Engineered Microenvironments for the Maturation and Observation of Human Embryonic Stem Cell Derived Cardiomyocytes

By
Max R. Salick

A dissertation submitted in partial fulfillment of
the requirements for the degree of

Doctor of Philosophy
(Materials Science)

at the
UNIVERSITY OF WISCONSIN-MADISON
2014

Date of final oral examination: 8/14/2014

The dissertation is approved by the following members of the Final Oral Committee:

Wendy C. Crone, Professor, Engineering Physics
Timothy J. Kamp, Professor, Medicine
Kristyn S. Masters, Associate Professor, Biomedical Engineering
Sean P. Palecek, Professor, Chemical and Biological Engineering
Lih-Sheng Turng, Professor, Mechanical Engineering

ABSTRACT

The human heart is a dynamic system that undergoes substantial changes as it develops and adapts to the body's growing needs. To better understand the physiology of the heart, researchers have begun to produce immature heart muscle cells, or cardiomyocytes, from pluripotent stem cell sources with remarkable efficiency. These stem cell-derived cardiomyocytes hold great potential in the understanding and treatment of heart disease; however, even after prolonged culture, these cells continue to exhibit an immature phenotype, as indicated by poor sarcomere organization and calcium handling, among other features. The lack of maturation that is observed in these cardiomyocytes greatly limits their applicability towards drug screening, disease modeling, and cell therapy applications.

The mechanical environment surrounding a cell has been repeatedly shown to have a large impact on that cell's behavior. For this reason, we have implemented micropatterning methods to mimic the level of alignment that occurs in the heart *in vivo* in order to study how this alignment may help the cells to produce a more mature sarcomere phenotype. It was discovered that the level of sarcomere organization of a cardiomyocyte can be strongly influenced by the micropattern lane geometry on which it adheres. Steps were taken to optimize this micropattern platform, and studies of protein organization, gene expression, and myofibrillogenesis were conducted. Additionally, a set of programs was developed to provide quantitative analysis of the level of sarcomere organization, as well as to assist with several other tissue engineering applications.

This dissertation is divided into several chapters, each describing a collection of studies conducted to investigate a specific topic.

Chapter 1: Background provides a succinct summary of the state of the field, and some of the physiology involved in this research. It begins by briefly describing heart disease as a whole, and quickly delves into the specific physiology of cardiomyocytes and stem cell technologies.

Chapter 2: Automated Image Analysis for Tissue Engineering Applications will cover three software packages utilizing Matlab that were developed for various investigations relating to tissue engineering. This includes particle-tracking software for applications in strain analysis of mechanical test samples, calcium transient curve analysis software for analyzing intracellular Ca^{2+} waveforms, and micropattern printing image analysis software to improve the accuracy of advanced micropatterning devices.

Chapter 3: Impact of Micropattern Geometry on Myofilament Structure describes the trends observed between micropatterned geometries and the sarcomere formation of cardiomyocyte populations seeded onto them. Specifically, it was found that micropatterned lanes of less than 100 μm produced aligned cardiomyocyte aggregates with more mature-like formation of their sarcomere structures.

Chapter 4: Micropattern Optimization continues off of this finding, with further steps to improve the consistency and mature cardiomyocyte modeling capacity of these micropatterns. The extracellular matrix coating, seeding density, and cardiomyocyte preparations were optimized to produce a more robust model of myofibrillogenesis.

Chapter 5: Scanning Gradient Fourier Transform (SGFT) Method for Assessing Sarcomere Structure describes software developed utilizing a novel combination of gradient analysis and one-directional Fourier transform techniques, allowing for a detailed quantification of sarcomere structure in intracellular protein stains.

Chapter 6: Assessment of hESC-CMs Culture on Optimized Micropattern Substrates includes several studies of the optimized micropatterned cardiomyocyte platforms. Immunostaining, qRT RT-PCR, and live cell timelapse imaging were conducted to investigate the means by which myofibrillogenesis was improved.

The appendices include data, protocols, and Matlab code to supplement these chapters. Readers are welcome and encouraged to use these protocols for their own research as much as possible. Readers are also encouraged to utilize and modify the published Matlab code for their own analyses, as long as proper acknowledgement is given.

DEDICATION

For my grandfather,

Del "Pompatch" Shobe

at 89, he is still the most youthful person I know

ACKNOWLEDGEMENTS

The number of people involved in this research extends far beyond the author lists. The willingness and helpfulness of my colleagues and advisors has been incredible, and I truly believe that true progress can only be made through such remarkable collaboration.

I'd first like to thank the fellow members of the Crone Lab. Chandler Benjamin and Suehelay Acevedo-Acevedo have been a great support during my time here. Brett Napiwocki and Shazhad Chindhy supported a large amount of this work, providing assistance with cell culture which can never be appreciated enough. Kevin Hart helped greatly with the design and production of the bioreactors used in some of my projects in the beginning of my research. Early on, the guidance provided by Barbara Calcagno, Maria del Carmen López García, and Adam Creuziger helped me to initiate my research career within the Crone Lab.

I would also like to thank the members of Bionates at the Wisconsin Institutes for Discovery. Lih-Sheng (Tom) Turng, Randolph Ashton, and Kris Saha have all helped me considerably along the way with their open, collaborative attitudes toward research, as well as their openness toward letting me use their equipment. A large portion of the knowledge I've gained has come from conversations with other students of Bionates, including Alex Laperle, Travis Cordie, and Ethan Lippmann. Hao-Yang Mi, Xin Jing, and Xiaofeng Wang have all been excellent collaborators, and I thoroughly enjoyed combining our varied expertise to produce some interesting research in the fields of material science. I would also like to thank Jin Sha, Gavin Knight, and Jason McNulty, whose development of the micropatterning scaffolds was critical for this research.

The lab of James Thomson has provided excellent advice, shared their equipment, and provided reagents that helped greatly for this research. In particular, I'd like to thank Nicholas Propson and Mitch Probasco for maintaining and providing advice for the flow cytometer. Nick was also kind enough to provide large amounts of vitronectin for these studies.

The lab of Timothy Kamp has been absolutely invaluable, as well. Their knowledge of cardiac biology is nearly infinite, and what little I know in the field can be attributed to them. Specifically, Chad Koonce, Jianhua Zhang, Pratik Lalit, and Kunil Raval have all been excellent collaborators throughout the years. I would also like to thank Gary Lyons and Jayne Squirrell for their helpful conversations. I would also like to thank Kristyn Masters, Sean Palecek, and their respective labs, for their excellent support in all aspects of this research. Kristyn helped me to get my qRT RT-PCR techniques established, and Sean has helped greatly with the ever-critical cardiomyocyte differentiation aspect of my work. Laurie Hazeltine and Xiaojun (Lance) Lian in particular have been excellent collaborators, as well.

I wish to thank Patricia Keely and the Laboratory for Optical and Computational Instrumentation, including Kevin Eliceiri and Yuming Liu, for providing image samples of breast cancer tissue, and for helpful conversations. Tenneille Ludwig and her colleagues at WiCell also deserve my thanks for their assistance with my stem cell work.

I'd like to thank Chris Lacey and Beth Misco for keeping everything running "behind the scenes" at the Wisconsin Institutes for Discovery, and Colleen Lavin and Roger Main from Nikon for their support with my intricate microscopy needs.

My friends and family may deserve the greatest acknowledgement of all. My family, for putting up with my absence during my studies. My friends, for drawing me away from them to remind me that there is more to life than research.

Lastly, I'd like to thank my advisor, Wendy Crone, for everything she's done to get me to this point. Wendy has given me the perfect amount of guidance, while also providing me with ample space to grow on my own. Wendy's knowledge of the scientific concepts, as well as her mastery of the 'soft skills' needed to get one's work fully recognized, has been invaluable during this project. Her guidance has been irreplaceable, and I'm sure I will be seeking her advice long after my time has finished in her lab.

This research was supported with funds from the National Institutes of Health Grant K18 HL105504 from the Heart, Blood and Lung Institute and the Graduate School of the University of Wisconsin-Madison.

TABLE OF CONTENTS

LIST OF TABLES

LIST OF FIGURES

CHAPTER 1: BACKGROUND

HEART DISEASE, CARDIOMYOCYTES, MYOFIBRILS, AND THE PLURIPOTENT STEM CELLS THAT HELP US TO UNDERSTAND THEM

HEART DISEASE

The impact of cardiovascular disease (CVD) on the world's population is staggering, regardless of the metric used to measure it. It is the largest cause of death globally, causing ~17.3 million mortalities every year [Alwan et al, 2011], with a projected increase to ~23 million by 2030, suggesting that it will remain the leading cause of death for the next several decades [Mathers and Loncar, 2006]. One in every three deaths in the United States can be attributed to CVD [Hoyert and Xu, 2012; Go et al, 2014], as is also observed in most European countries [Nichols et al, 2012]. Approximately half of these cases, or 1 in every 6 deaths overall, are due to coronary heart disease. ~620,000 new coronary attacks and ~295,000 recurring coronary attacks occur in the United States every year [Xu et al, 2010; Go et al, 2014], which includes the hundreds of thousands of estimated silent myocardial infarctions that go undetected.

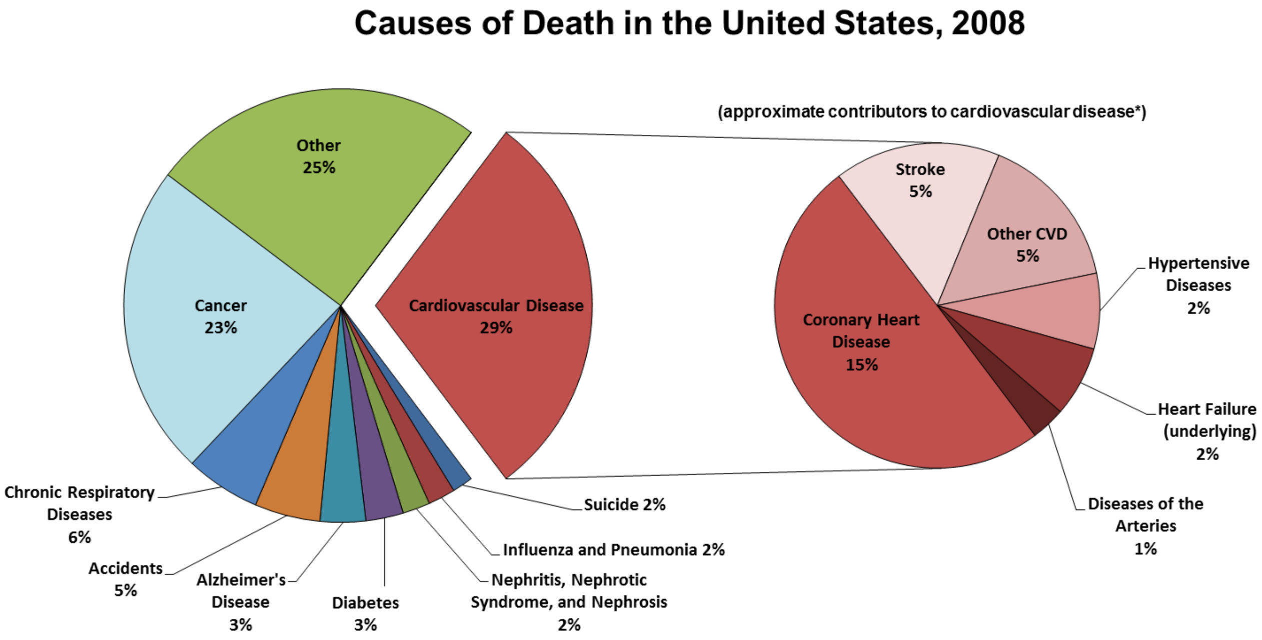

Figure 1-1. Overall mortality statistics for the United States in 2008. Cardiovascular disease is the single greatest cause of death in the United States, followed by cancer and chronic respiratory diseases. Approximate contributors to CVD are included. *It is important to note that death due to cardiovascular disease is complex and typically caused by a combination of factors. For example, atrial fibrillation, while typically not life-threatening, can often predispose patients to ischemia, stroke, and other components of cardiovascular disease. Figure compiled from data provided by the National Heart, Lung, and Blood Institute [Mussolino, 2012] and [Go et al, 2014].

The burden of cardiovascular disease goes beyond mortality rates, as well. The economic impact of CVD, consisting of direct medical costs and loss of productivity, amounts respectively to $273 billion and $172 billion in the United States. Additionally, due to the increasing population age, these costs are predicted to skyrocket, reaching $818 billion and $276 billion by 2030 [Heidenreich et al, 2011].

One of the leading causes of the extremely high mortality rate following MIs is the human heart's inability to regenerate. Unlike cells present in several other human tissues [Michalopoulos et al, 2007] or the hearts of some other species [Poss et al, 2002], the proliferation rate of human cardiomyocytes (cardiac muscle cells) is extremely low. As few as

1% of human cardiomyocytes replicate annually in adults of 25 years, and this number reduces to 0.45% by the age of 75 [Bergmann, 2009]. Carbon-dating studies have shown that less than 50% of cardiomyocytes are regenerated throughout an entire typical lifespan. This lack of proliferation is due to the transition of cardiomyocytes from a hyperplastic to hypertrophic phase, which is indicated by their binucleation, increase in myofibril density, and formation of intercalated discs [Pasumarthi and Field, 2002]. As a result of this inadequate regenerative capability, myocardial infarction triggers a complement cascade that produces a large region of collagen-dense scar tissue to replace the damaged myocardium [Frangogiannis et al, 2002]. Similarly, ischemic and dilated cardiomyopathies lead to a slow degradation of healthy myocardium which is unable to regenerate [Kang and Izumo, 2000]. This damaged tissue is significantly different from the surrounding healthy myocardium in both mechanical [Holmes et al, 2005] and electrophysiological [Bigger et al, 1984] properties. This heterogeneity and loss of heart function is what leads to spiraling heart disease and failure following an MI or other forms of heart disease.

In spite of the prevalence of CVD and the burden that it places on families throughout the world, there is still incredibly little that we know about the heart. Until the past decade, researchers have been forced to rely on animal models to understand the physiology of the heart. Fortunately, the emergence of new technologies and the discovery of pluripotent stem cells now allow researchers to examine human heart cells in ways that were impossible during the 20th century. Before delving into these stem cell advances, we will briefly review the physiology of the heart and the cells that populate it.

THE DEVELOPING HEART

To form hypotheses and to better understand how the process of cardiac differentiation may occur *in vitro*, an understanding of natural processes that occur *in vivo* is needed. In embryology, the heart is the first functional organ, though in a more primitive faculty, due to the nutrition requirements of the embryo that can no longer be met by direct diffusion of nutrients from the placenta. The first signs of human heart formation occur with the development of the primary and secondary heart fields. The heart fields are formed by cells of the mesodermal layer that is initially formed during gastrulation [Moorman et al, 2003].

The detailed complexities of cardiogenesis have been thoroughly studied in animal models and are beyond the scope of this review, but are briefly summarized as follows (for an excellent summary of cardiogenesis, readers are directed to [Burridge et al, 2012]). Spatially-varied NODAL expression within the mouse epiblast begins at embryonic day 5. This signaling leads to increased BMP4 expression, which in turn induces WNT3 expression in the proximal epiblast. WNT and NODAL in the anterior visceral endoderm are blocked by the antagonists Dkk1 and Lefty1/Cer1, respectively. During the same time, at day 5.75, WNT signaling in the posterior epiblast (where the primitive streak has now formed) leads to increased mesendodermal differentiation, as reflected by increased T (brachyury) expression, which in turn induces MESP1 expression.

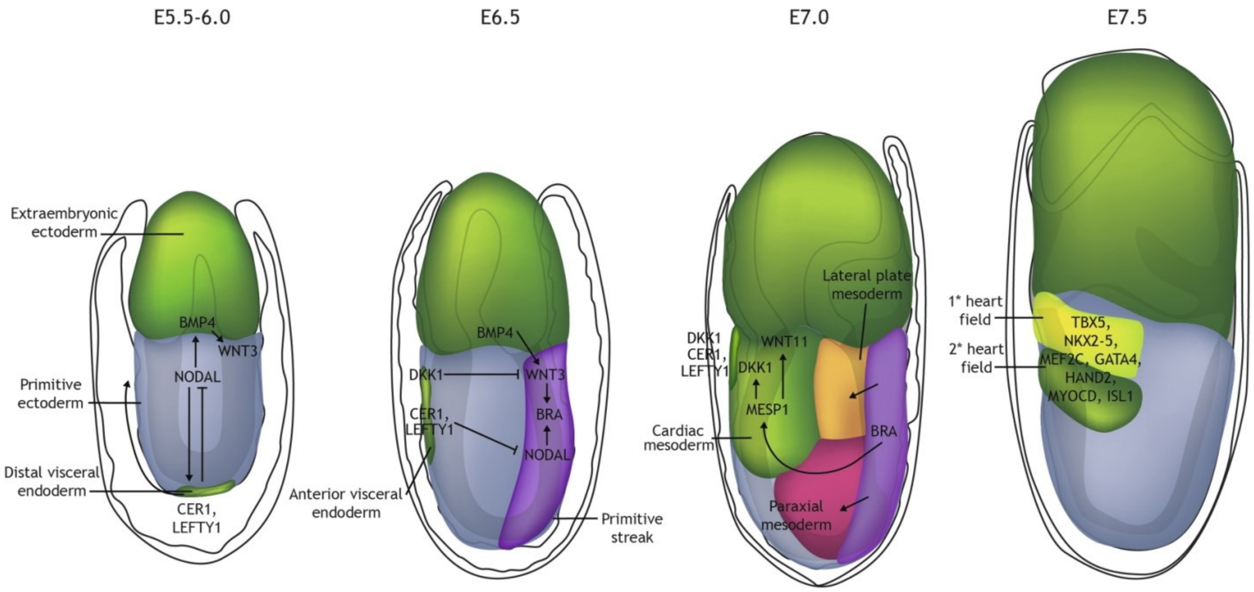

Figure 1-2. Mouse cardiogenesis. NODAL in the proximal epiblast induces BMP4 expression in the extraembryonic ectoderm. This in turn upregulates WNT3 expression in the proximal epiblast. During primitive streak formation, the distal visceral endoderm translates to the anterior epiblast, and continues to produce NODAL- and Wnt-blocking factors. T^+ cells transfer laterally, then ventrally, from the primitive streak to form the first and second heart fields. Figure from Burridge et al [2012].

These early mesoderm cells then migrate laterally and ventrally toward the anterior side of the embryo to form the lateral plate mesoderm, from which the first and second heart fields are derived [Arnold and Robertson, 2009]. It is from these early signaling patterns that researchers were first able to determine the pathways that induce cardiovascular development via testing of chick embryos [Schultheiss et al, 1997; Yatskievych et al, 1997; Marvin et al, 2001].

The next step of cardiogenesis is heart tube formation and heart tube looping. The first and second heart fields form primitive heart tubes, which then fuse along the midline of the embryo at day 8 (approximately day 20 for human). At this point, immature cardiomyocytes begin to contract, providing blood flow through the inflow and outflow tracts of the developing heart tube. It is important to note that a massive amount of heterogeneity in cardiac cell phenotype and gene expression has already been observed at this point in development [Christoffels et al, 2000; Nelson et al, 2014]. Minor constrictions form in the heart tube, segmenting it, cranially to caudally, into the bulbus cordis, ventricle, atrium, and sinus venosis. The heart tube then begins a complex folding process, in which the bulbus cordis and ventricle descend, the atrium ascends, and lastly, atrial and ventricular septa form to divide the functional chambers of the heart [Anderson et al, 2003]. The combination of mechanical loading and biological remodeling that occurs during heart looping is still not fully understood [Männer, 2000]. It was originally hypothesized that physical constraint of ends of the heart tube, in conjunction with uneven proliferation in the bulboventricular loop were the main causes of the intricate morphology that occurs during heart looping [Pensky, 1982]. However, it has been since found that looping still occurs when these constraints applied by the pericardial sac are removed [Larsen, 1997; Abdulla et al, 2004]

Of particular interest for our work, this combination of heart looping mechanics, along with the gradual conversion from hyperplasia (cell proliferation) to hypertrophy (cell growth), slowly lead to an adult phenotype of cardiomyocyte that is vastly different from its embryonic counterpart. The resulting tissue produces a reliable but dynamic organ that responds rapidly to short-term needs of the body [Fletcher et al, 2001], and steadily to long-term physiological factors [Cohn et al, 2000].

CELL TYPES OF THE HEART

Of the hundreds of cell types that populate the human body, there are four that are believed to predominate in the human heart: fibroblasts (extracellular matrix production and other supporting roles), endothelial cells (lining of the endocardium and coronary arteries), vascular smooth muscle cells (vasodilation of the coronary arteries), and cardiomyocytes (controlled contraction of the heart). While cardiomyocytes make up only 30-40% of the total cell number in the adult myocardium, they take up approximately 75% of the tissue's volume due to their enlarged size [Camelliti et al, 2005]. This review describes studies conducted solely on the force-producing cardiomyocytes; this does not suggest, however, that the various other cell types play a minimal role in the function of the heart. On the contrary, it is through exceedingly precise interactions among these cell types, as well as with their surrounding physical environment, that the heart is capable of its remarkable functionality. Hereafter, however, we will specifically examine the complex properties of the cardiomyocyte, including its differentiation *in vivo* and *in vitro*, myofibril production, and response to various engineering microenvironments.

THE CARDIOMYOCYTE

Ventricular, atrial, and sinoatrial nodal cardiomyocytes are the three distinctive phenotypes that form the multiple chambers and nodes of the heart, each with their own unique functional and electrophysiological properties [Ng et al, 2010]. Atrial cardiomyocytes exhibit faster active tension generation and relaxation compared to their ventricular counterparts; however, the resting and maximum tension in atrial cardiomyocytes is lower than in ventricular cardiomyocytes [van der Velden et al, 1999]. Sinoatrial nodal cardiomyocytes, also referred to as "pacemaker" cells, are located in the right atrium and are responsible for spontaneously firing action potentials which then propagate through the purkinje fibers and the chambers of the heart. The most robust method of identifying these cardiomyocyte phenotypes is by characterizing their notably differing action potentials [He et al, 2003]. While differentiation methods are capable of forming cardiomyocytes efficiently, there are still no well-established means of isolating these cardiomyocyte phenotypes without the use of costly and limiting flow cytometry or magnetic sorting techniques.

One of the most distinguishing components of a cardiomyocyte is its contractile apparatus. This is the highly organized structure formed by numerous cytoskeletal, motor, and binding proteins that enable the cell to produce force in response to calcium ion concentrations within the cytoplasm. The individual repeating unit of the contractile apparatus is the sarcomere, which is defined as one segment between neighboring Z-lines (Figure 1-3). These sarcomeres bundle together laterally and align end-to-end to produce long myofibrils that traverse the length of the cardiomyocyte. Depending on the maturation and condition of the cardiomyocyte, these organized myofibril structures can form up to 52% of the cell by volume [Barth et al, 1992].

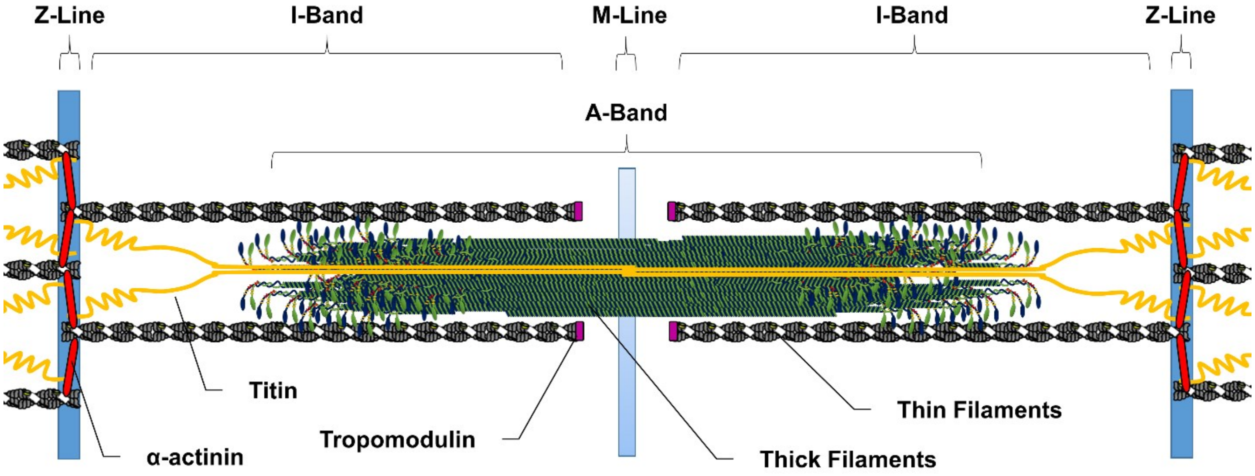

Figure 1-3. Diagram of a sarcomere. A single sarcomere consists of a wide variety of proteins, forming the thick filaments, thin filaments, M-line, Z-line, and other components. F-actin is anchored at the Z-line and provides binding sites for the globular myosin heads extending outward from the thick filaments. Titin, a giant protein that is also anchored to the Z-line, extends inward toward the M-line and is believed to provide elasticity and mechanical support to maintain the highly-organized structure of the myofibrils.

The I-band (standing for "isotropic") is made up of thin filaments consisting mostly of aligned F-actin, and is anchored at one end to a Z-line with the protein CapZ. These actin filaments extend toward the M-line at the center of the sarcomere, and are hypothesized to be limited in length by the giant protein nebulin [McElhinny et al, 2003; Labeit et al, 2011]. Troponin complexes consist of troponin C, cardiac troponin I, and one of several isoforms of cardiac troponin T [Gomes et al, 2002], and align with tropomyosin along the thin filaments, providing binding sites for myosin motors (Figure 1-4). When Ca^{2+} in the cytoplasm binds to the troponin C, a conformation change in the troponin complex occurs, temporarily removing troponin I from its neighboring F-actin, and providing a binding site for the myosin head. The myosin head (Figure 1-5) and neighboring actin produce a cross-bridge, and a structural change in the myosin results in a working stroke, which produces tension along the thick and thin filaments.

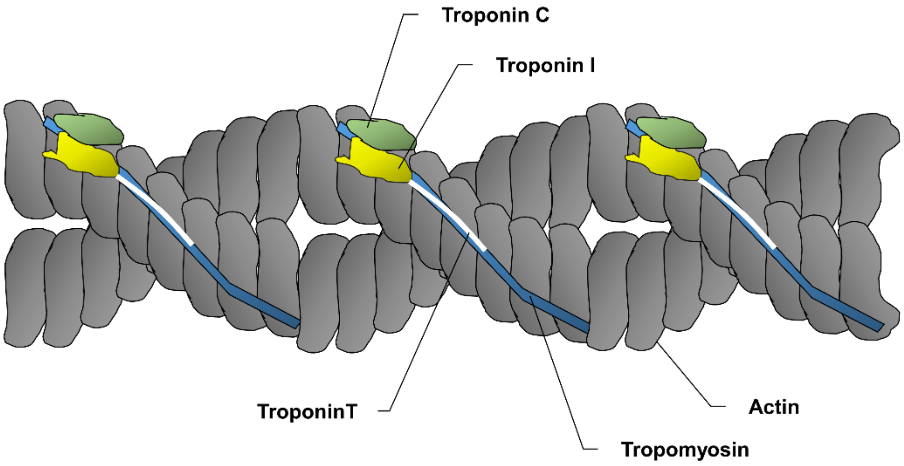

Figure 1-4. Diagram of F-actin forming the thin filament of a sarcomere. The actin fibers are lined with tropomyosin, which is bound to the troponin complex consisting of troponin C, troponin I, and cardiac troponin T. Slow (cardiac) troponin C is the only isoform of troponin C that is present in the heart [Parmacek and Leiden, 1991; Adamcova and Pelouch, 1999]. Isoform expression of troponin I changes with time; prenatal and neonatal hearts exhibit a combination of slow skeletal troponin I and cardiac troponin I, while adult cardiomyocytes contain solely cardiac troponin I [Hunkeler et al, 1991]. There are 4 isoforms of cardiac troponin T present in the heart [Anderson et al, 1991; Gomes et al, 2002]. Adapted from Adamcova and Pelouch [1999].

The A-band (standing for "anisotropic") forms along the center of the sarcomere, and consists of the myosin-dense thick filaments. While at least 24 classes of myosin exist in eukaryotic cells [Foth et al, 2006], only myosin II is present as the main motor protein in developed sarcomeres (it should be noted that nonmuscle myosin IIb is present in developing myofibrils, as explained in the next section). Each class II myosin is a hexamer (Figure 1-5), which includes two myosin heavy chains, two essential light chains, and two regulatory light chains [Reggiani et al, 2000]. One thick filament contains approximately 300 myosin molecules and extends to roughly 1.6μm in length. The expression of sarcomeric proteins is dependent on the phenotype and maturity of a cardiomyocyte. Thus, assessment of cardiomyocyte development often requires determination of the various isoforms that can make up the sarcomere.

There are two myosin heavy chain isoforms present in the heart: α-MHC and β-MHC. The α-MHC isoform is faster, exhibits higher ATPase activity, and produces more power than the β-MHC isoform [Miyata et al, 2000]. The ratio of these two isoforms is linked to heart disease, with α-MHC being observed in nonfailing left ventricles but not in failing left ventricles [Miyata et al, 2000; Lowes et al, 1997]. Additionally, a much larger amount of α-MHC is observed in atria than in the ventricles, and this percentage also decreases substantially in failing hearts. Lastly, the fetal heart contains a larger percentage of the α-MHC, with 95% and ~3-4% in the atria and ventricles, respectively. In comparison, the healthy adult myocardium consists of 86% and 2.5-5%, respectively [Reiser et al, 2001].

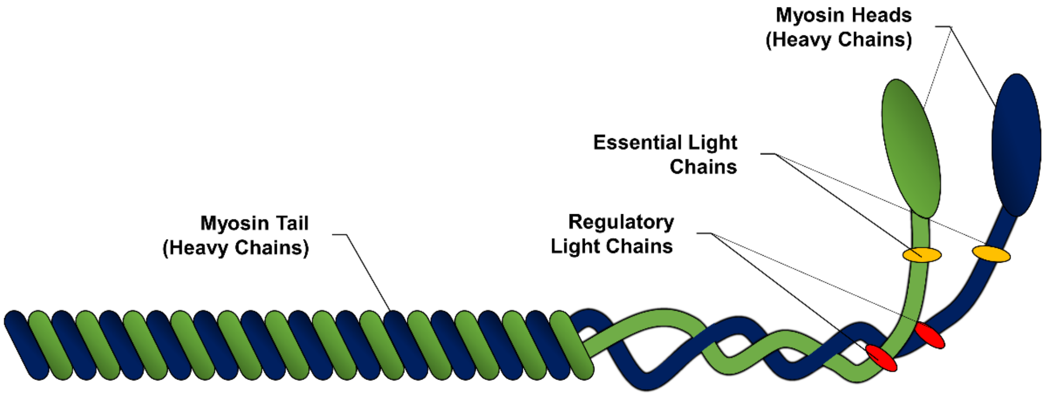

Figure 1-5. Class II myosin. The many classes of myosin result from a variety of multimers and contribute to a wide range of cellular functions, most of which involve mechanotransduction. In skeletal, smooth, and cardiac muscle, class II myosin molecules bundle together to form the thick filament of the sarcomere. Each myosin II molecule consists of two myosin heavy chains, two essential light chains, and two regulatory light chains [Reggiani et al, 2000].

Similarly, the two regulatory light chains MLC-2a and MLC-2v are variably expressed in the developing myocardium. Specifically, MLC-2a is present throughout the entire developing myocardium, and this expression declines postnatally only in the ventricles. Postnatal expression of MLC-2v in the developing ventricles increases in conjunction with this isoform switch [Chuva de Sousa Lopse et al, 2006]. Thus, MLC-2v expression may serve as an indicator of cardiomyocyte maturity, but only in the ventricular phenotype [Kubalak et al, 1994; O'Brien et al, 1993].

MYOFIBRILLOGENESIS

The formation of sarcomeres in developing and mature myocytes is termed myofibrillogenesis. Several of the mechanisms of myofibrillogenesis have been uncovered for embryonic chick, neonatal rat, and adult rat models [Dabiri et al, 1997; LoRusso et al, 1997].

Current models of myofibrillogenesis show that sarcomeres initially form along the myocyte's sarcolemma, or cell membrane [Sanger and Sanger, 2002]. Z-bodies, which are small clusters of α-actinin and possibly other binding proteins, form periodically along the sarcolemma. Loosely organized F-actin and nonmuscle myosin IIb accumulate between these Z-bodies, forming premyofibrils [Murakami et al 1993; Rhee et al, 1994; Tullio et al, 1997], which then detach and transfer medially towards the center of the cell. Multiple premyofibrils then begin to aggregate, as mediated by nonmuscle myosin IIb [Rhee et al, 1994], titin [Wang et al, 1988], and obscurin [Kontrogianni-Konstantopoulos et al, 2006]. Next, during the nascent myofibril stage, nonmuscle myosin IIb is replaced by muscle myosin II [LoRusso et al, 1997], the F-actin lengths are restricted by nebulin, and further condensation of Z-bodies occurs. Lastly, the Z-bodies merge to form Z-disks, and proteins such as talin, vinculin, and nebulin bind with the surrounding myoplasm and sarcolemma.

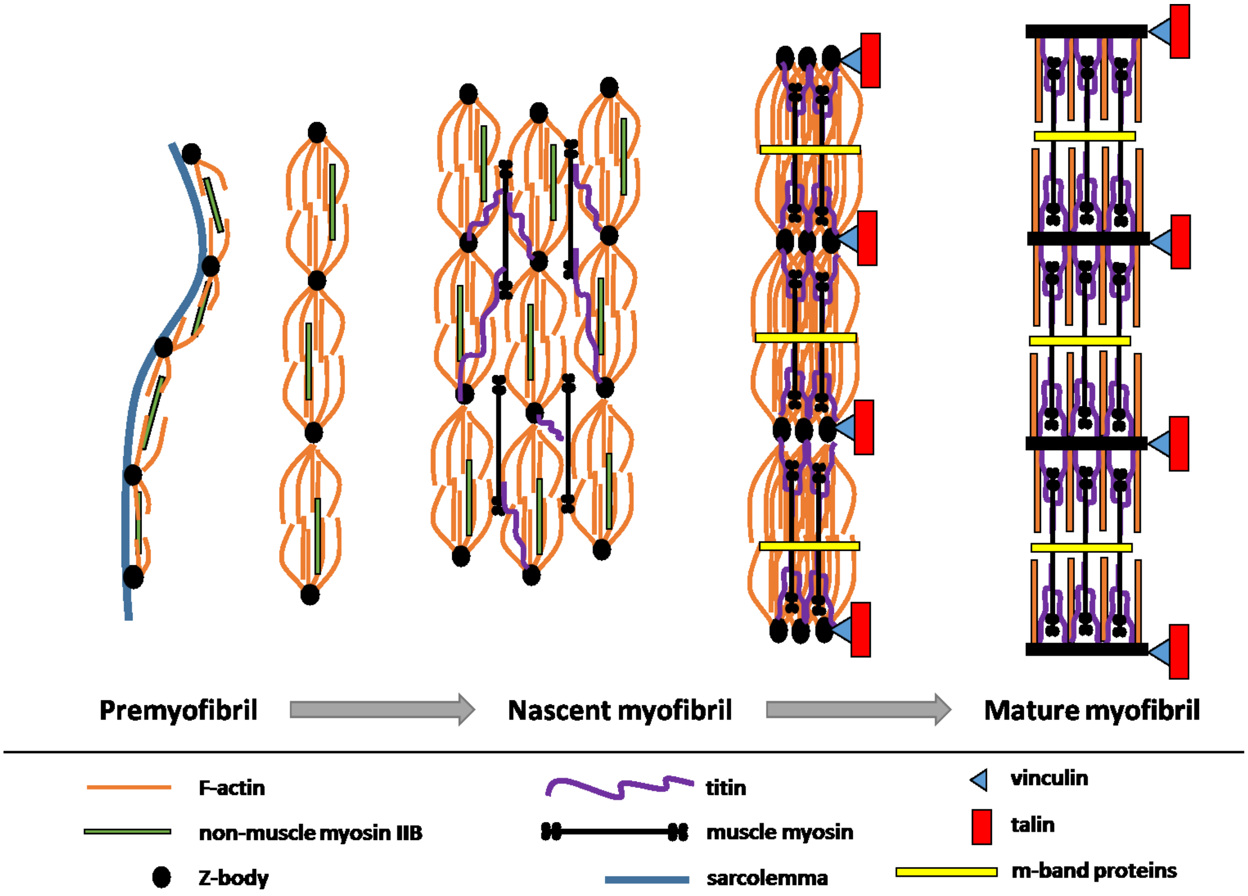

Figure 1-6. Current model of myofibrillogenesis. Premyofibrils form as aggregates of Z-bodies and loosely aligned F-actin and nonmuscle myosin IIb. These premyofibrils separate from the sarcolemma and cluster, as mediated by titin, nonmuscle myosin IIb, and obscurin, forming nascent myofibrils. Further alignment and constricting of the Z-bodies occurs, and the thick and thin filaments organize to form structured mature myofibrils. Figure adapted from Sanger and Sanger [2002].

POTENTIAL BENEFITS OF STEM CELL TECHNOLOGIES

Human embryonic stem cells (hESCs), which are pluripotent cells capable of long-term proliferation, were first successfully isolated from *in* vitro fertilization embryos in 1998 at the University of Wisconsin – Madison [Thomson et al, 1998]. This groundbreaking discovery has led to further breakthroughs in the fields of embryology, cellular biology, tissue engineering, and regenerative medicine. Following this discovery, an extensive number of researchers focused their efforts on developing methods for producing specific cell types through a wide variety of methods. As a result, we are now capable of producing a large number of specialized cell types, including oligodendrocytes [Faulkner and Keirstead, 2005], hepatocytes [Seo et al, 2005], pancreatic islets [Shim et al, 2007], and cardiomyocytes [Laflamme et al, 2007], to name a few.

With the rapid emergence of stem cell technologies, there is an exciting new opportunity to improve researchers' understanding of the human heart and develop effective new therapies to combat heart disease. With further investigation into the factors that control stem cell behavior and heart development, heart models of unprecedented physiological relevance could be produced that would streamline drug screening and accelerate future cardiac research. Moreover, a better understanding of these phenomena may lead to potentially life-saving cell-based therapies**.** Additionally, the more recent derivation of induced pluripotent stem cells (iPSCs) [Takahashi et al, 2007; Yu et al, 2007] can lead to development of disease models, improved drug screens, and clinical therapies that evade autoimmune rejection. In fact, cell-based therapies that involve direct implantation of stem cells to damaged tissue sites have already begun to enter clinical trials [Makkar et al, 2012].

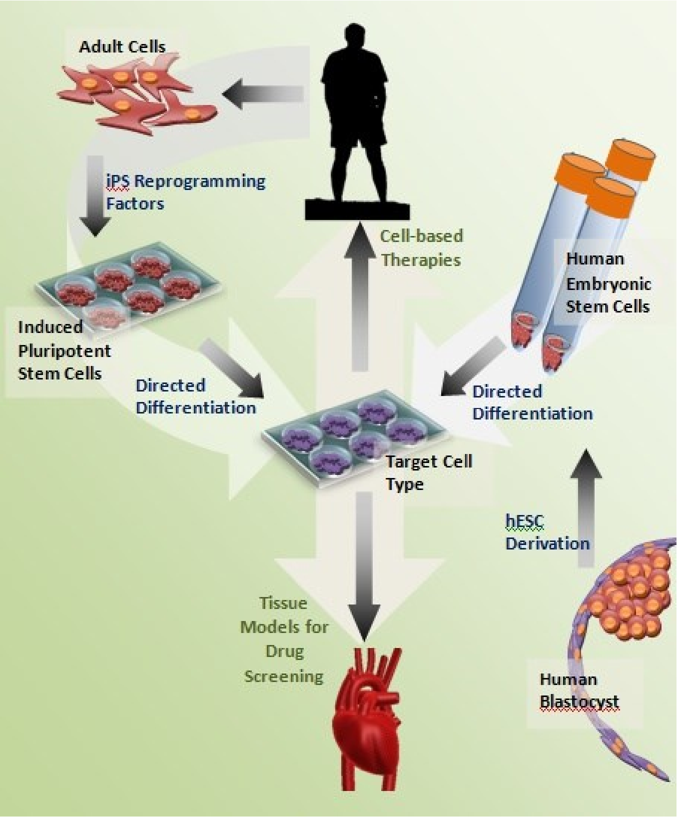

Figure 1-7. Stem cell technology continues to be an incredibly promising field. The development of cell-based therapies and tissue models from stem cells depends on effective directed differentiation of pluripotent stem cells.

BIOCHEMICALLY-INDUCED DIRECTED DIFFERENTIATION

After contracting cells were first observed in embryoid bodies formed from hESCs [Itskovitz-Eldor et al, 2000], researchers have made countless attempts to reproducibly derive cardiomyocytes from pluripotent stem cell sources. While this work showed that it was indeed possible to derive cardiomyocytes from hESCs, it was clear that steps would need to be taken to increase the differentiation efficiency to provide a workable number of cells for future applications**.** It was hypothesized that stem cell differentiation closely replicated embryogenesis, and as such it became clear that a thorough understanding of cardiomyogenesis would provide the first clues toward producing effective directed differentiation procedures.

Researchers utilized findings from cardiac embryology to induce cardiac differentiation of hESCs by applying Activin A and BMP4 to embryoid bodies [Kattman et al, 2011] and monolayers [Laflamme et al, 2007; Yang et al, 2008]. Unfortunately, the repeatability and efficiencies of these procedures had not reached desirable levels, and so further work has been done to improve the reliability of these treatment methods. Along these lines, recent investigations have developed alternative, more effective means of producing cardiomyocytes. These methods include small-molecule Wnt inhibition [Lian et al, 2012; Willems et al, 2011] and extracellular matrix sandwich methods [Zhang et al, 2012], and have reported efficiencies of up to 98%.

One obstacle facing stem cell technologies is the prevalence of non-specific differentiation. In order to create therapies and tissue models effectively, it is imperative that the cell fate can be properly controlled. Of particular relevance to this research, the presence of undifferentiated cells would greatly increase the variability within a population, making it much more difficult to derive reliable conclusions from the analysis. Additionally, it is critical from a clinical perspective to ensure that any cell-based therapies placed on the market do not contain pluripotent cells, as these cell types have repeatedly been shown to form teratomas upon implantation [Blum and Benvenisty, 2008]. For our purposes, a cardiac troponin-T promoter cell line, graciously provided by the Kamp Lab of the University of Wisconsin – Madison, allowed us to produce pure populations of cTnT$^+$ cells, ensuring that we were working with populations consisting of ~99% cardiomyocytes [Salick et al, 2014].

CARDIOMYOCYTE MATURATION

As described previously [Salick et al, 2014], the main limitation of all of these differentiation methods is that they produce cardiomyocytes with predominantly immature properties [Snir et al, 2003]. Specifically, rather than becoming organized, aligned “barrel”-shaped cells [Fernandez-Teran and Hurle, 1982] that are typically seen in native adult myocardium, the hESC-derived CMs form into randomly-aligned monolayers or clusters of contracting cells. Additionally, the multinucleation, myosin heavy chain isoform expression, Ca2+-handling, and biochemical response characteristics that are ordinarily exhibited by mature adult cardiomyocytes are not achieved by these immature cardiomyocytes [Binah et al, 2007].

Other studies, however, have shown that prolonged culture times of these immature cardiomyocytes over 60 days [Snir et al, 2003] and 120 days [Lundy et al, 2013] do appear to lead to more mature-like phenotypes. These cardiomyocytes displayed promising changes in morphology and function, including increased multinucleation, sarcomere length, and cell size, with reduced Ca2+ time-to-peak and decay time. However, while the long-term cultured cardiomyocytes exhibited improved sarcomere alignment, they still did not achieve the level of sarcomere structure and alignment observed in native adult cardiomyocytes [Bird et al, 2003; Robertson et al, 2013], and such long-term cultures would be limiting in their high cost and low throughput.

THE ROLE OF MECHANICS IN DIFFERENTIATION AND MATURATION

While these biochemical signaling pathways were being discovered, an entirely different set of researchers took a more physical approach to understanding differentiation. Heralded by Adam Engler and Dennis Discher’s work on mesenchymal stem cell (MSC) differentiation in response to substrate stiffness [Engler et al, 2006], researchers began to make connections between cellular mechanics and stem cell differentiation. While the influence of mechanics on *in vitro* stem cell differentiation has been a recent target for research, it has been known since the 19th century [Davis, 1867; Wolff, 1892] that the mechanical surroundings of a cell can strongly influence its behavior [Guilak et al, 2009]. For example, scientists discovered several years ago that cell shape, which is strongly influenced by a substrate's mechanical properties, greatly correlates to DNA synthesis and proliferation [Folkman and Moscona, 1978]. On a similar note, it had been shown that cell shape and alignment are highly dependent on their location within the embryonic heart tube during looping [Manasek and Burnside, 1972]. More recent studies have shown that culturing MSCs in either rounded or flattened morphologies can affect the lineage commitments of MSCs [McBeath et al, 2004], and this effect is hypothesized to correspond to cytoskeletal remodeling.

The stiffness of an underlying or surrounding substrate has also been shown to affect cell behavior in many ways, including migration [Pelham and Wang, 1997; Peyton and Putnam, 2005; Guo et al, 2006], proliferation [Hadjipanayi et al, 2009], maturation [Jacot et al, 2008; Jacot et al, 2010], apoptosis [Wang et al, 2000], and differentiation [Salick et al, 2010; Jacot et al, 2008; Engler et al, 2006; Chatterjee et al, 2010; Saha et al, 2008b]. Additionally, some studies have focused specifically on how myocytes interact with substrates of varying stiffness by investigating phenomena such as actin/myosin striation development [Engler et al, 2004] and cardiomyocyte contractility [Hazeltine et al, 2012].

Another collection of researchers has begun to examine how mechanical loading of a cell influences its behavior [Simmons et al, 2003; Thomas and el Haj, 1996; Sen et al, 2008]. All cells throughout the body experience a range of loading scenarios that may impact the way that they interact with their environment. Work as early as the 1930s and 1940s by A. Glucksmann [1942] showed a clear change in behavior of chondrocytes and osteoblasts in response to constant uniaxial tension. Until recently, most studies of the effects of mechanical loading were conducted strictly within the realm of orthopedics. More recent experiments, however, have shown that both internal and external cellular forces may play a key role in controlling stem cell differentiation. Work to create blood vessels with MSC-derived smooth muscle cells (SMCs) has utilized cyclic tension to promote differentiation and SMC alignment at the cost of a minor decrease in proliferation [Hamilton et al, 2004]. A similar study conducted at the same time determined that while biaxial loading reduced SMC differentiation, uniaxial loading increased SMC differentiation [Park et al, 2004].

Of particular relevance to our research, some studies have already been conducted on the response of immature cardiomyocytes to mechanical loading. It has been observed that 20%-strain, 2 Hz cyclic tensile loading of chick embryonic cardiomyocytes increased their rate of proliferation [Miller et al, 2000]. Another very thorough study conducted at the University of Washington determined that mechanical loading of embryonic cardiomyocytes within a coculture of supporting cells caused an increase in hypertrophy and proliferation [Tulloch et al, 2011].

CELLULAR MECHANOTRANSDUCTION

In an attempt to explain these phenomenological studies, models are now being created to examine precisely how these loading and adhesion scenarios translate into a biochemical reaction within the cell. It is now known that there are several sensing mechanisms used by cells to detect mechanical loads which ultimately influence cellular functions such as migration [Chien et al, 2005], attachment [Geiger and Bershadsky, 2002], and apoptosis [Hsieh and Nguyen, 2005]. While cellular mechanotransduction is still an open area of research, it is commonly hypothesized that the cytoskeleton, focal adhesions, tyrosine kinases, and ion channels are key cellular components that are directly influenced by mechanical loads [Ruknudin et al, 1993; Wozniak et al, 2004; Liu et al, 1996; Burridge and Chrzanowska-Wodnicka, 1996].

The Rho pathway has also shown a clear correlation to cellular mechanics. Activated by adhesion molecules, integrins, growth factors, and other signaling factors, the intricate Rho pathway controls a wide range of cellular processes, including actin cytoskeleton reorganization, mitogenesis, tumorigenesis, and transcription regulation. The three downstream subfamilies of the pathway include Rho, Rac, and CDC42, which induce stress fiber bundling/focal adhesion production, lamellipodia polymerization, and filopodia/microspike polymerization, respectively [Ridley and Hall, 1992; Ridley, 2006; Buoreux et al, 2007; Oleksy et al, 2006]. One of the most important proteins within the Rho pathways is Rho-associated protein kinase (ROCK), which plays a key role in controlling actomyosin contractility via myosin light chain (MLC) and myosin-binding subunit (MBS) phosphorylation [Torka et al, 2006; Tsai and Jiang, 2006]. Others have isolated 3 isoforms of a tension-induced/inhibited protein (TIP), which, as the name suggests, are upregulated and downregulated in response to external tensile loading. These TIPs act as nuclear receptor coregulators and can also regulate chromatin remodeling. TIPs have thus shown a strong connection to myogenic differentiation pathways [Jakkaraju et al, 2005].

A large number of tests have been done on neonatal rat cardiomyocytes to determine the biomolecular response to stretch [Sadoshima and Izumo, 1997]. These studies have shown that the MAP kinase cascade [Yamazaki et al, 1995] is transiently expressed immediately following stretch. Animal models have also revealed that a number of genes are activated by mechanical stretch, including c-fos, c-jun, Egr-1, and c-myc [Komuro et al, 1990; Sadoshima et al, 1993].

One of the most prominent biomechanical phenomena that occurs within cardiomyocytes is the Frank-Starling Law. Named after the physiologists Otto Frank and Ernest H. Starling, the Frank-Starling Law is based on the observation of a change in contractility upon modification of sarcomere length [Patterson and Starling, 1914]. This relation has been observed in skeletal and cardiac muscle in embryonic and adult tissues [Asnes et al, 2006], and in a variety of species [Shiels and White, 2006]. Contractility studies suggest that the Frank-Starling Law is due to changes in myofilament overlap, myofilament lattice spacing, and Ca^{2+} sensitivity within troponin complexes [Sheils and White, 2008; Solaro, 2007; Allen and Kentish, 1985; Shintani et al, 2014].

MICROPATTERNING OF CARDIOMYOCYTES

As described previously [Salick et al, 2014], while understanding of the biology continues to improve, a wide array of engineering innovations have been developed that have enabled researchers to more accurately mimic the cells' physiological environment while improving throughput, accuracy, and efficiency of these studies. Of these innovations, two-dimensional micropatterning and three-dimensional engineered topographies have proven to be exceptionally promising [Zhang et al, 2011; Falconnet et al, 2006; Flemming et al, 1999; Bettinger et al, 2009].

Two-dimensional micropatterning studies have indicated that the architecture of the extracellular environment influences cell behavior with respect to morphology [Lehnert et al, 2004], migration [Parker et al, 2002], cytoskeletal structure [McBeath et al, 2004], nuclear shape [Thomas et al, 2002], lineage determination [Kilian et al, 2010], and functionality [Kaji et al, 2003; Chen et al, 1997]. Several studies have been conducted in which neonatal rat and mouse cardiomyocytes were seeded onto two-dimensional micropatterns and observed. It has been consistently reported that these cells, when seeded as populations onto patterned stripes, are capable of forming myofibers with improved sarcomere organization, cell-cell junction protein expression, and contractile strength [Cimetta et al, 2009; McDevitt et al, 2002; Feinberg et al, 2012]. Additionally, micropatterned single-cell studies utilizing rat and mouse cardiomyocytes have shown trends between cell shape, sarcomere formation, and α-catenin expression [Bray et al, 2008; Chopra et al, 2012]. Further engineering innovations have led to studies involving PEG-and-groove combinations [Motlagh et al, 2003], poly(ethylene glycol) nanotopographies [Kim et al, 2009], and highly biomimetic micropattern designs [Badie et al, 2009].

With the previously-mentioned emergence of hESC-derived cardiomyocyte differentiation protocols, researchers have recently been able to begin testing human cardiomyocytes in similar ways. A study by Zhang et al [Zhang et al, 2013] has resulted in improved human cardiomyocyte maturation, E-C coupling, and sarcomere structure by culturing cell populations of varying cardiomyocyte purities onto mesh-like micropatterns. Another study has demonstrated that human cardiomyocytes can be micropatterned in arrays for high-throughput screening purposes [Serena et al, 2012].

CONCLUSION

This review covers a mere fraction of the dynamic mechanisms that are in constant activity within developing and adult hearts. The following chapters describe some of the contributions that we've made to the field, with particular focus on the response of human embryonic stem cell-derived cardiomyocytes to various mechanical stimuli. Micropatterned substrates have been used to influence embryonic human cardiomyocyte sarcomere formation. Several algorithms have been developed in order to streamline and quantitate complex mechanical and biological properties involved in the maturation of these cells. Lastly, an optimized platform based on these micropattern substrates was created, and myofibrillogenesis was assessed using immunohistochemistry, qRT RT-PCR, and time-lapse studies.

REFERENCES

Abdulla, R., Blew, G. A and Holterman, M. J. (2004). Cardiovascular embryology. *Pediatr. Cardiol.* **25**, 191–200.

Adamcova, M. and Pelouch, V. (1999). Isoforms of troponin in normal and diseased myocardium. *Physiol. Res.*

Allen, D. and Kentish, J. (1985). The cellular basis of the length-tension relation in cardiac muscle. *J. Mol. Cell. Cardiol.* **840**, 821–840.

Alwan, A. (2011). Global status report on noncommunicable diseases 2010. Geneva, Switzerland.

Anderson, P. A., Malouf, N. N., Oakeley, A. E., Pagani, E. D. and Allen, P. D. (1991). Troponin T isoform expression in humans. A comparison among normal and failing adult heart, fetal heart, and adult and fetal skeletal muscle. *Circ. Res.* **69**, 1226–1233.

Anderson, R. H., Webb, S., Brown, N. A., Lamers, W. and Moorman, A. (2003). Development of the heart: (2) Septation of the atriums and ventricles. *Heart* **89**, 949–58.

Arnold, S. and Robertson, E. (2009). Making a commitment: cell lineage allocation and axis patterning in the early mouse embryo. *Nat. Rev. Mol. cell Biol.* **10**, 91–103.

Asnes, C. F., Marquez, J. P., Elson, E. L. and Wakatsuki, T. (2006). Reconstitution of the Frank-Starling mechanism in engineered heart tissues. *Biophys. J.* **91**, 1800–10.

Badie, N., Satterwhite, L. and Bursac, N. (2009). A Method to Replicate the Microstructure of Heart Tissue In Vitro Using DTMRI-Based Cell Micropatterning. *Ann. Biomed. Eng.* **37**, 2510–2521.

Barth, E., Stämmler, G., Speiser, B. and Schaper, J. (1992). Ultrastructural quantitation of mitochondria and myofilaments in cardiac muscle from 10 different animal species including man. *J. Mol. ...* **681**, 669–681.

Bayraktar, M. and Männer, J. (2014). Cardiac looping may be driven by compressive loads resulting from unequal growth of the heart and pericardial cavity. Observations on a physical simulation model. *Front. Physiol.* **5**, 112.

Bergmann, O., Bhardwaj, R. D., Bernard, S., Zdunek, S., Barnabé-Heider, F., Walsh, S., Zupicich, J., Alkass, K., Buchholz, B. A, Druid, H., et al. (2009). Evidence for cardiomyocyte renewal in humans. *Science* 324, 98–102.

Bettinger, C. J., Langer, R. and Borenstein, J. T. (2009). Engineering Substrate Topography at the Micro- and Nanoscale to Control Cell Function. *Angew. Chemie Int. Ed.* **48**, 5406–5415.

Bigger, J. T., Fleiss, J. L., Kleiger, R., Miller, J. P. and Rolnitzky, L. M. (1984). The relationships among ventricular arrhythmias, left ventricular dysfunction, and mortality in the 2 years after myocardial infarction. *Circulation* **69**, 250–258.

Binah, O., Dolnikov, K., Sadan, O., Shilkrut, M., Zeevi-Levin, N., Amit, M., Danon, A. and Itskovitz-Eldor, J. (2007). Functional and developmental properties of human embryonic stem cells–derived cardiomyocytes. *ISCE 32nd Annu. Conf.* **40**, S192–S196.

Bird, S. D., Doevendans, P. A., van Rooijen, M. A., Brutel de la Riviere, A., Hassink, R. J., Passier, R. and Mummery, C. L. (2003). The human adult cardiomyocyte phenotype. *Cardiovasc. Res.* 58, 423–434.

Blum, B. and Benvenisty, N. (2008). The Tumorigenicity of Human Embryonic Stem Cells. *Adv. Cancer Res.* **100**, 133–158.

Boureux, A., Vignal, E., Faure, S. and Fort, P. (2007). Evolution of the Rho family of Ras-like GTPases in eukaryotes. *Mol. Biol. Evol.* **24**, 203–216.

Bray, M.-A., Sheehy, S. and Parker, K. (2008). Sarcomere alignment is regulated by myocyte shape. *Cell Motil. Cytoskel.* **65**, 641–651.

Burridge, K. and Chrzanowska-Wodnicka, M. (1996). Focal adhesions, contractility, and signaling. *Annu. Rev. Cell Dev. Biol.* **12**, 463–518.

Burridge, P. W., Keller, G., Gold, J. D. and Wu, J. C. (2012). Production of de novo cardiomyocytes: human pluripotent stem cell differentiation and direct reprogramming. *Cell Stem Cell* **10**, 16–28.

Camelliti, P., Borg, T. K. and Kohl, P. (2005). Structural and functional characterization of cardiac fibroblasts. *Cardiovasc. Res.* **65**, 40–51.

Chatterjee, K., Lin-Gibson, S., Wallace, W. E., Parekh, S. H., Lee, Y. J., Cicerone, M. T., Young, M. F. and Simon, C. G. (2010). The effect of 3D hydrogel scaffold modulus on osteoblast differentiation and mineralization revealed by combinatorial screening. *Biomaterials* **31**, 5051–5062.

Chen, C. S., Mrksich, M., Huang, S., Whitesides, G. M. and Ingber, D. E. (1997). Geometric Control of Cell Life and Death. *Science* **276**, 1425–1428.

Chien, S., Li, S., Shiu, Y.-T. and Li, Y.-S. (2005). Molecular basis of mechanical modulation of endothelial cell migration. *Front. Biosci.* **10**, 1985–2000.

Chopra, A., Patel, A., Shieh, A. C., A. Janmey, P. and Kresh, J. Y. (2012). α-Catenin localization and sarcomere self-organization on n-cadherin adhesive patterns are myocyte contractility driven. *PLoS One* **7**, e47592.

Christoffels, V. M., Habets, P. E., Franco, D., Campione, M., de Jong, F., Lamers, W. H., Bao, Z. Z., Palmer, S., Biben, C., Harvey, R. P., et al. (2000). Chamber formation and morphogenesis in the developing mammalian heart. *Dev. Biol.* 223, 266–78.

Chuva de Sousa Lopes, S. M., Hassink, R. J., Feijen, A., van Rooijen, M. a, Doevendans, P. a, Tertoolen, L., Brutel de la Rivière, A. and Mummery, C. L. (2006). Patterning the heart, a template for human cardiomyocyte development. *Dev. Dyn.* **235**, 1994–2002.

Cimetta, E., Pizzato, S., Bollini, S., Serena, E., Coppi, P. and Elvassore, N. (2009). Production of arrays of cardiac and skeletal muscle myofibers by micropatterning techniques on a soft substrate. *Biomed. Microdevices* **11**, 389–400.

Cohn, J. N., Ferrari, R. and Sharpe, N. (2000). Cardiac remodeling—concepts and clinical implications: a consensus paper from an international forum on cardiac remodeling. *J. Am. Coll. Cardiol.* **35**, 569–582.

Dabiri, G. A., Turnacioglu, K. K., Sanger, J. M. and Sanger, J. W. (1997). Myofibrillogenesis visualized in living embryonic cardiomyocytes. *Proc. Natl. Acad. Sci. U. S. A.* **94**, 9493–8.

Davis, H. G. (1867). *Conservative Surgery*. New York: D. Appleton & Co.

Engler, A. J., Griffin, M. A., Sen, S., Bönnemann, C. G., Sweeney, H. L. and Discher, D. E. (2004). Myotubes differentiate optimally on substrates with tissue-like stiffness: pathological implications for soft or stiff microenvironments. *J. Cell Biol.* **166**, 877–887.

Engler, A. J., Sen, S., Sweeney, H. L. and Discher, D. E. (2006). Matrix Elasticity Directs Stem Cell Lineage Specification. *Cell* **126**, 677–689.

Eurostat Regional Yearbook, 2013.

Falconnet, D., Csucs, G., Michelle Grandin, H. and Textor, M. (2006). Surface engineering approaches to micropattern surfaces for cell-based assays. *Biomaterials* **27**, 3044–3063.

Faulkner, J. and Keirstead, H. S. (2005). Human embryonic stem cell-derived oligodendrocyte progenitors for the treatment of spinal cord injury. *Transpl. Immunol.* **15**, 131–142.

Feinberg, A. W., Alford, P. W., Jin, H., Ripplinger, C. M., Werdich, A. A., Sheehy, S. P., Grosberg, A. and Parker, K. K. (2012). Controlling the contractile strength of engineered cardiac muscle by hierarchal tissue architecture. *Biomaterials* **33**, 5732–5741.

Fernandez-Teran, M. A. and Hurle, J. M. (1982). Myocardial fiber architecture of the human heart ventricles. *Anat. Rec.* **204**, 137–147.

Flemming, R. G., Murphy, C. J., Abrams, G. A., Goodman, S. L. and Nealey, P. F. (1999). Effects of synthetic micro- and nano-structured surfaces on cell behavior. *Biomaterials* **20**, 573–588.

Fletcher, G. F., Balady, G. J., Amsterdam, E. a., Chaitman, B., Eckel, R., Fleg, J., Froelicher, V. F., Leon, a. S., Pina, I. L., Rodney, R., et al. (2001). *Exercise Standards for Testing and Training: A Statement for Healthcare Professionals From the American Heart Association*.

Folkman, J. and Moscona, A. (1978). Role of cell shape in growth control. *Nature* **273**, 345–349.

Foth, B. J., Goedecke, M. C. and Soldati, D. (2006). New insights into myosin evolution and classification. *Proc. Natl. Acad. Sci. U. S. A.* **103**, 3681–6.

Frangogiannis, N. (2002). The inflammatory response in myocardial infarction. *Cardiovasc. Res.*. **53**, 31–47.

Geiger, B. and Bershadsky, A. (2002). Exploring the neighborhood: Adhesion-coupled cell mechanosensors. *Cell* **110**, 139–142.

Glucksmann, A. (1942). The role of mechanical stresses in bone formation in vitro. *J. Anat.* **76**, 231–239.

Go, A. S., Mozaffarian, D., Roger, V. L., Benjamin, E. J., Berry, J. D., Blaha, M. J., Dai, S., Ford, E. S., Fox, C. S., Franco, S., et al. (2014). *Heart disease and stroke statistics--2014 update: a report from the American Heart Association.*

Gomes, A. V, Guzman, G., Zhao, J. and Potter, J. D. (2002). Cardiac troponin T isoforms affect the Ca2+ sensitivity and inhibition of force development. Insights into the role of troponin T isoforms in the heart. *J. Biol. Chem.* **277**, 35341–9.

Grabarek, Z., Tao, T. and Gergely, J. (1992). Molecular mechanism of troponin-C function. *J. Muscle Res. Cell Motil.* **13**, 383–93.

Guilak, F., Cohen, D. M., Estes, B. T., Gimble, J. M., Liedtke, W. and Chen, C. S. (2009). Control of Stem Cell Fate by Physical Interactions with the Extracellular Matrix. *Cell Stem Cell* **5**, 17–26.

Guo, W., Frey, M. T., Burnham, N. A. and Wang, Y. (2006). Substrate rigidity regulates the formation and maintenance of tissues. *Biophys. J.* **90**, 2213–2220.

Hadjipanayi, E., Mudera, V. and Brown, R. A. (2009). Close dependence of fibroblast proliferation on collagen scaffold matrix stiffness. *J. Tissue Eng. Regen. Med.* **3**, 77–84.

Hamilton, D. W., Maul, T. M. and Vorp, D. A. (2004). Characterization of the Response of Bone Marrow-Derived Progenitor Cells to Cyclic Strain: Implications for Vascular Tissue-Engineering Applications. *Tissue Eng.* **10**, 361–369.

Hazeltine, L. B., Simmons, C. S., Salick, M. R., Lian, X., Badur, M. G., Han, W., Delgado, S. M., Wakatsuki, T., Crone, W. C., Pruitt, B. L., et al. (2012). Effects of substrate mechanics on contractility of cardiomyocytes generated from human pluripotent stem cells. *Int. J. Cell Biol.*

He, J. Q., Ma, Y., Lee, Y., Thomson, J. A. and Kamp, T. J. (2003). Human embryonic stem cells develop into multiple types of cardiac myocytes: action potential characterization. *Circ. Res.* **93**, 32–39.

Heidenreich, P. a, Trogdon, J. G., Khavjou, O. a, Butler, J., Dracup, K., Ezekowitz, M. D., Finkelstein, E. A., Hong, Y., Johnston, S. C., Khera, A., et al. (2011). Forecasting the future of cardiovascular disease in the United States: a policy statement from the American Heart Association. *Circulation* **123**, 933–44.

Holmes, J. W., Borg, T. K. and Covell, J. W. (2005). Structure and mechanics of healing myocardial infarcts. *Annu. Rev. Biomed. Eng.* **7**, 223–53.

Hoyert, D. L. and Xu, J. (2012). Deaths: Preliminary Data for 2011. *Natl. Vital Stat. Reports* **61**.

Hsieh, M. H. and Nguyen, H. T. (2005). Molecular mechanism of apoptosis induced by mechanical forces. *Int Rev Cytol* **245**, 45–90.

Hunkeler, N. M., Kullman, J. and Murphy, a. M. (1991). Troponin I isoform expression in human heart. *Circ. Res.* **69**, 1409–1414.

Itskovitz-Eldor, J., Schuldiner, M., Karsenti, D., Eden, A., Yanuka, O., Amit, M., Soreq, H. and Benvenisty, N. (2000). Differentiation of human embryonic stem cells into embryoid bodies compromising the three embryonic germ layers. *Mol. Med.* **6**, 88–95.

Jacot, J. G., McCulloch, A. D. and Omens, J. H. (2008). Substrate stiffness affects the functional maturation of neonatal rat ventricular myocytes. *Biophys. J.* **95**, 3479–3487.

Jacot, J. G., Kita-Matsuo, H., Wei, K. A., Chen, H. S. V., Omens, J. H., Mercola, M. and McCulloch, A. D. (2010). Cardiac myocyte force development during differentiation and maturation. *Ann N Y Acad Sci* 1188, 121–7.

Jakkaraju, S., Zhe, X., Pan, D., Choudhury, R. and Schuger, L. (2005). TIPs are tension-responsive proteins involved in myogenic versus adipogenic differentiation. *Dev. Cell* **9**, 39–49.

Kaji, H., Takii, Y., Nishizawa, M. and Matsue, T. (2003). Pharmacological characterization of micropatterned cardiac myocytes. *Biomaterials* **24**, 4239–4244.

Kang, P. M. and Izumo, S. (2000). Apoptosis and Heart Failure : A Critical Review of the Literature. *Circ. Res.* **86**, 1107–1113.

Kattman, S. J., Witty, A. D., Gagliardi, M., Dubois, N. C., Niapour, M., Hotta, A., Ellis, J. and Keller, G. (2011). Stage-specific optimization of activin/nodal and bmp signaling promotes cardiac differentiation of mouse and human pluripotent stem cell lines. *Cell Stem Cell* **8**, 228–240.

Kilian, K. A., Bugarija, B., Lahn, B. T. and Mrksich, M. (2010). Geometric cues for directing the differentiation of mesenchymal stem cells. *Proc. Natl. Acad. Sci.* **107**, 4872–4877.

Kim, D.-H., Lipke, E. A., Kim, P., Cheong, R., Thompson, S., Delannoy, M., Suh, K.-Y., Tung, L. and Levchenko, A. (2009). Nanoscale cues regulate the structure and function of macroscopic cardiac tissue constructs. *Proc. Natl. Acad. Sci.* **107**, 565–570.

Komuro, I., Kaida, T., Shibazaki, Y., Kurabayashi, M., Katoh, Y., Hoh, E., Takaku, F. and Yazaki, Y. (1990). Stretching cardiac myocytes stimulates protooncogene expression. *J. Biol. Chem.* 265, 3595–3598.

Kontrogianni-Konstantopoulos, A., Catino, D. H., Strong, J. C., Sutter, S., Borisov, A. B., Pumplin, D. W., Russell, M. W. and Bloch, R. J. (2006). Obscurin modulates the assembly and organization of sarcomeres and the sarcoplasmic reticulum. *FASEB J.* 20, 2102–11.

Kubalak, S. W., Miller-Hance, W. C., O'Brien, T. X., Dyson, E. and Chien, K. R. (1994). Chamber specification of atrial myosin light chain-2 expression precedes septation during murine cardiogenesis. *J. Biol. Chem.* **269**, 16961–70.

Labeit, S., Ottenheijm, C. a C. and Granzier, H. (2011). Nebulin, a major player in muscle health and disease. *FASEB J.* **25**, 822–9.

Laflamme, M. A., Chen, K. Y., Naumova, A. V, Muskheli, V., Fugate, J. A., Dupras, S. K., Reinecke, H., Xu, C., Hassanipour, M., Police, S., et al. (2007). Cardiomyocytes derived from human embryonic stem cells in pro-survival factors enhance function of infarcted rat hearts. *Nat. Biotechnol.* 25, 1015–1024.

Larsen, W. J. (1997). *Human Embryology*. Second. New York: Churchill Livingstone.

Lehnert, D., Wehrle-Haller, B., David, C., Weiland, U., Ballestrem, C., Imhof, B. A. and Bastmeyer, M. (2004). Cell behaviour on micropatterned substrata: limits of extracellular matrix geometry for spreading and adhesion. *J. Cell Sci.* **117**, 41–52.

Lian, X., Hsiao, C., Wilson, G., Zhu, K., Hazeltine, L. B., Azarin, S. M., Raval, K. K., Zhang, J., Kamp, T. J. and Palecek, S. P. (2012). Robust cardiomyocyte differentiation from human pluripotent stem cells via temporal modulation of canonical Wnt signaling. *Proc Natl Acad Sci U S A* **109**, E1848–57.

Liu, M., Qin, Y., Liu, J., Tanswell, A. K. and Post, M. (1996). Mechanical strain induces pp60 activation and translocation to cytoskeleton in fetal rat lung cells. *J. Biol. Chem.* **271**, 7066 – 7071.

LoRusso, S. M., Rhee, D., Sanger, J. M. and Sanger, J. W. (1997). Premyofibrils in spreading adult cardiomyocytes in tissue culture: evidence for reexpression of the embryonic program for myofibrillogenesis in adult cells. *Cell Motil. Cytoskeleton* **37**, 183–98.

Lowes, B. D., Minobe, W., Abraham, W. T., Rizeq, M. N., Bohlmeyer, T. J., Quaife, R. A., Roden, R. L., Dutcher, D. L., Robertson, A. D., Voelkel, N. F., et al. (1997). Changes in gene expression in the intact human heart. Downregulation of alpha-myosin heavy chain in hypertrophied, failing ventricular myocardium. *J. Clin. Invest.* **100**, 2315–2324.

Lundy, S., Zhu, W., Regnier, M. and Laflamme, M. A. (2013). Structural and functional maturation of cardiomyocytes derived from human pluripotent stem cells. *Stem Cells Dev.* **22**, 1991–2002.

Männer, J. (2000). Cardiac Looping in the Chick Embryo : A Morphological Review With Special Reference to Terminological and Biomechanical. *Anat. Rec.* **262**, 248–262.

Männer, J. (2009). The anatomy of cardiac looping: a step towards the understanding of the morphogenesis of several forms of congenital cardiac malformations. *Clin. Anat.* **35**, 21–35.

Makkar, R. R., Smith, R. R., Cheng, K., Malliaras, K., Thomson, L. E. J., Berman, D., Czer, L. S. C., Marban, L., Mendizabal, A., Johnston, P. V., et al. (2012). Intracoronary cardiosphere-derived cells for heart regeneration after myocardial infarction (CADUCEUS): A prospective, randomised phase 1 trial. *Lancet* **379**, 895–904.

Manasek, F. J. and Burnside, M. B. (1972). Myocardial cell shape change as a mechanism of embryonic heart looping. *Dev. Biol.* **29**, 349–371.

Marvin, M., Rocco, G. Di, Gardiner, A., Bush, S. M. and Lassar, A. B. (2001). Inhibition of Wnt activity induces heart formation from posterior mesoderm. *Genes Dev. Dev.* **15**, 316–327.

Mathers, C. D. and Loncar, D. (2006). Projections of global mortality and burden of disease from 2002 to 2030. *PLoS Med.* **3**, e442.

McBeath, R., Pirone, D. M., Nelson, C. M., Bhadriraju, K. and Chen, C. S. (2004). Cell shape, cytoskeletal tension, and RhoA regulate stem cell lineage commitment. *Dev. Cell* **6**, 483–495.

McDevitt, T. C., Angello, J. C., Whitney, M. L., Reinecke, H., Hauschka, S. D., Murry, C. E. and Stayton, P. S. (2002). In vitro generation of differentiated cardiac myofibers on micropatterned laminin surfaces. *J. Biomed. Mater. Res.* **60**, 472–479.

McElhinny, A. S., Kazmierski, S. T., Labeit, S. and Gregorio, C. C. (2003). Nebulin: the nebulous, multifunctional giant of striated muscle. *Trends Cardiovasc. Med.* **13**, 195–201.

Michalopoulos, G. K. (2007). Liver Regeneration. 286–300.

Miller, C. E., Donlon, K. J., Toia, L., Wong, C. L. and Chess, P. R. (2000). Cyclic strain induces proliferation of cultured embryonic heart cells. *Vitr. Cell Dev Biol Anim* **36**, 633–639.

Miyata, S., Minobe, W., Bristow, M. R. and Leinwand, L. a. (2000). Myosin heavy chain isoform expression in the failing and nonfailing human heart. *Circ. Res.* **86**, 386–390.

Moorman, A., Webb, S., Brown, N. a, Lamers, W. and Anderson, R. H. (2003). Development of the heart: (1) formation of the cardiac chambers and arterial trunks. *Heart* **89**, 806–14.

Motlagh, D., Hartman, T. J., Desai, T. A. and Russell, B. (2003). Microfabricated grooves recapitulate neonatal myocyte connexin43 and N-cadherin expression and localization. *J. Biomed. Mater. Res. Part A* **67A**, 148–157.

Mussolino, M. E. (2012). Morbidity and Mortality: 2012 Chart Book on Cardiovascular and Lung Diseases. *Bethesda, MD NIH.*

Murakami, N., Trenkner, E. and Elzinga, M. (1993). Changes in expression of nonmuscle myosin heavy chain isoforms during muscle and nonmuscle tissue development. *Dev. Biol.*

Nelson, D. O., Jin, D. X., Downs, K. M., Kamp, T. J. and Lyons, G. E. (2014). Irx4 identifies a chamber-specific cell population that contributes to ventricular myocardium development. *Dev. Dyn.* **243**, 381–92.

Ng, S. Y., Wong, C. K. and Tsang, S. Y. (2010). Differential gene expressions in atrial and ventricular myocytes : insights into the road of applying embryonic stem cell-derived cardiomyocytes for future therapies. 1234–1249.

Nichols, M., Townsend, N., Luengo-Fernandez, R., Leal, J., Gray, A., Scarborough, P. and Rayner, M. (2012). *European Cardiovascular Disease Statistics 2012*. Brussels, Belgium.

O'Brien, T. X., Lee, K. J. and Chien, K. R. (1993). Positional specification of ventricular myosin light chain 2 expression in the primitive murine heart tube. *Proc. Natl. Acad. Sci. U. S. A.* **90**, 5157–61.

Oleksy, A., Opaliński, Ł., Derewenda, U., Derewenda, Z. S. and Otlewski, J. (2006). The molecular basis of RhoA specificity in the guanine nucleotide exchange factor PDZ-RhoGEF. *J. Biol. Chem.* **281**, 32891–32897.

Park, J. S., Chu, J. S. F., Cheng, C., Chen, F., Chen, D. and Li, S. (2004). Differential effects of equiaxial and uniaxial strain on mesenchymal stem cells. *Biotechnol. Bioeng.* **88**, 359–368.

Parker, K. K., Brock, A. L., Brangwynne, C., Mannix, R. J., Wang, N., Ostuni, E., Geisse, N. A., Adams, J. C., Whitesides, G. M. and Ingber, D. E. (2002). Directional control of lamellipodia extension by constraining cell shape and orienting cell tractional forces. *FASEB J.* **16**, 1195–1204.

Parmacek, M. S. and Leiden, J. M. (1991). Structure, function, and regulation of troponin C. *Circulation* **84**, 991–1003.

Pasumarthi, K. B. S. and Field, L. J. . (2002). Cardiomyocyte Cell Cycle Regulation. *Circ. Res.* **90**, 1044–1054..

Patterson, S. and Starling, E. (1914). On the mechanical factors which determine the output of the ventricles. *J. Physiol.*

Pelham, R. J. and Wang, Y. l (1997). Cell locomotion and focal adhesions are regulated by substrate flexibility. *Proc. Natl. Acad. Sci. U. S. A.* **94**, 13661–13665.

Pensky, B. (1982). *Review of Medical Embryology*. New York: McMillan.

Peyton, S. R. and Putnam, A. J. (2005). Extracellular matrix rigidity governs smooth muscle cell motility in a biphasic fashion. *J. Cell. Physiol.* **204**, 198–209.

Poss, K. D., Wilson, L. G. and Keating, M. T. (2002). Heart regeneration in zebrafish. *Science* **298**, 2188–90.

Reggiani, C., Bottinelli, R. and Stienen, G. J. M. (2000). Sarcomeric Myosin Isoforms: Fine Tuning of a Molecular Motor. *News Physiol. Sci.* **15**, 26–33.

Reiser, P. J., Portman, M. A., Ning, X. H. and Schomisch Moravec, C. (2001). Human cardiac myosin heavy chain isoforms in fetal and failing adult atria and ventricles. *Am. J. Physiol. Heart Circ. Physiol.* **280**, H1814–H1820.

Rhee, D., Sanger, J. M. and Sanger, J. W. (1994). The premyofibril : evidence for its role in myofibrillogenesis. *Cell Motil. Cytoskeleton* **28**, 1–24.

Ridley, A. J. (2006). Rho GTPases and actin dynamics in membrane protrusions and vesicle trafficking. *Trends Cell Biol.* **16**, 522–529.

Ridley, A. J. and Hall, A. (1992). The small GTP-binding protein rho regulates the assembly of focal adhesions and actin stress fibers in response to growth factors. *Cell* **70**, 389–399.

Robertson, C., Tran, D. and George, S. (2013). Concise review: maturation phases of human pluripotent stem cell-derived cardiomyocytes. *Stem Cells* **31**, 829–837.

Ruknudin, A., Sachs, F. and Bustamante, J. O. (1993). Stretch-activated ion channels in tissue-cultured chick heart. *Am. J. Physiol.* **264**, H960–H972.

Sadoshima, J. and Izumo, S. (1997). The cellular and molecular response of cardiac myocytes to mechanical stress. *Annu Rev Physiol* **59**, 551–571.

Sadoshima, J. I., Xu, Y., Slayter, H. S. and Izumo, S. (1993). Autocrine release of angiotensin II mediates stretch-induced hypertrophy of cardiac myocytes in vitro. *Cell* **75**, 977–984.

Saha, S., Ji, L., De Pablo, J. J. and Palecek, S. P. (2006). Inhibition of human embryonic stem cell differentiation by mechanical strain. *J. Cell. Physiol.* **206**, 126–137.

Saha, K., Keung, A. J., Irwin, E. F., Li, Y., Little, L., Schaffer, D. V and Healy, K. E. (2008a). Substrate modulus directs neural stem cell behavior. *Biophys. J.* **95**, 4426–4438.

Saha, S., Ji, L., de Pablo, J. J. and Palecek, S. P. (2008b). TGFbeta/Activin/Nodal pathway in inhibition of human embryonic stem cell differentiation by mechanical strain. *Biophys. J.* **94**, 4123–4133.

Salick, M., Boyer, R., Koonce, C., Kamp, T., Palecek, S., Masters, K. and Crone, W. (2010). Differentiation of human embryonic stem cells encapsulated in hydrogel matrix materials. *2010 SEM Annu. Conf. Expo. Exp. Appl. Mech.*

Salick, M. R., Napiwocki, B. N., Sha, J., Knight, G. T., Chindhy, S. a, Kamp, T. J., Ashton, R. S. and Crone, W. C. (2014). Micropattern width dependent sarcomere development in human ESC-derived cardiomyocytes. *Biomaterials* **35**, 4454–64.

Sanger, J. W. and Sanger, J. M. (2002). Myofibrillogenesis in cardiac muscle. In *Myofibrillogenesis* (ed. Dube, D. K.), pp. 3–21. New York: Birkhauser Boston.

Schultheiss, T. M., Burch, J. B. and Lassar, a B. (1997). A role for bone morphogenetic proteins in the induction of cardiac myogenesis. *Genes Dev.* **11**, 451–62.

Sen, B., Xie, Z., Case, N., Ma, M., Rubin, C. and Rubin, J. (2008). Mechanical strain inhibits adipogenesis in mesenchymal stem cells by stimulating a durable beta-catenin signal. *Endocrinology* **149**, 6065–6075.

Seo, M. J., Suh, S. Y., Bae, Y. C. and Jung, J. S. (2005). Differentiation of human adipose stromal cells into hepatic lineage in vitro and in vivo. *Biochem. Biophys. Res. Commun.* **328**, 258–264.

Serena, E., Cimetta, E., Zatti, S., Zaglia, T., Zagallo, M., Keller, G. and Elvassore, N. (2012). Micro-arrayed human embryonic stem cells-derived cardiomyocytes for in vitro functional assay. *PLoS One* **7**, e48483.

Shiels, H. a and White, E. (2008). The Frank-Starling mechanism in vertebrate cardiac myocytes. *J. Exp. Biol.* **211**, 2005–13.

Shim, J. H., Kim, S. E., Woo, D. H., Kim, S. K., Oh, C. H., McKay, R. and Kim, J. H. (2007). Directed differentiation of human embryonic stem cells towards a pancreatic cell fate. *Diabetologia* **50**, 1228–1238.

Shimizu, N., Yamamoto, K., Obi, S., Kumagaya, S., Masumura, T., Shimano, Y., Naruse, K., Yamashita, J. K., Igarashi, T. and Ando, J. (2008). Cyclic strain induces mouse embryonic stem cell differentiation into vascular smooth muscle cells by activating PDGF receptor beta. *J Appl Physiol* **104**, 766–772.

Shintani, S. A., Oyama, K., Kobirumaki-Shimozawa, F., Ohki, T., Ishiwata, S. and Fukuda, N. (2014). Sarcomere length nanometry in rat neonatal cardiomyocytes expressed with α-actinin-AcGFP in Z discs. *J. Gen. Physiol.* **143**, 513–24.

Simmons, C. A., Matlis, S., Thornton, A. J., Chen, S., Wang, C. Y. and Mooney, D. J. (2003). Cyclic strain enhances matrix mineralization by adult human mesenchymal stem cells via the extracellular signal-regulated kinase (ERK1/2) signaling pathway. *J. Biomech.* **36**, 1087–1096.

Snir, M., Kehat, I., Gepstein, A., Coleman, R., Itskovitz-Eldor, J., Livne, E. and Gepstein, L. (2003). Assessment of the ultrastructural and proliferative properties of human embryonic stem cell-derived cardiomyocytes. *Am. J. Physiol. - Hear. Circ. Physiol.* **285**, H2355–H2363.

Solaro, R. J. (2007). Mechanisms of the Frank-Starling law of the heart: the beat goes on. *Biophys. J.* **93**, 4095–6.

Souders, C. a, Bowers, S. L. K. and Baudino, T. a (2009). Cardiac fibroblast: the renaissance cell. *Circ. Res.* **105**, 1164–76.

Taber, L. a, Lin, I. E. and Clark, E. B. (1995). Mechanics of cardiac looping. *Dev. Dyn.* **203**, 42–50.

Takahashi, K., Tanabe, K., Ohnuki, M., Narita, M., Ichisaka, T., Tomoda, K. and Yamanaka, S. (2007). Induction of pluripotent stem cells from adult human fibroblasts by defined factors. *Cell* **131**, 861–872.

Thomas, G. P. and El Haj, A. J. (1996). Bone marrow stromal cells are load responsive in vitro. *Calcif. Tissue Int.* **58**, 101–108.

Thomas, C. H., Collier, J. H., Sfeir, C. S. and Healy, K. E. (2002). Engineering gene expression and protein synthesis by modulation of nuclear shape. *Proc. Natl. Acad. Sci.* **99**, 1972–1977.

Thomson, J. a., Itskovitz-Eldor, J., Shapiro, S. S., Waknitz, M. A., Swiergiel, J. J., Marshall, V. S. and Jones, J. M. (1998). Embryonic stem cell lines derived from human blastocysts. *Science* **282**, 1145–1147.

Torka, R., Thuma, F., Herzog, V. and Kirfel, G. (2006). ROCK signaling mediates the adoption of different modes of migration and invasion in human mammary epithelial tumor cells. *Exp Cell Res* **312**, 3857–3871.

Tsai, M. H. and Jiang, M. J. (2006). Rho-kinase-mediated regulation of receptor-agonist-stimulated smooth muscle contraction. *Pflugers Arch. Eur. J. Physiol.* **453**, 223–232.

Tullio, a N., Accili, D., Ferrans, V. J., Yu, Z. X., Takeda, K., Grinberg, a, Westphal, H., Preston, Y. a and Adelstein, R. S. (1997). Nonmuscle myosin II-B is required for normal development of the mouse heart. *Proc. Natl. Acad. Sci. U. S. A.* **94**, 12407–12.

Tulloch, N. L., Muskheli, V., Razumova, M. V., Korte, F. S., Regnier, M., Hauch, K. D., Pabon, L., Reinecke, H. and Murry, C. E. (2011). Growth of engineered human myocardium with mechanical loading and vascular coculture. *Circ. Res.* **109**, 47–59.

Van der Velden, J., Klein, L. J., van der Bijl, M., Huybregts, M. a, Stooker, W., Witkop, J., Eijsman, L., Visser, C. a, Visser, F. C. and Stienen, G. J. (1999). Isometric tension development and its calcium sensitivity in skinned myocyte-sized preparations from different regions of the human heart. *Cardiovasc. Res.* **42**, 706–19.

Wang, S. M., Greaser, M. L., Schultz, E., Bulinski, J. C., Lin, J. J. and Lessard, J. L. (1988). Studies on cardiac myofibrillogenesis with antibodies to titin, actin, tropomyosin, and myosin. *J. Cell Biol.* **107**, 1075–83.

Wang, H. B., Dembo, M. and Wang, Y. L. (2000). Substrate flexibility regulates growth and apoptosis of normal but not transformed cells. *Am. J. Physiol. Cell Physiol.* **279**, C1345–C1350.

Willems, E., Spiering, S., Davidovics, H., Lanier, M., Xia, Z., Dawson, M., Cashman, J. and Mercola, M. (2011). Small-molecule inhibitors of the Wnt pathway potently promote cardiomyocytes from human embryonic stem cell-derived mesoderm. *Circ. Res.* **109**, 360–364.

Wolff, J. (1892). *The Law of Bone Remodeling*. Berlin: Heidelberg.

Wozniak, M. A., Modzelewska, K., Kwong, L. and Keely, P. J. (2004). Focal adhesion regulation of cell behavior. *Biochim. Biophys. Acta* **1692**, 103–119.

Xu, J., Kochanek, K. D. and Murphy, S. L. (2010). National Vital Statistics Reports Deaths : Final Data for 2007. *Statistics (Ber).* **58**, 135.

Yamazaki, T., Komuro, I., Kudoh, S., Zou, Y., Shiojima, I., Mizuno, T., Takano, H., Hiroi, Y., Ueki, K., Tobe, K., et al. (1995). Mechanical stress activates protein kinase cascade of phosphorylation in neonatal rat cardiac myocytes. *J Clin Invest* **96**, 438–446.

Yang, L., Soonpaa, M. H., Adler, E. D., Roepke, T. K., Kattman, S. J., Kennedy, M., Henckaerts, E., Bonham, K., Abbott, G. W., Linden, R. M., et al. (2008). Human cardiovascular progenitor cells develop from a KDR+ embryonic-stem-cell-derived population. *Nature* **453**, 524–528.

Yatskievych, T. A., Ladd, A. N. and Antin, P. B. (1997). Induction of cardiac myogenesis in avian pregastrula epiblast: the role of the hypoblast and activin. *Development* **124**, 2561 – 2570.

Yu, J., Vodyanik, M., Smuga-Otto, K., Antosiewicz-Bourget, J., Frane, J. L., Tian, S., Nie, J., Jonsdottir, G. a., Ruotti, V., Stewart, R., et al. (2007). Induced pluripotent stem cell lines derived from human somatic cells. *Science* **318**, 1917 – 1920.

Zhang, B., Xiao, Y., Hsieh, A., Thavandiran, N. and Radisic, M. (2011). Micro- and nanotechnology in cardiovascular tissue engineering. *Nanotechnology* **22**, 494003.

Zhang, J., Klos, M., Wilson, G. F., Herman, A. M., Lian, X., Raval, K. K., Barron, M. R., Hou, L., Soerens, A. G., Yu, J., et al. (2012). Extracellular matrix promotes highly efficient cardiac differentiation of human pluripotent stem cells: The matrix sandwich method. *Circ. Res.* **111**, 1125–1136.

Zhang, D., Shadrin, I. Y., Lam, J., Xian, H.-Q., Snodgrass, H. R. and Bursac, N. (2013). Tissue-engineered cardiac patch for advanced functional maturation of human ESC-derived cardiomyocytes. *Biomaterials* **34**, 5813–5820.

CHAPTER 2: AUTOMATED IMAGE ANALYSES FOR TISSUE ENGINEERING APPLICATIONS

INTRODUCTION

While investigating cardiomyocyte behaviors and responses to various stimuli, several instances occurred in which automated analysis methods were required. This chapter summarizes three of these instances, and describes the methods by which software was developed to provide solutions for these problems. The three software packages are as follows:

- **multiparticle_tracker.m** – designed for use during mechanical testing of soft biomaterials, this software allows a user to determine precise strains within materials using particle-tracking algorithms.
    - *Matlab code can be found in Appendix D: Multi-Particle Tracking Strain Analysis*

- **calcium_transient_analyzer.m** – this software accepts fluorescent intensity data that is gathered using voltage-sensitive and Ca^{2+}-detecting dyes, and produces valuable outputs such as intracellular Ca^{2+} time-to-peak and decay half-life.
    - *Matlab code can be found in Appendix E: Calcium Transient Auto Analysis*

- **micropattern_robot_alignment.m** – this software analyzes advanced lab-on-a-chip devices, utilizes the Horn quaternion method for determining array offsets, and suggests alignment corrections that improve the printing accuracy these micropatterning devices.
  - *Matlab code can be found in Appendix F: Micropatterning Robot Pattern Alignment Program*

MULTI-PARTICLE TRACKING FOR MECHANICAL TESTING OF SOFT AND BIOLOGICAL MATERIALS

This software and mechanical testing method was originally developed for publication in:

Hazeltine LB, Simmons CS, Salick MR, Lian X, Badur MG, Han W, Delgado SM, Wakatsuki T, Crone WC, Pruitt BL, Palecek SP (2012). Effects of substrate mechanics on contractility of cardiomyocytes generated from human pluripotent stem cells, Int J Cell Bio, 50829.

BACKGROUND

It has been well established that the mechanical properties of tissues and substrates play an extremely important role in the biological responses of cells that they encompass and contact [Engler et al, 2006; Pelham and Wang, 1997; Discher et al, 2005]. Tensile testing of such materials is a common method of determining their mechanical properties. During tensile testing, an increasing load is gradually applied to a material and the strain is recorded. Plotting the stress vs. strain in these materials provides a vast amount of information about the material, such as Young's Modulus (stiffness), regions of elasticity / plasticity, yield strength, ultimate tensile strength, and elastic recovery, to name a few. When possible, the most common sample geometry for testing is a dogbone shape, because it contains a neck region that exhibits a uniform stress throughout the cross-section. For most materials, strain gauges are utilized, which are placed at this neck region and give direct readouts of the strain being experienced by the sample. In soft and biological samples, however, strain gauges often cannot be applied, since the gauge itself interferes with the loading and displacements being applied to the material.

To overcome this obstacle, optical methods of strain determination are often used. This is done by coating the surface of the material with a speckled pattern or by placing beads within the sample. Depending on the relative sizes and volume percentage of beads placed in the sample, this has been shown not to significantly affect the material properties of the material being tested [Johnson et al, 2004]. The relative displacement of these beads is then measured frame-by-frame and correlated to the stress data produced by the tensile testing machine at the same time. This final step of bead tracking is highly labor-intensive, and is prone to large amounts of inaccuracy due to small sample sizes and human error. Thus, software was developed using Matlab to automatically track hundreds of beads and statistically determine the most likely strains at each frame, providing confidence predictions as well as a final stress vs. strain curve.

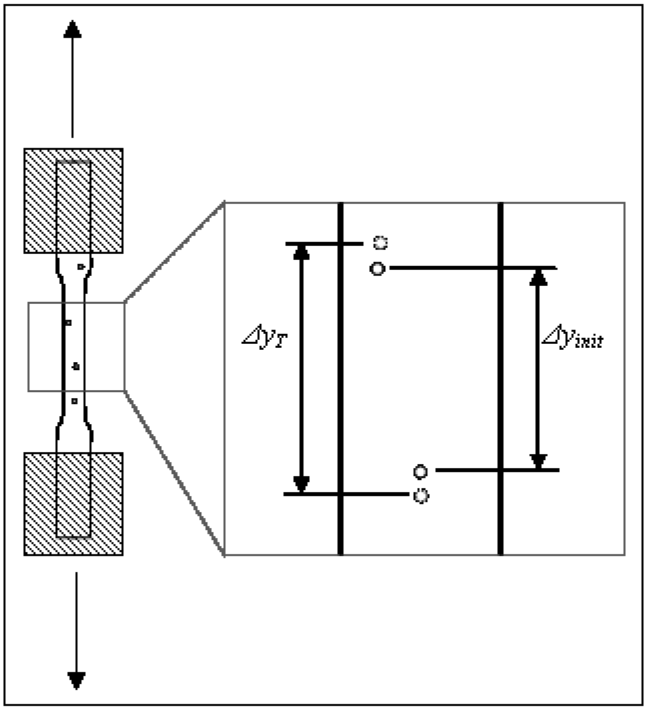

Figure 2-1. Optical strain determination. Distances along the Y-axis are compared between consecutive time steps, allowing strain determination without the implementation of strain gauges. [Salick, 2010]

METHODS AND MATERIALS

Mechanical Testing

Samples are first tested using a tensile testing machine as previously described [Hazeltine et al, 2012]. For our example, prepolymers of various bisacrylamide concentrations were prepared and 400 µL of prepolymer was pipetted to fill a dogbone-shaped Teflon mold. Glass beads with diameters of 30–50 µm (Polysciences, Inc.) were sprinkled over the prepolymer to allow for optical strain measurement during the test, and the prepolymer was covered with a polyethylene terephthalate transparency film. After 75 minutes of polymerization, the mold was disassembled, and samples were stored in HEPES buffer for 1–3 days before mechanical testing to allow the gels to reach hydrostatic equilibrium.

Prior to testing, additional glass beads with diameters of 30–50 μm were adhered to the surface of the samples. The samples were tested in an Instron 5548 MicroTester mechanical testing machine. The samples were secured using self-aligning grips with an abrasive surface at either end to prevent slipping of the sample during testing. The displacement rate of the test was 1 mm/min, which correlated to a strain rate of approximately 0.0025 sec^{-1}. This rate was fast enough that evaporation of the surrounding PBS was negligible but slow enough to reduce inertial and viscous effects. A 10 N load cell was used to measure load data at a rate of 1 Hz. The entire system was placed on a pneumatic air table to eliminate noise caused by environmental vibrations.

Temperature of the samples during testing was maintained at 37°C via a water-jacketed environmental chamber. The samples were also fully hydrated prior to testing and submerged in PBS during the test to simulate the salinity that the gels experienced during cell culture. During testing, the displacement of the grip apparatus displaces some of the PBS in the chamber, producing a change in buoyant loading which would skew test results if not taken into consideration. Thus, a buoyancy test was conducted, which was a complete duplication of the test but with no sample present. This provided a curve representing only the buoyant forces applied by the fluid on the apparatus, which was then subtracted from the original data.

Time-lapse microscopy was used to observe the locations of the beads at designated increments during the tensile test. During testing, the neck region of the sample was imaged as quickly as possible using QCapture Pro and a Q-Imaging MicroPublisher 5.0 RTV Camera.

Strain Determination

In the software, The user is first prompted to select a TIF stack or group of TIF images that contain the time-lapse footage of the beads during testing. The TIF images are then counted and converted to 8-bit arrays. The first round of particle detection is then conducted using algorithms designed by Prof. John C. Crocker of the University of Pennsylvania (available at physics.georgetown.edu/matlab/code.html) . Briefly, this set of algorithms identifies particles in the individual images based on relative pixel intensities. This data is quantified (Figure 2-2), and the XY locations of these particles are compared between neighboring timesteps. The root mean square of distances between particles across the two images are minimized. Once this step is completed, the XY positions of individual particles are known across all time steps.

Figure 2-2. Quantification of particle locations, conducted using track.m software developed by John C. Cocker of University of Pennsylvania. Raw images (A) are first filtered to improve the accuracy of particle detection (B). Once particle locations are quantified, they are plotted during analysis (C) to allow the user to observe the accuracy of the particle tracking software. Scale bar = 2 mm.

Next, the distance between each possible pair of beads is computed to acquire a population of strain values at each time step. Filters are then applied to improve the accuracy of the analysis. Specifically, particles are first only included if they are traveling in the upward direction during testing. This is because during standard tensile testing, the particles should all be moving in roughly the same direction. If the software indicates downward motion of particles, it is because a) the software is tracking debris within the submersion solution b) a bead has fallen off of the sample and is not representative of material motion or c) the software falsely selected a neighboring (lower) bead during the initial particle-tracking step.

The second filter that is applied ensures that only particles that are detected for long periods of time are included in the analysis. If a particle is only detected for a few frames, it is very likely that it is a floating piece of debris, it is near the edge of the capture window, or it is not properly illuminated. Removing these data points, referred to in the code as small particle chains, reduces the error in the ultimate computed strains.

With distances between particles determined and filtered accordingly, strain may now be calculated for each time step. This is done by taking a weighted average of strains of each particle pair across consecutive time steps. Particles that are farther apart from each other in the Y direction are weighted more heavily than those that are very close in the Y direction. This is because individual strain measurements across longer distances are more accurate than those taken across short distances. This is further amplified by image resolution restrictions, which considerably inhibit the accuracy achieved by two particles that are very close to each other.

The image frames are then matched to their closest time point from the mechanical test data, allowing the determined strains to be matched with their equivalent load values. The user is then prompted to include sample cross-section area, and the data is truncated in the event of any sample slipping that may have occurred. The user is prompted to select a region of interest along the stress vs. strain curve, and the slope, which is typically the Young’s Modulus of the linear elastic region, is output (Figure 2-3).

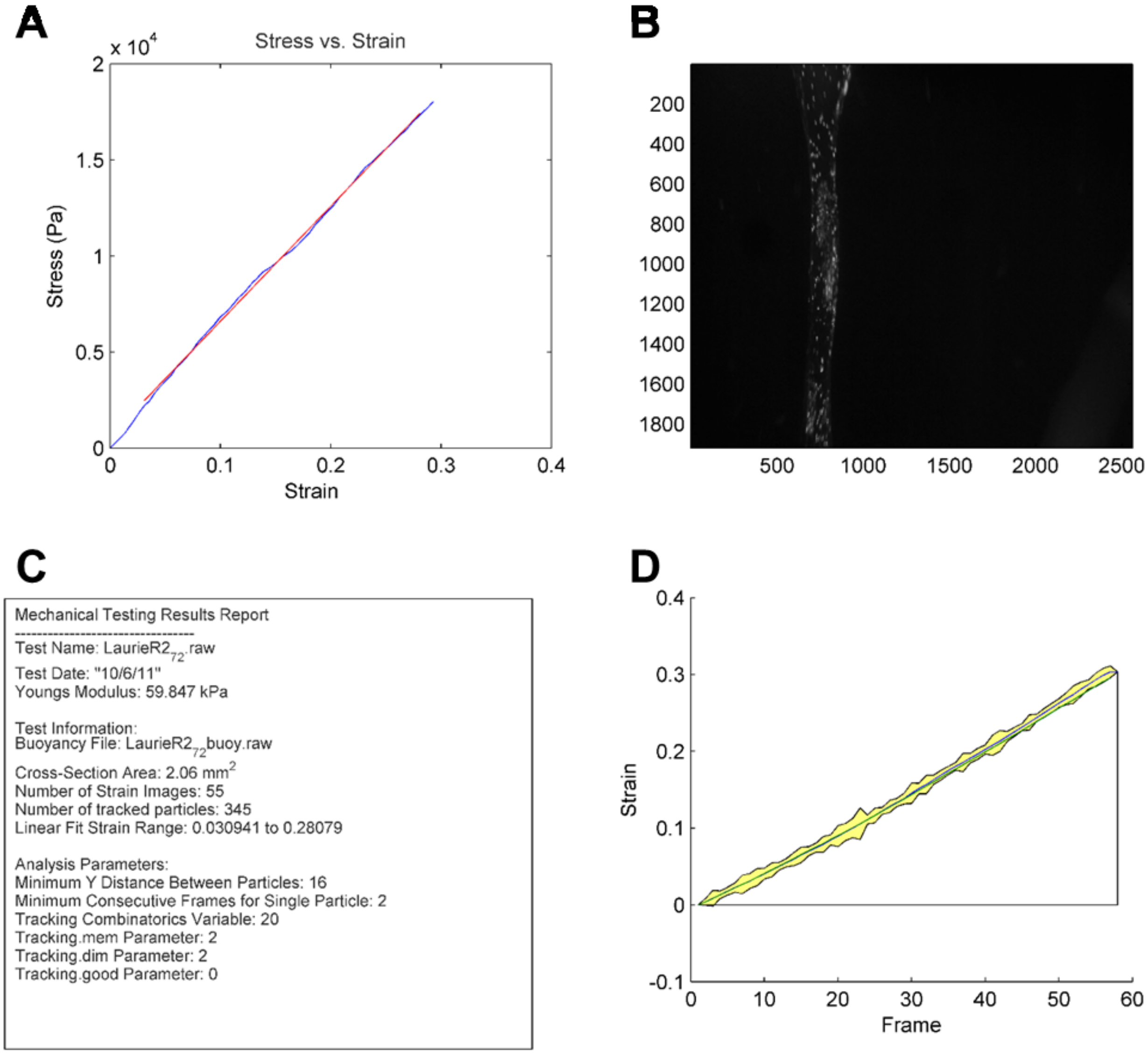

Mechanical Testing Results Report

Test Name: LaurieR2$_{72}$.raw
Test Date: "10/6/11"
Youngs Modulus: 59.847 kPa

Test Information:
Buoyancy File: LaurieR2$_{72}$buoy.raw
Cross-Section Area: 2.06 mm^2
Number of Strain Images: 55
Number of tracked particles: 345
Linear Fit Strain Range: 0.030941 to 0.28079

Analysis Parameters:
Minimum Y Distance Between Particles: 16
Minimum Consecutive Frames for Single Particle: 2
Tracking Combinatorics Variable: 20
Tracking.mem Parameter: 2
Tracking.dim Parameter: 2
Tracking.good Parameter: 0

Figure 2-3. An example of the report produced by multiparticle_tracker.m. A stress vs. strain plot is given (A), along with a single frame of the image stack (B). The report (C) includes Young's Modulus, as well as the parameters used for analysis and number of particles detected. The strain vs. frame plot (D) shows the optically determine strain (green line), along with the confidence (yellow area) which is determined by the standard deviation of strains calculated by the individual particle pairs for each time step.

SUMMARY

Optical methods of determining strain are typically used for samples in which standard strain gauges cannot be used. This is usually necessary for soft and biological samples. The developed Matlab software allows users to quickly input collections of images taken during mechanical testing, and through a series of particle-tracking, filtering, and statistical computations, the strain of the sample is determined. Using this strain information, mechanical properties of the material may be determined with considerable reduction in error.

AUTOMATED CALCIUM TRANSIENT ASSESSMENT

BACKGROUND

Calcium ions are utilized routinely within cells to facilitate biological functions in a tremendously wide range of cell types [Berridge et al, 2000; Grienberger and Konnerth, 2012]. Within cardiomyocyte alone, Ca^{2+} signaling is responsible for facilitating transcription, cell survival, and energy metabolism, in addition to controlling the contractile cycle [Pleger et al, 2014; Bers, 2008]. The network of transporters, pumps, channels, sensors, and other proteins involved in Ca^{2+} signaling is vast and complex [Berridge et al, 2000], and dependent on cell type and maturity. In cardiomyocytes, two membrane potential-dependent calcium currents, L-type ($I_{Ca,L}$) and T-type ($I_{Ca,T}$) exist, depending on cell maturation and phenotype. $I_{Ca,T}$, which is present in pacemaking and conducting regions of the adult heart [Bers et al, 2008; Chen et al, 2007], has also been observed in embryonic and immature cardiomyocytes. Additionally, it has been observed that the sarcoplasmic reticulum, which plays a key role in storing and controlling the release of Ca^{2+} ions into the cytoplasm, is poorly formed in immature cardiomyocytes [Liu et al, 2007; Sartiani et al, 2007], affecting the waveform of intracellular Ca^{2+}. Specifically, the rate of rise and decay are both much lower in prenatal cardiomyocytes [Seki et al, 2003]. Thus, measurement of Ca^{2+} waveforms within the cytoplasm provides a useful method of assessing cardiomyocyte maturation and phenotype.

One method of assessing the state of the calcium-handling mechanisms of a cell is by directly observing Ca^{2+} using indicator dyes that are based off of Ca^{2+} chelators ethylene glycol tetraacetic acid (EGTA), aminophenol triacetic acid (APTRA), and 1,2-bis(o-aminophenoxy)ethane-N,N,N',N'-tetraacetic acid (BAPTA) [Tsien, 1980]. These indicator dyes indicate changes in Ca^{2+} concentration through wavelength shifts in their emission/excitation spectrum, or by increases in fluorescence intensity. For this set of experiments, Rhod-2 AM Ester (Life Technologies) was utilized.

MATERIALS AND METHODS

Cell Culture

Human embryonic stem cell-derived cardiomyocytes (hereafter described as hESC-CMs) were cultured using methods previously described [Salick et al, 2014]. Briefly, hESCs were maintained in E8 media on vitronectin, and were passaged every 3-4 days as needed. Cells were differentiated using the Wnt-agonist method [Lian et al, 2012], and purified for cTnT+ cardiomyocytes using the Zeocin-resistant properties of the cTnT-GFP promoter line [Salick et al, 2014]. Purified cardiomyocytes were maintained in RPMI (Life Technologies) supplemented with B27 supplement (Life Technologies), which was replaced every three days. Cells were maintained in these conductions and were tested for calcium handling at day 12 (immediately after purification), 27, and 42.

Calcium Detection

Calcium handling assessment was conducted using Rhod-2 AM Ester (Life Technologies) and the fluorescent intensity analysis software described in the following sections. 50 µg of Rhod-2 were diluted into 44.5 µL DMSO to produce a 100X indicator dye solution. The dye was then diluted in RPMI/B27 media at 1:100 and added to the cells at a volume necessary to thoroughly coat the hESC-CMs. Cells were then incubated for 15 minutes, washed twice with 37°C PBS, and fed with normal RPMI/B27. The cells were then allowed to incubate for 30 minutes at 37°C before imaging. During imaging, the cells were maintained in a microscope stage incubator, since variations in temperature have strong effects on the contractility of cardiomyocytes. Images were taken every 90ms using a Photometrics CoolSnap HQ2 camera on a Nikon Ti-E epifluorescent microscope using NIS-D Elements software (Figure 2-4); this is enough to provide approximate assessment of Ca^{2+} waveform. However, it should be noted that confocal line-scanning is recommended for future studies to improve the temporal resolution of the detected waveforms.

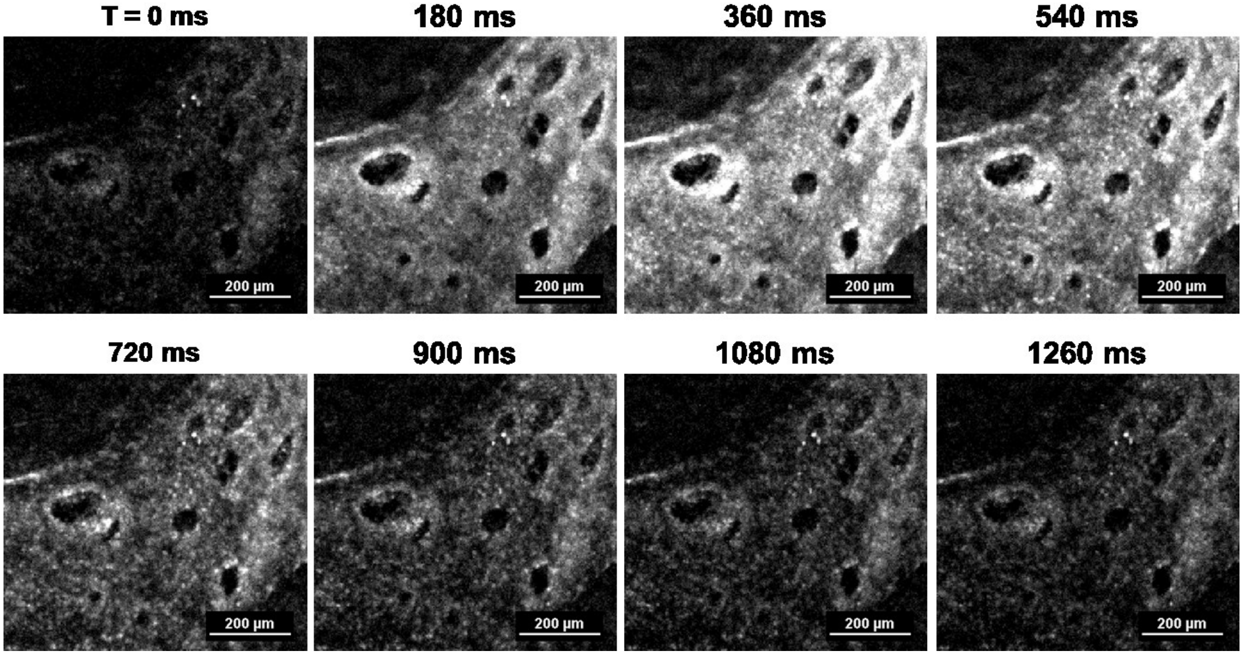

Figure 2-4. Rhod-2 fluorescence during a single contraction of a sheet of hESC-CMs. Through direct observation, it is clear that the rate of increasing Ca^{2+} is faster than the decay rate. The exact values of these rates requires quantification such as that described in the following sections, however. At low magnification (2X), this dye is capable of showing the user how quickly calcium propagates through large hESC-CM populations.

Calcium Analysis of Heterogeneous hESC-CM Structures

Along with the assessment of Ca^{2+} waveforms across multiple hESC-CM ages, an additional study was conducted to determine if differences in waveforms occurred based on the geometry of the CM structures. Beginning approximately 6 days after differentiation is first initiated, the hESC-CMs typically form heterogeneous structures consisting of monolayers, fibers, and holes. During prolonged cultures, these structures persist and are often modified by the mechanical forces of the contracting hESC-CMs. For this second study, hESC-CMs were imaged after 10 days (before purification), using the Rhod-2 protocol described above. Regions of interest (ROIs) were taken at various points within these structures, and their waveforms were analyzed (Figure 2-5).

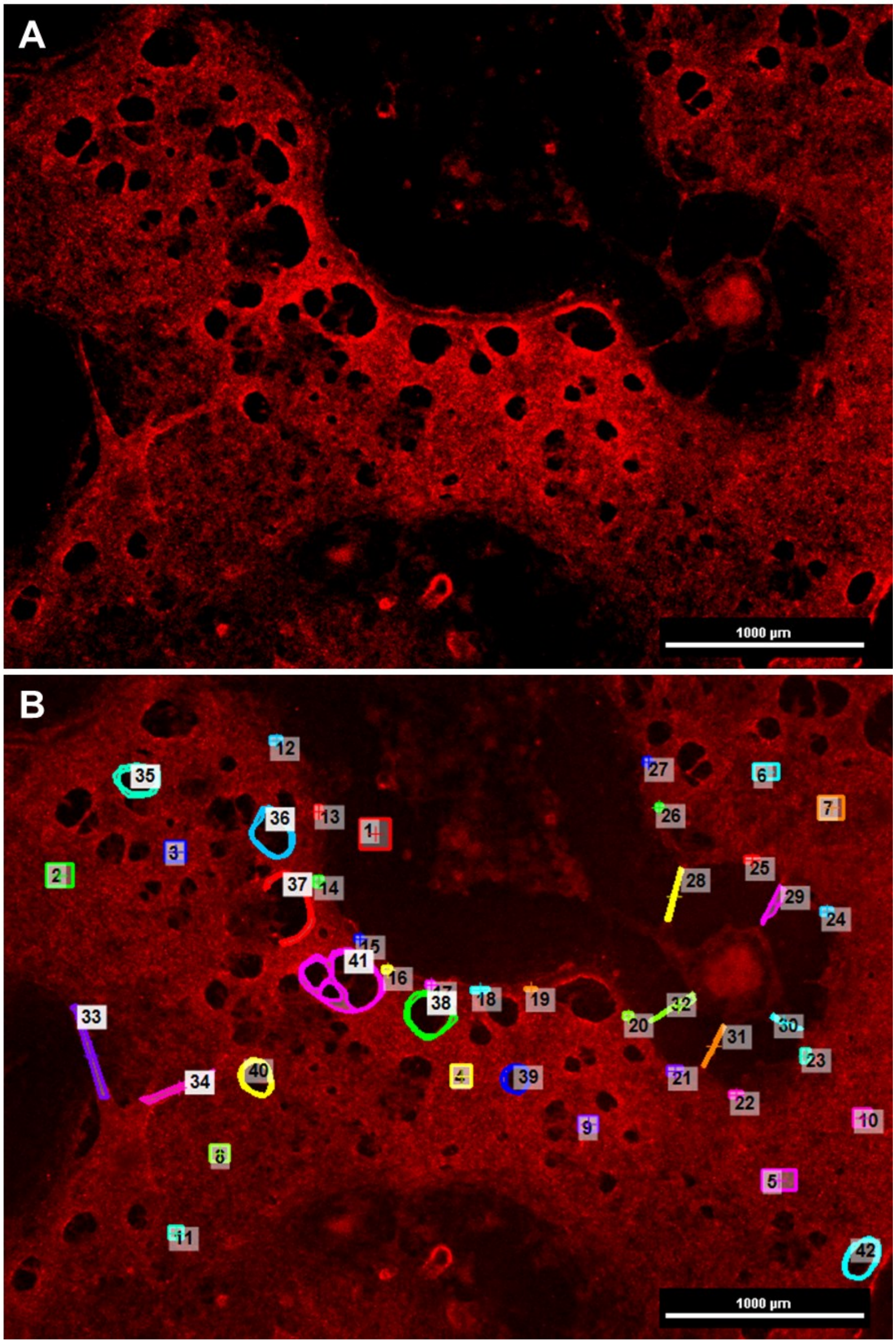

Figure 2-5. Region of interest (ROI) selection for heterogeneous hESC-CM structures. After ~6 days of differentiation, the immature hESC-CMs often form a variety of tissue structures such as monolayers, fibers, and holes (A). These regions were specifically selected (B) and analyzed using the curve analysis software. Resulting time-to-peak and decay half-life values were grouped based on region type.

Automated Curve Analysis

Matlab software was developed to allow automated, unbiased assessment of the intracellular Ca^{2+} readings provided by the Rhod-2 stains. First, curves of Rhod-2 fluorescence were determined at multiple ROIs for each region assessed (Figure 2-6). An additional ROI is assigned, indicating a region at which there are no cells present, to provide the software with a background fluorescence intensity curve that is subtracted from the positive-signal curves. These curves were then smoothed using spline methods and normalized. The peak (overall maximum) of each curve was detected for a single contraction. The timing of initial calcium uptake was then detected using a variety of criteria based off of the original curve and the derivative of this curve. Specifically, the software seeks a point at which the calcium concentration is decreasing steadily over multiple frames, in which the fluorescence is also less than 40% of the maximum previously determined. The duration between these this point and the curve maximum is determined as the ***uptake time***, or ***time-to-peak,*** for the curve.

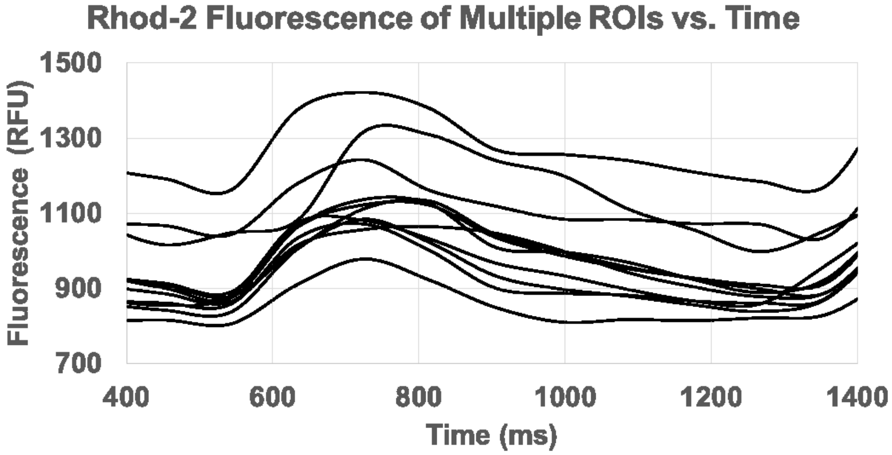

Figure 2-6. Example dataset of raw fluorescence data from 10 ROIs examined within a single frame during calcium transient analysis. The timespan is truncated to include a single contraction.

The decay half-life is determined next. The points at which the curve reaches 80% and 20% of the maximum following the peak are determined. The log of the curve between these two points is matched to a polynomial using Matlab's `polyfit` function (Eq. 2-1), where t and F(t) are the time and fluorescent values, respectively, between 80% and 20% of the decay curve. The ***decay half-life*** of this curve is then determined by dividing –ln(2) by the slope of the polyfit line (Eq. 2-2).

Eq. 2-1 $$[\,p(0), p(1)\,] = polyfit\,\big(t\,, \log\big(F(t)\big), 1\big)$$

Eq. 2-2 $$t_{1/2} = \frac{-\ln(2)}{p(1)}$$

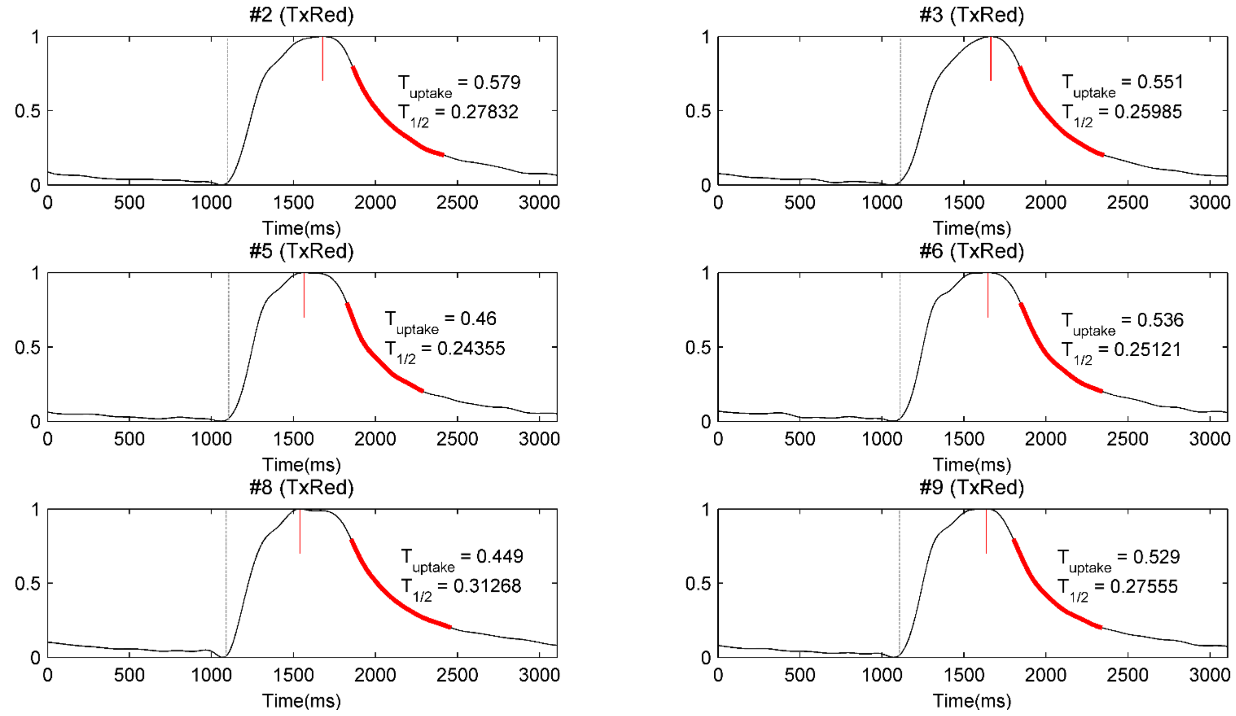

Figure 2-7. Example of report files generated after automatic calcium transient analysis. The batch function of the code allows for analysis of virtually unlimited numbers of curves to be analyzed, which helps with statistical analysis of large numbers of ROIs.

RESULTS

Intracellular Ca^{2+} was determined using Rhod-2 calcium indicator dyes, and analysis software was developed to automatically quantify the curves caused by increased intracellular Ca^{2+} during hESC-CM contraction. The first study investigated the Ca^{2+} transients of hESC-CMs after 12, 27, and 42 days in culture. A clear trend was observed in the time-to-peak values output by the software (Figure 2-8), with a considerable decrease in time-to-peak in the 42 day cultures. The decay half-life, however, showed less variability with age, but showed no overall rate change between day 12 and day 42. It should be noted that the contractile rate, which is closely linked to calcium kinetics, was also variable between samples. Specifically, time between contractions was 827±32 ms, 1123±161 ms, and 685±73 ms for day 12, day 27, and day 42 cardiomyocytes, respectively.

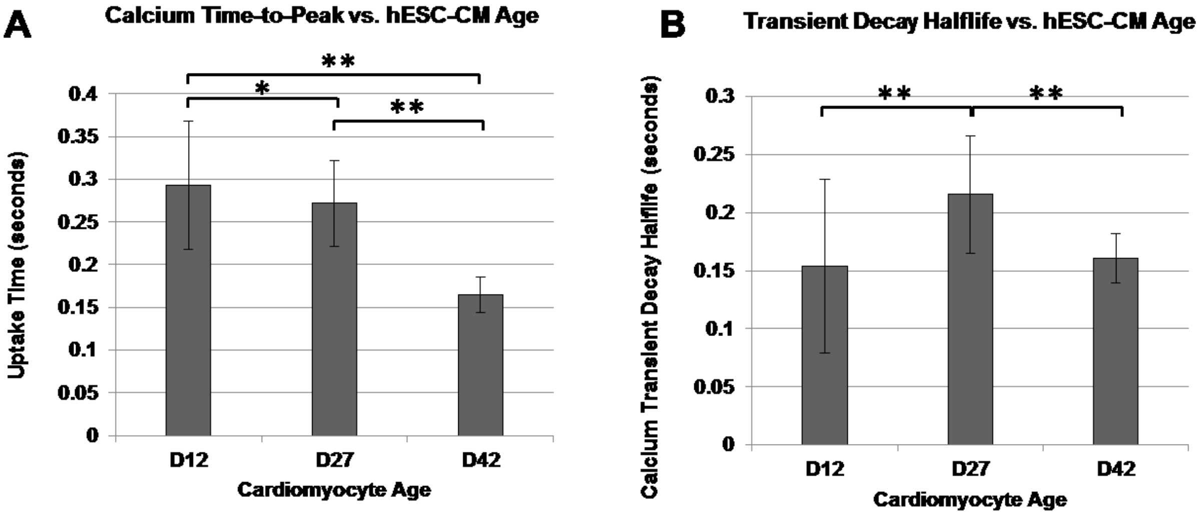

Figure 2-8. Results of curve quantification for hESC-CM age study (n > 65 for all cases). A significant reduction in calcium time-to-peak was observed over 30 days of culture (A). The decay half-life became more consistent, though the hESC-CMs exhibited no change in average half-life (B). (* significant at $p<0.05$; ** significant at $p<0.001$ under t-test)

The second study investigated regional calcium transients in heterogeneous structures produced by hESC-CMs (Figure 2-5). The ROIs were grouped into four categories: monolayer center, monolayer edges, fibers, and edges of holes. Calcium transient analysis was conducted as previously described. The results indicate that there is no significant difference in calcium handling between hESC-CMs in these regions (Figure 2-9).

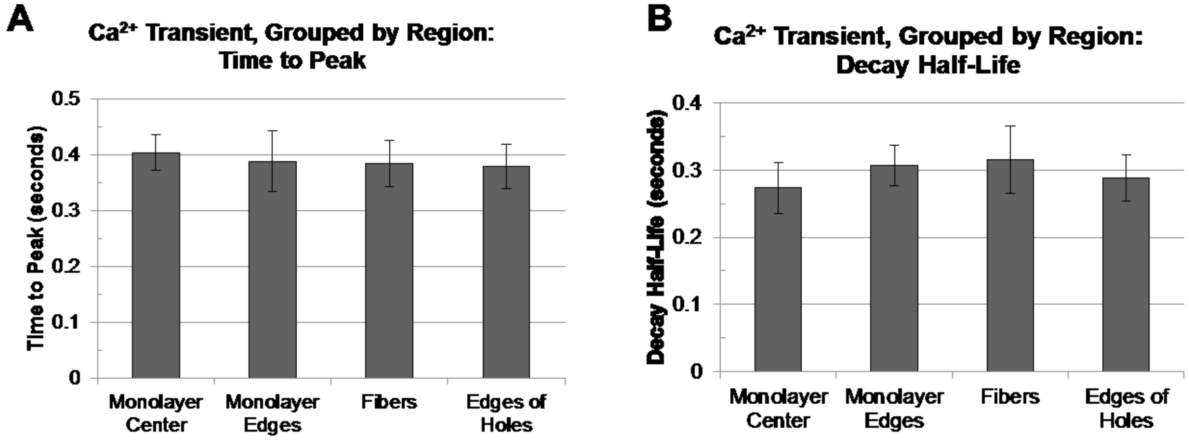

Figure 2-9. Time-to-peak and decay half-life for day 10 hESC-CMs in different regions of heterogeneous cultures. There was no significant difference in calcium transient rates between these groups. It should be noted that the time-to-peak is slightly higher than the values reported in the hESC-CM age study. This matches the observed trend of immature hESC-CMs showing slower calcium transient waveforms. Similarly, the decay half-life was larger than the values previously shown for older hESC-CMs, though this may be due to the large variability in decay half-life reported for the earlier cultures of hESC-CMs.

SUMMARY

hESC-CMs were cultured for various durations and their intracellular Ca^{2+} was assessed using a Rhod-2 indicator dye. Automated analysis software was developed in Matlab, allowing for rapid computation of time-to-peak and best-fit decay half-life values. These values were determined for hESC-CMs cultured to day 12, day 27, and day 42, with a notable decrease in time-to-peak across these sample sets. This supports claims that further development of calcium handling mechanisms such as the endoplasmic reticulum occurs well after contractile function begins. Interestingly, decay half-life did not show such a trend, suggesting a decoupling between development of the various Ca^{2+} uptake and release mechanisms within the hESC-CM. An additional study was conducted to gauge the calcium transients of hESC-CMs in various regions within large populations. ROIs were taken for cells in monolayers, along monolayer edges, within fibers, and outlining holes in the cellular constructs. No significant difference in time-to-peak or decay half-life was observed in any of these regions. Although the mechanical loading experienced by cells at different regions can be widely different, this data suggests that this is not enough to induce a response in the cells' calcium handling mechanisms.

MICROPATTERNING ROBOT ALIGNMENT CALCULATOR

This software and technique has been published in:

McNulty JD, Klann T, Sha J, Salick MR, Knight GT, Turng LS, Ashton RS (2014). High-precision robotic microcontact printing (R-µCP) utilizing a vision guided selectively compliant articulated robotic arm, Lab on a Chip, 14, 1923-1930.

BACKGROUND

In biology, the locations and morphologies of cells play a key role in the way they interact. To examine these interactions, researchers have often utilized microcontact printing to print proteins [Kane et al, 1999; Mrkich et al, 1997; Ashton et al, 2007] in controlled geometries. Seeding cells onto proteins in these distinct geometries enables a wide range of microfluidics and high-throughput microarray studies to be conducted.

In collaboration with the Ashton Lab of the University of Wisconsin – Madison, a microcontact printing robot has been constructed that is capable of printing multiple overlapping patterns of different geometries and components through extremely precise controlled actuation [McNulty et al, 2014]. This robot is capable of printing designs within microns of their target to match geometries at the cellular scale. There is, however, slight error within the multiple actuating arms that form the robot; thus, image analysis software was developed to calculate the exact translational and rotational errors that the robot was experiencing, which can then be corrected.

MATERIALS AND METHODS

As this chapter is focused primarily on the alignment-correction software, the details regarding microcontact printing and sample preparation will not be discussed. For further information concerning these steps, readers are directed to [McNulty et al, 2014].

Printing of Alignment Patterns

Alignment patterns consisting of gridded circles were constructed from PDMS and used to calibrate the alignment of the microprinting robot. These three patterns (Figure 2-10) were consecutively used to pattern a single sample, such that patterns A and C were placed concentrically, and pattern B was placed at a 600 µm offset in the X and Y directions (Figure 2-11). The micropatterns were functionalized with fluorescent molecules [Sha et al, 2013] and imaged using a Nikon A1R confocal microscope.

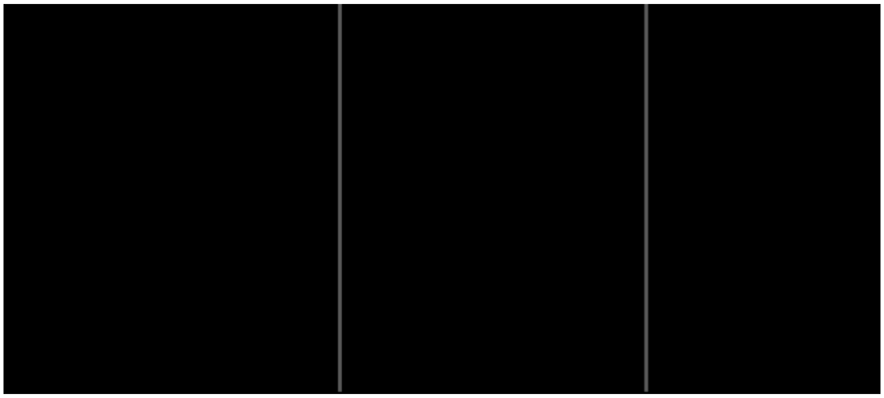

Figure 2-10. Microstamp patterns used to determine alignment of the robot during consecutive stamps. The patterns consist of annuli (A, B) and circles (C) spaced 1200 µm apart to form square grids. Image adapted from [McNulty et al, 2014].

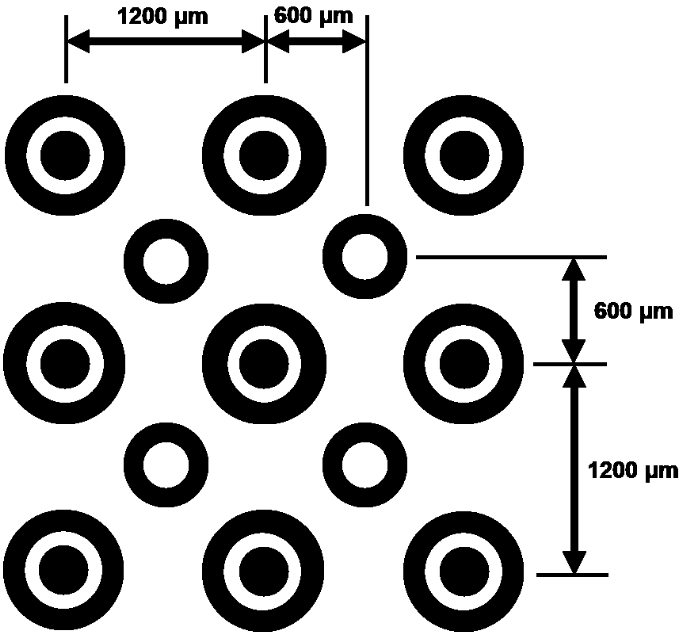

Figure 2-11. Overlapping microcontact printed patterns. The 3 stamps are consecutively printed using the high-precision robot. It is designed such that stamps A and C are concentric, with stamp B offset by 600 µm in the X and Y directions. Variations off of this target alignment are detected by the software, allowing determination of the robot's overall translational and rotational error. Image adapted from [McNulty et al, 2014].

Alignment Assessment

Fluorescent images of the consecutively-stamped samples are then imported into Matlab and converted into 8-bit arrays. Local contrast filters are then applied to the image to ensure uniformity of the intensity, and improve the software's ability to detect features with lower signal-to-noise ratios. The user is prompted to input the number of "populations," where each population is a specific type of geometry that has been printed. In the case of this example, there are three populations, each representing an annulus or circle by the three respective stamps. Next, using a graphic user interface (Figure 2-12), thresholds are applied across the image, converting the image to a binary layer. The binary layer is then converted to a collection of ROIs, where each set of neighboring pixels is grouped into a single ROI. The user is then prompted to select a few ROIs that represent each population. In this case, the user must indicate a few examples each of the large annulus, small annulus, and circle.

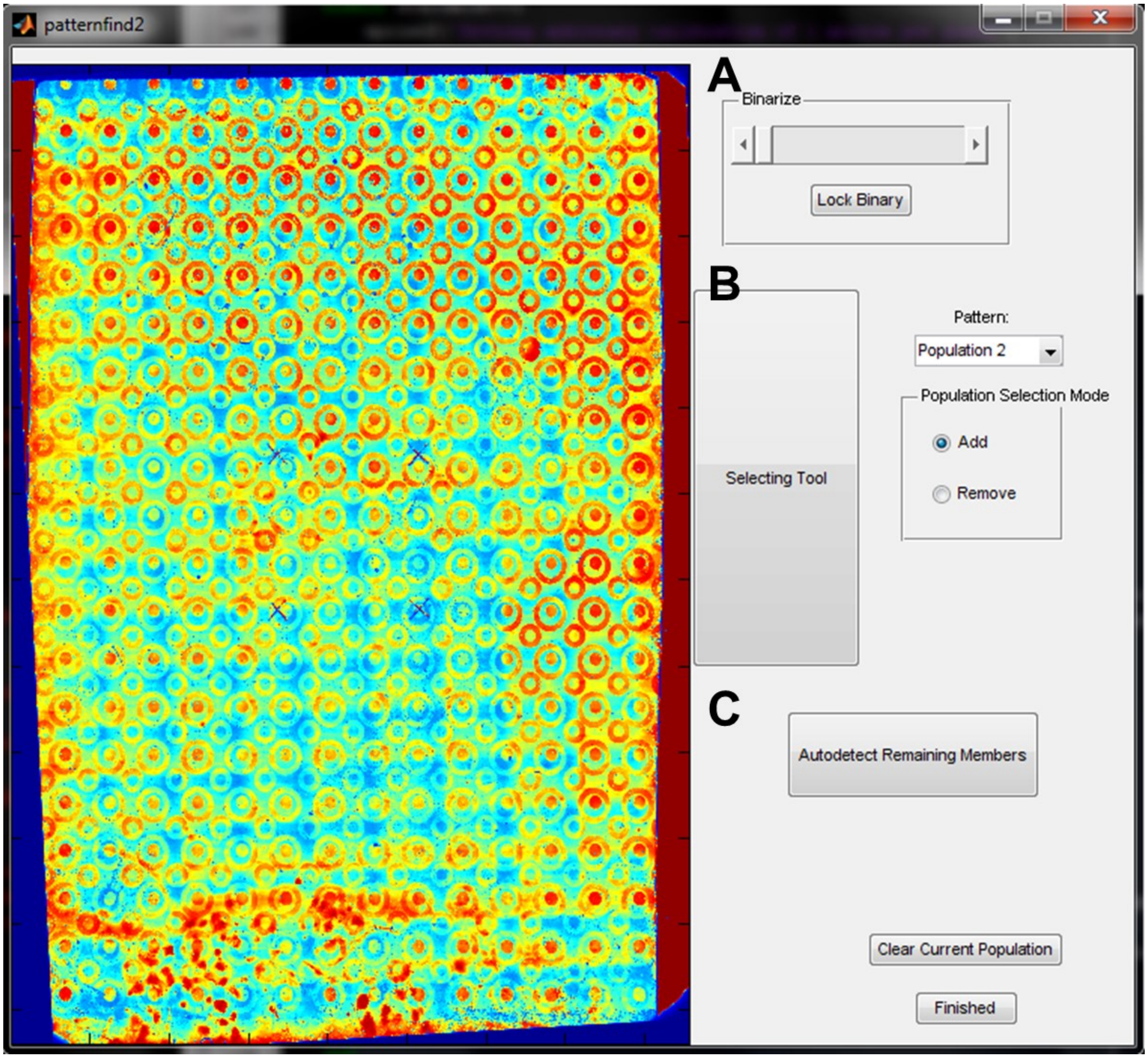

Figure 2-12. Graphic user interface for population defining and detecting. First the image must be binarized and converted to an ROI array (A). Next, the user sets representative members of each population manually (B). Once 3-5 features of each population are selected, the "Autodetect Remaining Members" option (C) automatically finds all other members of the population that match the morphological characteristics of the selected features.

Next, the software automatically detects all other members of each population by comparing each ROI's geometric properties with those of the representative samples. Specifically, the ***area***, ***extent***, and ***filledarea*** for the representative ROIs are determined. All other ROIs within the image that contain values that closely match the representative ROIs are considered to be a match. Once all members of each population are determined, their centroids are then calculated, and thus the coordinates of each stamped feature are found. Since microprinting error can take the form of both translation and rotation, the origin of the sample must be defined. This is indicated automatically by the robot by etching 4 crosses that designate the location of the robot's vertical axis. The software prompts the user to select these 4 crosses that are clearly located within the fluorescent image.

Once the members of each population have been located, in addition to the origin of the coordinate system, the software is capable of comparing these locations to determine the error in consecutive stamps. To do this, the Horn's quaternion method for absolute orientation is applied [Horn, 1987]. This algorithm is designed to detect the translation and rotation that must be applied to multiple populations to maximize the amount of overlap that occurs between nearest-neighbor members. This is done by minimizing the root-mean-square distances between these nearest-neighbor features. The suggested translation and rotation values are then included as an offset for the robot for concurrent sample preparations. The errors produced by the robot are considerably reduced once these corrections are applied (Figure 2-13).

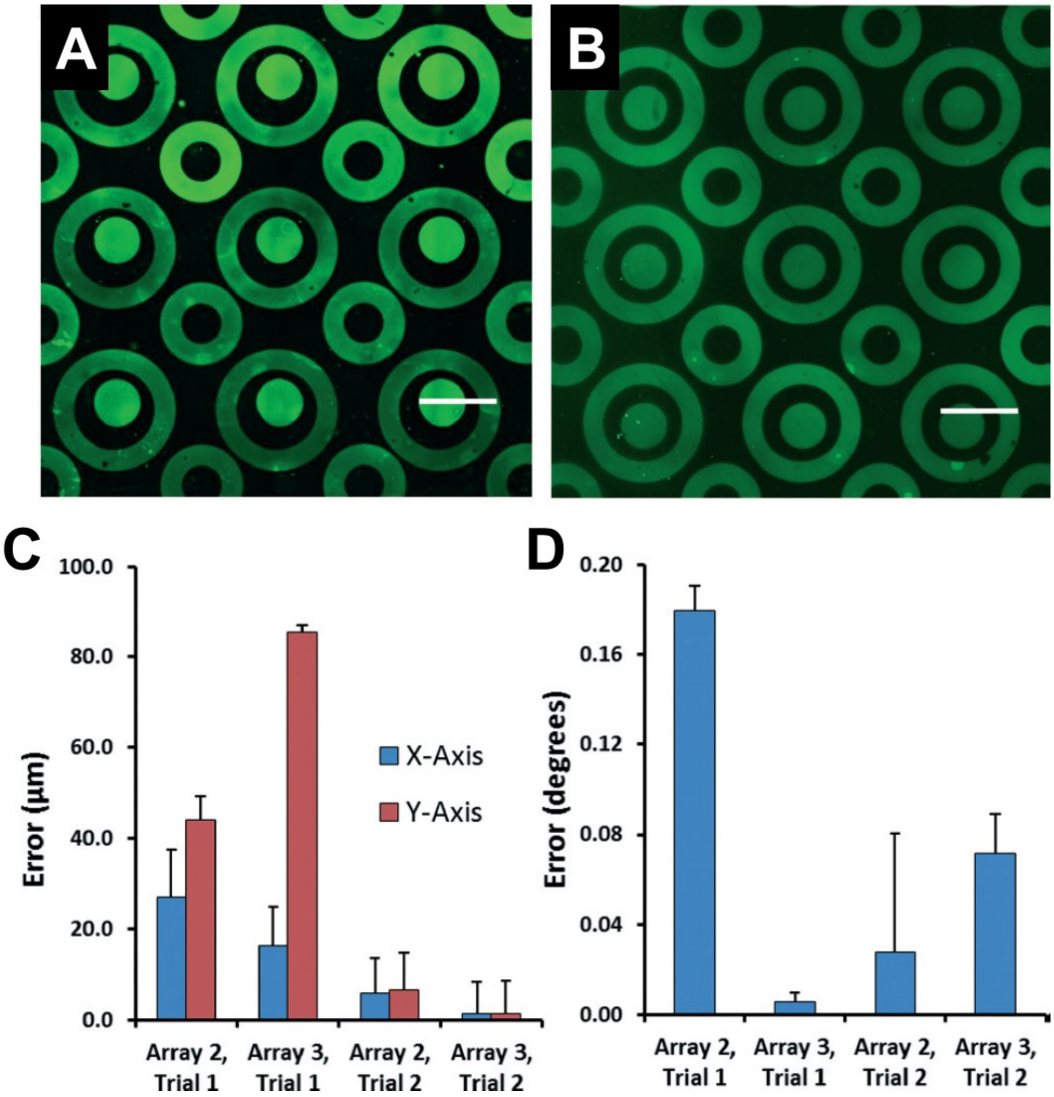

Figure 2-13. Errors of consecutive stamps before and after error correction is applied. Trial 1 labels the original sample set (A), Trial 2 labels samples that had been corrected using the software (B). Translational error was reduced significantly (C), while extremely limited rotational error was detected (less than 0.2 degrees) across all trials (D). Scale bar = 500 µm. Image from [McNulty et al, 2014].

SUMMARY

The capability of micropatterning multiple features of different morphologies and compositions onto the same surface could enable research into complex biological systems. In its original state, the micropatterning robot was incapable of printing consecutively without producing large amounts of error that would make most cell-scale studies impossible. Once the error is determined and corrected using this software, however, the micropatterning robot is capable of printing at resolutions of less than 10 microns.

REFERENCES

Ashton, R. S., Peltier, J., Fasano, C. a, O'Neill, A., Leonard, J., Temple, S., Schaffer, D. V and Kane, R. S. (2007). High-throughput screening of gene function in stem cells using clonal microarrays. *Stem Cells* **25**, 2928–35.

Bers, D. M. (2008). Calcium cycling and signaling in cardiac myocytes. *Annu. Rev. Physiol.* **70**, 23–49.

Discher, D. E., Janmey, P. and Wang, Y.-L. (2005). Tissue cells feel and respond to the stiffness of their substrate. *Science* **310**, 1139–1143.

Engler, A. J., Sen, S., Sweeney, H. L. and Discher, D. E. (2006). Matrix Elasticity Directs Stem Cell Lineage Specification. *Cell* **126**, 677–689.

Grienberger, C. and Konnerth, A. (2012). Imaging calcium in neurons. *Neuron* **73**, 862–85.

Hazeltine, L. B., Simmons, C. S., Salick, M. R., Lian, X., Badur, M. G., Han, W., Delgado, S. M., Wakatsuki, T., Crone, W. C., Pruitt, B. L., et al. (2012). Effects of substrate mechanics on contractility of cardiomyocytes generated from human pluripotent stem cells. *Int. J. Cell Biol.*

Horn, B. K. P. (1987). Closed-form solution of absolute orientation using unit quaternions. *J. Opt. Soc. Am. A* **4**, 629.

Johnson, B., Bauer, J. M., Niedermaier, D. J., Crone, W. C. and Beebe, D. J. (2004). Experimental Techniques for Mechanical Characterization of Hydrogels at the Microscale. *Exp. Mech.* **44**, 21–28.

Kane, R. S., Takayama, S., Ostuni, E., Ingber, D. E. and Whitesides, G. M. (1999). Patterning proteins and cells using soft lithography. *Biomaterials* **20**, 2363–76.

Liu, J., Fu, J. D., Siu, C. W. and Li, R. a (2007). Functional sarcoplasmic reticulum for calcium handling of human embryonic stem cell-derived cardiomyocytes: insights for driven maturation. *Stem Cells* **25**, 3038–44.

Lundy, S., Zhu, W., Regnier, M. and Laflamme, M. A. (2013). Structural and functional maturation of cardiomyocytes derived from human pluripotent stem cells. *Stem Cells Dev.* **22**, 1991–2002.

McNulty, J. D., Klann, T., Sha, J., Salick, M., Knight, G. T., Turng, L.-S. and Ashton, R. S. (2014). High-precision robotic microcontact printing (R-μCP) utilizing a vision guided selectively compliant articulated robotic arm. *Lab Chip* **14**, 1923–30.

Pelham, R. J. and Wang, Y. l (1997). Cell locomotion and focal adhesions are regulated by substrate flexibility. *Proc. Natl. Acad. Sci. U. S. A.* **94**, 13661–13665.

Pleger, S. T., Raake, P., Katus, H. a and Most, P. (2014). Cardiac calcium handling on trial: targeting the failing cardiomyocyte signalosome. *Circ. Res.* **114**, 12–4.

Salick, M. R., Napiwocki, B. N., Sha, J., Knight, G. T., Chindhy, S. a, Kamp, T. J., Ashton, R. S. and Crone, W. C. (2014). Micropattern width dependent sarcomere development in human ESC-derived cardiomyocytes. *Biomaterials* **35**, 4454–64.

Salick, M. R. (2010). Stiffness of three-dimensional poly(ethylene glycol) environment impacts differentiation of encapsulated embryoid bodies.

Sartiani, L., Bettiol, E., Stillitano, F., Mugelli, A., Cerbai, E. and Jaconi, M. E. (2007). Developmental changes in cardiomyocytes differentiated from human embryonic stem cells: a molecular and electrophysiological approach. *Stem Cells* **25**, 1136–44.

Seki, S., Nagashima, M., Yamada, Y. and Tsutsuura, M. (2003). F etal and postnatal development of Ca 2 1 transients and Ca 2 1 sparks in rat cardiomyocytes. **58**, 535–548.

Sha, J., Lippmann, E. and McNulty, J. (2013). Sequential Nucleophilic Substitutions Permit Orthogonal Click Functionalization of Multicomponent PEG Brushes. … **14**, 3294–3303.

Tsien, R. Y. (1980). New calcium indicators and buffers with high selectivity against magnesium and protons: design, synthesis, and properties of prototype structures. *Biochemistry* **19**, 2396–2404.

CHAPTER 3: IMPACT OF MICROPATTERN GEOMETRY ON MYOFILAMENT STRUCTURE

A substantial portion of this work has been published as:

Salick MR, Napiwocki BN, Sha J, Knight GT, Chindhy SA, Kamp TJ, Ashton RS, Crone WC (2014). Micropattern width dependent sarcomere development in human ESC-derived cardiomyocytes, Biomaterials, 35(15): 4454-64.

INTRODUCTION

In this study, we closely examined how a multi-cell micropattern shape may play a role in controlling sarcomere morphology in pure populations of human cardiomyocytes derived from embryonic stem cells. We hypothesized that the widths and aspect ratios of rectangular micropatterns may lead to changes in costamere development, which in turn could influence cell shape, alignment, polarization, and sarcomere structure. We also examined whether these varied micropattern shapes led to altered gap junction plaque formation and calcium propagation rates within the human cardiomyocyte aggregates.

MATERIALS AND METHODS

HESC CULTURE

The cardiomyocytes used for all studies were derived from an engineered H9 hESC line containing a cardiac troponin T GFP (cTnT-GFP) promoter. The cTnT-GFP promoter line also exhibited resistance to the antibiotic Zeocin in conjunction with cardiac troponin T expression. This allowed for purification of cTnT-expressing cells, leading to a ~98% purity of cardiomyocyte cultures for the described studies (Figure 3-1).

Prior to differentiation, these hESCs were maintained on vitronectin-coated polystyrene plates, and E8 media [Chen et al, 2011] was replaced daily. The E8 media was produced in-house using DMEM/F-12 (Life Technologies), L-ascorbic acid 2-phosphate sesquimagnesium salt hydrate, sodium selenite, sodium bicarbonate, holo-transferrin, insulin, βFGF (WiCell), and TGFβ (Peprotech). Unless otherwise mentioned, these reagents were purchased from Sigma-Aldrich. The cells were passaged at a 1:12 ratio every 4 days using versene (Life Technologies) and were seeded with ROCK Inhibitor (Tocris).

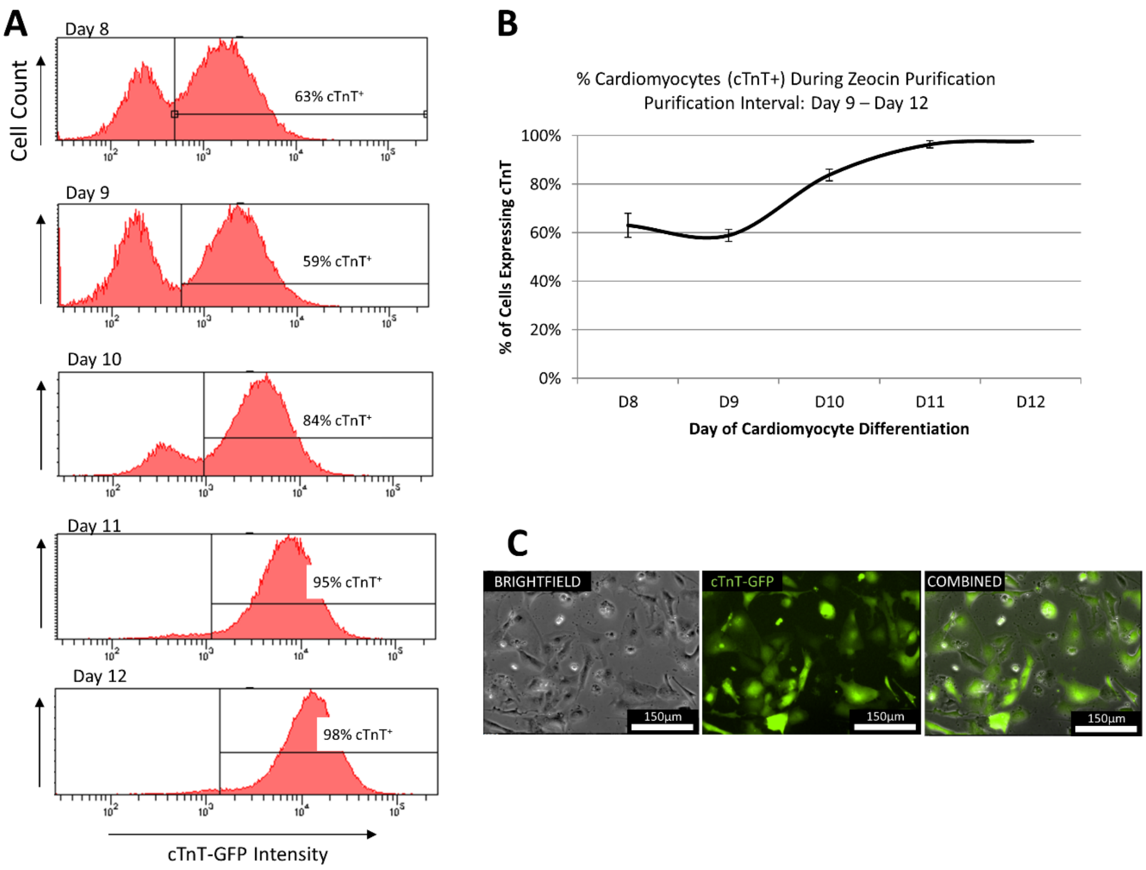

Figure 3-1. Purification of hESC-derived cardiomyocyte population. The zeocin resistance of cTnT-expressing hESC-CMs was used to purify out a population of ~98% cardiomyocytes. Daily flow cytometry (A-B) indicated that this was achieved after three days of zeocin purification (n = 3). Epifluorescent imaging after purification reinforced this by showing that all visible cells were positive for cTnT-GFP protein (C).

HESC CARDIOMYOCYTE DIFFERENTIATION

A modified version of the small molecule Wnt-agonist method of differentiation [Lian et al, 2012] was used to produce a high percentage of cardiomyocytes from the cTnT-promoting H9 hESC line. Briefly, the cTnT-GFP hESCs were seeded on day -3 into matrigel-coated (BD Biosciences) 12-well plates at a density of 400,000 cells per well. The seeding solution was E8 medium supplemented with 5µm ROCK Inhibitor (Tocris). On day -1, cells were fed again with E8 medium. On day 0, exactly 72 hours after the initial seed, cells were treated with RPMI (Life

Technologies) supplemented with B27-insulin (Life Technologies), 10.5 µM of the Wnt agonist CHIR 99021 (Tocris), and 1µg/mL of insulin (Sigma). On day 1, cells were fed with RPMI supplemented with B27-insulin only. On day 3, cells were treated with RPMI supplemented with B27-insulin and 2.5 µM of the Wnt inhibitor IWP4 (StemGent). Cells were then fed on day 5 with RPMI containing B27-insulin and then treated with RPMI containing B27 complete on days 7,8, and 9, and every 3 days thereafter. Once contractions were observed between day 9 and day 12, zeocin treatments were applied in which 100µg/mL per day were added to the RPMI/B27 medium for 3 days to remove non-cTnT expressing cell types. The resulting cells were confirmed by flow cytometry to be ~98% cardiomyocytes.

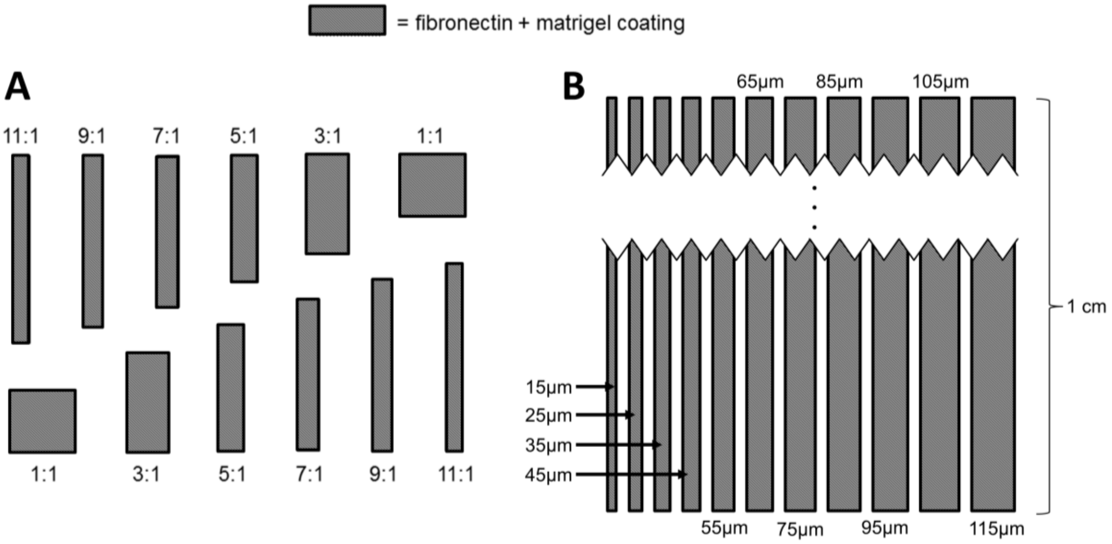

Figure 3-2. Micropattern designs. Extracellular matrix proteins were micropatterned in rectangles of varying sizes and aspect ratios. Two types of patterns were formed. (A) Features were grouped by surface area; while the features shown have varying aspect ratios, they would all have the same surface area within the same grouping. The dimensions of features within each grouping are shown in table 1. (B) Once it was determined that lane width was more important in eliciting a biological response than aspect ratio, long lanes of varying widths were formed. These lanes provided a more efficient use of space and were long enough to enable observation of calcium propagation through the hESC-CM aggregates. Dimensions shown indicate the thickness of each lane. Various spacings between neighboring lanes were attempted.

2D Micropattern Design and Stamp Production

The patterning technique in this study utilized a microcontact printing technique on a gold-coated glass substrate. Several steps were required to create the stamp used for printing. First, a template with the feature designs was created in AutoCAD (Autodesk) and sent to the Stanford Microfluidics Foundry for the fabrication of a photomask and a 4-inch patterned Si wafer (Stanford University, Santa Clara County, CA). Using soft photolithography techniques, the Si wafer was spin-coated with an SU-8 negative photoresist and exposed to UV light which yielded features with a height of 15 µm. The first round of testing incorporated features on the Si master consisting of rectangles with aspect ratios ranging from 1:1 – 11:1. The following aspect ratios were chosen: 1:1, 3:1, 5:1, 7:1, 9:1 and 11:1 with a starting dimension of 100 µm, 200 µm, 300 µm and 400 µm, respectively. For each starting dimension, as the aspect ratio increased the surface area within the feature was held constant. The dimensions used for each feature are listed in Table 1. After the first round of testing determined that lane width, rather than overall aggregate aspect ratio, played the largest role in affecting cell behavior, a new design was created. This additional design type (Figure 3-2) incorporated long lanes with widths ranging from 15 µm to 115 µm. These lanes allowed calcium transient analysis to be conducted due to their long length, in addition to providing more efficient utilization of the seeding surface.

Table 3-1. Dimensions for each feature. All features within each grouping contain varied aspect ratios, but identical surface areas.

Grouping (surface area)	**Feature Dimensions at Various Aspect Ratios (µm)**											
	1:1		**1:3**		**1:5**		**1:7**		**1:9**		**1:11**	
	Width	*Length*	*Width*	*Length*	*Width*	*Length*	*Width*	*Length*	*Width*	*Length*	*Width*	*Length*
A (2500µm^2)	50	50	29	87	22	112	19	132	17	150	15	166
B (10,000µm^2)	100	100	58	173	45	224	38	265	33	300	30	332
C (40,000µm^2)	200	200	115	346	89	447	76	529	67	600	60	663
D (90,000µm^2)	300	300	173	520	134	671	113	794	100	900	90	995
E (160,000µm^2)	400	400	231	693	179	894	151	1058	133	1200	121	1327
	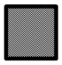		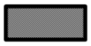									

Elastomeric stamps used for microcontact printing were generated by standard soft lithographic techniques. The silicon master was rendered inert by overnight exposure in vapors of (tridecafluoro-1, 1, 2, 2-tetrahydrooctyl) trichlorosilane. Then, poly (dimethyl siloxane) (PDMS) (Sylgard 184 Kit) was used to create replicas of the silicon master by curing a 10:1 mixture of PDMS and curing agent overnight at 60°C. Fisherbrand microscope cover glass (24×50 #1) slides were cleaned by sequential washes in toluene and methanol followed by sonication for 1 minute in acetone.

μCP OF Ω-MERCAPTOUNDECYL BROMOISOBUTYRATE ON AU-COATED SLIDES

After drying, 35 Å of titanium (Ti) followed by 180 Å of gold (Au) were deposited onto cover glass slides using a CHA-600 Telemark focused electron-beam evaporation system (Wisconsin Center for Applied Microelectronics). Au-coated glass substrates were rinsed with absolute ethanol prior to use. To make micropatterned substrates, PDMS stamps were coated with ω-mercaptoundecyl bromoisobutyrate (2mM in absolute ethanol), dried under nitrogen, and then brought in conformal contact with Ti/Au-coated glass slides. Finally, the chemically modified slides were incubated in absolute ethanol for 2h prior to being dried under nitrogen.

SURFACE-INITIATED ACTIVATOR GENERATED BY ELECTRON TRANSFER ATOM TRANSFER RADICAL POLYMERIZATION (SI-AGET ATRP) OF OEGMEMA

The macromonomer OEGMEMA (8g, 16.7mmol), water (7.5mL), methanol (7.5mL), copper(II) bromide (0.08mmol, 17.9mg) and 2'2-Bipyridine (0.24mmol, 37.5mg) were added to a Schlenk flask, sealed, and stirred for 30 min. Then, the flask was degassed with three freeze-vacuum-thaw cycles, and backfilled with nitrogen. Next, the mixture was transferred by syringe to a reaction flask containing micropatterned glass slides under vacuum. To start the reaction, L-ascorbic acid (0.8mmol, 140.9mg) in deionized water was injected into the flask. The reaction continued for 16h to generate micropatterned thick PEGMEMA brushes. Polymerization was stopped by adding air, and the slides were rinsed with ethanol, water, and ethanol sequentially before drying under nitrogen. Prior to cell culture, the slides were immersed in a large volume of ethanol for 2h to ensure complete removal of copper ions.

ADSORPTION OF ADHESION LIGANDS

Once the slides were prepared, they were coated with a mixture of extracellular components overnight at 37°C, which allowed adsorption of attachment ligands onto the slides' features. This controlled adsorption of adhesion ligands was caused by the PEGMEMA's extremely limited binding affinity for these proteins in comparison to the gold-coated feature regions of the slides. The ECM solution consisted of DMEM (Life Technologies) containing 12μg/mL fibronectin from bovine plasma (Sigma) and 83μg/mL matrigel (WiCell). Through prior experimentation, this combination of extracellular matrix proteins was found to be the most successful in ensuring attachment of pure immature human cardiomyocyte cultures.

HESC-CM SEEDING AND CULTURE

Purified hESC-CMs were seeded onto micropatterns within 1 to 3 days after the purification step had been finished. Since the purification step was dependent on the time at which contractions were first observed, this seeding step typically occurred between days 13 – 16 of overall cardiomyocyte culture. The purified hESC-CMs were first washed 3 times with PBS to remove unnecessary debris that may interfere with binding onto the treated glass slides. The cells were then dissociated from their original culture dish via 15-20 minute exposure to TrypLE (Life Technologies). Every five minutes during the dissociation, the plates were gently agitated in order to help to break up the significant cell-cell binding and ECM deposits that form in these cultures. Cells were then rinsed in 10% serum-containing media and plated onto the treated glass slides in B27-supplemented RPMI medium. The hESC-CMs were seeded at a density of 30,000 cells/cm^2, which allows for confluent cell attachment while avoiding excessive "piling up" of seeded cells. Spent medium was replaced with fresh RPMI+B27 every day thereafter.

IMMUNOFLUORESCENCE AND IMAGING

Samples were stained and imaged after 5 days of culture. Cells were washed once with PBS, followed by a 15-minute exposure to 4% paraformaldehyde (PFA) (Electron Microscopy Sciences) at room temperature. Cells were washed once more, and were then treated for 6 minutes at room temperature with 0.1% Triton (Sigma) to permeabilize the cell membrane. Cells were washed once again with PBS and treated for 60 minutes with a blocking solution consisting of PBS, 2% FBS, 0.1% Triton, 11.2 mg/mL glycine, and 50µg/mL BSA. Cells were then treated with a primary antibody, consisting of mouse anti-α-actinin (1:60 dilution, Abcam) or mouse anti-connexin43 (1:100 dilution, BD Biosciences) overnight. The following day, cells were washed once with PBS for 5 minutes, and treated for 1 hour with blocking solution containing the secondary antibody, Cy5-conjugated goat anti-mouse (1:1000 dilution, Abcam). Cells were washed once more, and phalloidin conjugated to tetramethylrhodamine B isothiocyanate (TRITC) (Sigma) was applied at a 50µg/mL concentration to label actin filaments, and DAPI was applied at a 1:10,000 dilution to label nuclei. Cells were washed with PBS and transferred to coverslips, where they were mounted using ProLong Gold Antifade (Life Technologies).

Samples were imaged on a Nikon A1RSi Confocal Microscope with attached Photometrics CoolSNAP HQ2 camera. Nis-D Elements – Advanced Research v.3.22 software was used for image acquisition and analysis.

MEASUREMENT OF CELL NUCLEI ALIGNMENT

Alignment of cardiomyocytes was assessed via measurement of nuclear alignment, which is commonly used to determine the directionality of populations of cells [Maniotis et al, 1997]. Using the Nis-D Elements – AR software, threshold values were set within the DAPI (nuclear) channel of the confocal images. Size and shape filters were set in the Nikon Nis-D Elements software to remove debris and imaging artifacts from the analysis. Nuclei that were overlapping each other were manually separated, to keep them from being quantified as a single nucleus. The major axis of the nuclei was then determined automatically, and the angle of this axis was used to determine cell alignment. It should be noted that cardiomyocytes at this stage of maturity may often have multiple nuclei; however, this phenomenon should not play a large role in changing their directionality. Once alignments were quantified, cells were then defined as “aligned” if their major axis was within 20° of the axis of the micropatterned feature on which the cell was adhered.

Measurement of Calcium Propagation Rate

While actin, α-actinin, and nuclear staining provided characterization of the structural changes of hESC-CMs seeded on lanes of varying widths, further tests were conducted to determine the level of calcium ion conduction present in the aggregates. Thus, connexin 43 immunostaining (described above) and calcium transient analysis were conducted. For these experiments, the long micropattern designs were used (Figure 2B) since they were long enough to allow detection of the rapid calcium propagation rate throughout the aggregates. For calcium signaling assessment, the Rhod-2 acetoxymethyl (AM) ester (Life Technologies) calcium indicator dye was used. This cell-permeant dye exhibits an increase in fluorescence upon binding with cytoplasmic Ca^{2+}, providing a direct means of observing calcium propagation through aggregates of contracting cardiomyocytes.

The Rhod-2 dye was first reconstituted to a 100X concentration of 1 mM Rhod-2 in DMSO, which was then diluted in RPMI/B27 medium and applied to the day 5 patterned cells for 15 minutes at 37°C. The cells were then washed twice with PBS, fed with RPMI/B27, and incubated for an additional 30 minutes. Dyed micropattern samples were then loaded into a heated microscope stage incubator and videos of calcium transient fluorescence were taken. The rates of these calcium transients were high enough to be undetectable by the naked eye, so ROI analysis was conducted using Nikon Nis-D Elements software on extreme ends of each aggregate (Figure 3). By comparing the Rhod-2 intensities of the two ROIs, we were able to approximate the rate of calcium propagation between the two regions.

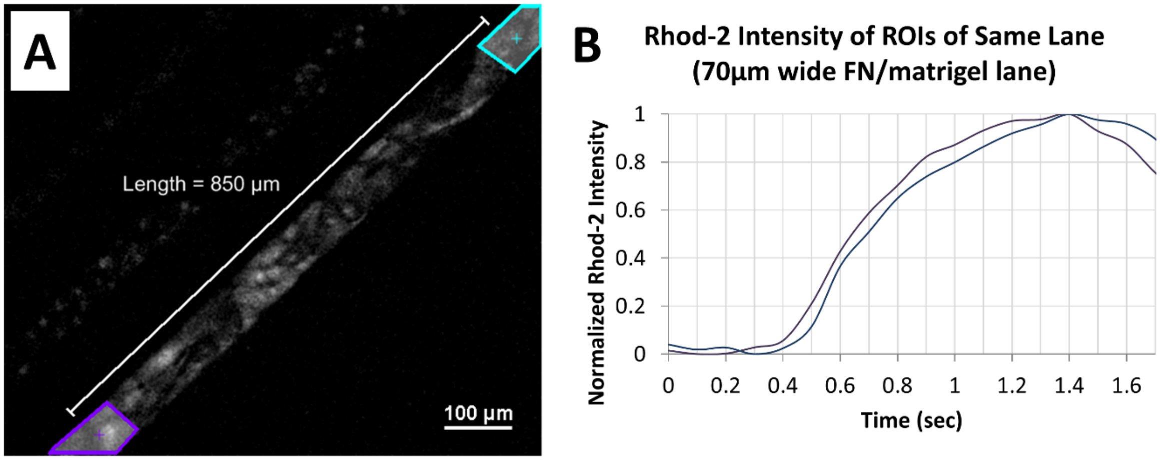

Figure 3-3. Calcium transient analysis of hESC-CMs seeded onto lanes of varying widths. Live fluorescent imaging was conducted, and intensities were measured for ROIs at opposite ends of each lane (A). By comparing normalized calcium transient intensity over time (B) between the two ROIs, and using the distance between the ROIs, the calcium propagation rate was determined for each micropattern width. ROI=region of interest, FN=fibronectin.

Results

Cell Attachment and Spontaneous Contraction on Micropatterned Surfaces

Brightfield images were taken regularly to assess the level of attachment of the pure hESC-CMs onto the matrigel/fibronectin-coated features (Figure 3-3). As expected, there was a small amount of debris present at day 1, most of which was washed away during routine feeding. Qualitative analysis of timelapse images between day 1 and 3 revealed that the seeded cardiomyocytes changed shape slightly to fill in any empty spaces available on the micropattern (data not shown), though they did not migrate significantly after they adhered. On a select few of the micropatterns, large aggregates of cells detached at one or more locations on a feature while still remaining anchored at another point. Additionally, cells occasionally “bridged” the distance between two features, creating a linkage.

The hESC-CMs had already begun spontaneously contracting well before being seeded onto the micropattern. Immediately after seeding, however, while the cells were under stress due to dissociation, no contraction was observed. Subtle contractions were then observed 24 hours after being seeded onto the micropattern slides, and they continued to increase in strength over the next 24-48 hours. Contractions among cells within a single feature were completely synchronized. There were multiple cases in which linkage cells bridged the gap between separate features, which caused synchronization between these two features. Conversely, features did not synchronize with one another when such linkages were not present.

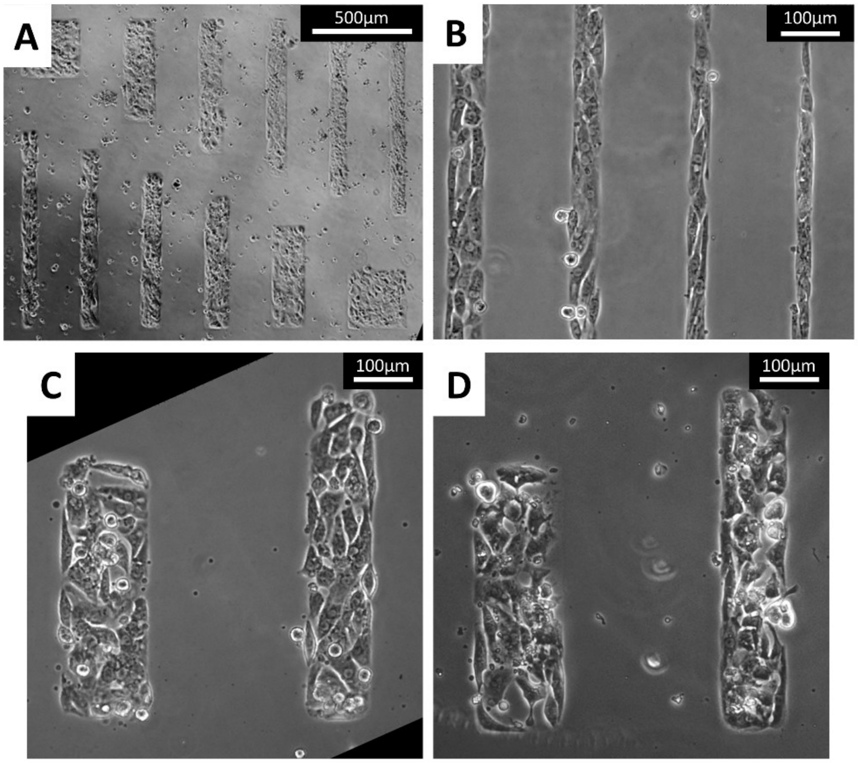

Figure 3-4. Representative brightfield images of micropatterned hESC-CMs. Cells seeded onto the micropatterned matrigel-fibronectin features matched the printed geometries very closely. (A) The first pattern design produced hESC-CM aggregates of varying aspect ratios (cells shown at day 7). All aggregates within a single grouping, as shown above, presented the same surface area. (B) The second design produced long lanes of varying widths (cells shown at day 3). As shown, the cells bound tightly to these geometric constraints and aligned clearly along the direction of the patterns. (C-D) The alignment of cells was clearly dependent on feature width, with the outermost cells aligning significantly more than cells located toward the center of each aggregate (cells shown at days 2 and 3, respectively)

ACTIN AND A-ACTININ ALIGNMENT ON PATTERNED HYDROGELS

Expression of select components of the sarcomere structure was determined via phalloidin and α-actinin immunostaining and confocal imaging. Qualitative analysis of both reveals significant improvement in sarcomere alignment within micropatterned cardiomyocytes (Figure 3-4). Sarcomere structures within individual cells generally aligned with each other, and the alignments of neighboring cells also tended to match direction. This phenomenon has been observed previously in rat and mouse cardiomyocytes, but this level of alignment had not yet been seen in this type of two-dimensional micropatterned structure for human cardiomyocytes.

Of particular interest was the relative level of sarcomere development among the multiple feature geometries that were tested. It was clear that the aspect ratios of the features were less important in inducing well-structured sarcomeres than the widths of the features themselves. That is, while a cell's alignment and internal structure was influenced by an edge of a micropattern, it was not heavily influenced by the aspect ratio. Specifically, it appeared that features with widths of 30µm – 80µm produced hESC-CMs with the most organized sarcomere structures.

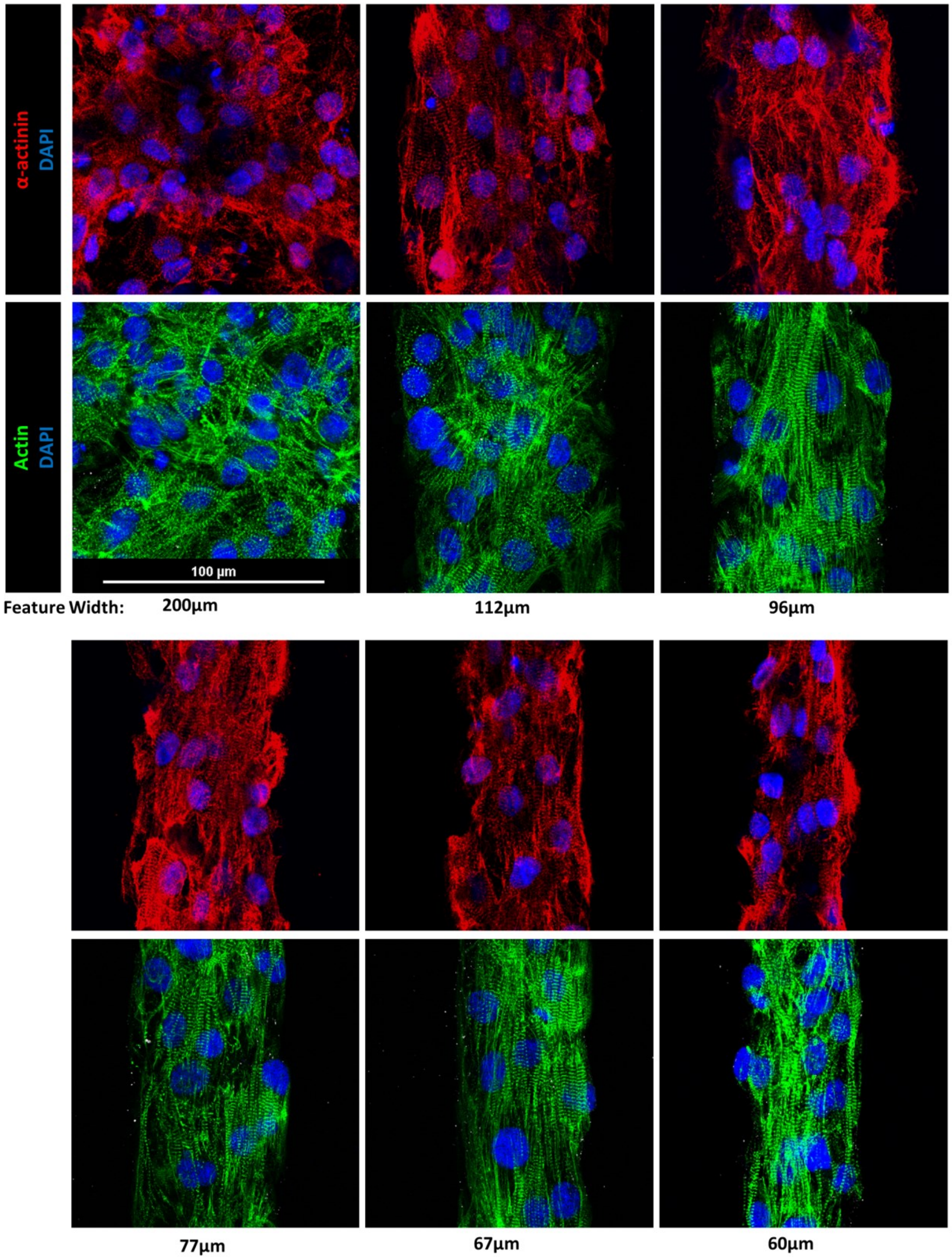

Figure 3-5. α-actinin, actin, and DAPI stains of cardiomyocytes after 5 days of culture on features of varying widths. Both myofilament markers show clearly improved cellular alignment, sarcomere organization, and sarcomere alignment in features under ~100 µm in width. As anticipated, cells seeded onto square features (200 µm in this set) show no favor towards any specific direction. A slight difference of 0 – 5 µm was observed between the designed pattern width and the actual width of the patterned cells. This is likely due to a small amount of swelling in the PDMS stamps during the curing step, as well as some mild mismatch between the feature edges and the cells' exact boundaries.

Connexin 43 Immunofluorescence

Antibody staining of connexin 43, a common gap junction protein, was conducted to assess the effects of aggregate width on cell-cell conduction. Connexin 43 gap junction channels couple cardiomyocytes in the ventricular myocardium enabling rapid electrical conduction between cells. In the normal adult ventricle, Connexin 43 gap junctions are preferentially in high abundance on the ends of cells and less on the sides. Immunostaining of monolayer cultures, as well as micropatterned aggregates of varying widths (Figure 3-6) revealed highly variable connexin 43 expression; unlike in sarcomere expression, there was no discernible pattern between connexin 43 expression and micropattern width. Gap junction plaques were highly punctate and occurred almost entirely within cell-cell junctions, as anticipated. These gap junctions localized to both lateral and axial edges of cardiomyocytes, however at day 5 there was no correlation found, regardless of cell shape, cell cytoskeleton orientation, or pattern width.

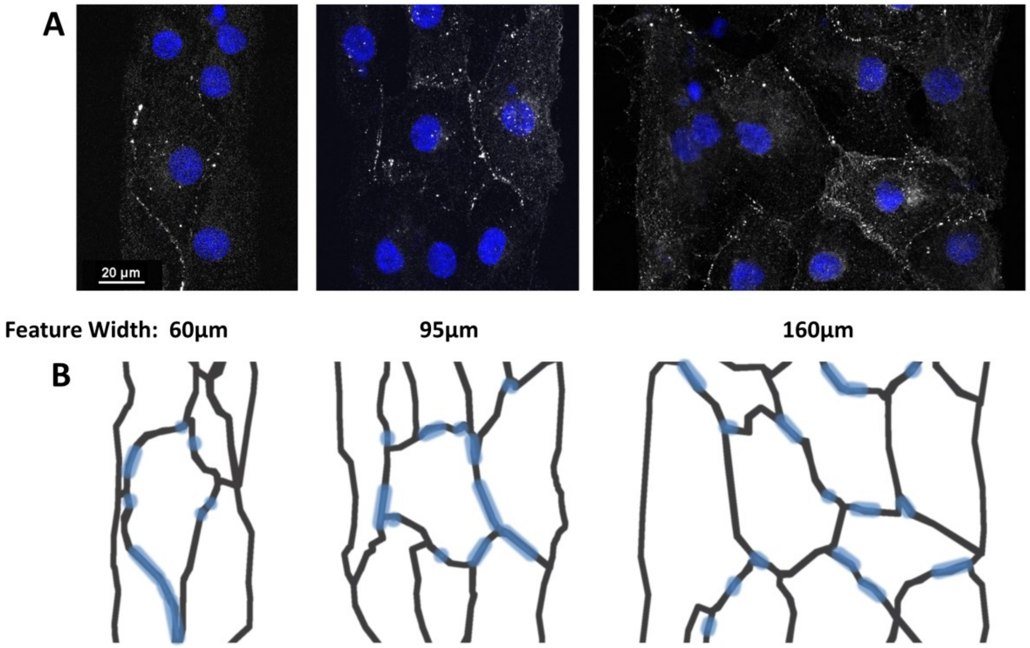

Figure 3-6. Connexin 43 expression of pure hESC-CMs seeded onto micropatterned matrigel/FN features of varying widths. Connexin 43 immunostaining with DAPI (A) shows a highly punctate and variable expression of gap junction plaques within the aggregates. Gap junction plaques were present along both lateral and axial edges of cardiomyocytes. A diagram (B) is included to indicate cell boundaries, as determined by phalloidin co-stain.

NUCLEAR ALIGNMENT ON PATTERNED SUBSTRATES

To gain quantitative insight regarding the level of directionality in the cultures, nuclear alignment was also assessed for the immature cardiomyocytes cultured on micropatterns of varying sizes and aspect ratios. As previously described, the patterns were organized into groups based on their surface area. Within each grouping, a variety of aspect ratios was examined. A nucleus was considered "aligned" if the direction of its major axis was within 20 degrees of the direction of the feature on which it was seeded. The measured directionalities of the nuclei closely matched the qualitative assessments of z-disk alignment observed in the immunostains mentioned above (Figure 3-5). That is, the overall width of the micropatterns played a large role in determining cell orientation, rather than the aspect ratio of the feature as a whole.

As shown in figure 3-7, the cells' nuclei were far more aligned on features with widths in the 30µm – 80µm range. For features with widths larger than this range, the nuclei were aligned only roughly 22% of the time, which is the expected value for cells that have no directionality. Cells on the outer-most edges of the features appeared to show the highest level of alignment and nuclear elongation. Cells that were not on the outer edge of a feature still exhibited a large amount of alignment, as long as the feature width was less than approximately 100µm. We hypothesize that there is still considerable restriction in cell shape for the more centrally-located neighboring cells, created by the laterally adjacent cells that are in direct contact with the feature boundary.

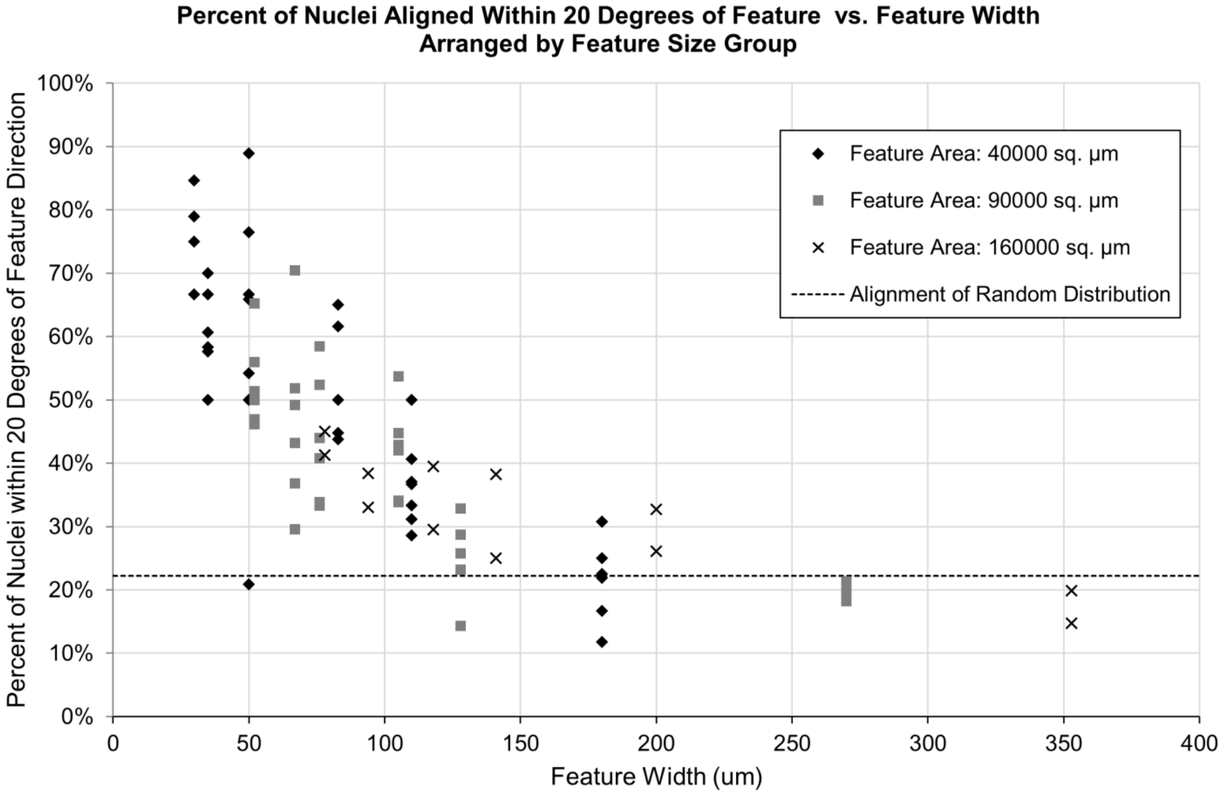

Figure 3-7. Percentage of aligned nuclei of cells on varying features. It is clear that nuclei showed much stronger alignment on features with widths of 30 µm – 80 µm. The aspect ratios of the features as a whole, however, did little to affect the alignment of the hESC-CMs.

CALCIUM ION PROPAGATION RATES

Rhod-2 AM ester calcium indicator dye was used to measure the rate at which calcium signaling passes through aggregates of various sizes. A large number of lanes were tested, with widths ranging from 20µm to 110µm. The resulting calcium propagation rates, shown in figure 3-8, suggest that there is no clear link between aggregate width and calcium propagation rate for the observed cells. Most lanes exhibited calcium propagation rates within the range of 0.5cm/sec to 2cm/sec.

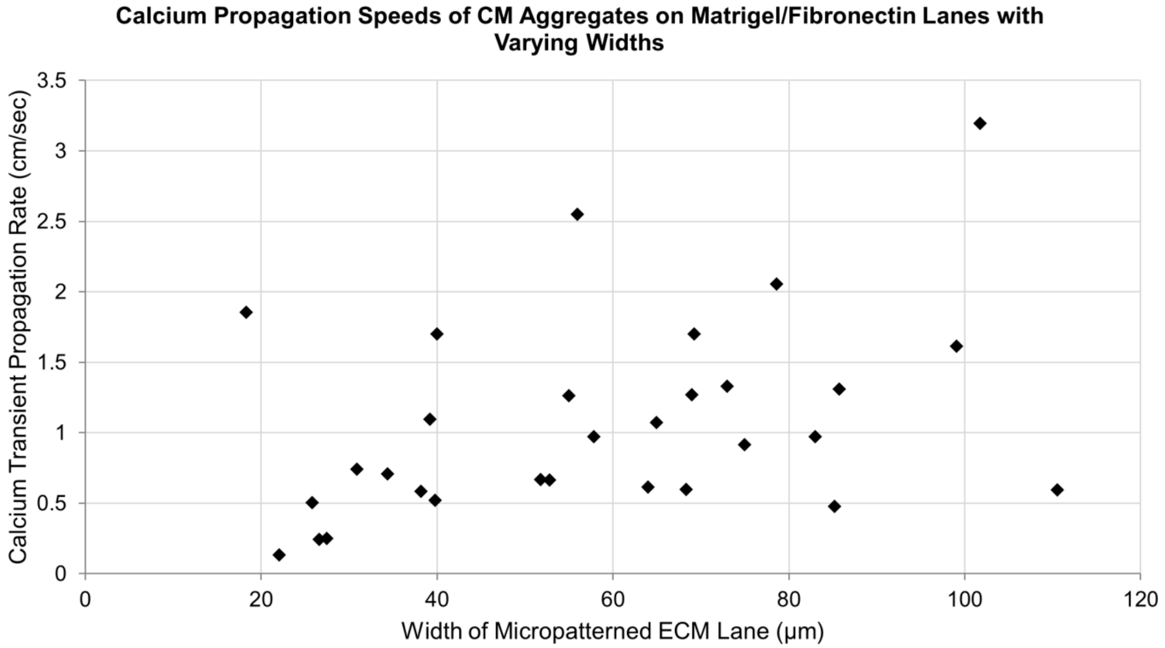

Figure 3-8. Calcium propagation speeds of hESC-CM aggregates on matrigel/fibronectin lanes with varying widths. Rhod-2 AM ester indicator dye was used to determine the rate at which calcium waves propagated through the cardiomyocyte aggregates. A compilation of all assessed lane widths indicates that there was no clear trend between lane width and calcium transient propagation rate. Calcium propagation rates typically ranged between 0.5 cm/sec and 2 cm/sec.

DISCUSSION

Methods that promote cardiomyocyte alignment have the potential to lead to an exciting new range of studies on human embryonic stem cell-derived cardiomyocytes. Emerging methods of differentiating hESCs into cardiomyocytes have shown great promise in their repeatability, efficiency, and reduced cost. However, these protocols continue to only achieve an immature phenotype of cardiomyocytes, with limited cell size and elongation, low levels of multinucleation, and immature action potential characteristics. It is clear that the next challenge facing cardioregenerative biology is the achievement of a more mature phenotype that will allow for more accurate modeling of native myocardium for pharmacological studies and for potential cell therapies. We hypothesize that the mechanisms facilitating the improved sarcomere structure involve a combination of focal adhesion/costamere confinement, improved polarization due to cell elongation, and controlled directionality of cell-cell junctions and the resulting contraction-induced mechanical loading.

Focal adhesions, which are intricate protein complexes that enable binding between a cell's cytoskeleton and the surrounding ECM, play a substantial role in the formation and alignment of actin stress fibers and force transduction. By restricting the locations at which the focal adhesions were able to form, both the cell and its stress fibers were aligned in the direction of the underlying features. In muscle cells, the laterally-located ECM-binding domains are more commonly referred to as costameres, which are highly related to focal adhesions both in function and protein composition [Quach and Rando, 2006]. Costameres form in conjunction with peripherally-located myofibrils along the z-disks, and their formation has been shown to be dependent on electrical coupling and mechanical loading of the cardiomyocyte [Ervasti, 2003; Bezakova and Lomo, 2001; Sharp et al, 1997].

In addition to cell-ECM binding, cell-cell contacts are also highly influenced by the micropatterned geometry. In standard two-dimensional cultures of cardiomyocytes, the cells form cell-cell junctions in all directions and are still capable of producing synchronously contracting sheets. This system is not physiologically relevant, however, since native cardiomyocytes form extremely polarized, fibrous tissue structures. The cell-cell junctions within native cardiomyocyte tissues reflect on this cellular polarity, with large differences in expression of cell-cell junction proteins in the axial versus lateral directions. Specifically, cardiomyocytes form intercalated discs with neighboring cells in the axial direction, while forming the costameres that bind to ECM ligands in the lateral direction. The intercalated discs are membrane-bound protein complexes that consist largely of adherens junctions and desmosomes to provide robust mechanical coupling between cells, as well as gap junctions to provide electrical coupling [Noorman et al, 2009]. Due to the improved polarity of our cultured cardiomyocytes, there is a much higher likelihood of the formation of physiologically-relevant intercalated discs and costameres. This new platform can lead to further studies of the many pathologies related to cell-cell junction mutations, such as arrhythmogenic right ventricular dysplasia/cardiomyopathy (ARVD/C), which has been linked to mutations in genes that encode desmosomal proteins [Rampazzo et al, 2002].

While sarcomere formation and alignment were improved within the thin feature widths, there was no significant difference in gap junction plaque expression and calcium propagation rate among these micropatterns. The connexin 43 immunostaining revealed punctate gap junction distribution along both lateral and axial edges of cardiomyocytes, which indicates that the cells may not yet have reached the level of polarity found in mature cardiomyocytes. Additionally, calcium propagation rates ranged around 0.5cm/sec to 2cm/sec, which is significantly lower than what is typically observed *in vivo* in neonatal myocardium (~20 cm/sec), adult ventricles (~100 cm/sec), and adult conduction systems (~300 cm/sec). These results agree in suggesting that the calcium conduction system has yet to be fully developed at day 5 in these micropatterned systems. This also agrees with previously reported results indicating that heterogeneous connexin 43 expression, in which at least 50% of cells present limited numbers of gap junctions, may lead to slower calcium propagation rates [Beauchamp et al, 2012]. It is possible, however, that a longer culture period within these fibrous aggregates will provide the cells with enough time to develop more robust calcium handling mechanisms.

The development of organized, structured sarcomeres is only one of many steps towards cardiomyocyte maturation that need to be better understood before a proper mature model of human cardiomyocytes can be thoroughly established. In addition to the numerous biochemical and epigenetic factors of cardiomyocyte maturation, there are other biomechanical aspects which will need to be addressed, such as substrate stiffness and mechanical loading, which were at non-physiological levels for this study. Additionally, the authors acknowledge that the use of matrigel as one of the components of the ECM substrate does provide some variability in the system; however, we believe that substituting this with laminin or other ECM components may allow for improved reproducibility and traceability. Regardless of these shortcomings, this system shows that a highly aligned, mature-like population of pure human cardiomyocytes can be produced in an exceedingly controlled manner from hESCs. We are confident that additional targeted studies of this platform will uncover fascinating mechanisms of cardiomyocyte development.

CONCLUSION

Organized cellular alignment is critical to controlling tissue micro-architecture and biological function. In this study, a pure population of human cardiomyocytes derived from embryonic stem cells was seeded onto micropatterns of varying geometries. The effects of these geometries on sarcomere development and nuclear alignment of the seeded cells were assessed and it was determined that a range of 30μm - 80μm is the ideal feature width to promote alignment of pure immature hESC-CMs, leading to improved sarcomere formation. By effectively inducing strong alignment of pure human cardiomyocyte cultures, we are now able to form much more physiologically-relevant models of heart tissues *in vitro*.

DISCLOSURES

One author (TJK) holds founding shares in Cellular Dynamics International, Inc. This company produces and sells cardiomyocytes from human stem cells. This company, however, has no connection with the stated research and had no part in funding or advising the direction of this research.

REFERENCES

Annabi, N., Tsang, K., Mithieux, S. M., Nikkhah, M., Ameri, A., Khademhosseini, A. and Weiss, A. S. (2013). Highly elastic micropatterned hydrogel for engineering functional cardiac tissue. *Adv. Funct. Mater.* **23**, 4950-4959.

Azarin, S. M., Lian, X., Larson, E. A., Popelka, H. M., de Pablo, J. J. and Palecek, S. P. (2012). Modulation of Wnt/β-catenin signaling in human embryonic stem cells using a 3-D microwell array. *Biomaterials* **33**, 2041–2049.

Balaban, N. Q., Schwarz, U. S., Riveline, D., Goichberg, P., Tzur, G., Sabanay, I., Mahalu, D., Safran, S., Bershadsky, A., Addadi, L., et al. (2001). Force and focal adhesion assembly: a close relationship studied using elastic micropatterned substrates. *Nat Cell Biol* **3**, 466–472.

Beauchamp, P., Desplantez, T., McCain, M. L., Li, W., Asimaki, A., Rigoli, G., Parker, K. K., Saffitz, J. E. and Kleber, A. G. (2012). Electrical coupling and propagation in engineered ventricular myocardium with heterogeneous expression of connexin43. *Circ. Res.* **110**, 1445–1453.

Bezakova, G. and Lømo, T. (2001). Muscle activity and muscle agrin regulate the organization of cytoskeletal proteins and attached acetylcholine receptor (achr) aggregates in skeletal muscle fibers. *J. Cell Biol.* **153**, 1453–1464.

Bursac, N. (2002). Cardiomyocyte cultures with controlled macroscopic anisotropy: a model for functional electrophysiological studies of cardiac muscle. *Circ. Res.* **91**, 45e–54.

Cao, F., Wagner, R. A., Wilson, K. D., Xie, X., Fu, J.-D., Drukker, M., Lee, A., Li, R. A., Gambhir, S. S., Weissman, I. L., et al. (2008). Transcriptional and functional profiling of human embryonic stem cell-derived cardiomyocytes. *PLoS One* **3**, e3474.

Chen, G., Gulbranson, D. R., Hou, Z., Bolin, J. M., Ruotti, V., Probasco, M. D., Smuga-Otto, K., Howden, S. E., Diol, N. R., Propson, N. E., et al. (2011). Chemically defined conditions for human iPSC derivation and culture. *Nat Meth* **8**, 424–429.

Chiu, L. L. Y., Janic, K. and Radisic, M. (2012). Engineering of oriented myocardium on three-dimensional micropatterned collagen-chitosan hydrogel. *Int. J. Artif. Organs* **35**, 237–250.

Dalby, M. J., Riehle, M. O., Sutherland, D. S., Agheli, H. and Curtis, A. S. G. (2004). Use of nanotopography to study mechanotransduction in fibroblasts – methods and perspectives. *Eur. J. Cell Biol.* **83**, 159–169.

Deutsch, J., Motlagh, D., Russell, B. and Desai, T. A. (2000). Fabrication of microtextured membranes for cardiac myocyte attachment and orientation. *J. Biomed. Mater. Res.* **53**, 267–275.

Domian, I. J., Chiravuri, M., van der Meer, P., Feinberg, A. W., Shi, X., Shao, Y., Wu, S. M., Parker, K. K. and Chien, K. R. (2009). Generation of functional ventricular heart muscle from mouse ventricular progenitor cells. *Science* **326**, 426–429.

Engelmayr, G. C., Cheng, M., Bettinger, C. J., Borenstein, J. T., Langer, R. and Freed, L. E. (2008). Accordion-like honeycombs for tissue engineering of cardiac anisotropy. *Nat Mater* **7**, 1003–1010.

Entcheva, E. and Bien, H. (2003). Tension Development and nuclear eccentricity in topographically controlled cardiac syncytium. *Biomed. Microdevices* **5**, 163–168.

Grosberg, A., Kuo, P.-L., Guo, C.-L., Geisse, N. A., Bray, M.-A., Adams, W. J., Sheehy, S. P. and Parker, K. K. (2011). Self-organization of muscle cell structure and function. *PLoS Comput. Biol.* **7**, e1001088.

Lian, X., Hsiao, C., Wilson, G., Zhu, K., Hazeltine, L. B., Azarin, S. M., Raval, K. K., Zhang, J., Kamp, T. J. and Palecek, S. P. (2012). Robust cardiomyocyte differentiation from human pluripotent stem cells via temporal modulation of canonical Wnt signaling. *P. Natl. Acad. Sci. USA*.

Lim, J. Y. and Donahue, H. J. (2007). Cell sensing and response to micro- and nanostructured surfaces produced by chemical and topographic patterning. *Tissue Eng.* **13**, 1879–1891.

Maniotis, A. J., Chen, C. S. and Ingber, D. E. (1997). Demonstration of mechanical connections between integrins, cytoskeletal filaments, and nucleoplasm that stabilize nuclear structure. *Proc. Natl. Acad. Sci.* **94**, 849–854.

McDevitt, T. C., Woodhouse, K. A., Hauschka, S. D., Murry, C. E. and Stayton, P. S. (2003). Spatially organized layers of cardiomyocytes on biodegradable polyurethane films for myocardial repair. *J. Biomed. Mater. Res. Part A* **66A**, 586–595.

Motlagh, D., Senyo, S. E., Desai, T. A. and Russell, B. (2003). Microtextured substrata alter gene expression, protein localization and the shape of cardiac myocytes. *Biomaterials* **24**, 2463–2476.

Noorman, M., van der Heyden, M. A. G., van Veen, T. A. B., Cox, M. G. P. J., Hauer, R. N. W., de Bakker, J. M. T. and van Rijen, H. V. M. (2009). Cardiac cell–cell junctions in health and disease: electrical versus mechanical coupling. *J. Mol. Cell. Cardiol.* **47**, 23–31.

Orlova, Y., Magome, N., Liu, L., Chen, Y. and Agladze, K. (2011). Electrospun nanofibers as a tool for architecture control in engineered cardiac tissue. *Biomaterials* **32**, 5615–5624.

Parrag, I. C., Zandstra, P. W. and Woodhouse, K. A. (2012). Fiber alignment and coculture with fibroblasts improves the differentiated phenotype of murine embryonic stem cell-derived cardiomyocytes for cardiac tissue engineering. *Biotechnol. Bioeng.* **109**, 813–822.

Quach, N. L. and Rando, T. A. (2006). Focal adhesion kinase is essential for costamerogenesis in cultured skeletal muscle cells. *Dev. Biol.* **293**, 38–52.

Rampazzo, A., Nava, A., Malacrida, S., Beffagna, G., Bauce, B., Rossi, V., Zimbello, R., Simionati, B., Basso, C., Thiene, G., et al. (2002). Mutation in human desmoplakin domain binding to plakoglobin causes a dominant form of arrhythmogenic right ventricular cardiomyopathy. *Am. J. Hum. Genet.* **71**, 1200–1206.

Sasaki, D., Shimizu, T., Masuda, S., Kobayashi, J., Itoga, K., Tsuda, Y., Yamashita, J. K., Yamato, M. and Okano, T. (2009). Mass preparation of size-controlled mouse embryonic stem cell aggregates and induction of cardiac differentiation by cell patterning method. *Biomaterials* **30**, 4384–4389.

Sharp, W., Simpson, D. and Borg, T. (1997). Mechanical forces regulate focal adhesion and costamere assemblv in cardiac mvocvtes. *Am. J. Physiol. - Hear. Circ. Physiol.* **273**, H546–H556.

Singhvi, R., Stephanopoulos, G. and Wang, D. I. C. (1994). Effects of substratum morphology on cell physiology. *Biotechnol. Bioeng.* **43**, 764–771.

CHAPTER 4: MICROPATTERN OPTIMIZATION

INTRODUCTION

With clear trends existing between micropattern lane widths and hESC-CM sarcomere formation, further attempts were made to augment the level of sarcomere formation in order to produce the most organized, mature-like myofibril structure possible. This would provide an improved model of myofibrillogenesis in human embryonic cardiomyocytes, and may help researchers to understand the mechanisms by which these myofibrils form. Thus, a series of experiments were conducted to optimize the various parameters involved in the micropatterning platform, including cell seeding density, substrate extracellular matrix composition, and timing of seeding.

MATERIALS AND METHODS

hESC CULTURE AND CARDIOMYOCYTE DIFFERENTIATION

All studies were conducted using cardiomyocytes derived from a cTnT-GFP promoter cell line graciously provided by the Kamp Lab of the University of Wisconsin – Madison. Cell culture and cardiomyocyte differentiation were conducted as previously described in Chapter 3. Briefly, hESCs were maintained in E8 media on vitronectin, and were passaged every 3-4 days as needed. Cells were differentiated using the Wnt-agonist method [Lian et al, 2012], and purified for cTnT+ cardiomyocytes using the Zeocin-resistant properties of the cTnT-GFP promoter line [Salick et al, 2014]. Purified cardiomyocytes were maintained in RPMI (Life Technologies) supplemented with B27 supplement (Life Technologies), which was replaced every three days. The parameter hereafter described as cardiomyocyte "age," is defined as the number of days after differentiation was first initiated; thus, the earliest age at which purified cardiomyocytes could be seeded was around day 12.

MICROPATTERNED EXTRACELLULAR MATRIX OPTIMIZATION

Original methods of micropatterning utilized a matrigel/fibronectin mixture to provide a binding substrate for patterned cardiomyocytes. Due to the undefined nature of matrigel, as well as the potential for improved binding to other extracellular matrix proteins, an alternative matrix protein was sought. A large number of extracellular matrices, including some combinations of multiple matrices, were tested to determine the ideal substrate for embryonic hESC-CM culture (Table 4-1).

Table 4-1. Extracellular matrix substrates tested for micropattern optimization. Combinations of some of the shown substrates were also tested.

Substrate	Source	Preparation
Collagen Type I	Ibidi (rat tail)	9.1 µL of 11 mg/mL collagen type I solution (Ibidi) was added to 1.7 µL 3M acetic acid and 2.5 mL H_2O to provide a 40 µg/µL working solution with a pH of 7.4. 250 µL of this solution was quickly added to each of 9 wells of a 24-well plate, since the collagen I begins to polymerize at this pH. Coating was allowed for one hour at room temperature.
Collagen Type IV	BD Biosciences (EHS lathrytic mouse tumor)	90 µL of 1 mg/mL BD BioCoat Collagen IV was added to 1.25 mL 0.1N HCl and 1.25 mL H_2O. 250 µL of this solution was quickly added to each of 9 wells of a 24-well plate. Coating was allowed for one hour at room temperature.
Fibrin	Fibrin – Chemicon Thrombin – Sigma (bovine plasma)	Fibrinogen and thrombin solutions were prepared separately and combined prior to experimentation. The fibrinogen solution consisted of 280 µL 33 mg/mL fibrinogen stock, mixed with 1.395 mL HEPES buffer and 417 µL DMEM. The thrombin solution consisted of 42.5 µL thrombin stock mixed with 6.5 µL 1N CaCl and 337 µL DMEM. These solutions were mixed to produce fibrin and 250 µL of this solution was quickly added to each of 9 wells of a 24-well plate.
Fibronectin	Sigma (bovine plasma)	90 µL 1 mg/mL fibronectin solution were mixed with 2.5 mL DMEM. 250 µL of this solution was quickly added to each of 9 wells of a 24-well plate.
Gelatin	Sigma (porcine skin)	500 mg gelatin were mixed with 500 mL MilliQ ultrapure H_2O and autoclaved to sterilize, producing a 0.1% gelatin stock solution. 250 µL of this solution was quickly added to each of 9 wells of a 24-well plate.
Laminin 1-1-1	R&D – Cultrex (EHS lathrytic mouse tumor)	90 µL 1 mg/mL laminin 1-1-1 solution were mixed with 2.5 mL DMEM. 250 µL of this solution was quickly added to each of 9 wells of a 24-well plate.
Matrigel	BD (EHS lathrytic mouse tumor)	Matrigel lot was initially screened and approved for compatibility with cell culture by WiCell, University of Wisconsin - Madison. 180 µL 1 mg/mL matrigel solution were mixed with 2.5 mL DMEM. 250 µL of this solution was quickly added to each of 9 wells of a 24-well plate.
Vitronectin	Thomson Lab (E. Coli)	Purified vitronectin for cell culture was graciously provided by Nick Propson of the Thomson Lab, University of Wisconsin – Madison. 90 µg were diluted in 2.5 mL cold PBS. 250 µL of this solution was quickly added to each of 9 wells of a 24-well plate.

Cardiomyocytes were produced and seeded onto tissue culture polystyrene wells coated with the above ECM proteins. It was hypothesized that integrin expression, and thus binding affinity to various ECM, may change with time. Thus, cardiomyocytes at day 13, day 95, and day 130 were seeded onto these substrates at a seeding density of 50,000 cells per cm^2. Images were taken at

1, 2, and 5 days after this seed, and qualitative assessment of attachment percentage and cell spreading were recorded (n=3 for all ECM / cell age / timestep combinations). During qualitative assessment, the number of cells attached to the matrix and the overall spreading of the cells were given a score of 0 – 5. Summing these numbers provided the attachment / spreading index shown in Figure 4-2.

SEEDING DENSITY OPTIMIZATION

The seeding density of the immature cardiomyocytes also needed to be fine-tuned. Seeding too many cells into the micropattern platforms causes them to compete for space, limiting their ability to spread and consequently reducing their ability to form robust sarcomeres. Conversely, however, immature cardiomyocytes appear to survive under conditions in which each cell is in contact with at least one other cell. Thus, seeding the cells too sparsely limited cell health and reduced survival. Seeding the cells densely enough to produce cell-cell contacts provides the added advantage of producing primitive adherens junctions between the cells, as well, the mechanisms of which can be further studied using this platform.

12-well tissue culture polystyrene culture plates were coated with 10 μg/cm^2 matrigel and 1.5 μg/cm^2 fibronectin diluted in DMEM. Immature day 13 hESC-CMs were seeded onto these wells at densities of 10 × 10^3 cells/cm^2, 50 × 10^3 cells/cm^2, and 150 × 10^3 cells/cm^2. Cells were monitored and imaged for 14 days to determine spreading and cell attachment.

CELL AGE / PRE-SEEDING OPTIMIZATION

During several prior experiments, it was observed that the hESC-CM age (time since differentiation was initiated) had an effect on the level of spreading and myofibrillogenesis that occurred on the micropattern platforms. Additionally, re-seeding the cells into a new culture well prior to micropatterning appeared to "prime" the cells, leading to highly organized sarcomere formation upon transfer to micropatterned lanes. We hypothesized that a small amount of maturation naturally occurred after initial differentiation for a few weeks, but that this level of maturation could only occur in more sparse cultures that are not provided by the conditions in which the hESC-CMs are initially differentiated. Experiments were subsequently conducted to determine the best method combination of pre-seeds and maintenance periods to lead to improved myofibrillogenesis (Figure 4-1).

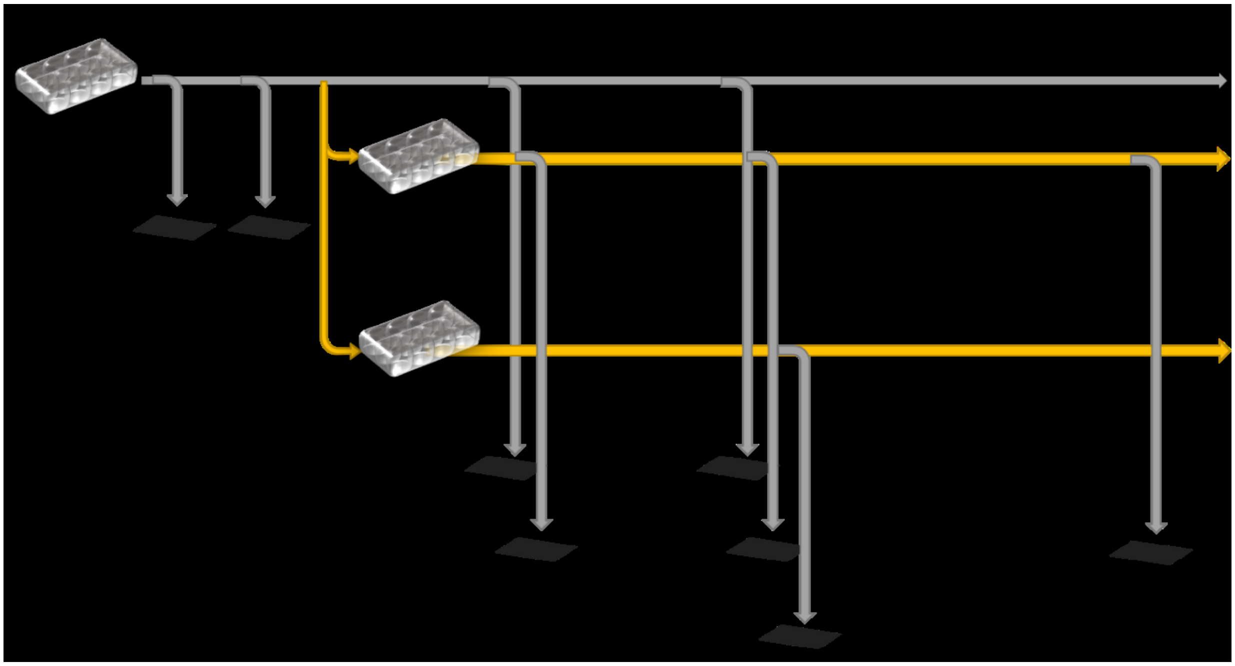

Figure 4-1. Workflow for pre-seed optimization. Upon hESC-CM differentiation and purification, micropatterns were seeded at various timings. Once purification was completed, cells were first passaged at a 1:2 ratio onto a new TCPS plate (shown by tissue culture plate at D13). Cells were transferred directly from this plate at D14 and D15. Additional pre-seeds were conducted, in which hESC-CMs were seeded into additional 12-well tissue culture polystyrene plates prior to being transferred onto the micropatterned cover slips. This provided the hESC-CMs with time to spread at a more sparse seeding density, which increased the amount of sarcomere organization and spreading that ultimately occurred on the micropatterned platforms.

RESULTS

MICROPATTERNED EXTRACELLULAR MATRIX OPTIMIZATION

hESC-CM attachment and spreading on a wide range of ECM proteins was examined for cells at three different ages. The results indicated a clear improvement of attachment on laminin-containing substrates (Figure 4-2). The best attachment occurred on matrigel, laminin 1-1-1, or a mixture of the two. We thereafter used laminin 1-1-1 as the ECM coating for further micropatterns, since it is more defined and less variable than matrigel.

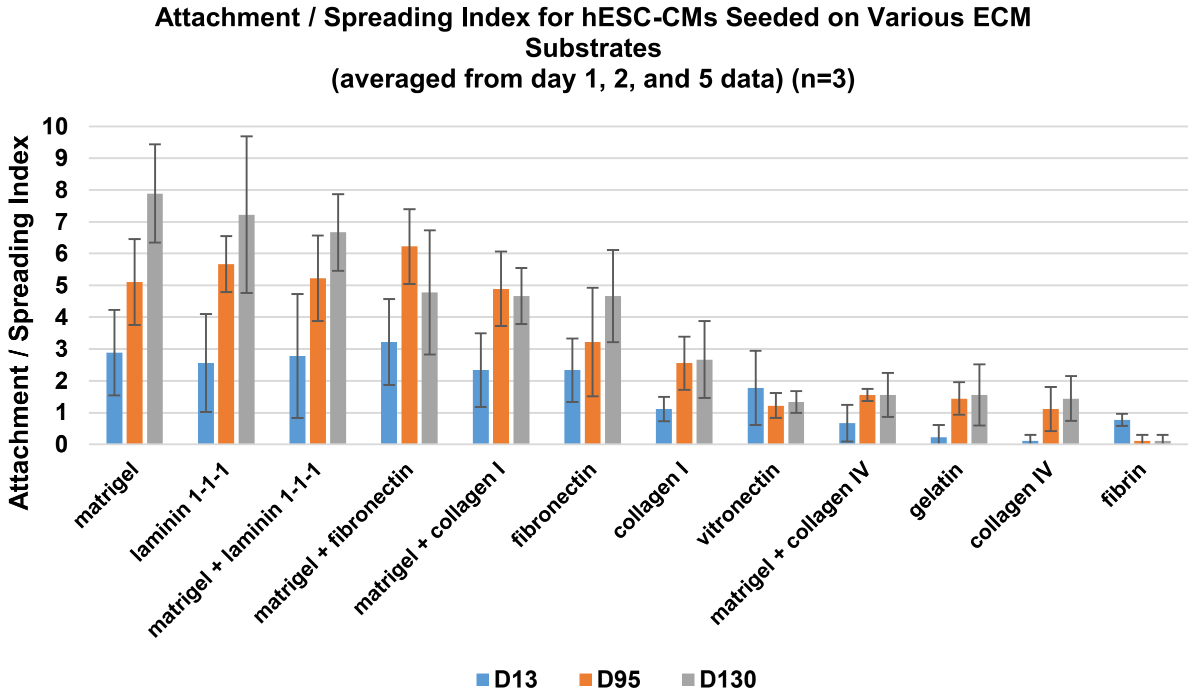

Attachment / Spreading Index for hESC-CMs Seeded on Various ECM Substrates (averaged from day 1, 2, and 5 data) (n=3)

Figure 4-2. Results of ECM substrate test, organized from strongest to weakest attachment / spreading. Level of attachment and spreading were qualitatively assessed and given a score that was combined to produce the index shown. The substrates containing laminin (either in purified laminin 1-1-1 form or within matrigel) provided the best hESC-CM attachment and spreading. Overall attachment and spreading was greater for hESC-CMs that had been maintained in culture for prolonged periods of time, further suggesting that some level of development occurs over time with no stimulus applied to the cells.

SEEDING DENSITY OPTIMIZATION

Day 13 hESC-CMs were seeded onto matrigel / fibronectin coated micropatterned cover slips at densities of 10 × 10^3 cells/cm^2, 50 × 10^3 cells/cm^2, and 150 × 10^3 cells/cm^2. Note that seeding densities are reported as the number of cells seeded over the total area of the well; this includes both patterned and unpatterned parts of the cover slip, as well as the surrounding well. Cells that land on PEG-coated areas wash away upon routine feeding. The cells were observed and imaged for 14 days. It was clear from direct observation that the lower seeding density resulted in complete cell detachment and apoptosis, while the higher densities had higher number of attaching cells, which remained attached over the course of the experiments. The highest seeding density had considerable cell crowding, preventing individual cells from spreading out and producing robust, organized myofibrils (Figure 4-3). Once the approximate ideal seeding density was determined, further testing revealed that a density of 30 × 10^3 to 50 × 10^3 cells/cm^2 is ideal for this application.

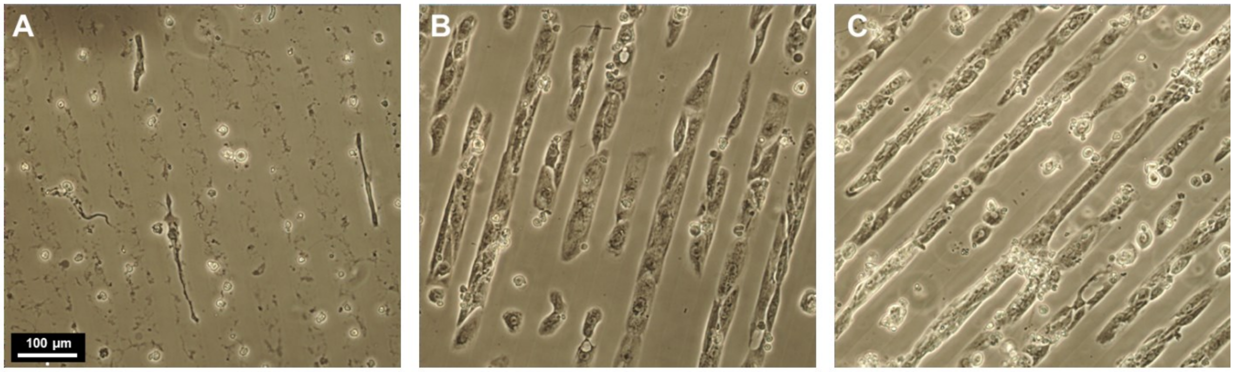

Figure 4-3. Brightfield images, taken 14 days after hESC-CMs were seeded onto micropattern lanes at (A) 10 × 10^3 cells/cm^2, (B) 50 × 10^3 cells/cm^2, and (C) 150 × 10^3 cells/cm^2. Since cell-cell contacts appear to improve hESC-CM attachment and survivability, all cells had detached by day 14 in the low-density samples. Crowding was observed in the higher-density samples, preventing mature-like formation of sarcomeres that was observed in the mid-range seeding densities.

Cell Age / Pre-Seeding Optimization

Pre-seeding hESC-CMs onto a TCPS plate prior to transfer onto micropatterns appeared to improve overall myofibrillogenesis. Cells were seeded at a density of 30×10^3 cells/cm^2 after multiple pre-seeding conditions (see Figure 4-1). Since this was on the lower end of the suggested seeding density, cell survival only occurred if cell-cell contacts were made early on in the attachment process; cells that failed to spread on the micropatterned lanes tended to undergo apoptosis and detachment. The results of the pre-seed experiments are shown in Figure 4-4. Trajectories on this graph that show increasing cell area with time are desired. It appeared that pre-seeding was beneficial for ultimate micropatterned-cell spreading and attachment, as long as this pre-seed was not too sparse. Providing the cells with over 14 days to spread on their pre-seed plate also appeared to improve their ultimate spreading and myofibrillogenesis.

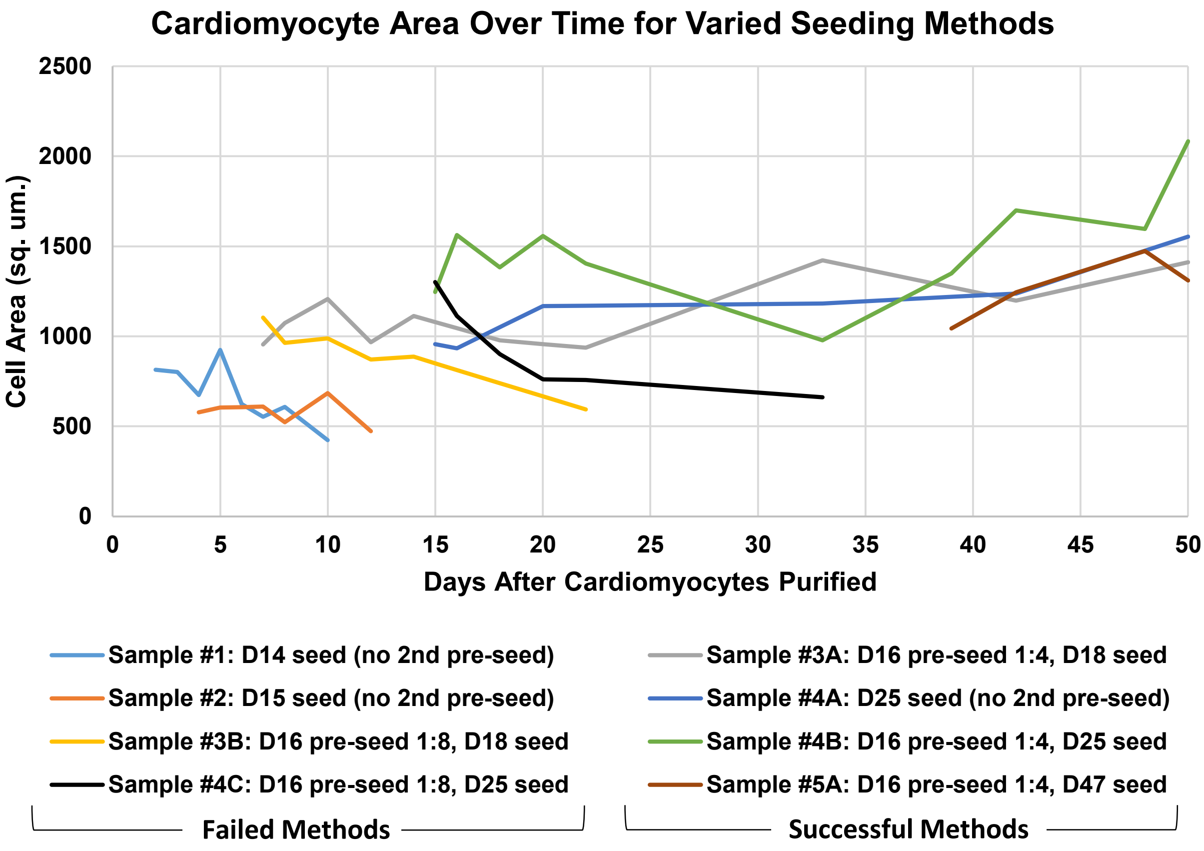

Figure 4-4. Results of pre-seed testing of hESC-CMs. Cell areas were measured manually using Nikon Nis-D Elements software. Cell area tended to decline with poor health of the cells, while increased spreading has been observed to be linked closely to the level of myofibrillogenesis. Cells seeded early (#1 / #2), and pre-seeded too sparsely (#3B / #4C) tended to shrink and detach. Cells that were given at least 14 days on a pre-seeded substrate before transfer to the micropatterns (#3A / #4A / #4B / #5A), and that were not pre-seeded too sparsely tended to spread and thrive on the micropatterned substrates.

DISCUSSION

As discussed in chapter 3, there was a distinct response of hESC-CMs to the geometry of their underlying micropatterned substrate. As the lane widths approached smaller sizes, single cells were capable of spanning an entire lane, and these cells often formed spread, brick-shaped morphologies that very closely resembled those of mature cardiomyocytes. To produce a model in which this occurs regularly, the many parameters involved in the platform required optimization.

Extracellular matrix substrate studies indicated that laminin was a substantial factor in inducing hESC-CM attachment and spreading. ECMs that included matrigel or laminin tended to perform much better than the other examined proteins. This corresponds to observations made *in* vivo, in which laminin was not observed in the developing heart before stage 11, but was found to be critical in heart formation at times after this stage [Yarnitsky and Volk, 1995; Oliviero et al, 2000]. The ECM of the developing heart is highly dynamic, consisting of a large number of extracellular proteins such as proteoglycans, hyaluronans, collagens, elastin, and fibronectin [Lockhart et al, 2011; Fomovsky et al, 2010]. It was thus hypothesized that developing cardiomyocytes may alter their integrin expression, and subsequently would attach and spread differently with time in culture. Indeed, there were considerable differences with cell attachment and spreading with age, with some ECM components providing better attachment for older hESC-CMs and vice versa. For example, on the substrates containing large concentrations of laminin, attachment and spreading increased greatly with cardiomyocyte age. Conversely, on the matrigel/fibronectin and matrigel/collagen I substrates, spreading and attachment decreased for the oldest hESC population. One future study of interest could probe for integrin expression of developing cardiomyocytes to see exactly which ligands these cells would prefer as they age.

During the differentiation process, cardiomyocytes form large, contracting monolayers and fibrous webs. While exhibiting strong coupling and contractile properties, the cells are small and densely packed, and they stay in this configuration seemingly indefinitely, as shown by year-long cultures under these conditions (data not shown).

Seeding these cells onto TCPS plates before micropatterning provides them with a chance to spread and grow in size, and may initiate a hypertrophic response similar to what occurs naturally during growth or pathologically under several forms of disease. Pre-seed testing showed that transferring the cells at ~100,000 cells/cm^2 onto matrigel-coated TCPS for approximately 14 days prior to micropatterning could help to induce long-term survival and spreading of the micropatterned cells.

CONCLUSIONS

Micropatterned lanes are capable of increasing sarcomere organization and alignment of hESC-derived cardiomyocytes. In order to produce a repeatable platform for observation of this robust sarcomere formation, several parameters were optimized. The micropattern lane width, ECM substrate, cell seeding density, and pre-seeding culture conditions were adjusted to develop a repeatable method of producing highly aligned, single-cell wide cardiomyocyte fibers. The cells that formed these fibers exhibited a brick-like morphology that matches *in vivo* observations more closely than in unaligned cultures.

REFERENCES

Fomovsky, G., Thomopoulos, S. and Holmes, J. (2010). Contribution of extracellular matrix to the mechanical properties of the heart. *J. Mol. ...* **48**, 490–496.

Lian, X., Hsiao, C., Wilson, G., Zhu, K., Hazeltine, L. B., Azarin, S. M., Raval, K. K., Zhang, J., Kamp, T. J. and Palecek, S. P. (2012). Robust cardiomyocyte differentiation from human pluripotent stem cells via temporal modulation of canonical Wnt signaling. *P. Natl. Acad. Sci. USA*.

Lockhart, M., Wirrig, E., Phelps, A. and Wessels, A. (2011). Extracellular matrix and heart development. *Birth Defects Res. ...* 1–31.

Oliviéro, P., Chassagne, C., Salichon, N., Corbier, a, Hamon, G., Marotte, F., Charlemagne, D., Rappaport, L. and Samuel, J. L. (2000). Expression of laminin alpha2 chain during normal and pathological growth of myocardium in rat and human. *Cardiovasc. Res.* **46**, 346–55.

Salick, M. R., Napiwocki, B. N., Sha, J., Knight, G. T., Chindhy, S. a, Kamp, T. J., Ashton, R. S. and Crone, W. C. (2014). Micropattern width dependent sarcomere development in human ESC-derived cardiomyocytes. *Biomaterials* **35**, 4454–64.

Sanger, J. W. and Sanger, J. M. (2002). Myofibrillogenesis in cardiac muscle. In *Myofibrillogenesis* (ed. Dube, D. K.), pp. 3–21. New York: Birkhauser Boston.

Sha, J., Lippmann, E. and McNulty, J. (2013). Sequential Nucleophilic Substitutions Permit Orthogonal Click Functionalization of Multicomponent PEG Brushes. … **14**, 3294–3303.

Yarnitzky, T. and Volk, T. (1995). Laminin is required for heart, somatic muscles, and gut development in the Drosophila embryo. *Dev. Biol.* **169**, 609–618.

CHAPTER 5: SCANNING GRADIENT FOURIER TRANSFORM (SGFT) METHOD FOR ASSESSING SARCOMERE ORGANIZATION

A substantial portion of this work has been submitted for publication as:

Salick MR, Napiwocki BN, Knight GT, Ashton RS, Crone WC (2014). The scanning gradient Fourier transform (SGFT) method for assessing sarcomere organization, alignment, and heterogeneity.

INTRODUCTION

Recent advances in stem cell biology have allowed researchers to efficiently produce large numbers of cardiomyocytes from various pluripotent cell sources. Unfortunately, these cells exhibit properties that are characteristic of immature cardiomyocytes such as poor sarcomere organization, limited calcium handling, and reduced cell size and alignment. Specifically, the actin-myosin motor proteins that form the sarcomeres within these cardiomyocytes fail to produce the large, highly-ordered repeating structures that are indicative of adult myocytes. Instead, these cells produce heterogeneous sarcomeres that vary in thickness, alignment, spacing, and level of organization. This study focuses on a series of algorithms that provide a quantitative analysis technique to characterize these heterogeneous sarcomere structures within aggregates and single cardiomyocytes. The scanning gradient Fourier transform (SGFT) method incorporates gradient analysis along with fast Fourier transforms to determine regions of sarcomere organization within individual cells, and allows a quantitative method of determining sarcomere quality at the sub-cellular scale. Trends between sarcomere length and location are observed in immature cardiomyocytes, and utilization of the SGFT technique was demonstrated for additional applications, such as breast cancer collagen microstructure and neural rosette patterning.

As researchers develop methods to advance the maturation of cardiomyocytes, a robust method of assessing the sarcomere structures of these cells is needed. Multiple methods of sarcomere assessment currently exist in the literature, but they are limited in their ability to assess unaligned or heterogeneous myofibrils. The most common of these methods involves application of a one-directional Fourier transform to a linear intensity profile taken across a large region of an entire cell or cellular aggregate (Gannier et al., 1993; Dobesh et al., 2002; Mansour et al., 2004; Bray et al., 2008), typically to determine sarcomere length with considerable accuracy. A more recent study utilized an intensity profile curve-fitting approach to achieve nanometer-precision measurement of sarcomere lengths (Shintani et al., 2014). These studies have been able to make fascinating connections between sarcomere length and other physiological and functional properties of the cardiomyocytes (Mansour et al., 2004; Dobesh et al., 2001; Gannier et al., 1993); however, this method of analysis is only applicable for cardiomyocytes that have already established highly organized, unidirectional sarcomeres.

The condition in which the myofilaments fail to align in an anisotropic manner is referred to as myofibrillar disarray. *In vivo*, myocyte/myofibrillar disarray is regularly observed in patients suffering from hypertrophic cardiomyopathy (HCM) (Ferrans et al., 1972; Francalanci et al., 1995; Karlon et al., 2000). HCM is the most common of all inherited heart defects, affecting 1 out of every 500 people in the United States (Maron et al., 2003). Not surprisingly, the root causes of myofibrillar disarray in HCM are mutations in genes encoding the sarcomeric proteins, particularly beta-myosin heavy chain, myosin-binding protein C, and cardiac troponin-T (Bashyam et al., 2003). It is still largely unknown how these mutations ultimately lead to the hypertrophic response of the heart; thus, more rigorous examination of the cellular response at the protein level may lead to improved understanding of the mechanisms involved. *In vitro*, myofibrillar disarray is observed in embryonic cardiomyocytes (Lundy et al., 2013), cardiomyocytes with constrained boundaries (Bray et al., 2008), or cardiomyocytes being cultured in non-physiological conditions (Jacot et al., 2008). This lack of sarcomeric organization, both examined *in vivo* and *in vitro*, cannot be analyzed using the previously mentioned unidirectional Fourier transform methods. In these cases, researchers often utilize gradient-based methods (Karlon et al., 1998; Hong et al., 1998; Bray et al. 2008, Kabir et al., 2013), Hough transforms (Karlon et al., 1998), or two-dimensional Fourier transforms (Rao et al., 2009) to determine their orientations, though these techniques are incapable of determining sarcomere organization or length in these unaligned myofibrils.

While prior techniques are robust and computationally rapid, they are limited in their determination of the sarcomere characteristics at the sub-cellular scale. The scanning gradient Fourier transform (SGFT) method described here incorporates gradient techniques to initially determine local sarcomere directionality, followed by a large number of 1-dimensional fast

Fourier transforms to determine the sarcomere properties of individual myofibrils within cells and aggregates. The main values that are determined using this method include myofibril direction, sarcomere length, and the level of sarcomere organization.

MATERIALS AND METHODS

The workflow described below is depicted in full in Figure 5-1. The initial image to be analyzed can be any fluorescent stain that has heterogeneous repeating striped patterns; thus, this method may be used for applications other than cardiomyocyte sarcomere striation. In the examples shown in this paper, α-actinin immunostains (Abcam, Cambridge, UK) and TMRho-conjugated phalloidin (Sigma-Aldrich, St. Louis MO, USA) stains were used to label the striated sarcomere structures of cardiomyocytes. Images were captured using a Nikon A1RSi Confocal Microscope (NikonUSA, Melville NY, USA) with attached Photometrics CoolSNAP HQ2 camera (Photometrics, Tucson AZ, USA). Nis-D Elements – Advanced Research v3.22 (NikonUSA, Melville NY, USA) software was used to prepare images for analysis. Images were taken using an oil-immersion 100X objective. Not surprisingly, it was observed that the objective, and thus the resulting image resolution, has a large impact on the ultimate quality of the SGFT analysis. Images with resolutions of at least 4 μm per pixel were sufficient for analysis. After initial image preparation, all following analysis was conducted on MATLAB (version R2013) (MathWorks, Natick MA, USA).

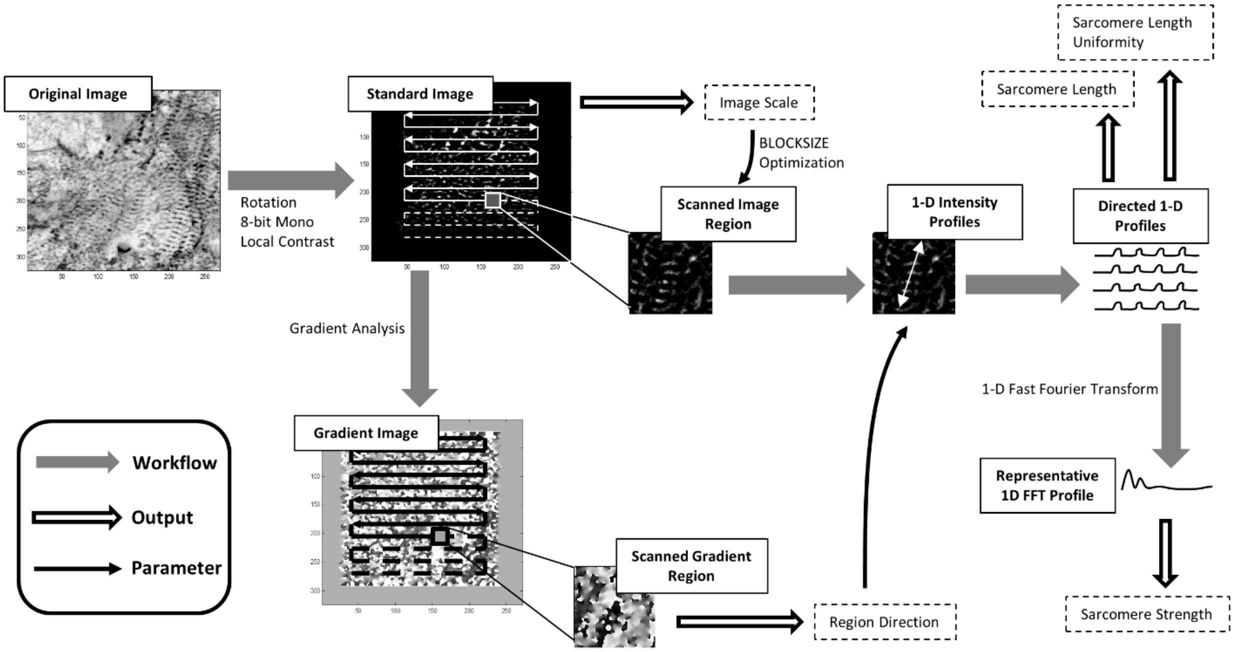

Figure 5-1. Workflow of SGFT method. The original image is first rotated, converted into 8-bit monochromatic format, and modified using a local contrast filter. A separate array is also produced by taking the gradient of the standardized image; this is used to determine the local directions of the sarcomere structures. A scanning loop is then applied on small regions throughout the gradient array, determined by the BLOCKSIZE and SCANJUMP parameters. Directional statistics are applied to this local region to determine the orientation that exhibits the largest gradient, which accurately determines the direction of the sarcomere patterns. After determining the direction of strongest gradient, one-dimensional intensity profiles of the standard image are taken in this direction. The spacing and consistency of these profiles are then used to determine the sarcomere length and uniformity. One-dimensional Fourier transforms are then taken of each profile, which are then averaged to produce a low-noise representative 1D fast Fourier transform profile. Analysis is then conducted on the representative curve to determine the strength of sarcomere organization.

CARDIOMYOCYTE DIFFERENTIATION AND CULTURE

Cardiomyocytes were differentiated and purified from human embryonic stem cells (hESCs), as described in Lian, et al. [2012] and Salick, et al. [2014]. Cells were seeded on multiple platforms, including micropatterned laminin lanes and unpatterned laminin wells, as described in the previous chapters.

IMAGE PREPARATION AND PARAMETER DETERMINATION

Fluorescent images were converted to monochrome 8-bit format and rotated such that the cells were aligned in the vertical direction using Nis-D Elements – Advanced Research v3.22. This rotation was done to streamline analysis, and is not necessary for the SGFT method to work properly. In Matlab, the μm/pixel ratio was determined and the ***blocksize*** parameter was set. ***blocksize*** sets the height and width of the small sections of the image that are analyzed individually. It was found that a ***blocksize*** that includes 8 sarcomeres acquires the clearest signal, while achieving adequate resolution to measure sub-cellular sarcomere regions. b***locksize*** was also rounded to a non-prime value, as fast Fourier transforms utilizing the Cooley-Tukey algorithms (Cooley and Tukey, 1965) are considerably slower for data sets with prime dimensions. A local contrast filter was then applied to the image to account for immunostaining artifacts that tend to lead to nonuniformity in the final images. Local contrast filtering also helps to detect sarcomeres that are located in regions that may have some non-specific binding of the stain. The ***scanjump*** parameter was set, which provides the number of pixels that are skipped between individual scans. ***scanjump*** determines the resolution of the SGFT analysis, at a cost of computation time. The image was then normalized.

IMAGE FILTERING AND GRADIENT PRODUCTION

To speed processing, the software initially scanned the image and removed regions containing empty space from the analyzed regions of interest. This prevented unnecessary application of fast Fourier transforms on regions that clearly contain no sarcomeres. Additionally, a smoothing function was applied to the edges of the region of interest to prevent these edges from creating a false-positive artifact that is often detected during fast Fourier transform analysis of images. Next, a gradient image was produced by taking the discrete derivatives of the original image in the X and Y directions, independently. The image was then split into several small blocks, specified by the ***blocksize*** and ***scanjump*** parameters. The following steps describe the analysis conducted during each individual scan.

DIRECTION DETERMINATION

The direction of patterns was determined using directional statistics of the gradient image of the current scan area. First, the principal axis of the strongest gradient was determined in each pixel. This was done by taking the numerical gradient in the X and Y directions within the full image, shown as the partial derivatives $\frac{\partial f}{\partial x}$ and $\frac{\partial f}{\partial y}$ in Eq. 5-1. The inverse tangent of these values then provides the principal axis of variation θ at each point, as shown in Eq. 5-2.

Eq. 5-1 $$\nabla f = \left[i\frac{\partial f}{\partial x} + j\frac{\partial f}{\partial y}\right]$$

Eq. 5-2 $$\theta = atan2\left(-\frac{\partial f}{\partial y}, \frac{\partial f}{\partial x}\right)$$

The average directions of the individual scans were then determined using θ. Weighted directionality was determined using Eqs 5-3, 5-4, 5-5. The weighting values were determined by the intensity of the original image; this prevented negative regions of the image from skewing direction results. For directional analysis, θ was replaced with 2θ, since the algorithm is working with axial ($0 < \theta < \pi$) rather than circular ($0 < \theta < 2\pi$) data:

Eq. 5-3 $$\bar{C} = \frac{1}{n}\frac{\sum_{j=1}^{n} I_j \cos(2\theta_j)}{\sum_{j=1}^{n} I_j}$$

Eq. 5-4 $$\bar{S} = \frac{1}{n}\frac{\sum_{j=1}^{n} I_j \sin(2\theta_j)}{\sum_{j=1}^{n} I_j}$$

Eq. 5-5
$$2\bar{\theta} = \begin{cases} tan^{-1}\left(\frac{\bar{S}}{\bar{C}}\right) & if\ \bar{C} > 0 \\ tan^{-1}\left(\frac{\bar{S}}{\bar{C}}\right) + \pi & if\ \bar{C} < 0 \end{cases}$$

The mean direction of the transformed patterns is $\bar{\theta}$, while I_j and θ_j represent the absolute intensities and angles of individual pixels within the image and gradient, respectively (Mardia and Jupp, 2000).

SARCOMERE ORGANIZATION AND SPACING DETERMINATION

With the mean direction determined, multiple parallel intensity profiles of the filtered image were taken in this direction to determine the organization of the pattern signal, as well as the pattern spacing (sarcomere length, in this example). An example of the resulting 1D Fourier transforms is shown in Figure 5-2. These 1D Fourier transform profiles were then averaged to reduce the noise level and halved due to symmetry to reduce computation time. The decreasing minimum of this curve is then determined and subtracted from the averaged 1D Fourier transform profile. Next, the maximum of this curve is located. The height of this maximum, which corresponds strongly with the organization of the repeating pattern in the direction, was used to determine the sarcomere pattern organization $\bar{P}$**,** as shown in Figure 5-2.

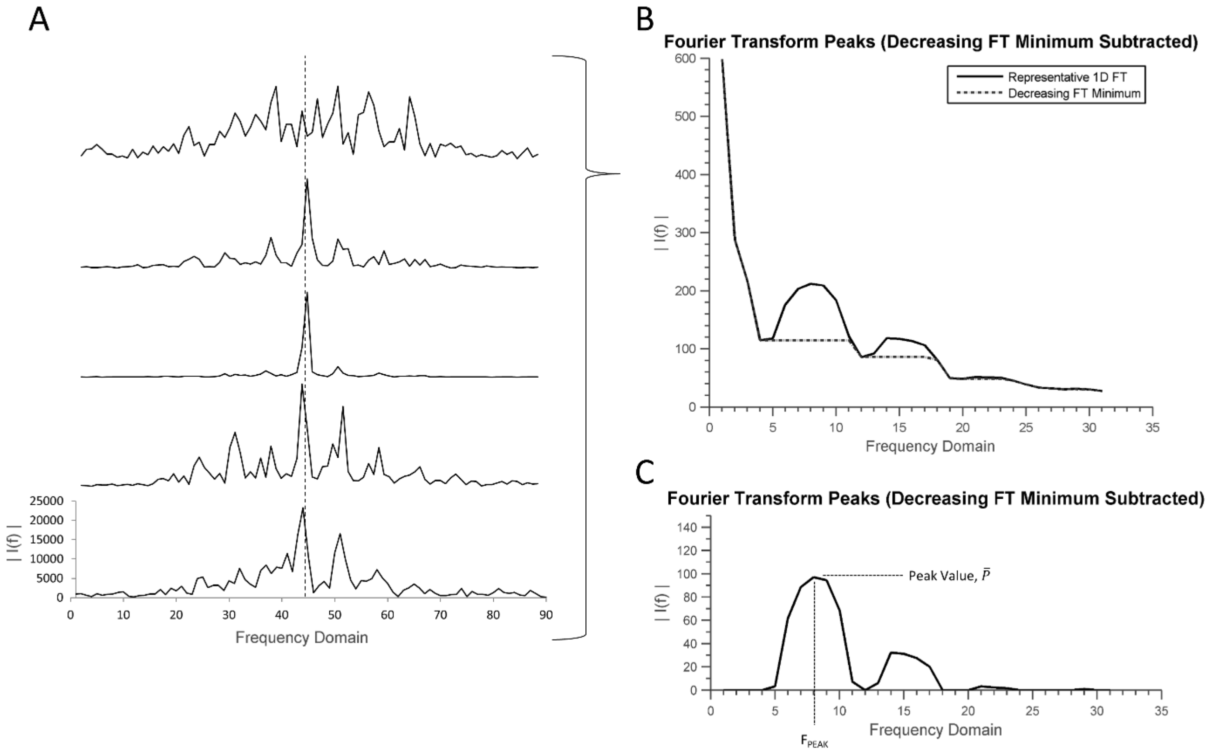

Figure 5-2. An example of five one-directional Fourier transforms taken in the determined myofibril direction (A). These transforms are then averaged, and the resulting curve is smoothed (B). The decreasing minimum of the averaged FT is then determined and subtracted from the original curve (C). The maximum of the resulting curve is then located. The Fourier transform signal intensity at this point is used to define the sarcomere pattern organization of the current scanned section, and the location of the peak along the x-axis (frequency domain) can be used to determine the pattern spacing.

Eq. 5-6
$$\overline{D}_{FREQ} = \frac{n}{F_{PEAK}}\left(\frac{microns}{pixel}\right)$$

In addition to the organization of the sarcomere signal, the sarcomere length, or wavelength of the repeating pattern, was determined based on the location of the greatest local maximum of the representative 1D Fourier transform curve using Eq. 5-6. This spacing, $\overline{D}_{FREQ}$, is determined by the peak location F_{PEAK}, the sample size of the 1D Fourier transforms n, and the µm-to-pixel ratio of the image. Due to limitations in the sampling frequency, however, it was found that the sarcomere spacing determined in the spatial domain was considerably more accurate and precise than $\overline{D}_{FREQ}$, found in the frequency domain. Since immature cardiomyocytes have shorter and more variable sarcomeres, this output of local sarcomere spacing is another useful feature of the SGFT method.

SPATIAL DETERMINATION OF SARCOMERE SPACING

Measurement of sarcomere spacing using the peak frequency in the 1D fast Fourier transform is limited due to its low resolution. Thus, sarcomere spacing was determined in the spatial domain, using the intensity profiles of the filtered images in the pattern direction previously determined as $\overline{\theta}$. To compute this spacing, the locations at which the intensity profiles crossed their mean value were detected (Figure 5-3).

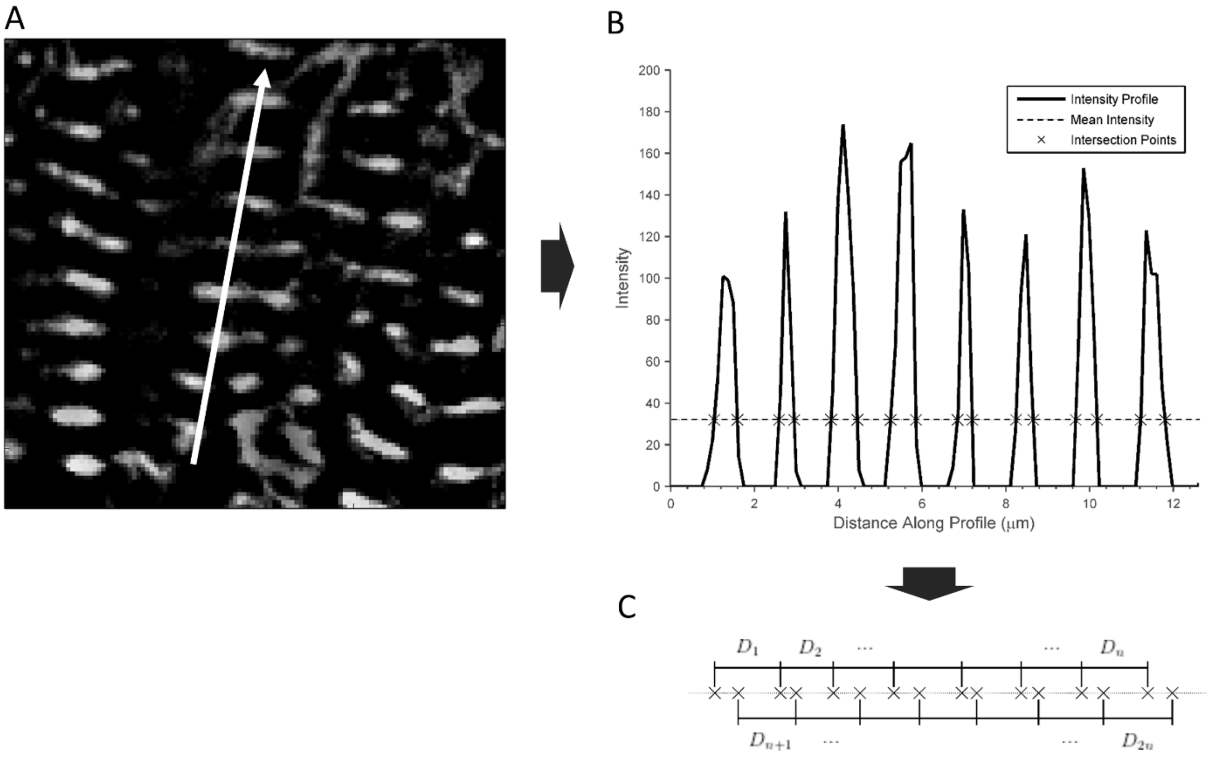

Figure 5-3. Spatial determination of sarcomere spacing. Intensity profiles are taken in the direction of strongest gradient (A), and thus run parallel to the myofibrils and cross multiple z-lines within the image section. Locations at which this intensity profile crosses its own mean are then detected (B). The spacings between the rising edges and falling edges of neighboring z-lines (C) are then automatically measured and averaged. Dk values that are well outside of the physiological range of possible sarcomere lengths are not included in the analysis.

Eq. 5-7
$$\overline{D}_{SPATIAL} = \frac{\sum_{k=1}^{2n} D_k}{2n}$$

Next, the spacings between these intersects were determined and averaged (Eq. 5-7). In addition to producing a robust method of determining pattern spacing, the uniformity of these spacings was observed to provide a secondary method of calculating the pattern organization $\overline{P}$; this, however, has not shown to be as effective as the fast Fourier transform peak method.

RESULTS

SARCOMERE MAPPING

With the local sarcomere direction, organization, and spacings known, maps of these values and overall analysis can be produced for the cell or aggregate being assessed. For our applications, quiver plots and heatmaps were used to visualize the sarcomere direction and sarcomere organization, respectively (Figure 5-5). Overall assessment of sarcomere alignment could also be determined by weighing the direction values with this new sarcomere quality parameter. As shown in Figure 5-5I, highly aligned sarcomere structures are clearly shown in a quantitative manner via a quality-weighted histogram of sarcomere directions.

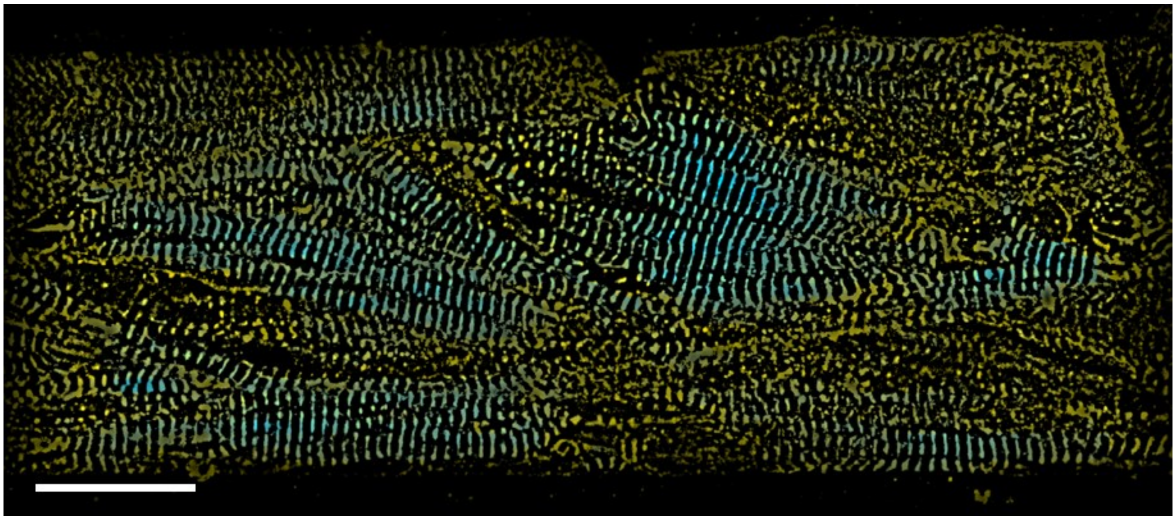

Figure 5-4. Example of map output produced by SGFT technique. This output is a combination of the local contrasted image with the strength map produced by detecting Fourier transform peaks. Regions that are stained positive are tinted yellow, while regions that are determined to have strong sarcomere patterning are automatically tinted teal. This analysis was done on a 60 µm micropattern lane, and the frame of this image contains ~6 hESC-CMs. Scale bar = 20 µm.

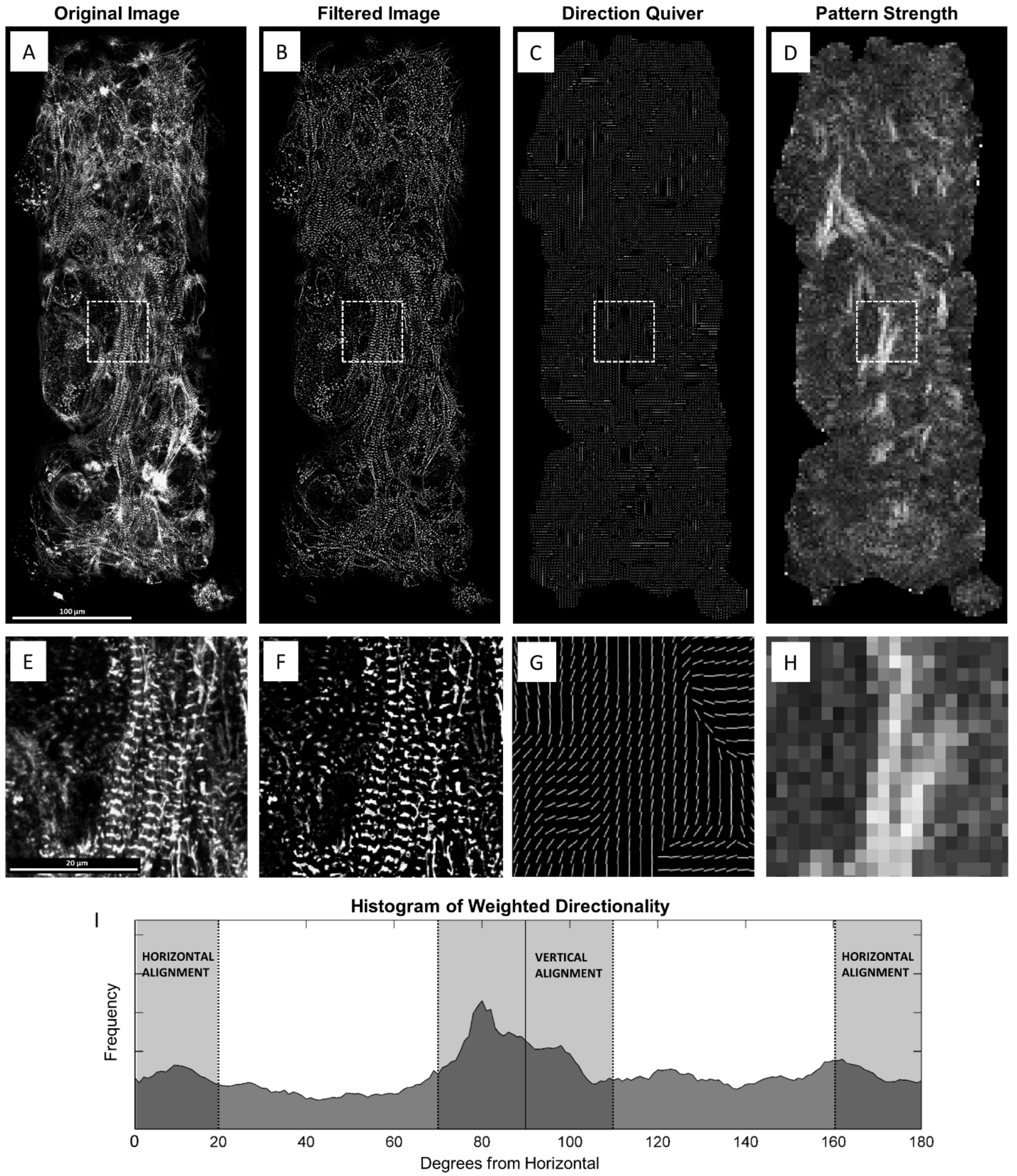

Figure 5-5. Sarcomere mapping of cardiomyocyte aggregates. The original image (A) is first filtered to improve signal-to-noise ratio and account for imaging artifacts (B). Gradient analysis allows quiver plots of sarcomere direction to be produced (C), and lastly, sarcomere pattern strength maps can be produced (D) to indicate regions that have high levels of repeated patterning. Inlays (E-H) show focused view of regions indicated by dashed box. Once the directions and pattern strengths are indicated, the overall distribution of pattern orientations can be determined (I). In this example, the overall population of sarcomeres is clearly oriented more strongly in the vertical direction.

Assessment of Varied Micropattern Lanes Using SGFT

The SGFT technique was used to assess sarcomere patterning of hESC-CMs seeded onto micropatterns of varying lanes, as described in Chapter 3. Actin and α-actinin images of day 30 hESC-CMs, acquired via phalloidin and antibody staining, respectively, were analyzed. The resulting quantitative alignment values of the sarcomeres along these various lane widths matched the qualitative assessments made during initial analysis. Alignment was much higher along micropatterned surfaces with lanes below 100 µm in width. Micropatterns less than 62 µm expressed myofibrils that were over 80% aligned (Figure 5-6).

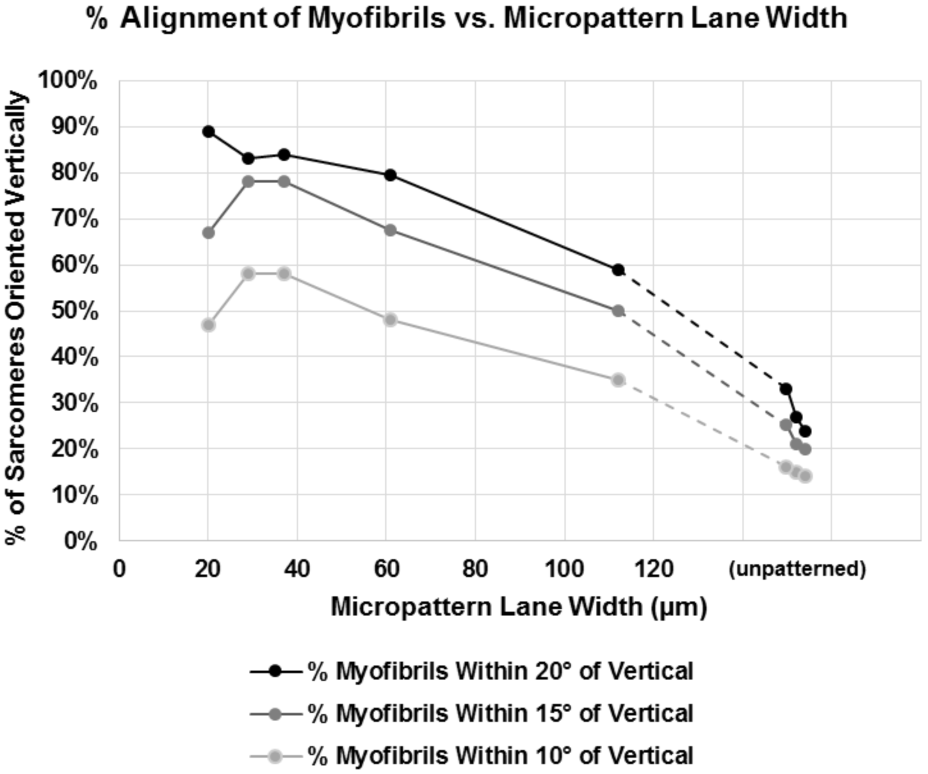

Figure 5-6. Alignment of myofibrils along micropatterns of varying lane widths, determined via SGFT techniques. Micropatterns with widths of less than 100 µm showed a clear improvement in myofibril alignment when compared to very wide or unpatterned substrates.

Additional analysis was conducted to observe how the level of organization, also referred to as the sarcomere strength index, changed with position within micropatterned lanes. A small trend was indeed observed, in that the overall sarcomere strength distribution was noticeably higher in regions that were less than 30 µm away from the nearest micropatterned lane edge.

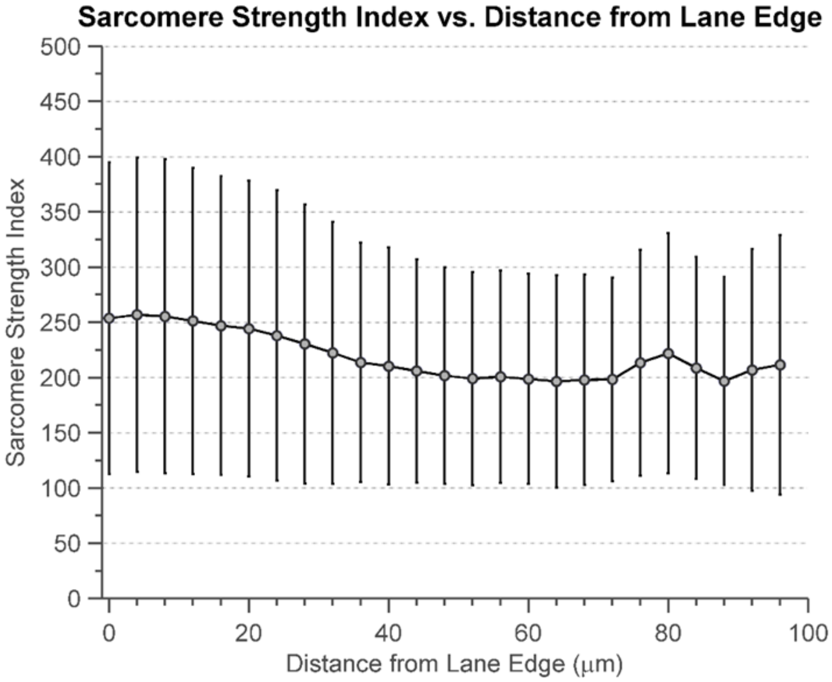

Figure 5-7. Sarcomere strength index vs distance from lane edge. A slight increase in sarcomere strength index was observed for regions within hESC-CM aggregates that were less than 30 µm away from the nearest micropatterned edge. These numbers indicate that the peak detected by the Fourier transform was ~20% higher along the outer regions of micropatterned hESC-CMs. Data compiled from multiple lane widths, and filtered for only regions that contain myofibrils.

QUANTIFICATION OF SARCOMERE LENGTH

A massive amount of data is produced by the SGFT technique, and this section will describe some of these notable findings regarding sarcomere length. First, the sarcomere lengths of hESC-CMs were observed to increase naturally over time, regardless of micropattern environment (Figure 5-8). While other studies have shown increases with sarcomere length over time [Lundy et al, 2013], the magnitude of increase detected by SGFT was even larger than previously reported.

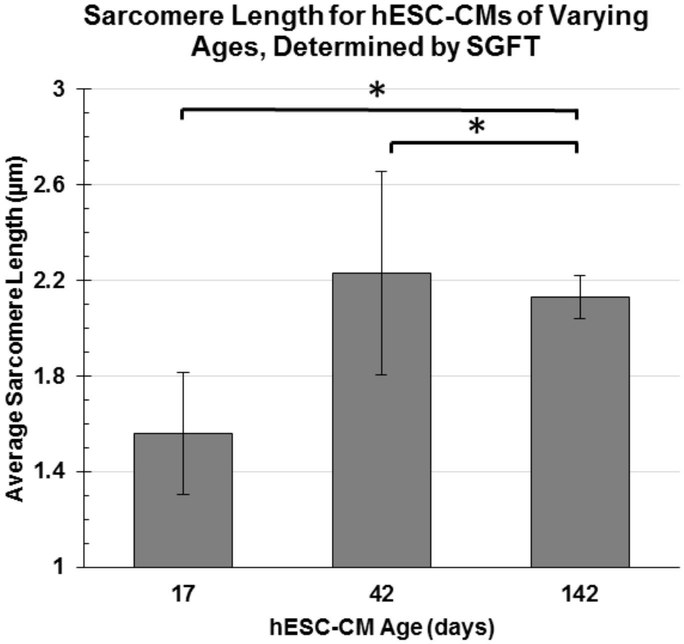

Figure 5-8. Change in sarcomere length with hESC-CM age. A large amount of sarcomere lengthening occurred between day 17 and 42, as determined by the SGFT technique. Upon reaching 2.2 µm, however, no more lengthening seemed to occur. Rather, the sarcomere lengths converge onto this sarcomere length, likely as they align with eachother and are further modified by regulating proteins such as titin and nebulin.). (* significant at $p<0.05$ under t-test)

Another interesting phenomenon that was detected by the SGFT technique was the relation between sarcomere length and the location within a cell or cell aggregate. Striations located within 10 µm of a cell or aggregate edge were considerably shorter than those located inward (Figure 5-9). We hypothesize that this is due to the method of myofibrillogenesis previously described, in which unorganized Z-bodies tend to cluster together at shorter intervals before spreading and forming longer myofibrils.

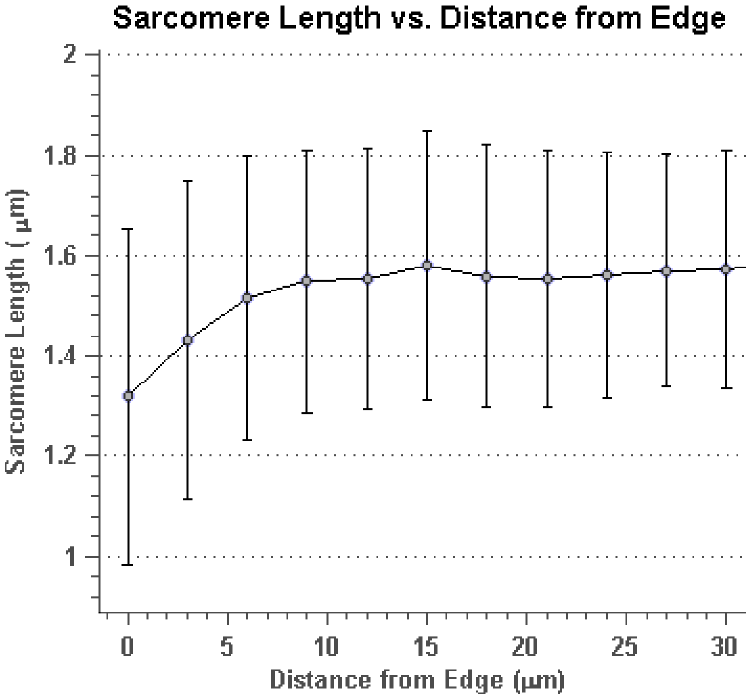

Figure 5-9. Sarcomere length vs. distance from edge of hESC-CM aggregate. Sarcomeres were roughly 200 nm shorter along the outside edges of micropatterned aggregates. This is likely because premyofibrils and nascent myofibrils, whose lengths aren't yet properly mediated by titin and nebulin, were forming along these edges.

DISCUSSION

SIGNIFICANCE FOR CARDIAC PHYSIOLOGY

Myofibrillar disarray occurs in healthy, developing myocardium within embryonic cardiomyocytes, as well as in the diseased myocardium in cases of hypertrophic cardiomyopathy. To the best of our knowledge, no technique has yet been developed that allows analysis of heterogeneous, multidirectional, striated myofibrils. By combining gradient methods with fast Fourier transforms, we have developed a method of quantifying myofibril structure in these cells with considerable accuracy. This level of analysis, in conjunction with, for example, emerging studies of mutation effects on sarcomere assembly, has the potential to produce a substantial amount of insight regarding the mechanisms underlying myofibillogenesis and cardiomyopathies. Additionally, this technique may be used to assess the level of sarcomeric organization achieved in stem cell-derived cardiomyocytes. Quantitative comparisons can then be made between these cells and the target adult cardiomyocyte phenotype to determine their current stage of differentiation.

As mentioned, we observed a clear dependence of sarcomere length on the location within the cellular aggregate. While a decrease of 200 nm is only a ~10% change in overall sarcomere length, it has been well established that even subtle changes in sarcomere length can have dramatic effects on a cell's contractility, as shown by the Frank-Starling Law (Patterson et al., 1914; Allen and Kentish, 1985; Shintani et al., 2014). Since most studies observing sarcomere length measure only an average across entire myofibrils, a more precise measurement of heterogeneous sarcomere lengths could be quite useful for further examination of this length-tension relationship. Similarly, using advanced microscopy techniques, researchers have observed local changes in calcium ion concentrations within contracting cardiomyocytes (Neher, 1998; Bers, 2002; Rizzuto and Pozzan, 2006). Measuring the regional sarcomere lengths within single cardiomyocytes using the SGFT technique could help to discern how these regional Ca^{2+} sparks influence nearby myofibril dynamics.

Another potentially beneficial application of the SGFT technique would be in the investigation of myofibril dynamics over time. Utilizing time-lapse studies, one could observe how values such as sarcomere length distribution, myofibril alignment, and overall myofibril density change with time within a single cell or population of cells.

ADDITIONAL APPLICATIONS IN CLINICAL DIAGNOSIS OF EXTRACELLULAR MATRIX PROTEINS

While this study has been focused largely on the assessment of heterogeneous sarcomere structures in cardiomyocytes, there are several other potential applications for the SGFT technique. The only requirement for the SGFT technique to work properly is for the object under examination to have a patterned, striated morphology. These striations must be regionally aligned, but this alignment can be quite heterogeneous across an entire image.

One such application involves the links between extracellular matrix microstructure and disease states, wound healing, and angiogenesis (Bogenrieder and Herlyn, 2003; Chang and Werb, 2001; Sottile, 2004). For example, recent work has shown that the morphology of collagen fibers in breast cancer tissue is a strong prognostic indicator of the malignancy of the tumor (Provenzano et al., 2006; Conklin et al., 2011). These studies have designated three different categories, referred to as tumor-associated collagen signatures (TACS) that relate to the density, alignment, and relative orientation of collagen fibers to the tumor that they surround. There are several promising techniques that have emerged to provide rapid, unbiased determination of such collagen structures based on elliptical Fourier analysis (Falzon et al., 2008), two-dimensional Fourier transforms (Bayan et al., 2009; Frisch et al., 2012), fractal dimensions (Frisch et al., 2012), curvelet filtering (Bredfeldt et al., 2014), and other advanced fiber tracking methods (Bredfeldt et al., 2014).

The SGFT technique, by combining gradient-based determination of orientation with averaged one-dimensional Fourier transforms, supplements previously established methods by determining more localized trends in pattern strength, fiber spacing, and alignment in heterogeneous collagen biopsies. To test this hypothesis, identical methods to those used for sarcomere analysis were applied on images graciously provided by Jeremy Bredfeldt and Yuming Liu of the UW-Madison Laboratory for Optical and Computational Instrumentation (Y. Liu, personal communication). Human breast cancer biopsies were prepared and imaged using methods described in Bredfeldt et al. (2014), and the resulting analyses are shown in Figure 5-10 and Figure 5-11. The distributions of collagen organization and orientation were clearly detected using the SGFT technique, and statistical analysis of these distributions could be used to provide automated assessment of collagen alignment, which may ultimately be combined with current methods to provide TACS assessment of such samples.

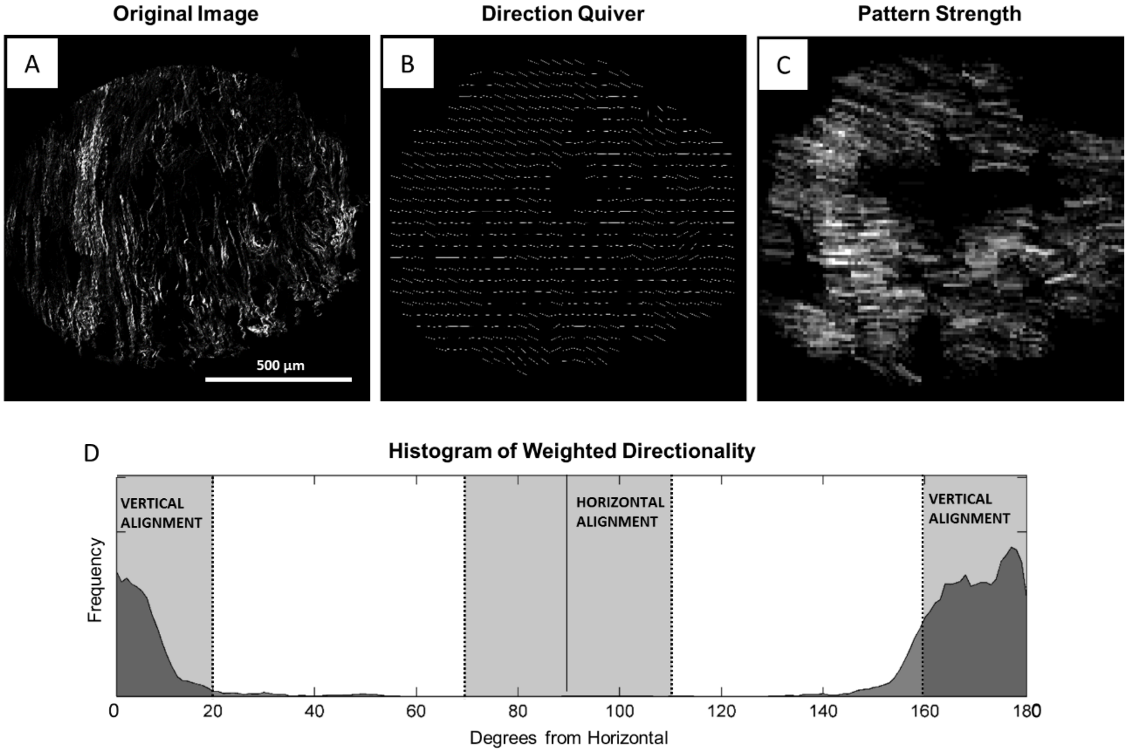

Figure 5-10. Analysis of human breast cancer tissue biopsy, with collagen detected via second-harmonic generation (A). Fiber directionality and pattern strength (B-C) were detected using the SGFT technique. A distribution of fiber orientation (D) clearly indicates strong alignment of the fibers in the vertical direction. Such strong alignment may be indicative of a TACS-2 or TACS-3 prognosis. Including tumor boundaries and calculating relative pattern orientation to the tumor may help to further specify the exact extracellular dynamics at work. (original images provided by Jeremy Bredfeldt and Yuming Liu of LOCI)

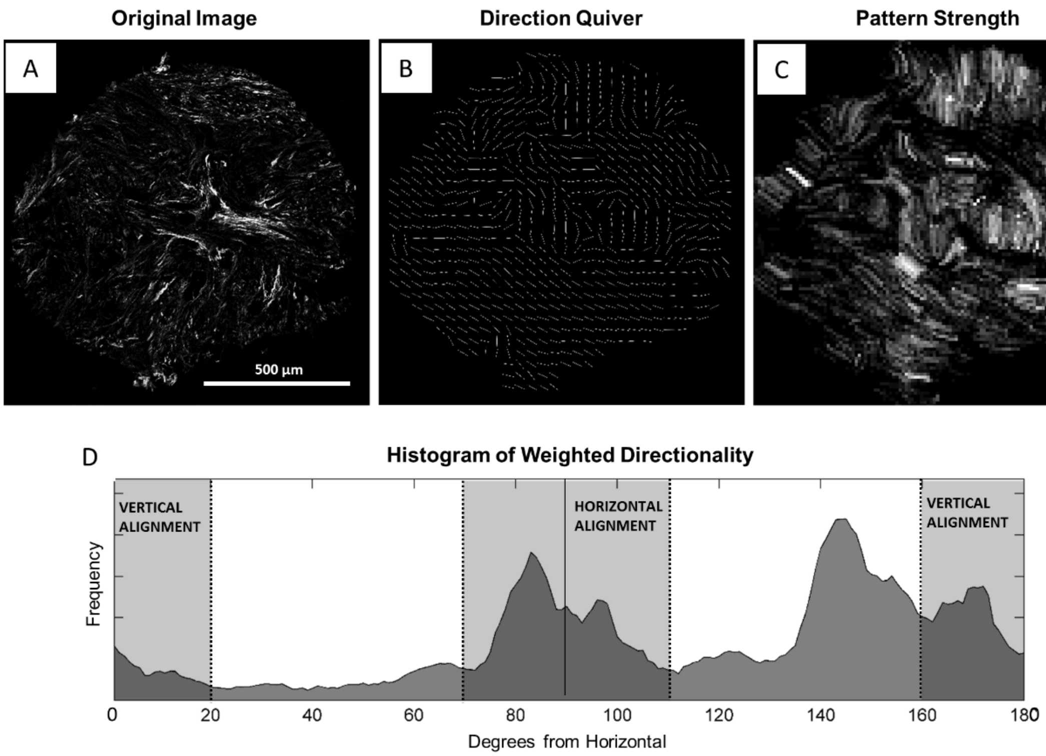

Figure 5-11. Analysis of a more randomly-aligned human breast cancer tissue biopsy, with collagen detected via second-harmonic generation (A). Fiber directionality and pattern strength (B-C) were still effectively detected using the SGFT technique. Unlike in the aligned sample, a more random distribution of fiber orientations was detected (D), suggesting a TACS-1 prognosis. (original images provided by Jeremy Bredfeldt and Yuming Liu of LOCI)

Additional Applications in Neural Rosette Patterning Assessment

Potentially any biological or non-biological processes that produce repeating but heterogeneous/anisotropic striated patterns may be analyzed using the SGFT approach. To test the universality of the technique, neural rosettes formed *in vitro* using pluripotent stem cell sources were also assessed. These rosettes, when successfully formed, produce highly structured, radially symmetric structures with a clear laminin alpha 1 localization along the periphery, and a robust, apical polarization of N-cadherin that branches out radially from the center (Lippmann et al., 2014). SGFT analysis indeed detected this N-cadherin pattern of expression, successfully detecting the radial morphology and pattern organization of the cell-cell junctions within these neural rosettes (Figure 5-12).

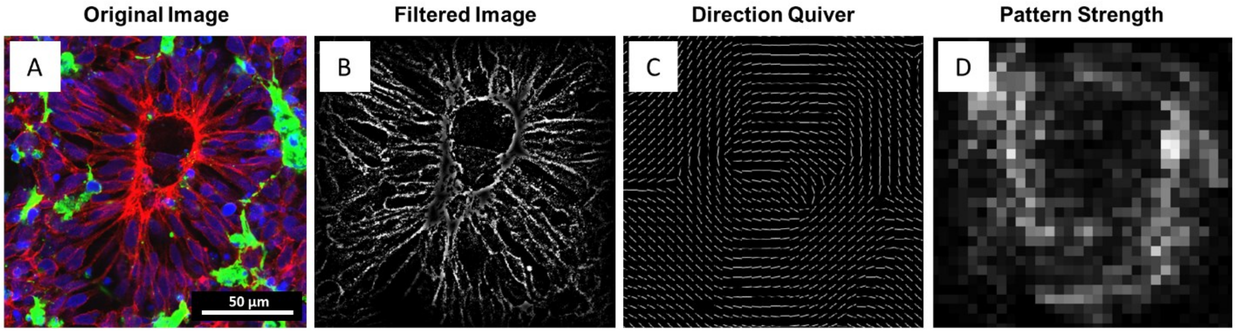

Figure 5-12. Analysis of neural rosettes formed *in vitro* using the SGFT technique. The original image consisted of DAPI (blue), N-cadherin (red), and laminin alpha 1 (green) imunostains (Abcam, Cambridge, UK) (A). The N-cadherin channel was selected and filtered (B). After gradient analysis, a quiver plot showed clear detection of the radial alignments of cell-cell junctions (C). Analysis of the pattern strengths (D) showed clear detection of N-cadherin patterning in specific regions of the image. The method successfully determined the orientations and pattern strength of N-cadherin within the developing neural rosettes.

DRAWBACKS OF THE SGFT TECHNIQUE

While this technique is quite powerful in its ability to detect heterogeneous striated patterns, there are some drawbacks that must be considered during application. First, the computational intensity of this technique is considerably higher than that of most previously-reported techniques. The requirement of the SGFT to conduct thousands of one-directional Fourier transforms produces a great computational demand, particularly when conducting analysis of large cell aggregates with a high analytical resolution. This makes the SGFT approach impractical for real-time analysis of sarcomere dynamics.

Second, the currently proposed techniques are designed for analysis of two-dimensional images only. For ideal modeling and assessment of biological processes, three-dimensional culturing and imaging are required. Translation into the third dimension would be conceptually quite simple, though it would increase the computational demands substantially. To include the third dimension, the gradient-based orientation determination step would simply include a Z component, similar to Eqs. 5-3 and 5-4. Once the three-dimensional direction is determined, intensity profiles could once again be taken; however, pixel intensities along this profile in three dimensions would likely require interpolation between the 8 surrounding pixels.

CONCLUSIONS

Heterogeneous, striated patterning occurs in countless instances in both biology and elsewhere. During this study, we combined gradient methods of orientation determination with 1-dimensional Fourier transform analysis and spatial pattern detection to quantify these patterns. We focused particularly on myofibril formation and organization in immature human cardiomyocytes, though this technique may be used in a variety of other applications. We were able to determine the level of organization and alignment within immature cardiomyocyte myofibers, and also detected a slight increase in sarcomere length at regions toward the center of hESC-derived cardiomyocyte aggregates. The SGFT method was shown to indicate regions of clear radial cellular alignment in developing neural rosettes. Additionally, the SGFT method was utilized to analyze collagen fiber patterning in breast cancer tissue biopsies, resulting in thorough quantification of fiber orientation and organization.

REFERENCES

Allen, D., and Kentish, J. (1985). The cellular basis of the length-tension relation in cardiac muscle. *J. Mol. Cell. Cardiol.* **840**, 821–840.

Bashyam, M. D., Savithri, G. R., Kumar, M. S., Narasimhan, C., and Nallari, P. (2003). Molecular genetics of familial hypertrophic cardiomyopathy (FHC). *J. Hum. Genet.* **48**(2), 55–64.

Bayan, C., Levitt, J. M., Miller, E., Kaplan, D., and Georgakoudi, I. (2009). Fully automated, quantitative, noninvasive assessment of collagen fiber content and organization in thick collagen gels. *J. Appl. Phys.* **105**(10), 102042.

Bers, D. (2002). Cardiac excitation–contraction coupling. *Nature* **415**, 198-205.

Bogenrieder, T., and Herlyn, M. (2003). Axis of evil: molecular mechanisms of cancer metastasis. *Oncogene* **22**(42), 6524–36.

Bray, M.-A., Sheehy, S., and Parker, K. (2008). Sarcomere alignment is regulated by myocyte shape. *Cell Motil. Cytoskel.* **65**(8), 641–651.

Bredfeldt, J. S., Liu, Y., Pehlke, C. A., Conklin, M. W., Szulczewski, J. M., Inman, D. R., Keely, P. J., Nowak, R. D., Mackie, T. R. and Eliceiri, K. W. (2014). Computational segmentation of collagen fibers from second-harmonic generation images of breast cancer. *J. Biomed. Opt.* **19**, 16007.

Bub, G., Camelliti, P., Bollensdorff, C., Stuckey, D. J., Picton, G., Burton, R. A. B., Clarke, K. and Kohl, P. (2010). Measurement and analysis of sarcomere length in rat cardiomyocytes in situ and in vitro. *Am. J. Physiol-Heart C.* 1616–1625.

Chang, C. and Werb, Z. (2001). The many faces of metalloproteases: cell growth, invasion, angiogenesis and metastasis. *Trends Cell Biol.* **11**, S37–43.

Chen, G., Gulbranson, D., Hou, Z., Bolin, J., Ruotti, V., Probasco, M. D., Smuga-Otto, K., Howden, S. E., Diol, N. R., Propson, N. E., et al. (2011). Chemically defined conditions for human iPSC derivation and culture. *Nat. Methods* **8**, 424–429.

Colella, M., Grisan, F., Robert, V., Turner, J. D., Thomas, A. P. and Pozzan, T. (2008). Ca2+ oscillation frequency decoding in cardiac cell hypertrophy: role of calcineurin/NFAT as Ca2+ signal integrators. *P. Natl. Acad. Sci. USA* **105**, 2859–64.

Conklin, M. W., Eickhoff, J. C., Riching, K. M., Pehlke, C. a, Eliceiri, K. W., Provenzano, P. P., Friedl, A. and Keely, P. J. (2011). Aligned collagen is a prognostic signature for survival in human breast carcinoma. *Am. J. Pathol.* **178**, 1221–32.

Cooley, J. and Tukey, J. (1965). An algorithm for the machine calculation of complex Fourier series. *Math. Comput.* **19**, 297–301.

Dabiri, G. A., Turnacioglu, K. K., Sanger, J. M. and Sanger, J. W. (1997). Myofibrillogenesis visualized in living embryonic cardiomyocytes. *P. Natl. Acad. Sci. USA* **94**, 9493–8.

Dobesh, D. P., Konhilas, J. P. and de Tombe, P. P. (2002). Cooperative activation in cardiac muscle: impact of sarcomere length. *Am. J. Physiol-Heart C.* **282**, H1055–H1062.

Falzon, G., Pearson, S. and Murison, R. (2008). Analysis of collagen fibre shape changes in breast cancer. *Phys. Med. Biol.* **53**, 6641–52.

Ferrans, V. J., Morrow, A. G. and Roberts, W. C. (1972). Myocardial ultrastructure in idiopathic hypertrophic subaortic stenosis: a study of operatively excised left ventricular outflow tract muscle in 14 patients. *Circulation* **45**, 769–792.

Francalanci, P., Gallo, P., Bernucci, P., Silver, M. D. and D'Amati, G. (1995). The pattern of desmin filaments in myocardial disarray. *Hum. Pathol.* **26**, 262–6.

Frisch, K. E., Duenwald-Kuehl, S. E., Kobayashi, H., Chamberlain, C. S., Lakes, R. S. and Vanderby Jr., R. (2012). Quantification of collagen organization using fractal dimensions and Fourier transforms. *Acta Histochem.* **114**, 140–4.

Gannier, F., Bernengo, J. C., Jacquemond, V. and Darnier, D. (1993). Measurements of sarcomere dynamics simultaneously with auxotonic force in isolated cardiac cells. *IEEE T. Bio-Med. Eng.* **40**, 1226–1232.

Go, A. S., Mozaffarian, D., Roger, V. L., Benjamin, E. J., Berry, J. D., Blaha, M. J., Dai, S., Ford, E. S., Fox, C. S., Franco, S., et al. (2014). *Heart disease and stroke statistics--2014 update: a report from the American Heart Association.*

Hong, L., Wan, Y. and Jain, A. (1998). Fingerprint image enhancement: algorithm and performance evaluation. *IEEE T. Pattern Anal.* **20**, 777–789.

Jacot, J., McCulloch, A. and Omens, J. (2008). Substrate stiffness affects the functional maturation of neonatal rat ventricular myocytes. *Biophys. J.* **95**, 3479–3487.

Kabir, M. M., Inavalli, V. V. G. K., Lau, T.-Y. and Toussaint Jr., K. C. (2013). Application of quantitative second-harmonic generation microscopy to dynamic conditions. *Biomed. Opt. Express* **4**, 2546–54.

Karlon, W. J., Covell, J. W., McCulloch, a D., Hunter, J. J. and Omens, J. H. (1998). Automated measurement of myofiber disarray in transgenic mice with ventricular expression of ras. *Anat. Rec.* **252**, 612–25.

Karlon, W. J., McCulloch, a D., Covell, J. W., Hunter, J. J. and Omens, J. H. (2000). Regional dysfunction correlates with myofiber disarray in transgenic mice with ventricular expression of ras. *Am. J. Physiol-Heart C.* **278**, H898–906.

Kattman, S., Witty, A., Gagliardi, M., Dubois, N., Niapour, M., Hotta, A. and Keller, G. M. (2011). Stage-specific optimization of activin/nodal and BMP signaling promotes cardiac differentiation of mouse and human pluripotent stem cell lines. *Cell Stem Cell* **8**, 228–240.

Katz, A. M. (2002). Ernest Henry Starling, his predecessors, and the "law of the heart." *Circulation* **106**, 2986–2992.

Korte, F. S. and McDonald, K. S. (2007). Sarcomere length dependence of rat skinned cardiac myocyte mechanical properties: dependence on myosin heavy chain. *J. Physiol.* **581**, 725–39.

Laflamme, M. A. and Murry, C. E. (2005). Regenerating the heart. *Nat. Biotechnol.* **23**, 845–56.

Laflamme, M. A., Chen, K. Y., Naumova, A. V, Muskheli, V., Fugate, J. A., Dupras, S. K., Reinecke, H., Xu, C., Hassanipour, M., Police, S., et al. (2007). Cardiomyocytes derived from human embryonic stem cells in pro-survival factors enhance function of infarcted rat hearts. *Nat. Biotechnol.* **25**, 1015–1024.

Lian, X., Hsiao, C., Wilson, G., Zhu, K., Hazeltine, L. B., Azarin, S. M., Raval, K. K., Zhang, J., Kamp, T. J. and Palecek, S. P. (2012). Robust cardiomyocyte differentiation from human pluripotent stem cells via temporal modulation of canonical Wnt signaling. *P. Natl. Acad. Sci. USA*.

Lippmann, E. S., Estevez-Silva, M. C. and Ashton, R. S. (2014). Defined human pluripotent stem cell culture enables highly efficient neuroepithelium derivation without small molecule inhibitors. *Stem Cells* **32**, 1032–42.

Lundy, S., Zhu, W., Regnier, M. and Laflamme, M. A. (2013). Structural and functional maturation of cardiomyocytes derived from human pluripotent stem cells. *Stem Cells Dev.* **22**, 1991–2002.

Mandenius, C.-F., Steel, D., Noor, F., Meyer, T., Heinzle, E., Asp, J., Arain, S., Kraushaar, U., Bremer, S., Class, R., et al. (2011). Cardiotoxicity testing using pluripotent stem cell-derived human cardiomyocytes and state-of-the-art bioanalytics: a review. *J. Appl. Toxicol.* **31**, 191–205.

Mansour, H., de Tombe, P. P., Samarel, A. M. and Russell, B. (2004). Restoration of resting sarcomere length after uniaxial static strain is regulated by protein kinase Cε and focal adhesion kinase. *Circ. Res.* **94**, 642–649.

Mardia, K. V. and Jupp, P. E. (2000). *Directional Statistics*. New York: John Wiley & Sons.

Maron, B. J., McKenna, W. J., Danielson, G. K., Kappenberger, L. J., Kuhn, H. J., Seidman, C. E., Shah, P. M., Spencer, W. H., Spirito, P., Ten Cate, F. J., et al. (2003). American College of Cardiology/European Society of Cardiology clinical expert consensus document on hypertrophic cardiomyopathy. *J. Am. Coll. Cardiol.* **42**, 1687–1713.

Nectow, A., Gil, E., Kaplan, D. L. and Kilmer, M. E. (2013). A statistical algorithm for assessing cellular alignment. *J. Biomed. Mater. Res. A* **101**, 884–891.

Nectow, A., Kilmer, M. E. and Kaplan, D. L. (2014). Quantifying cellular alignment on anisotropic biomaterial platforms. *J. Biomed. Mater. Res. A* **102**, 420-428.

Neher, E. (1998). Vesicle pools and Ca 2+ microdomains: new tools for understanding their roles in neurotransmitter release. *Neuron* **20**, 389–399.

Patterson, S. and Starling, E. (1914). On the mechanical factors which determine the output of the ventricles. *J. Physiol.* **48**, 357-379.

Provenzano, P. P., Eliceiri, K. W., Campbell, J. M., Inman, D. R., White, J. G. and Keely, P. J. (2006). Collagen reorganization at the tumor-stromal interface facilitates local invasion. *BMC Med.* **4**, 38.

Rao, R. A. R., Mehta, M. R. and Toussaint Jr., K. C. (2009). Fourier transform-second-harmonic generation imaging of biological tissues. *Opt. Express* **17**, 14534–42.

Rizzuto, R. and Pozzan, T. (2006). Microdomains of intracellular Ca2+: molecular determinants and functional consequences. *Physiol. Rev.* **86**, 369–408.

Robertson, C., Tran, D. and George, S. (2013). Concise Review: Maturation Phases of Human Pluripotent Stem Cell-Derived Cardiomyocytes. *Stem Cells* **31**, 829–837.

Salick, M. R., Napiwocki, B. N., Sha, J., Knight, G. T., Chindhy, S. A., Kamp, T. J., Ashton, R. S. and Crone, W. C. (2014). Micropattern width dependent sarcomere development in human ESC-derived cardiomyocytes. *Biomaterials* **35**, 4454–64.

Shintani, S. A., Oyama, K., Kobirumaki-Shimozawa, F., Ohki, T., Ishiwata, S. and Fukuda, N. (2014). Sarcomere length nanometry in rat neonatal cardiomyocytes expressed with α-actinin-AcGFP in Z discs. *J. Gen. Physiol.* **143**, 513–24.

Sottile, J. (2004). Regulation of angiogenesis by extracellular matrix. *Biochim. Biophys. Acta* **1654**, 13–22.

Stout, A. L., Wang, J., Sanger, J. M. and Sanger, J. W. (2008). Tracking changes in Z-band organization during myofibrillogenesis with FRET imaging. *Cell Motil. Cytoskel.* **65**, 353–67.

Tarar, S. and Kumar, E. (2013). Fingerprint Image Enhancement: Iterative Fast Fourier Transform Algorithm and Performance Evaluation. *IJHIT* **6**, 11–20.

Willems, E., Spiering, S., Davidovics, H., Xia, Z., Dawson, M., Cashman, J. and Mercola, M. (2011). Small-molecule inhibitors of the Wnt pathway potently promote cardiomyocytes from human embryonic stem cell–derived mesoderm. *Circ.* **109**, 360 –364.

Xu, F., Beyazoglu, T., Hefner, E., Gurkan, U. A. and Demirci, U. (2011). Automated and adaptable quantification of cellular alignment from microscopic images for tissue engineering applications. *Tissue Eng. Pt. C-Meth.* **17**, 641–649.

Yang, L., Soonpaa, M., Adler, E., Roepke, T. K., Kattman, S. J., Kennedy, M., Henckaerts, E., Bonham, K., Abbott, G. W., Linden, R. M., et al. (2008). Human cardiovascular progenitor cells develop from a KDR+ embryonic-stem-cell-derived population. *Nature* **453**, 524–528.

Yaniv, Y., Juhaszova, M., Wang, S., Fishbein, K. W., Zorov, D. B. and Sollott, S. J. (2011). Analysis of mitochondrial 3D-deformation in cardiomyocytes during active contraction reveals passive structural anisotropy of orthogonal short axes. *PLoS One* **6**, e21985.

Zhang, J., Klos, M., Wilson, G. F., Herman, A. M., Lian, X., Raval, K. K., Barron, M. R., Hou, L., Soerens, A. G., Yu, J., et al. (2012). Extracellular matrix promotes highly efficient cardiac differentiation of human pluripotent stem cells: the matrix sandwich method. *Circ. Res.* **111**, 1125–1136.

CHAPTER 6: ASSESSMENT OF hESC-CMs CULTURED ON OPTIMIZED MICROPATTERN SUBSTRATES

INTRODUCTION

Once the micropattern platform was optimized, single-cell wide lanes of cardiomyocytes with robust, aligned sarcomere structures and mature-like cell-cell junctions were formed, matching *in vivo* cardiomyocyte morphologies more closely than in previous cellular *in vitro* models. Next, in order to understand the mechanisms of sarcomere organization in human cardiomyocytes, several methods of assessment were conducted in order to investigate the causes behind this improved sarcomere structure. This section describes these assessments, which consist of immunostaining of cytoskeletal and cell-cell junction proteins, qRT-RT PCR analysis of micropatterned and unpatterned hESC-CMs, and live imaging studies using fluorescent actin to observe myofibrillogenesis in real time. During these studies, multiple modes of myofibrillogenesis were detected and cell boundary constraints were observed to play a large role in how these myofibrils were formed.

MATERIALS AND METHODS

IMMUNOSTAINING

Several stains were conducted to observe how hESC-CMs responded to the optimized micropatterned substrate. α-actinin and connexin-43 stains were utilized to observe myofibril structure and cell-cell junction formation, respectively. Mitochondrial stains utilizing MitoTracker Red (Life Technologies) were used to assess mitochondrial localization within these cardiomyocytes.

Antibody staining for α-actinin and connexin-43 were conducted as previously described [Salick et al, 2014] in chapter 3. Briefly, hESC-CMs were cultured on micropatterned substrates for variable periods of time. The cells were fixed with 4% paraformaldehyde (Electron Microscopy Sciences), permeabilized with 0.1% Triton (Sigma), and treated with blocking solution. Primary antibody solution was applied for two hours, and secondary antibody solution was applied for one hour, followed by treatment with ProLong Gold Antifade (Life Technologies) and mounting. Samples were imaged on a Nikon A1RSi Confocal Microscope with attached Photometrics CoolSNAP HQ2 camera. Nis-D Elements – Advanced Research v.3.22 software was used for image acquisition and analysis.

For mitochondrial assays, MitoTracker Red (Life Technologies) was diluted to 1mM in DMSO (Sigma) and stored in aliquots at -20°C. This was diluted to 200nM in RPMI/B27 prior to staining, which was then used to treat the cells. Cells were allowed to incubate in this medium for 30 minutes. Two PBS washes were then applied, and the cells were fed with normal RPMI/B27 medium. Cells were then immediately fixed and immunostained (see above) for co-stain studies.

QRT RT-PCR

Three sample conditions were studied: control, patterned, and unpatterned. hESC-CMs were differentiated and purified, and pre-seeded at 1:3 on day 17. On day 25, the control cells were maintained on TCPS coated with laminin 1-1-1, and cells for the patterned and unpatterned samples were seeded onto laminin 1-1-1 coated coverslips. As the name implies, some of the coverslips contained 37 µm micropatterned lanes, while others were uniformly coated with laminin 1-1-1. Cells were cultured for 4 days on these varying surfaces, after which their RNA was isolated.

Compared to most other cell types, myocytes exhibit low transcriptional activity. For this reason, high-sensitivity assessment of RNA production is needed. For RNA extraction, an RNAqueous Micro Kit (Ambion) was found to be the most effective, compared to TRI Reagent (Life Technologies) methods and the RNeasy Plus Mini Kit (Qiagen) (Figure 6-1).

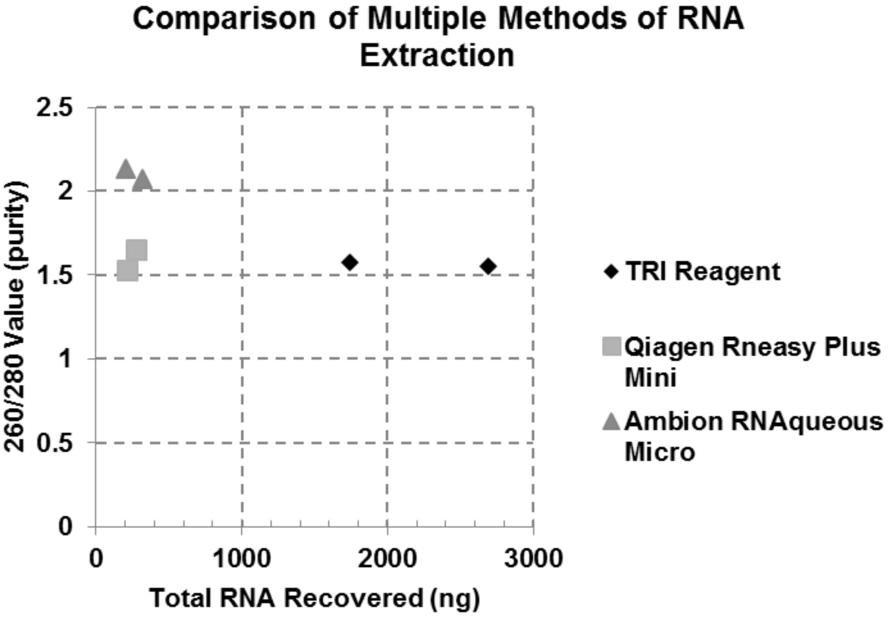

Figure 6-1. Results from various RNA Isolation methods. A 260/280 spectrum value, acquired via Nanodrop, should be around 2.0 for samples of high RNA purity. While TRI reagent methods produced more RNA, which is often lacking in myocyte cultures, it was determined that the purity of the Ambion RNAqueous Micro Kit was required.

For this method, cells are dissociated with Trypsin for 10 minutes for monolayers, or 15 minutes for tightly grouped fibrous structures. The trypsin is then deactivated with a 10% FBS media, and the cells are lysed. A series of washes and treatments are conducted using spin tubes. Once isolation is completed, DNAse treatment is applied to ensure that genomic DNA is not included in the samples. RNA samples are then immediately used or stored at -80°C.

RNA purities and concentrations were determined via Nanodrop 2000 (Thermo Scientific), and reverse transcription was conducted using a QuantiTect Kit (Qiagen). No-amplification controls were conducted and standard curve samples were also prepared, using genomic human DNA samples (Life Technologies) at controlled concentrations. Standard curve analysis showed efficiencies between 1.95 and 2.05 for select TaqMan primers.

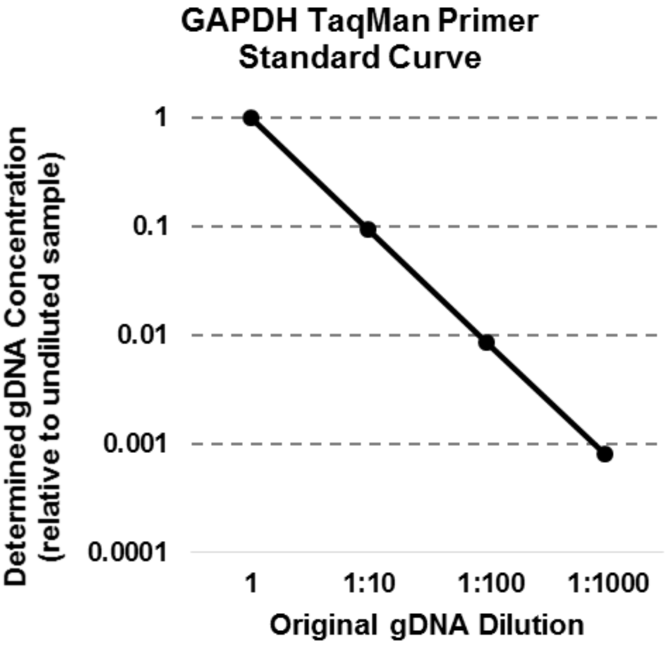

Figure 6-2. Example standard curve of TaqMan primers utilizing known concentrations of gDNA. Curves showed efficiencies between 1.95 and 2.05 for tested primers.

qRT RT-PCR was then conducted using TaqMan Fast Advanced Master Mix (Life Technologies), TaqMan Primers (Life Technologies), and the sample cDNA. 20 µL reactions were conducted on a StepOne Plus PCR machine. The examined genes were GAPDH (Glyceraldehyde 3-phosphate dehydrogenase), MYH6 (alpha myosin heavy chain), MYH7 (beta myosin heavy chain), ACTA2 (alpha smooth muscle actin), TNNT2 (cardiac troponin T), and ATP2A2 (sarco/endoplasmic reticulum Ca^{2+}-ATPase).

LIVE CELL OBSERVATION

Live high-magnification imaging of F-actin was conducted to observe how myofibrillogenesis occurred in these cultures, in order to gain a better understanding of the means by which the highly organized sarcomeres develop over time. Once the lane width, ECM, seeding density, and seeding age parameters were optimized, a live-imaging apparatus was constructed. To construct the apparatus, the bottom surface of a 12-well tissue culture polystyrene plate was coated with a biocompatible, high-adhesive, double-sided tape (9472LE acrylic adhesive transfer tape, 3M). Precautions were made to ensure that the tape was flush with the bottom surface of the plate, since any folds would induce leakage. 6mm holes were then drilled through the tape and bottom surface of the plate and micropatterned cover slips were attached face-up to the plates. ECM coating and cell seeding were then conducted normally on these modified plates.

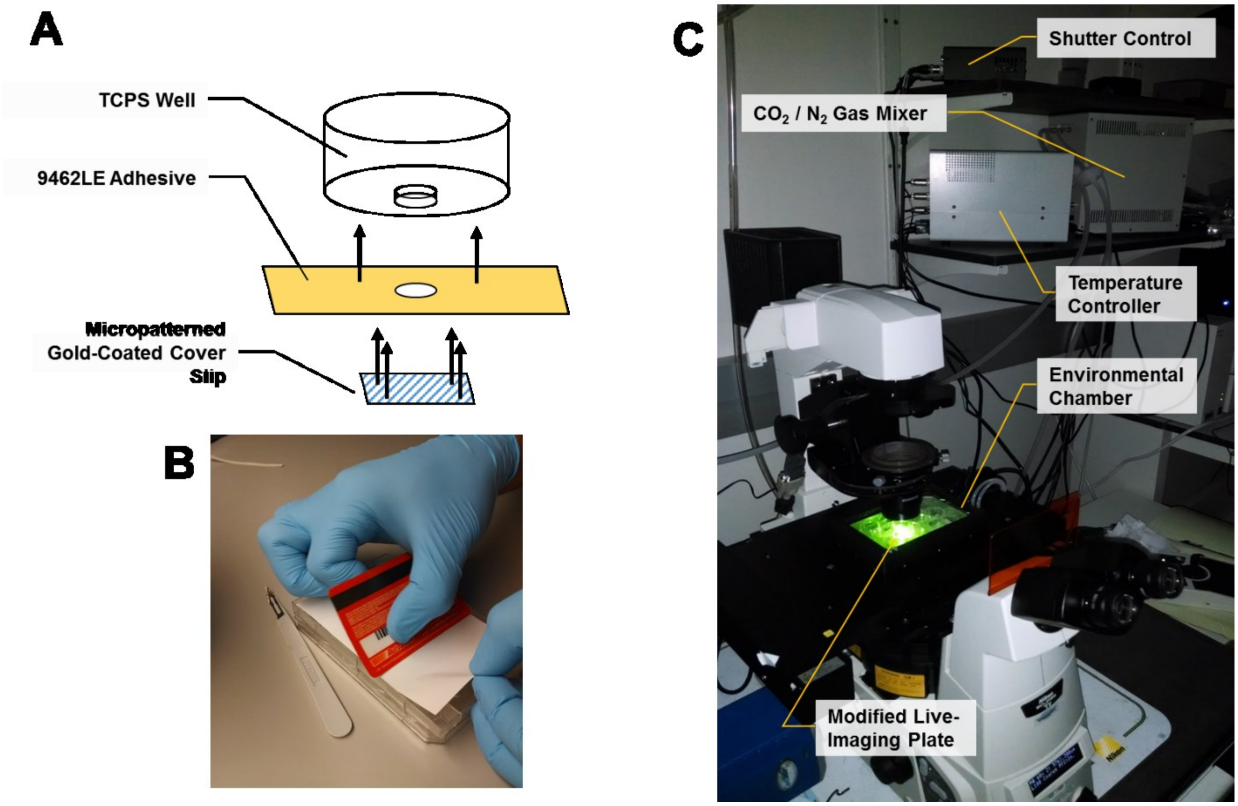

Figure 6-3. Sample preparation and live imaging setup. Biocompatible 9462LE double-sided adhesive was placed on the bottom of a tissue culture polystyrene plate, and a 6mm hole was drilled through them. A micropatterned gold-coated cover slip was then placed over the hole from below (A). Care was taken to ensure a tight seal between the adhesive film and the plate (B). The incubated imaging setup consisted of a Nikon Ti-E epifluorescent microscope, automated using NIS-D Elements software (C). A temperature controller was utilized to maintain physiological temperatures for the environmental chamber. Since oil objectives were used, the objective was also heated to 37°C to ensure that heat did not diffuse too rapidly through the oil contact at the bottom of the sample. Standard cell culture conditions (20% O_2) were maintained in the environmental chamber using a Tokai Hit gas mixer.

F-actin was imaged using CellLight BacMam 2.0 Actin-RFP (Life Technologies), which is a fusion construct of human actin and TagRFP. The vector for the construct is an insect baculovirus, which does not replicate in human cells. The cells were transfected at 10 particles per cell (PPC) and imaged 2 days after transfection, when it was easy to detect the cells that had been transfected. At day 2 after infection, hESC-CMs were seeded onto the modified live-imaging plates containing a micropatterned glass slide with 37 µm laminin 1-1-1 lanes. The cells were given 7 hours to begin attachment onto the micropatterns, and were then imaged every 7.5 minutes for 16 hours.

The live-imaging setup consisted of a Nikon Ti-E epifluorescent microscope utilizing Perfect Focus and running Nis-D Elements Software. The cells were maintained at 37°C in a temperature-controlled, hydrated environmental chamber. The 60X oil objective used for imaging was also maintained at 37° to prevent heat from diffusing through the oil. The gas mixture was maintained at 20% O_2 using a Tokai Hit gas mixer.

RESULTS

IMMUNOSTAINING

hESC-CMs cultured on the optimized micropattern platforms exhibited extremely robust sarcomere organization (Figure 6-4). This high level or sarcomere organization was visible within 5 days of culture on the micropatterned substrates, and persisted for more than 130 days on these substrates. Using the SGFT technique for quantification, approximately 90% of myofibrils were aligned within 20° of vertical in these culture conditions.

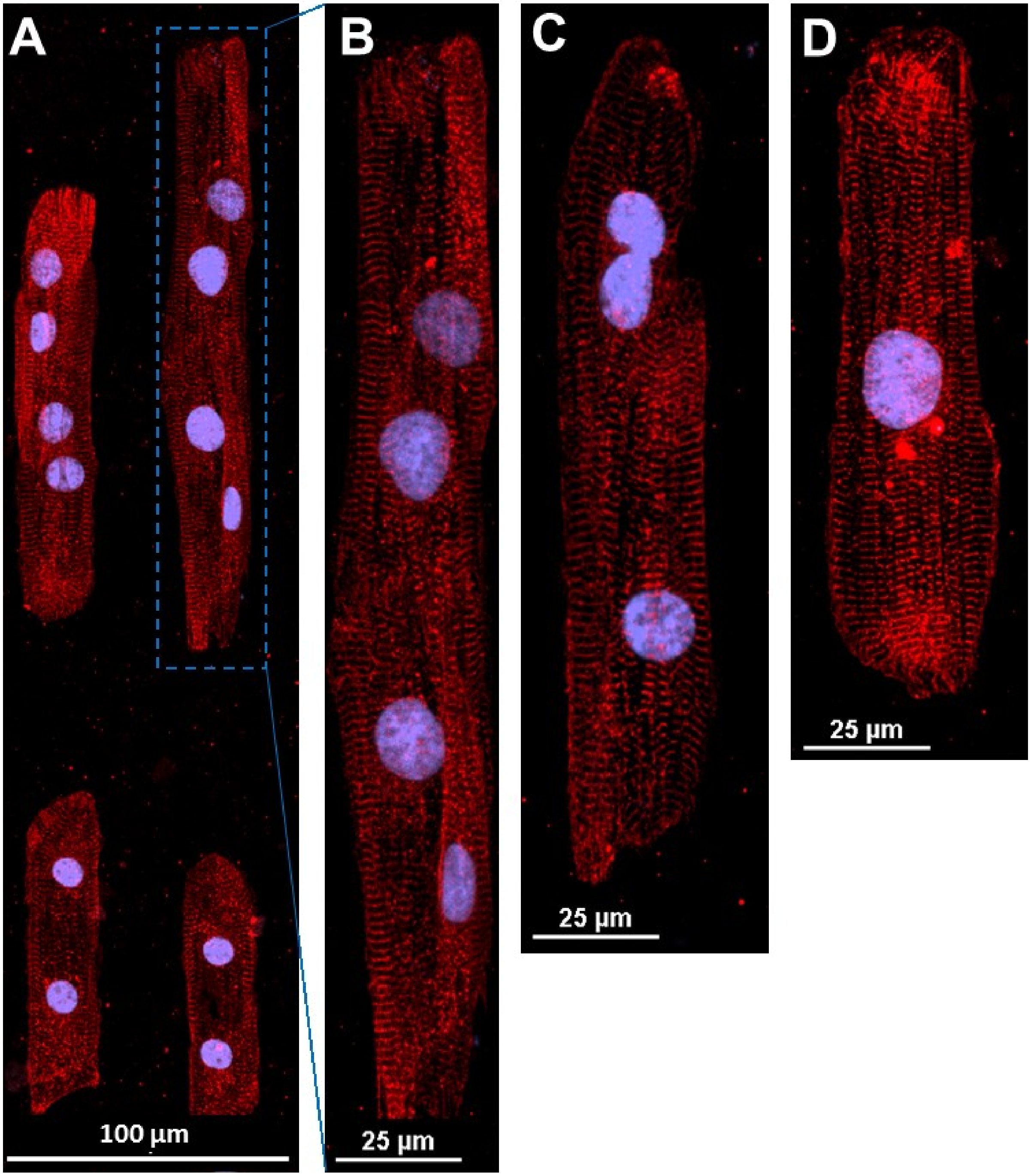

Figure 6-4. hESC-CMs seeded onto optimized platform and immunostained for α-actinin (red) and DAPI (blue). A large number of hESC-CMs formed brick-shaped morphologies with extremely robust, aligned sarcomere structures. Most cells appeared multinucleated, and many cells were grouped into fibers consisting of 2 or more cells (B, C), though several lone and mononucleated hESC-CMs were still present (D). These cells were imaged after 30 days of culture on the optimized platform; however, this level of striation is visible as early as 5 days after seeding onto the micropatterns.

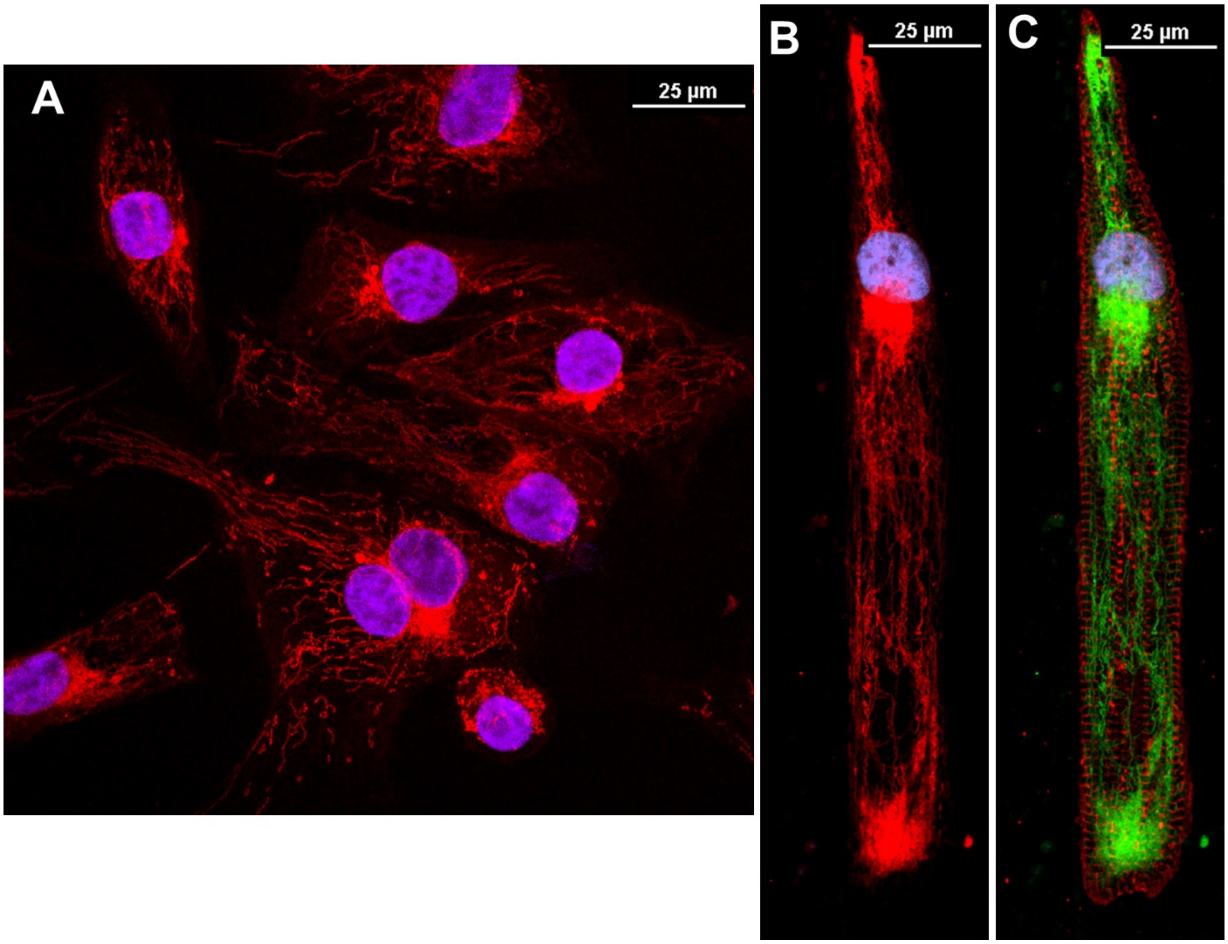

Figure 6-5. Comparison of mitochondria expression in normally-cultured vs. micropatterned, aligned cardiomyocytes. Mitochondria shown in red, DAPI in blue. Immature hESC-CMs cultured normally on matrigel-coated TCPS (A) express more randomly-oriented mitochondria. Micropatterned cardiomyocytes express mitochondria that align strongly with the micropattern direction (B). Co-stains with alpha-actinin (red), mitochondria (green) and DAPI (blue) show that mitochondria align alongside myofibrils, as is typically seen in mature cardiomyocytes (C).

Mitochondrial expression also appeared to match physiological morphologies more closely on the aligned, optimized micropattern cultures (Figure 6-5). In unaligned cultures, mitochondria localize near nuclei, and have a random distribution within the cytoplasm. In micropatterned cultures, there is still considerable nuclear localization, as well as an interesting localization at the polar ends of the cardiomyocytes. Additionally, strong alignment of the mitochondria was observed, matching the organization of the myofibrils. Thus, this model could likely help researchers to investigate mitochondrial morphogenesis in addition to myofibrillogenesis.

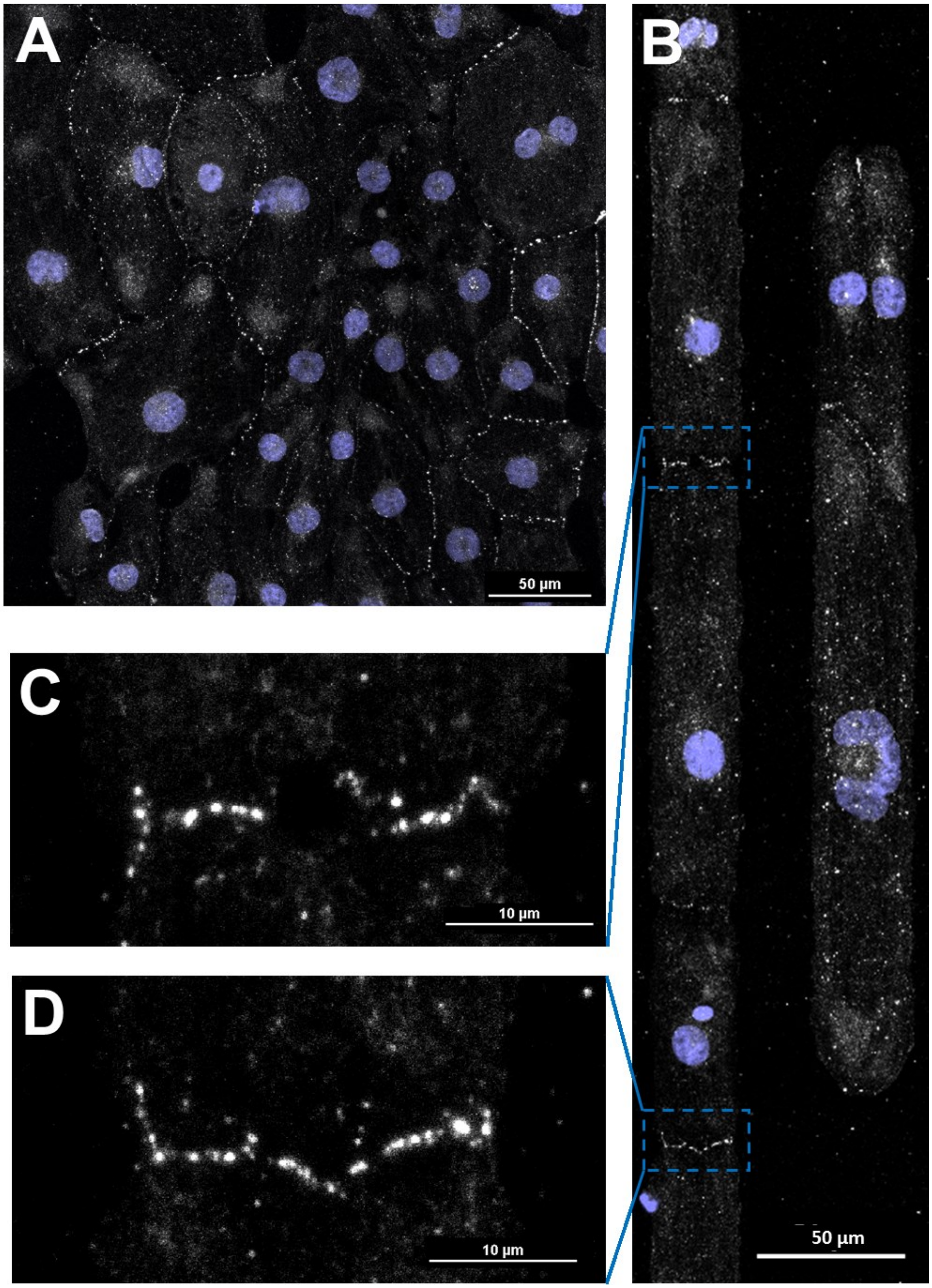

Figure 6-6. Connexin 43 (white) and DAPI (blue) staining of unpatterned and pattern hESC-CMs. In unpatterned culture, Cx43 is clearly expressed in a punctate manner along all cell-cell boundaries. Cells are typically in uniform contact with other hESC-CMs in all directions, so the Cx43 expression is not polarized (A). In the micropatterned platform, hESC-CMs form single-cell well fibers, and thus only have cell-cell contacts on polar ends of the cell, which is more physiologically relevant (B). (C) and (D) show focused views of select cell-cell junctions.

Lastly, connexin 43, a common gap junction protein, was imaged. The presence of connexin 43 between cells indicates that some level of cell coupling is occurring, which is required for proper modeling of hESC-CM function. Connexin 43 forms into gap junction plaques, which are concentrated regions along the intercalated disks of neighboring cardiomyocytes. This tendency to cluster is what gives connexin 43 its punctate appearance during high-resolution microscopy. Our studies showed that both unpatterned and patterned hESC-CMs expressed strong connexin 43 signaling along cell-cell junctions (Figure 6-6). In the patterned substrates, however, the hESC-CMs form into single-cell wide fibers, and thus cell-cell junctions are only possible at the polar ends of the cells. Connexin 43 only localized along these ends, resulting in a polarized expression that is more representative of physiological expression than in randomly-oriented hESC-CMs.

QRT RT-PCR

Most of the genes examined showed little to no change in response to the different culturing platform. ATP2A2, ACTA2, and TNNT2 all showed only a slight increase in expression on the laminin 1-1-1 coated cover slips (Figure 6-7). Additionally, there was no significant difference in RNA expression between patterned and unpatterned coverslips, indicating that the differences in sarcomeric organization may not be occurring strongly at the transcriptional level.

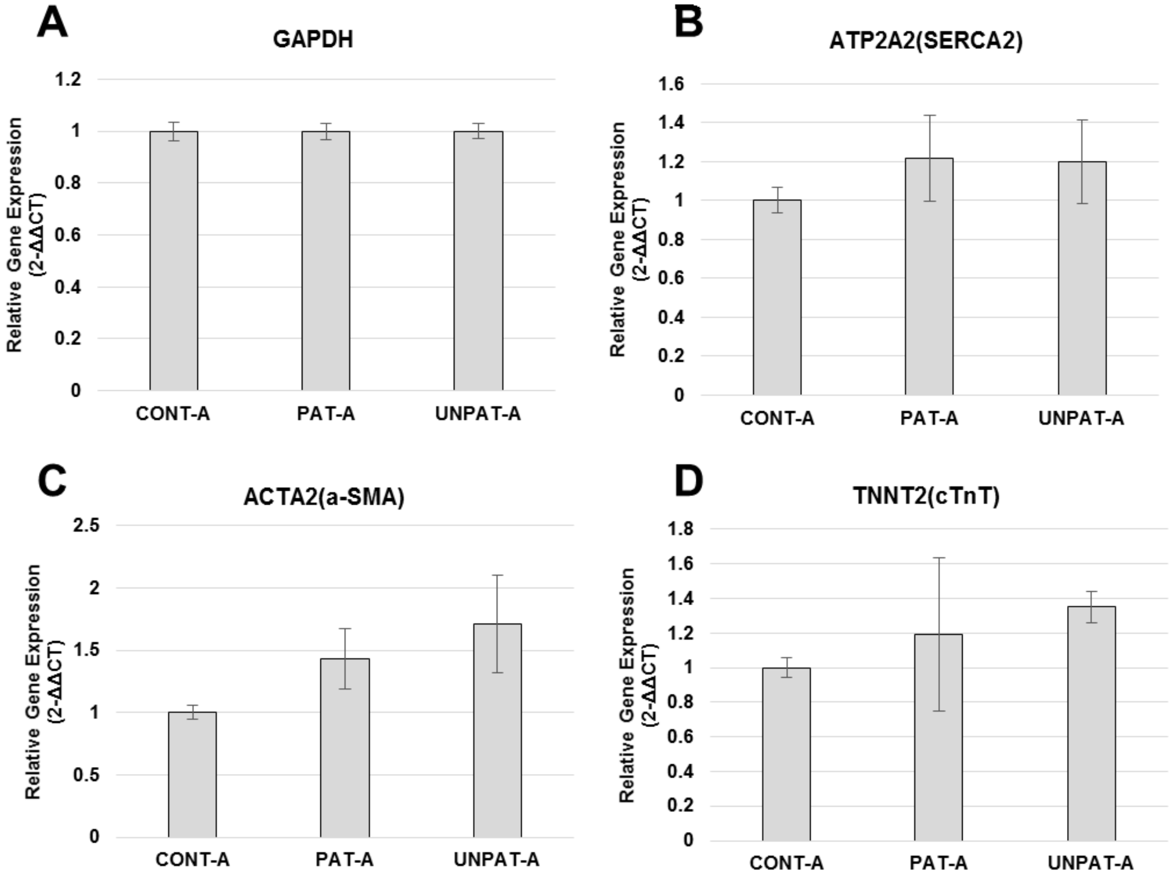

Figure 6-7. qRT RT-PCR results for control, patterned, and unpatterned hESC-CMs. GAPDH, used as a housekeeping gene (A) showed minimal variation within each sample type. ATP2A2 was selected to determine level of sarcoplasmic reticulum development. A slight increase was observed on both patterned and unpatterned samples (B), though this increase was minimal. ACTA2 showed a slight increase as well (C); alpha smooth muscle actin is often used as an indicator of immaturity of cardiomyocytes, so this small change may suggest that the hESC-CMs are not, in fact, reaching a more mature phenotype. TNNT2 showed a minimal increase (D) on patterned and unpatterned samples.

Notable differences did occur, however, in the gene coding for alpha myosin heavy chain expression (Figure 6-8). MYH6 increased 4.5 fold between the control and cover slip samples. Once again, however, no difference was noted between patterned and unpatterned cover slips. Importantly, MYH7, the gene encoding for beta myosin heavy chain, did not change considerably across these samples. This means that the α:β ratio between these culture conditions is quite different. Since the α:β myosin heavy chain ratio has several implications regarding development, pathology, contractile rate, etc., this is something that should be further investigated in later studies.

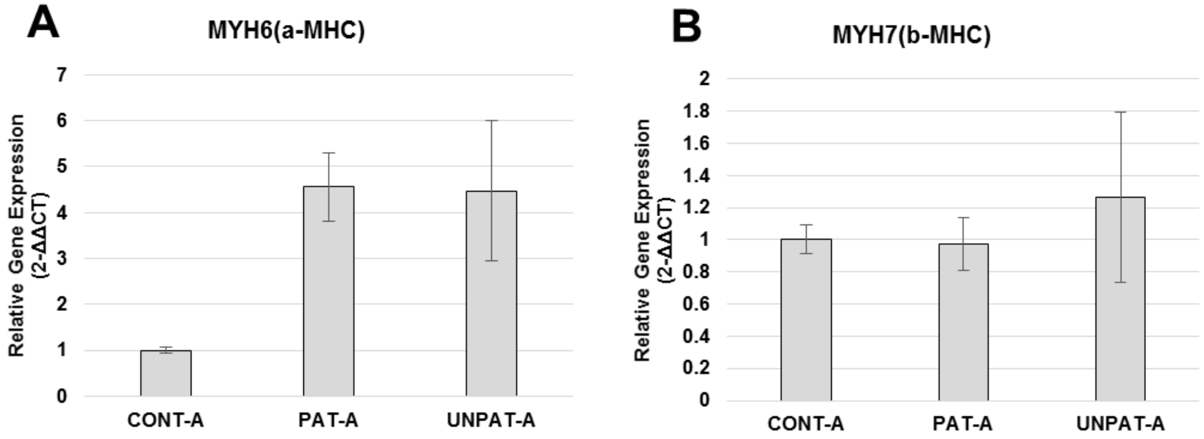

Figure 6-8. MYH6 and MYH7 gene expression in control, patterned, and unpatterned samples. A large increase in the alpha myosin heavy chain gene occurred on the glass cover slip samples, while the beta myosin heavy chain gene remained constant. This indicates a large change in α:β ratio between the culture conditions. Note that there was still no notable difference between patterned and unpatterned sample types.

LIVE CELL OBSERVATION

To better understand how myofibrillogenesis is improved by the aligned micropatterned lanes, we conducted live observation of the F-actin within the cells using an actin-RFP insect baculovirus. The live-cell imaging apparatus was constructed and several individual cells were observed over a period between 7 hours and 22 hours after being seeded onto the micropatterned substrate. Multiple modes of myofibrillogenesis were observed, in addition to other myofilament modifications such as Z-disk addition, alignment, and complete myofibril deconstruction.

Unconstrained edge myofibrillogenesis

Cells seeded onto the micropatterned lanes exhibited constrained and unconstrained edges. That is, cell boundaries that lined up with the edges of micropatterned lanes were constrained in motion, while boundaries that could expand along uncovered regions of ECM-coated lanes were unconstrained in motion. Myofibrillogenesis occurring along the unconstrained edges matched the theories described in Chapter 1 quite closely. Specifically, lamellipodia extend along the unconstrained boundaries of the cell, and large stress fibers, parallel to the cell edge, are formed as focal adhesions are established. These stress fibers likely contain interspersed α-actinin, which then condense into Z-bodies as the stress fibers move in from the lamellipodia into the lamellum (Figure 6-9, Figure 6-10). The Z-bodies, forming nascent myofibrils, then organize further and bind laterally with neighboring mature myofibrils in an additive manner to form sarcomeres that are parallel to the cell edge. This is likely the phenomenon that occurs in unpatterned cardiomyocytes *in vitro*, leading to their often circumferential patterning of sarcomeres.

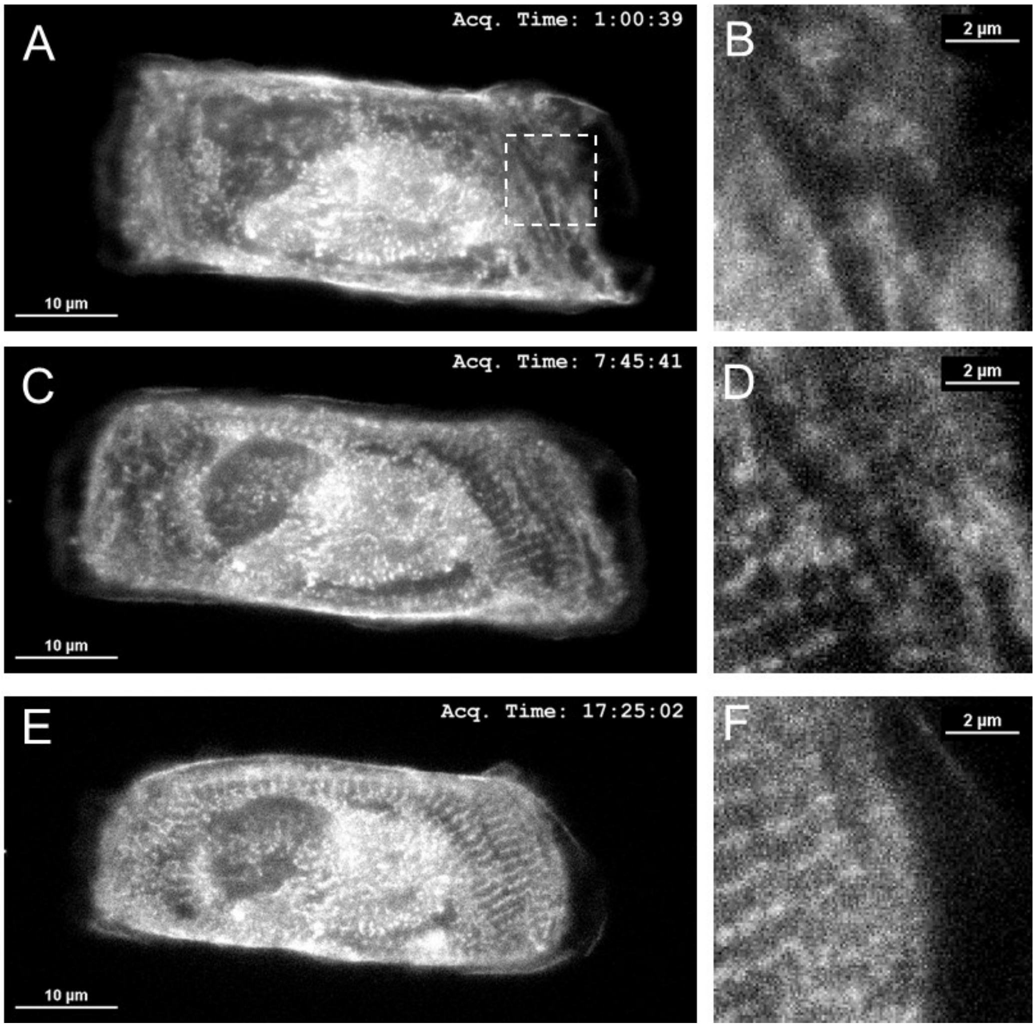

Figure 6-9. Example of unconstrained edge myofibrillogenesis. hESC-CMs were seeded onto horizontally-oriented, 37 µm-wide, micropatterned laminin 1-1-1 lanes. A single cell is shown (A, C, E) with focus on the unconstrained on the right side of the cell (B, D, F). Stress fibers originate along the dynamic lamellipodia and translate inward from the outside edge. As they reach ~8-15 µm from the outside edge, z-bodies begin to condense and form nascent myofibrils (D). As time progresses, nascent myofibrils bind to neighboring mature myofibrils to form large, organized structures parallel to the cell edge (F).

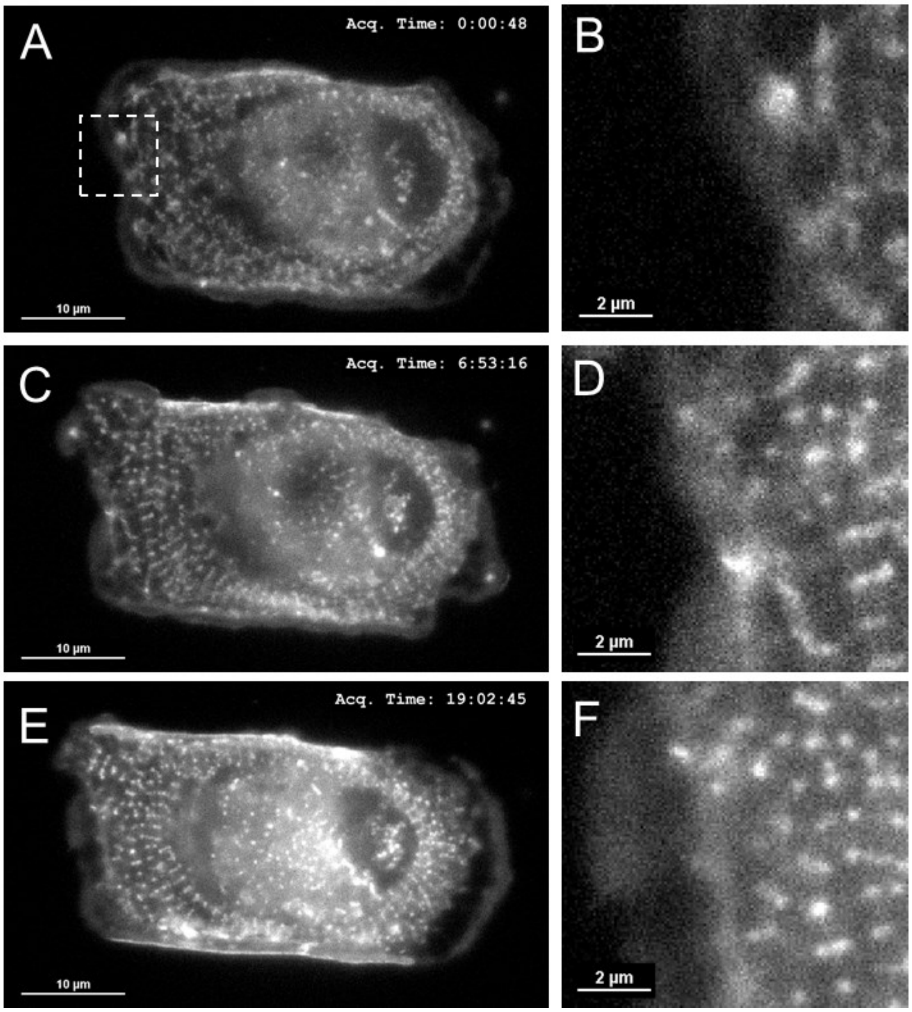

Figure 6-10. Additional example of unconstrained edge myofibrillogenesis. A single hESC-CM is shown (A, C, E) with emphasis on the unconstrained boundary on the left side of the cell (B, D, F). At ~7 and ~19 hours after seed, a large number of premyofibrils and nascent myofibrils were observed, as shown by the loosely organized z-bodies. Toward the center of the cell, nascent myofibrils clustered to form more organized sarcomere structures.

Constrained edge myofibrillogenesis

Within this system, cells had one or two constrained edges, depending on whether or not they were spanning the entire lane. Along these constrained cell edges, myofibrillogenesis appeared to occur in a different manner. Rather than having stress fiber-like premyofibrils translating inward from lamellipodia, myofibrils appeared to build in from the outside surface directly

(Figure 6-11, Figure 6-12). The resulting myofibrils are parallel to the constrained surface and thus parallel to the micropatterned lane. In most cells, this myofibril organization dominates the cell, which leads to the aligned, organized sarcomere patterning that is regularly observed in this system.

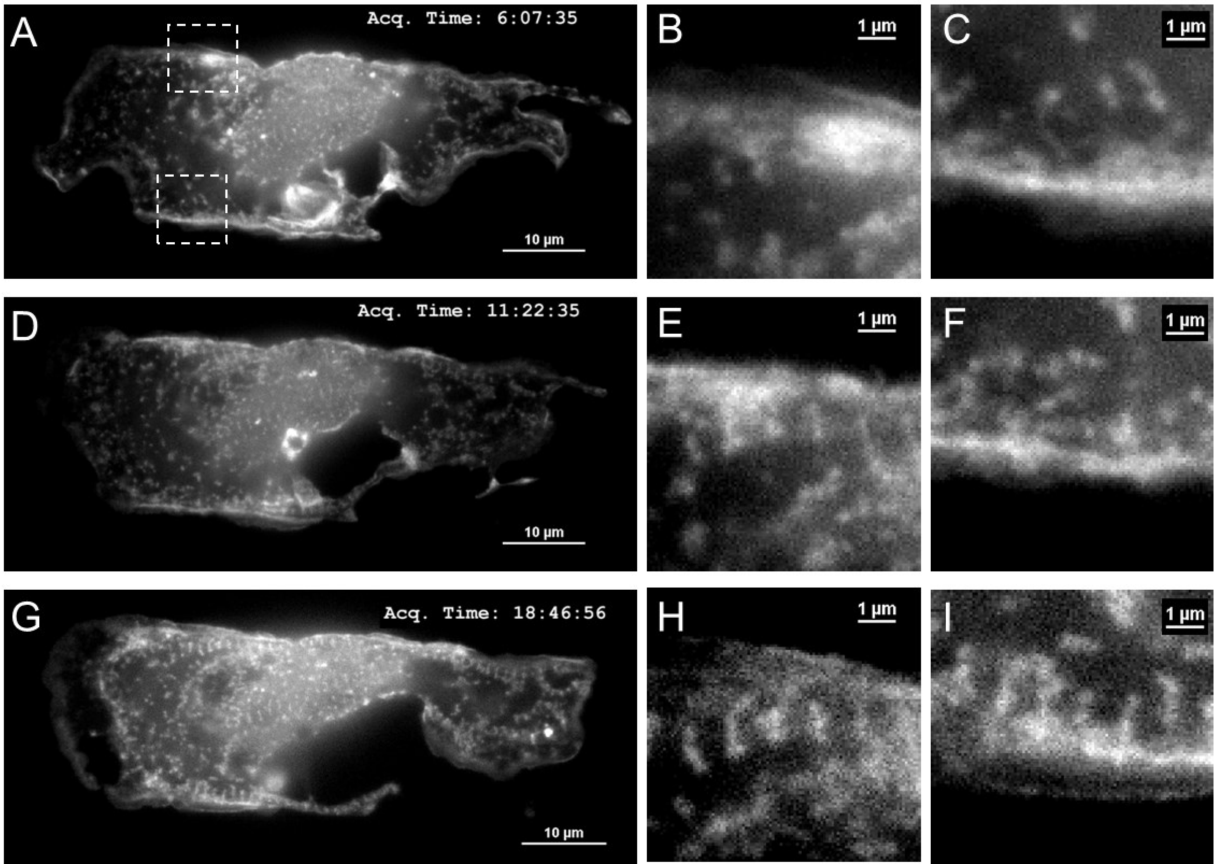

Figure 6-11. Example of constrained edge myofibrillogenesis. hESC-CMs were seeded onto horizontally-oriented, 37 µm-wide, micropatterned laminin 1-1-1 lanes. A single cell is shown (A, D, G) with focus on the constrained edges on the top and bottom of the cell (B-C, E-F, H-I). As of 6 hours after seeding, the hESC-CM showed minimal sarcomere structure (A-C). Premyofibrils were visible 11 hours of seeding (D-F), which expanded inward (G-I). Note that striations are visible within 1 µm of the cell edge along constrained boundaries, unlike in myofibrillogenesis that occurs within the lamella.

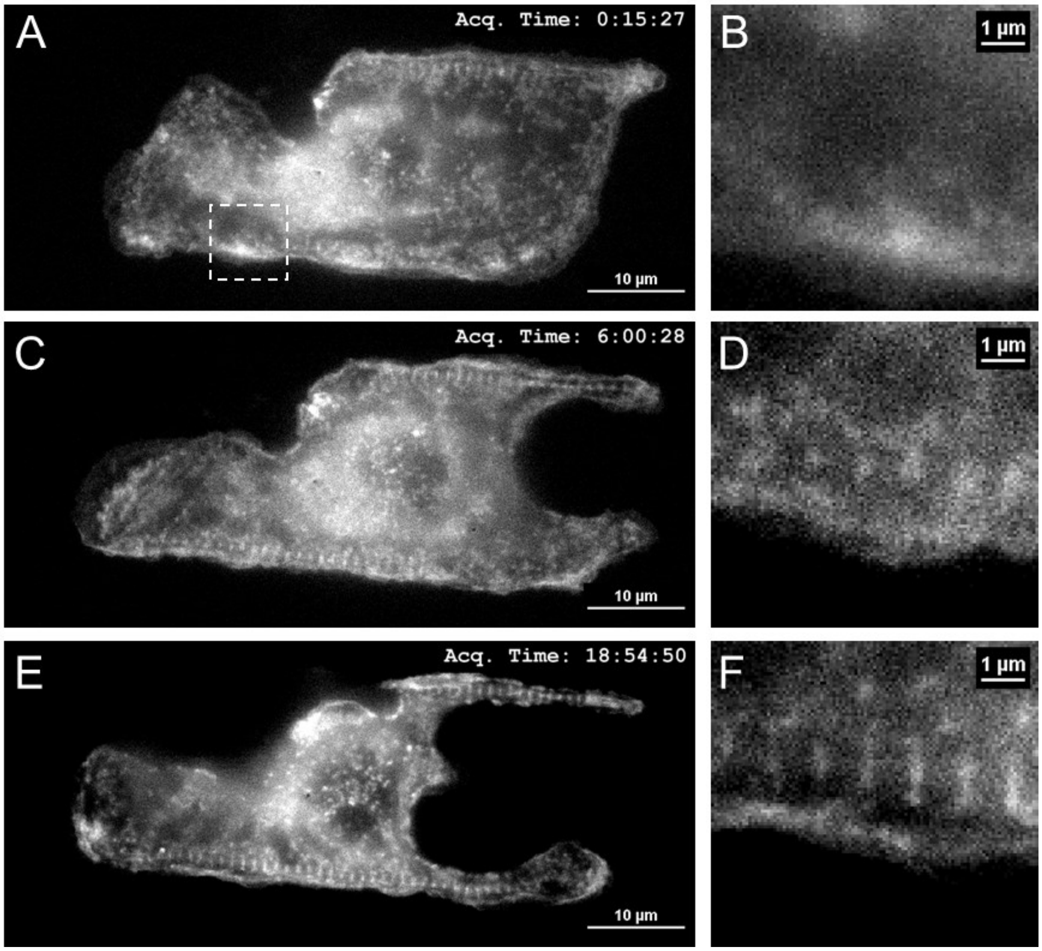

Figure 6-12. An additional example of constrained edge myofibrillogenesis. This is once again showing a single cell (A, C, E), though this particular example has a neighboring cell on the right that is pressing in, as shown by the large indent that forms over time. In this case, premyofibrils were present within 6 hours of being seeded (C-D). Once again, organized sarcomere structures are formed within ~1 µm of the cell boundary along constrained edges (D, F).

Medial myofibrillogenesis

The third observed mode of myofibrillogenesis was by far the least common, though its potential existence could promote some theories of myofibrillogenesis that are less well known and less frequently discussed [Sanger et al, 2005]. This mode, referred to as medial myofibrillogenesis, occurred when the hESC-CMs had already produced considerable striated structures on their periphery based on the other two previously-mentioned modes. When myofibril structures from opposite ends of a cell approach each other, such that spacings of ~5 µm existed between connected myofibrils, a rapid polymerization of Z-disks was observed in this space along the period of only 6 hours (Figure 6-13).

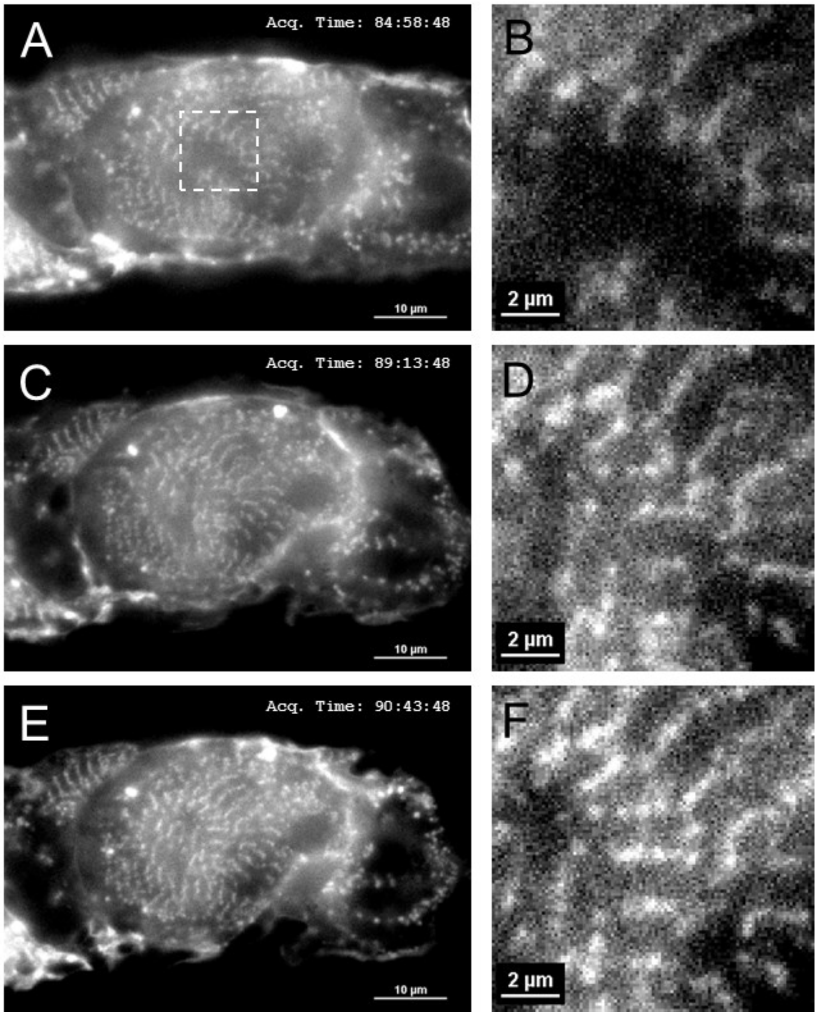

Figure 6-13. Medial myofibrillogenesis observed in hESC-CM. A single cell is shown (A, C, E), with emphasis on the center (B, D, F). Rather than developing along cell edges, myofibrils appear to form off of existing sarcomeres. Note that this occurs between ~85 hours and ~91 hours after seeding, which is far later than the other two forms of observed myofibrillogenesis. It is hypothesized that mature myofibrils must first surround a region before it can be "filled in" by nascent myifbrils (D, F). Note that the newly forming z-disks still show a punctate morphology, with highly variable sarcomere lengths typical of nascent of myofibrils. This further suggests that these are, indeed, newly-forming sarcomeres.

DISCUSSION

Immunostaining of the micropatterned hESC-CM showed that the sarcomeres, mitochondria, and cell-cell junctions were forming morphologies similar to those observed *in vivo*. Previous chapters have discussed the importance of organized sarcomere structure on cardiomyocyte function. The presence and localization of mitochondria around these myofibrils, however, is another critical component of proper cardiomyocyte function. The heart is extremely metabolically active due to its high energy demands, which is why heart disease often correlates to mitochondrial disorders [Williams, 1995]. Since this model provides a much more accurate representation of mitochondrial assembly in hESC-CMs, it could be quite useful for further studies into the mechanisms and interactions between mitochondria and myofibrils. Similarly, the polarized expression of connexin 43 along cell-cell junctions produces the appearance of primitive intercalated disks. An easily producible *in vitro* model of intercalated disk formation could be extremely beneficial for investigations into cell coupling.

The qRT RT-PCR results indicated no distinct change in RNA expression between patterned and unpatterned cells among the genes examined. This doesn't necessarily indicate, however, that the protein composition of the cells is identical. Further protein-focused studies will need to be conducted to see if expression is truly identical between culture conditions. One interesting finding during qRT RT-PCR analysis was the increase in α:β myosin heavy chain expression in cells cultured on coated glass cover slips. As discussed in chapter 1, the ratio between alpha and beta chains varies significantly, depending on the maturation [Reiser et al, 2001], location, and pathology of the cardiomyocytes being observed [Miyata et al, 2000; Lowes et al, 1997]. Generally, α-MHC is higher in fetal hearts when compared to adult hearts. It is also more common in atria than in the ventricles. Lastly, α-MHC is present in nonfailing left ventricles, but not in failing left ventricles. More thorough analysis of the causality behind this trend *in vitro* may provide insight regarding why this phenomenon occurs *in vivo*.

The live observation of F-actin in this system was novel in several ways. First, to the best of our knowledge, this is the first direct observation of myofibrillogenesis in human cardiomyocytes. Second, this is the first time active myofibrillogenesis has been observed in constrained and unconstrained surfaces. Lastly, the presence of a third, medial mode of myofibrillogenesis was observed, which may contribute to further understanding of the mechanisms involved in sarcomere development.

Current models of myofibrillogenesis state that z-bodies form along the sarcolemma and translate inward, grouping up to form organized z-disks and mature myofibrils [Sanger and Sanger, 2002]. Our observations of this mechanism along unconstrained edges of cardiomyocytes matched this theory quite closely. That is, stress fiber-like actin bundles translated inward from lamellipodia, and Z-bodies formed within these stress fibers that eventually clustered together with previously-established myofibrils to form large, mature myofibrils. Along constrained edges, however, myofibrils containing clear Z-disks appeared to be growing inward, directly from the sarcolemma. One likely reason for this is that focal adhesions are already strongly expressed along these edges, and thus the stress fibers along these sides form larger bundles more quickly. We hypothesize that, instead of starting as curved, amorphous actin structures, these stress fibers are more quickly forming as large, load-bearing structures, and this tension within the stress fibers may play a role in the progression toward nascent myofibrils.

The medial myofibrillogenesis observed in this model does not match the sarcolemmal z-body theory that describes the unconstrained- and possibly constrained- modes of sarcomere development. It is possible that the free surface in the vertical direction- that is, the tightly-adhered bottom of the cell or the unattached top- are still producing premyofibrils that are extending inwards. However, one would still expect to see long, stress fiber-like premyofibrils extending toward existing mature myofibrils if this were the case. Rather, this mode would be more congruous with previous theories of myofibrillogenesis [Sanger et al, 2005; Costa et al, 2002; Ehler et al, 1999; Lu et al, 1992] that state that some thick and thin filaments may form independently or may build in from previously established myofibrils. While examples of the z-body theory has been shown repeatedly here and in previous studies [Murakami et al 1993; Rhee et al, 1994; Tullio et al, 1997], there does stand the possibility of multiple modes working simultaneously, and perhaps cooperatively, to form the robust, organized sarcomeres that are seen in mature cardiomyocytes. Further studies are needed to expound on this possibility.

CONCLUSIONS

Purified hESC-CMs were cultured on the optimized micropattern platform and their protein expression, gene expression, and myofibrillogenesis were observed. Particular focus was placed on the means by which the myofibrils aligned on the micropatterned substrates. Immunostaining showed highly organized, aligned myofibrils on the optimized micropatterned lanes. α-actinin, connexin 43, and mitochondria stains showed mature-like localization within the micropatterned hESC-CMs. qRT RT-PCR analysis showed a consistent expression profile between patterned and unpatterned cells for all examined genes. A difference was observed, however, in the α:β myosin heavy chain ratio on cells cultured on glass cover slips rather than on the standard TCPS.

Live observation showed differences between constrained and unconstrained myofibrillogenesis, as well as a sudden increase in myofibril density in the centers of a few cells. These combined observations indicate that the micropatterned hESC-CMs could act as a valuable model for observing sarcomere dynamics, in addition to other protein cardiomyocyte functions.

REFERENCES

Costa, M. L., Escaleira, R. C., Rodrigues, V. B., Manasfi, M. and Mermelstein, C. S. (2002). Some distinctive features of zebrafish myogenesis based on unexpected distributions of the muscle cytoskeletal proteins actin, myosin, desmin, alpha-actinin, troponin and titin. *Mech. Dev.* **116**, 95–104.

Ehler, E., Rothen, B. M., Hämmerle, S. P., Komiyama, M. and Perriard, J. C. (1999). Myofibrillogenesis in the developing chicken heart: assembly of Z-disk, M-line and the thick filaments. *J. Cell Sci.* **112 (Pt 10)**, 1529–1539.

Lowes, B. D., Minobe, W., Abraham, W. T., Rizeq, M. N., Bohlmeyer, T. J., Quaife, R. A., Roden, R. L., Dutcher, D. L., Robertson, A. D., Voelkel, N. F., et al. (1997). Changes in gene expression in the intact human heart. Downregulation of alpha-myosin heavy chain in hypertrophied, failing ventricular myocardium. *J. Clin. Invest.* **100**, 2315–2324.

Lu, M. H., DiLullo, C., Schultheiss, T., Holtzer, S., Murray, J. M., Choi, J., Fischman, D. A. and Holtzer, H. (1992). The vinculin/sarcomeric-alpha-actinin/alpha-actin nexus in cultured cardiac myocytes. *J. Cell Biol.* **117**, 1007–1022.

Miyata, S., Minobe, W., Bristow, M. R. and Leinwand, L. a. (2000). Myosin Heavy Chain Isoform Expression in the Failing and Nonfailing Human Heart. *Circ. Res.* **86**, 386–390.

Murakami, N., Trenkner, E. and Elzinga, M. (1993). Changes in expression of nonmuscle myosin heavy chain isoforms during muscle and nonmuscle tissue development. *Dev. Biol.*

Reiser, P. J., Portman, M. A., Ning, X. H. and Schomisch Moravec, C. (2001). Human cardiac myosin heavy chain isoforms in fetal and failing adult atria and ventricles. *Am. J. Physiol. Heart Circ. Physiol.* **280**, H1814–H1820.

Rhee, D., Sanger, J. M. and Sanger, J. W. (1994). The Premyofibril : Evidence for Its Role in Myofibrillogenesis. *Cell Motil. Cytoskeleton* **28**, 1–24.

Sanger, J. W. and Sanger, J. M. (2002). Myofibrillogenesis in Cardiac Muscle. In *Myofibrillogenesis* (ed. Dube, D. K.), pp. 3–20. New York: Birkhauser Boston.

Sanger, J. W., Kang, S., Siebrands, C. C., Freeman, N., Du, A., Wang, J., Stout, A. L. and Sanger, J. M. (2005). How to build a myofibril. In *Journal of Muscle Research and Cell Motility*, pp. 343–354.

Tullio, a N., Accili, D., Ferrans, V. J., Yu, Z. X., Takeda, K., Grinberg, a, Westphal, H., Preston, Y. a and Adelstein, R. S. (1997). Nonmuscle myosin II-B is required for normal development of the mouse heart. *Proc. Natl. Acad. Sci. U. S. A.* **94**, 12407–12.

Williams, R. S. (1995). Cardiac involvement in mitochondrial diseases, and vice versa. *Circulation* **91**, 1266–1268.

CHAPTER 7: FUTURE WORKS

This section summarizes some of the promising findings that have been made during these studies, and ways in which the field would benefit from further inquiry.

STRAIN DETERMINATION

The calcium analysis and micropatterning alignment software are complete, and little can be recommended to improve their effectiveness or range of applications. The particle tracking software could be improved, however, in one aspect in particular. The Poisson's ratio is a material property that indicates the strain that occurs perpendicularly to the direction of the applied stress. Determination of this parameter would be quite valuable for engineering applications of the material being assessed. The X-axis locations of the particles are indeed detected by the software; the strains experienced in the X direction must merely be determined in a way similarly to that of the Y direction, and the Poisson's ratio could thus be determined. Some considerations would have to be made regarding the imaging resolution. In most tensile tests, the strains exhibited parallel to the applied stress are much greater than those in the perpendicular directions. Additionally, the initial distances between particles in these perpendicular directions are also usually much smaller. These factors must all be kept in mind when deriving the Poisson's ratio.

SGFT TECHNIQUE

Much of the work that could be done on this topic would involve the adaptation of the algorithms toward additional applications. Images may come in many formats, and additional front-end components of the software could be added to help to standardize these images for analysis. Some early attempts have been made to utilize curvelets rather than gradients to determine fiber orientation, which may make the software even more reliable for more challenging images. Additionally, as mentioned in chapter 5, the SGFT technique could be taken into the third dimension at the cost of increased computation time.

MICROPATTERN OPTIMIZATION

It was discovered early on in this analysis that cells that could reach across a lane and contact both ends tended to produce extremely organized sarcomeres. Thus, the ideal micropatterns were small enough to fit only one fully-stretched cardiomyocyte, while large enough to allow some spreading. I theorize that inducing some level of hypertrophy, whether through biochemical signals such epinephrine or angiotensin II or through other means, may increase cell spreading and thus allow wider patterns to produce large cardiomyocytes with improved sarcomere development. Additionally, utilizing a softer substrate would more closely match the physiological environment that the cells experience. However, micropatterning of soft substrates is far more challenging, and a decrease in optical quality for imaging applications may also be unavoidable. The ideal model would lead to three-dimensional cultures of cardiomyocytes, though attempts to lift single-cell wide fibers from the substrates have not been effective.

hESC-CM OBSERVATION ON OPTIMIZED SUBSTRATE

There are a number of studies that should be conducted on this platform. The early studies of myofibrillogenesis are particularly promising, and further inquiry along these lines are greatly recommended. For example, examining how hESC-CMs develop myofibrils compared to primary cardiomyocytes could lead to a better understanding to how the mechanisms of myofibrillogenesis may change with age. Similarly, the sarcomere's response to biochemical stimuli may also be observed over time. Myofibril remodeling could also be assessed, and the repair mechanisms of human cardiomyocytes can be observed *in vitro*. Actin dynamics during contraction have been witnessed under this platform, as well. Combining the real-time detection of contracting myofibrils with mechanistic computer models could reveal a great amount of information regarding the contractile apparatus.

Disease models using iPSCs would also benefit greatly from this platform. Comparing myofibrillogenesis of healthy patients with those experiencing one of any number of myopathies could expose some of the underlying causes of these diseases. All of these studies, conducted finally on human cells, could provide valuable insights regarding the behavior of developing cardiomyocytes.

CHAPTER 8: CONCLUDING REMARKS

This body of work can be organized into two groups. The first sections describe several software packages that have been developed to analyze images and produce useful quantitative data for tissue engineering applications. The particle tracking software, which allows strain to be determined from optical measurements, has implications in several other fields, including the studies of rheology and microfluidics. The calcium transient analysis provides a rapid and easy way of testing large numbers of regions for their intracellular calcium waveforms. The micropatterning robot alignment software helps to ensure that the advanced micropatterned designs are capable of influencing cellular behaviors down to the microscale.

The scanning gradient Fourier transform (SGFT) technique has the potential to be used in numerous applications, both in and outside of biology. Heterogeneous patterning can be observed everywhere in nature, whether it is formed by waves along the ocean surface, cumulous clouds overhead, or in our own fingerprints. The examples mentioned here were focused specifically on microscopy, however, and showed that this analysis technique is capable of assessing sarcomere structure, breast cancer collagen morphology, and neural rosette formation.

The unique combination of gradient techniques and Fourier transforms provides detailed levels of quantification that are not achieved by most image analysis techniques.

The second body of work investigated the effects of micropatterning on human embryonic stem cell-derived cardiomyocytes. Much of this research began as a simple attempt to align cells. The final product was a cardiomyocyte model that met and exceeded expectations in its ability to mimic cellular behaviors *in vivo*.

Initial observations showed that hESC-CM aggregates produced more robust, aligned sarcomeres on micropatterned lanes when those lanes approached below 100 µm in width. Further investigations yielded optimized ways of producing these micropatterns and culturing cells beforehand to produce the most mature-like phenotypes possible. Assessments of these optimized cardiomyocytes revealed that the cells expressed sarcomeres, mitochondria, and cell-cell junctions quite similarly to what is observed *in vivo*. Lastly, a series of live imaging studies was conducted, and it was observed that myofibrillogenesis takes on different appearances depending on the region of the cell in which it is occurring.

Much like the organisms that we study, cellular biology is constantly growing and evolving as new technologies emerge. As stem cell technologies merge with advances, for example, in genetic screening and epigenetics, we can look forward to a new era of medical innovations that will truly improve the quality of life for generations to come. Humans are both empowered and limited by the tools at their disposal, and it is for this reason that a large component of my work has involved the development of such tools. By handing on these tools, as well as some of the interesting findings I’ve made along the way, I hope to bring the field slightly closer to a better understanding of cardiac biology.

APPENDIX A: PROCEDURES

E8 MEDIA LARGE BATCH PRODUCTION

Max Salick, 3/2/2012
Rev 1: 3/14/2012 MS
Rev 2: 3/15/2012 EL
Rev 3: 8/17/2012 MS: Adjusted some pricing and catalog numbers of reagents

This procedure describes the large-batch preparation of E8 media, which is a defined stem cell culture media that is capable of replacing TeSR media in most circumstances. Media preparation occurs in two steps: the initial large batch preparation, and the small batch preparation. The result of this procedure is 48L (96 x 500mL bottles) of modified DMEM, which is then frozen down for storage. These aliquots are then taken out as needed, and the remaining 4 components of the media are added at that time.

Frozen aliquots can be stored at -80C for a prolonged period of time. After thawing, it is recommended to use or dispose of the media within 2-3 weeks. Estimated final cost of the media is ~$50 per liter ($273 after growth factor addition). For reference, WiCell charges $360 per liter of mTeSR1. Each 48L batch will cost roughly $2,500 to produce. Initial startup costs for equipment and initial reagents is $2,200.

To summarize, the first batch overall will cost $4,700 and all successive batches will cost $2,500.

Shared reagents (Purchasing)

Reagent	Supplier	Cat #	Qty	Cost
DMEM/F12, HEPES	Invitrogen	11330057	100x500mL	2429.90
L-Ascorbic acid 2-phosphate sesquimagnesium salt hydrate	Sigma-Aldrich	A8960-5G	5 g	51.00
Sodium Selenite Solution(0.7 mg/mL in PBS)	Sigma-Aldrich	214485-100G	100 g	77.10
Sodium Bicarbonate	Sigma-Aldrich	S3817-500G	500 g	34.40
Sodium Chloride	Sigma-Aldrich	S7653-250G	250 g	31.70
1M Sodium Hydroxide	Sigma-Aldrich	71463-1L	1 L	22.70

Reagents (Usage)

Reagent	Amount Used
DMEM/F12, HEPES	48 L
L-Ascorbic acid 2-phosphate sesquimagnesium salt hydrate	3.072 g
Sodium Selenite Solution(0.7 mg/mL in PBS)	930.86 uL
Sodium Bicarbonate	26.064 g
Sodium Chloride	(as needed to adjust osmolarity)
1M Sodium Hydroxide	(as needed to adjust pH)

Individual lab reagents

Reagent	Supplier	Cat #	Qty	Cost	Qty per 500mL	Cost per 500mL
TGF-β1	Peprotech	100-21	5 ug	195	1 ug	13.72 (bulk order price)
Basic FGF	WiCell	N/A	100 ug	90	50 ug	45
Insulin	Sigma	I2643	250 mg	628	9.7 mg	24.37
Transferrin	Sigma	T0665	500 mg	307	5.25 mg	3.28

Equipment

- 50L Dispensing Carboy
- Fisher 02-963C - $189.39
- High-Capacity Stirrer
- HyClone Maxi Stirrer
- Fisher 14-259-122 - $1781.89
- Osmometer
- Advanced® Model 3320 Micro-Osmometer,Advanced Instruments, Inc. – Quote: $10,870.00
- pH Meter
- -20C Freezer
- -80C Freezer

Procedure

Note: Sterilization is done during the growth-factor-addition step of media preparation. This procedure is done openly in a non-sterile environment.

Note: To avoid contamination of the media by residues on the equipment, it is best to have a set of dedicated tools for media preparation. All equipment involved should be labeled as such.

1) Set up 50L carboy on the large-capacity stirrer at a lab bench
2) Turn on stirrer to a medium stirring speed
3) Pour 48L of DMEM/F12+HEPES into carboy by hand, saving the bottles
4) Add additional reagents to the DMEM/F12 to create the modified DMEM
    a. Add 26064mg of **sodium bicarbonate**
    b. Add 3072mg of **L-ascorbic acid 2-phosphate**
    c. Add 930.9uL of **sodium selenite solution** (0.7mg/mL in PBS)
        i. Measurement of sodium selenite solution should be done in a biosafety cabinet or fume hood
        ii. Take care in handling sodium selenite solution, as it is extremely toxic
5) Allow solution to mix for 20 minutes
6) Alternate between osmolarity tests and pH tests until both are the proper values:

Osmolarity Test

Pour out an aliquot of solution into one of the empty DMEM bottles, and test the solution for osmolarity. Target media osmolarity is **340±5 mOsm/kg**. When testing osmolarity, dab off the meniscus that forms at the bottom of the needle. To determine how many grams of NaCl to add, use the following equation:

$$(340 - x) * 1.44 = \#\ of\ grams\ of\ NaCl\ to\ add$$

Where *x* is the current osmolarity reading.

It is important to note that it is best to 'undershoot' the osmolarity, since one cannot remove NaCl once it has been added.

Pour unused sample back into the large carboy, and add the determined amount of NaCl. Allow 5-10 minutes of stirring before testing again.

pH Test

Make sure pH reader is calibrated before beginning testing. Rinse electrode before and between all pH tests. The target pH is **7.4±0.05** .

Pour out a 250mL aliquot into an empty DMEM bottle and test its pH. The pH usually starts at ~5.8. Pour in ~5mL of 1M NaOH by hand if pH is still below 7.4. Pour test sample back into the carboy and allow 5-10 minutes of stirring before testing again.

7) As you get close to the target values, check the pH twice and the osmolarity three times to make sure the readings are consistently within the target ranges
8) Once pH and osmolarity are satisfactory, aliquot solution back into 500mL bottles and label as 'modified E8 DMEM'
9) Freeze bottles in -20C freezer for the first day, then move them into the -80C for long-term storage the following day
10) Wash out large carboy thoroughly, but <u>do not autoclave</u> it

E8 ALIQUOT PREPARATION

Max Salick, 6/23/2012
Revision 1: MS, 7-25-2012: Adjusted purchasing information
Revision 2: MS, 8-17-2012: Fixed BFGF sourcing information, added freeze temperatures

Notes

This protocol describes the preparation of aliquots for the additional four components that should be added to the "E4" base media to create E8. This protocol was developed in the Thomson lab, and further information can be found in the article listed below:

Chen, G., et al. (2011). Chemically defined conditions for human iPSC derivation and culture. *Nat Meth*, *8*(5), 424–429.

Reagents (Purchasing)

Reagent	**Supplier**	**Cat #**	**Qty**	**Cost**
Recombinant Human TGF-beta 1	R&D	240-B-001MG/CF	200ug	$2000
Recomb. Human TGF-beta 1 (alternative)	Peprotech	100-21	Variable	Variable
Recombinant Human FGF	WiCell	-	100ug	$90
Holo – Transferrin	Sigma	T0665-100MG	100mg	$104
Recombinant Human Insulin	Sigma	I2643	50mg	$204
HCl	Sigma	H9892-100ML	100mL	$20
Recombinant Human Albumin	Sigma	A7223	1g	$337
PBS				

Aliquot Information

Reagent	**Amount per Aliquot**	**Aliquots Produced**	**$ per Aliquot**
Recombinant Human TGF-beta 1	0.8725ug in 500uL	573 per 500ug vial	$10
Recombinant Human FGF	50ug in 500uL	2 per 100ug vial	$45
Holo – Transferrin	5.335mg in 500uL	186 per 1G	$10
Recombinant Human Insulin	0.5mg in 500uL (varies)	5 per 50mg	$5 - $41

Procedure

<u>Recombinant Human TGF-Beta 1</u>

- Peprotech provides significant bulk purchase discounts, so it is best to coordinate TGF preparation with other labs
- 1000X = 1.745 ug/mL
- Prepare 500ug in 286.5mL

1) Dissolve 286.5mg recombinant human albumin in 4mM HCl (citric acid can also be used)
2) Add 500ug TGF-Beta to solution
3) Filter
4) Aliquot 500uL per tube and freeze at -80C as quickly as possible (this will produce a very large number of aliquots)

Recombinant Human FGF

- 1000X = 100ug/mL

1) Order bFGF aliquots directly from WiCell
2) When making media, directly pipette half (500uL) of the bFGF contents of one glass vial into the solution, mark the vial as “50ug remaining” and return to -80C storage

Holo – Transferrin

- 1000X = 10.67mg/mL

1) Weigh out 100mg and dissolve in 9.37mL PBS
2) Filter
3) Aliquot 500uL per tube and freeze at -20C

Recombinant Human Insulin

- 1000X = 20mg/mL
- Lower concentrations may be acceptable, down to even 50ug/mL

1) Dissolve 50mg in 2.5mL of 0.010 N HCl
2) Aliquot 500uL per tube and freeze at -20C
3) May also take one aliquot and further dilute it by 1:20 to produce 1mg/mL and so on to produce low-concentration aliquots

PASSAGING hESCS FROM VITRONECTIN TO VITRONECTIN

Max Salick, 5/5/2011
Suehelay Acevedo, 7/30/2012- Adapted Matrigel passaging protocol to vitronectin coating and E8 media.
Max Salick, 7/30/2012 – Minor adjustments to timings

Time Requirement

1.5 – 2 hours

Reagents

- **PBS**
- **E8**
- **ROCK Inhibitor**
- **Versene**
- **Vitronectin Aliquots**
- **6-well Plates**

Procedure

Prep Vitronectin

1) Place intended number of new plates in biosafety cabinet; Keep in mind that this passage is done at a ratio of 1:12, so it only takes a few wells to make several new plates
2) Place **cold** PBS in hood
3) Remove vitronectin aliquots (# aliquots = # of new plates) from -80C freezer and place in hood
    a. Aliquots are set beforehand to provide enough vitronectin for a certain number of plates
    b. Each well requires 6µg of matrigel, and most aliquots are typically made with 36µg of vitronectin per tube. This means that each aliquot will provide enough vitronectin for **1** full plate.
4) Quickly add 1mL of cold PBS to each vitronectin aliquot
5) Pipette these aliquots up and down to thaw vitronectin into PBS, and transfer all aliquots to a 50mL conical tube
6) Add enough PBS to this solution to provide 1mL/well of solution to each new plate.
    a. i.e. 4 new plates will need 22mL added in addition to the 2mL used to dissolve the vitronectin
7) Add 1mL to each well of new plates and ensure that the entire well surface is covered by solution
8) Label plates "vitronectin" and allow them to sit in hood for one hour and a half before plating cells onto them

Passage hESCs

9) After 1.5 hours (no less), prepare E8 / ROCK inhibitor solution
    a. Begin thawing ROCK inhibitor
    b. Transfer 2mL/well of E8 to 50mL conical tube(s), for each well of the new plates
        i. i.e. 4 new plates would require 48 mL of E8
    c. Add ROCK inhibitor to create 5uM solution
        i. Note: Typically ROCK inhibitor is diluted to a concentration such that it will require a 1:1000 ratio to create a 5uM solution. In other words, 48mL of E8 will require 48uL of ROCK inhibitor
10) Aspirate the PBS/vitronectin solution from the wells leaving a small amount in the well to prevent the vitronectin coating to dry out.
11) As quickly as possible, add 2mL/well of E8 +ROCK inhibitor solution to vitronectin-coated plates
12) Identify non-differentiated cells in nearly-confluent old plates for passaging

13) Aspirate media from passaging wells and treat with 1mL versene
14) Allow versene to react for 5-6 minutes in hood
15) Aspirate versene and immediately add 2mL E8/well
16) Use high-pressure pipetting to break cells off of the well and transfer cell solution to 15mL tube
    a. Versene singularizes cells, so these cells will form more of a cloud than clumps
17) Spin down cells at 1000rpm for 3 minutes
18) Aspirate supernatant
19) Resuspend in .5mL/well E8
    a. i.e. 4 new plates will require 12mL E8
20) Seed cells into new plates in a drop-wise manner, at .5mL/well
21) Place new plates in incubator and shake to evenly distribute cells

PASSAGING HESCS FROM MATRIGEL TO MATRIGEL

Max Salick, 5/5/2011

Time Requirement

1.5 – 2 hours

Reagents

- **PBS**
- **DMEM/F12**
- **mTeSR1**
- **ROCK Inhibitor**
- **Versene**
- **Matrigel Aliquots**
- **6-well Plates**

Prep Matrigel

1) Place intended number of new plates in biosafety cabinet; Keep in mind that this passage is done at a ratio of 1:12, so it only takes a few wells to make several new plates
2) Place **cold** DMEM/F12 in hood
3) Remove matrigel aliquots (# aliquots = # of new plates / 2) from -80C freezer and place in hood
    a. Aliquots are set beforehand to provide enough matrigel for a certain number of plates
    b. Each plate requires 0.5mg of matrigel, and most aliquots are typically made with 1mg of matrigel per tube. This means that each aliquot will provide enough matrigel for **2** new plates.
4) Quickly add 1mL of cold DMEM/F12 to each matrigel aliquot
5) Pipette these aliquots up and down to thaw matrigel into DMEM/F12, and transfer all aliquots to a 50mL conical tube
6) Add enough DMEM/F12 to this solution to provide 1mL/well of solution to each new plate.
    a. i.e. 4 new plates will need 22mL added in addition to the 2mL used to dissolve the matrigel
7) Add 1mL to each well of new plates and ensure that the entire well surface is covered by solution
8) Label plates “matrigel” and allow them to sit in hood for one hour before plating cells onto them

Passage hESCs

9) After 1 to 1.5 hours (no more, no less), prepare mTeSR1 / ROCK inhibitor solution
    a. Begin thawing ROCK inhibitor
    b. Transfer 2mL/well of mTeSR1 to 50mL conical tube(s), for each well of the new plates
        i. i.e. 4 new plates would require 48 mL of mTeSR1
    c. Add ROCK inhibitor to create 5uM solution
        i. Note: Typically ROCK inhibitor is diluted to a concentration such that it will require a 1:1000 ratio to create a 5uM solution. In other words, 48mL of mTeSR1 will require 48uL of ROCK inhibitor
10) Wash matrigel solution with 1mL PBS in each well
11) Add 2mL/well of mTeSR +ROCK inhibitor solution to matrigel-coated plates
12) Identify non-differentiated cells in nearly-confluent old plates for passaging
13) Aspirate media from passaging wells and treat with 1mL versene
14) Allow versene to react for 3 minutes in hood
15) Aspirate versene and immediately add 2mL mTeSR/well

16) Use high-pressure pipetting to break cells off of the well and transfer cell solution to 15mL tube
    a. Versene singularizes cells, so these cells will form more of a cloud than clumps
17) Spin down cells at 1000rpm for 5 minutes
18) Aspirate supernatant
19) Resuspend in .5mL/well mTeSR
    a. i.e. 4 new plates will require 12mL mTeSR
20) Seed cells into new plates in a drop-wise manner, at .5mL/well
21) Place new plates in incubator and shake to evenly distribute cells

SMALL MOLECULE CARDIAC PROTOCOL

Max Salick, 12/15/2012
Rev 1: Included D0 Insulin, reduced CHIR, and altered seeding density, MS 2-21-2013
Rev 2: Fixed reagents lists, other minor edits MS 5-2-2013
Rev 3: Included Day -1 to Day 0 24-hour tip, and details about Zeocin MS 7-2-2014

Notes

This protocol is Xiaojun (Lance) Lian's Wnt-signaling directed-differentiation protocol. The protocol involves solely small molecule treatments. The protocol begins at day -3, differentiation is induced at day 0, and beating typically begins around day 8-9. The culture is particularly sensitive to mechanical shock, especially during days 0 to 5. Be extremely careful when handling the culture and changing media to prevent damage to the cells during this time.

Flow cytometry can be conducted to determine the efficiency of a single batch. It should be noted that H9 hESCs tend to have lower differentiation efficiencies when compared to iPS cell lines. Once beating, the cells tend to keep beating for several weeks after this protocol is finished.

Reagents (Purchasing)

Reagent	**Supplier**	**Cat #**	**Qty**	**Cost**
E8				
ROCK Inhibitor (Y-27632)	Tocris	1254	10mg	$225
Accutase	Invitrogen	A11105-01	100mL	$39
PBS	Invitrogen	14190144	500mL	$8.11
RPMI	Invitrogen	11875085	1L	$30.43
B27 Supplement	Invitrogen	17504044	10mL	$77.50
B27 –Insulin	Invitrogen	0050129SA	10mL	$95.75
CHIR-99021 (CT99021)	Tocris	4423	10mg	$199
Stemolecule™ Wnt Inhibitor IWP-4	StemGent	04-0036	2mg	$124
Insulin	Sigma	I2643-50mg	50mg	$208

Procedure

Day -3

1) Prep new 12-well plates with matrigel coating for at least 1.5 hours before seeding
2) Accutase treat cells and seed onto new wells of a 12-well plate at 400,000 cells per well, using ROCK inhibitor in new media. Each well should have 2.5mL of cell solution + ROCK.

Day -1

3) Feed cells with 2.5mL E8 per well. Ideally, cells will be mostly confluent, and will show 'star' morphology (visible at 10X-20X). It is important that there are at least 24 hours between this step and the following (CHIR application) step.

Day 0

4) Treat cells with RPMI/B27-insulin/CHIR/Insulin solution
   a. This amounts to the following amounts per 12-well (WELL) [plate volume]:

2.5mL RPMI	**[30mL]**
50uL B27-Insulin	**[600uL]**
2.19uL CHIR99021 (12mM sol'n)	**[26.28uL]**
2.5uL Insulin Solution (1mg/mL)	**[30uL]**

Day 1 (exactly 24 hours after previous treatment)

5) Exchange medium with RPMI/B27-Insulin
   a. This amounts to the following amounts per 12-well (WELL):

2.5mL RPMI	**[30mL]**
50uL B27-Insulin	**[600uL]**

Day 3 (exactly 48 hours after previous treatment)

6) Apply IWP4 treatment to cells
   a. 5uM IWP4 in RPMI/B27-insulin; this amounts to the following amounts per 12-well (WELL):

2.5mL RPMI	**[30mL]**
50uL B27-Insulin	**[600uL]**
1.25uL of 10mM IWP4 Sol'n	**[15uL]**

Dqy 5

7) Replace medium with RPMI/B27-Insulin (2.5mL/well)

Day 7

8) Replace medium with RPMI/B27 complete (2.5mL/well)

Day 8

9) Replace medium with RPMI/B27 complete (2.5mL/well) and continue replacing this medium every three days

Purification Option:

Day 9, 10, 11 - Replace medium RPMI/B27 complete/Zeocin(1:1000)
(Use Zeocin only if culturing cTnT-GFP Zeocin resistant cell line)

IMMUNOFLUORESCENCE PROTOCOL FOR CELLS

Max Salick, 4/12/2011

Rev. 1 – 10/3/2011 MS – Added phalloidin/DAPI option, antibody dilutions, time requirements, notes on quantities, and minor edits
Rev. 2 – 1/27/2012 MS – Fixed units for BSA for blocking solution prep
Rev. 3 – 5-1-2013 MS – Added 150mM glycine to blocking solution recipe
Rev. 4 – 8-31-2013 MS – Reduced concentration of phalloidin from 5/500 to 2/500uL

Notes

The following protocol uses quantities for 1 well of a 6-well plate. Scale quantities directly for additional wells. For 1 well of a 12-well plate, reduce all quantities by ½. For multiple wells of a 12-well plate, scale appropriately.

Time Requirement

Day 1: ~3 hours
Day 2*: ~3 hours
Day 3 or later: Imaging (varies)

*Entire stain can be conducted on day 1, with 2-hour gap between "day 1" and "day 2" segments. Total is ~8 hours.

Reagents

PBS
16% EM-grade Paraformaldehyde in 10mL ampoules
Blocking solution aliquots
Triton X
Bovine Serum Albumin (BSA)
Primary antibodies
Secondary antibodies
DAPI (optional)

Procedure

Prep (Aliquots)

If aliquots are not already prepared, prepare paraformaldehyde solution in chemical fume hood
NOTE: Paraformaldehyde is highly toxic and releases toxic fumes. Make sure to wear goggles if splashing is possible, and always work in a fume hood.

1) Take 16% EM grade PFA in 10mL sealed ampules and dilute in PBS to 40mL
2) Aliquot into 5mL per 15mL conical tube (8 x 15mL conical tubes)
3) Store tubes at -20C, use within 2-3 months of freezing

If aliquots are not already prepared, prepare blocking solution
Mix the following reagents (assuming all at 1X)

- 42 mL PBS
- 2.25 mg BSA
- 900 uL Serum (serum should be from same animal that secondary antibodies were produced from)
- 45 uL Triton X
- 506.7mg Glycine

Aliquot into 5mL per 15mL conical tube and freeze at -20C

Day 1: Sample Fixation / Blocking and Primary Antibody Application

1) Thaw / heat the following reagents
    - 5mL aliquot of paraformaldehyde solution
    - 2x5mL aliquot of blocking solution
    - PBS
    - Triton X
    - Primary antibodies
2) Aspirate media from all wells and wash 3 times with 2mL PBS per well
3) Add 800uL paraformaldehyde solution to each well and allow to sit for 15 minutes at room temperature in biosafety cabinet
    a. ***3D/Intercellular Samples:*** While waiting, add 3uL of Triton X to 3mL of PBS to the side
        i. *Due to the viscosity of Triton X, this may take a few more gradual dilutions*
4) Wash once with 2 mL PBS per well
    a. ***3D/Intercellular Samples:*** Add 2mL of diluted Triton X solution to each well and allow to permeablize for 6 minutes
5) Wash off Triton X solution once with 2mL PBS per well
6) Add 800uL blocking solution to each well and allow to block for 30 – 90 minutes (time does not affect effectiveness; use time as convenient)
7) Dilute primary antibodies in blocking solution (dilution depends on specific antibody; may take tweaking)
8) Aspirate current blocking solution and replace with 800uL per well of primary-antibody blocking solution
9) Allow reaction overnight at 4C or for 2 hours at room temperature

Day 2 (or late 1): Secondary Antibody Application and Imaging

NOTE: Be sure to keep the secondary antibodies from being exposed to light. Keep in opaque containers and dim the lights when working with them. The plate being tested may also be wrapped in tin foil to avoid exposure.

1) Thaw / heat the following reagents
    - 5mL aliquot of blocking solution
    - PBS
    - Secondary antibodies
    - DAPI
    - Antifade agent

2) Wash wells once with 2mL PBS per well, waiting 5 minutes during wash
3) Dilute the secondary antibodies in blocking solution (per company recommendation, usually around 1:500)
    a. If not doing a later DAPI stain, you can mix DAPI stain with the secondary antibody solution to get a strong DAPI signal
4) Apply 800uL per well of secondary antibody solution. Allow reaction at room temperature for 1 hour (may want to cover plate or keep in dark for this; a closed drawer works fine)
5) Wash 3 times with 2mL PBS per well for 5 minutes each time.
    a. **Optional:** Conduct phalloidin and DAPI stain
6) Mount sample and image (this will depend on sample type). Ideally, find a way place the cells directly on a coverslip and image with the coverslip facing downward.

Optional phalloidin / DAPI stain:

1) Make phalloidin stain solution consisting of 2uL phalloidin solution and 498uL PBS
2) Apply phalloidin stain to sample and incubate for 1 hour
3) Wash sample 3 times with 2mL PBS
4) Apply DAPI stain directly onto sample via dropper

FLOW CYTOMETRY SAMPLE PREPARATION

Max Salick, 4/18/2012
Rev 1: Made universal for all antibodies, included dilutions 1-15-2013 MS
Rev 2: Protocol reduced to eliminate unnecessary steps 3-31-2013 MS

Notes

This protocol is for conducting immunostaining followed by flow cytometry. It is often required to reserve time on a flow cytometer ahead of time, so make sure to allocate enough time to conduct the preparation beforehand. After preparation is done, there can be a delay of a few hours before the flow work is done, as long as the samples are kept on ice.
This protocol has been optimized for cardiomyocytes.

Time Requirement

Sample Preparation: 4 hours
Flow Cytometry: 1 hour
[1.5 hours active, 30 minutes waiting, 30 minutes active, (overnight), 30 minutes active, 1 hour wait, 1.5 hours active]

Reagents

TrypLE
DMEM/F12
FBS
PBS
Paraformaldehyde
Methanol (Keep cold; store at start of procedure)
Triton
Primary Antibody
Secondary Antibody

Procedure

1) Sample Preparation [for X wells of cells]
2) Prepare FACS buffer by mixing PBS with 2% FBS. Usually about 30mL of FACS buffer is enough per well tested. This amounts to 30mL of PBS and 600uL of FBS.
3) Conduct 3 PBS washes of samples to remove debris
4) Add 1mL of TrypLE. Incubate for 15-20 minutes at 37C.
5) While waiting for singularization, prepare 2*X mL of DMEM/F12 with 10% FBS
    a. (X = mL of TrypLE used)
6) Also prepare 10mL of 90% methanol and keep on ice
7) Gently pipette treated cells 5-10 times with 5mL pipette to break up chunks. Transfer to 15mL conical tube.
8) Dilute with 2mL of DMEM/F12 + 10% FBS solution for every 1mL of trypsin
9) Spin down vials
10) Resuspend cells in 2mL FACS buffer and spin down (wash)
11) Resuspend cells in 1mL PBS per conical tube
12) Add paraformaldehyde so that the final concentration is ~0.8% PF and fix for 10 minutes in a 37C water bath. If using a 4% PF aliquot, 250uL of this aliquot should reach the desired concentration
13) Spin down fixed cells
14) Resuspend cells in 2mL FACS buffer and spin down (wash)
15) Resuspend cells in 1mL per tube of ice-cold 90% methanol
16) Incubate tubes on ice for 30 minutes

At this point, proceed with staining or store the cells at -20C in the 90% methanol solution.

17) Prepare 0.25% triton wash buffer
18) Add 2mL Triton-X100 to 8mL PBS
19) Add 312uL of diluted (Triton-X10) solution to 25mL of FACS buffer
20) Once 30 minutes have passed, spin down cells
21) Resuspend in 2-3mL of 0.25% triton wash buffer and spin down (triton wash)
22) Pour off supernatant and add 100uL of antibody solution (per tube) at designated concentration

Primary Antibody Dilution (use antibody #2 row if conducting a co-stain)

Volume of PBS ________uL

Antibody #1 Name ___________ Dilution _____:_____ Volume of Antibody __________uL

Antibody #2 Name ___________ Dilution _____:_____ Volume of Antibody __________uL

23) Incubate at 4C overnight or at least 45 minutes at room temperature (overnight stains are typically more effective)
24) Add 1mL FACS buffer and spin down (wash)
25) Aspirate supernatant
26) Resuspend in 100uL (per tube) of secondary antibody

Secondary Antibody Dilution (use antibody #2 row if conducting a co-stain)

Volume of PBS ________uL

Antibody #1 Name ___________ Dilution _____:_____ Volume of Antibody __________uL

Antibody #2 Name ___________ Dilution _____:_____ Volume of Antibody __________uL

27) Incubate in the dark at room temperature for 1-2 hours
28) Add 1mL FACS buffer and spin down (wash)
29) Resuspend cells in 150uL FACS buffer and transfer to flow cytometry tubes
30) Keep tubes on ice in the dark until ready to run flow

FLOW CYTOMETRY ON FACSCANTO III

Max Salick, 9/13/2012
Rev 1: Several small details (controls, grammar, machine warm-up) – MS 10/3/2012
Rev 2:

This procedure describes how to run flow cytometry on a FACSCanto III cytometer. This is only for cell counting, and not for cell sorting. See the procedure on 'Flow Cytometry Sample Preparation.'

It is very helpful to include a control sample, as well. Ideally these will be the same cell type, but without fluorescence (i.e. by replacing the primary antibody solution with PBS).

Procedure

Startup

1) Press large green button on left side of FACSCanto III
2) Turn on computer
3) Check fluid levels; PBS should be high, waste should be low
4) If out of PBS, replace with full PBS bottle on floor near machine
5) If waste is getting high, take off both caps and replace with empty waste container on ground.
6) There should already be bleach in the containers, but make sure it smells a little 'bleachy' before dumping the full container out into the sink.
7) Log into FACSDiva software
8) Make sure that small, round metal arm attached to swinging lever is pointing <u>in</u> toward the cytometer – at this point, the lever should be pushed over slightly by the brown coupling attached to the inlet
9) Allow machine to warm up. This can take roughly 10 minutes.
10) In software, run 'startup' (Menu -> Cytometer -> Startup). This will take another 10 minutes or so.
11) Once finished, remove brown coupling (some force may be needed to loosen it) and set down somewhere in the machine

Preparing Experiment

1) Press 'start new experiment'
2) Name specimen by date
3) Add a tube in the software for each tube to test, including negatives **-OR-** Add plate if running plates
4) On 'cytometer' screen, delete unneeded parameters
5) If this option is not available, make sure you have a sample selected via the green button at the left in the sample menu
6) Make sure 'SIT Flush' is selected. This cleans the system out of the previous sample.

Running Samples

1) Mix tube for ~1 second on vortexer
2) Push over lever and lift tube onto inlet until it clicks
3) At first, set flow rate to low
4) Under 'cytometer', set FSC threshold to ~20,000 to remove debris from data
5) Press 'acquire data' to begin running sample
6) Tweak voltages as necessary
7) Take data (~10,000 events) and adjust gates and thresholds to make sure you are finding the right populations
8) It is not advised to leave the cytometer running during this time, or you will waste sample

9) Once voltages and gates are all properly tuned, take data again
10) Remove tube and put back on ice
    a. **NOTE – When removing samples, make sure that the lever gets a moment to rotate ALL THE WAY BACK so that the system can purge**
11) Prepare next tube (starting at step 14) and select corresponding tube in software

Shutdown

1) Data is saved automatically during acquisition
2) Rotate round metal arm so it is pointing inward toward cytometer
3) **Place brown coupling back onto inlet, and screw the coupling so that it is tightly attached – the lever should be pushed to the side by the coupling at this point**
4) Close the doors around the HTS (plate loader)
5) Run the shutdown protocol from software; there may be a slight delay before it initializes
6) Hit OK to begin shutdown process
7) Once shutdown is complete, turn off computer and make sure cytometer is off
8) Check fluid levels

RNA ISOLATION USING AMBION RNAQUEOUS-MICRO KIT

Max Salick, 2/21/2014

Rev 1:

Reagents

- Ambion RNAqueous Micro Kit (spin columns and reagents)
- RNAse-free ethanol
- RNAse-free water
- RNAse decontaminant (i.e. RNAseZap)
- RNAse-free microcentrifuge tubes
- Centrifuge for microtubes
- Trypsin (or accutase)
- FBS-containing media (DMEM + 10% FBS)

Procedure

Preparation

1) If this is the first time using the kit…
    a. Add 10.5mL of RNAse-free 100% ethanol to the **Wash Soln 1 Concentrate** bottle
    b. Add 22.4mL of RNAse-free 100% ethanol to the **Wash 2/3 Concentrate** bottle
2) Label a Micro Filter Cartrige Assembly and a Micro Elution Tube for each sample
3) Warm **Wash Solution 2/3** to room temperature
4) Heat an aliquot of **Elution Solution** in a tightly-closed RNAse-free tube to 75°C in a thermocycler
    a. The amount aliquoted depends on the number of samples; prepare 25µL per sample, and prepare at least 50µL

RNA Isolation

5) Dissociate cells using trypsin or accutase
6) Deactivate trypsin(accutase) with 10% FBS(PBS dilution) and spin town to pellet
    a. Aspirate supernatant
7) Add 100µL **Lysis Solution** and vortex vigorously
8) Add 50µL of 100% ethanol and vortex briefly but thoroughly
9) Transfer the 150µL solution to a **Micro Filter Cartridge Assembly** and spin down for 10 seconds at maximum speed
10) Add 180µL of **Wash Solution 1** to the filter and centrifuge for 10 seconds at 13,400 – 16,500 x g (~13,000 rpm)
11) Add 180µL of **Wash Solution 2/3** to the filter and centrifuge for 10 seconds at 13,400 – 16,500 x g (~13,000 rpm)
12) Add 180µL of **Wash Solution 2/3** to the filter and centrifuge for 10 seconds at 13,400 – 16,500 x g (~13,000 rpm)
13) Pour out the collection tube
14) Place the **Micro Filter Cartridge** back into the same collection tube and centrifuge for 1 minute at maximum speed
15) Transfer the **Micro Filter Cartridge** to a **Micro Elution Tube**
16) Apply 5-10µL of **Elution Solution** (preheated to 75C) and store for 1 minute at room temperature
17) Centrifuge the assembly for 30 seconds at 13,400 – 16,500 x g (~13,000 rpm)
18) Add another 5-10µL of **Elution Solution**, allow 1 minute to dissolve RNA, and centrifuge once again for 30 seconds at 13,400 – 16,500 x g (~13,000 rpm)

DNAse Treatment

19) Add 1/10 volume(1-2µL, depending on elution) **10X DNase I Buffer** and 1 µL **DNase I** to the sample, and mix gently but thoroughly
20) Incubate the DNase reaction for 20 minutes at 37C
    a. During this time, remove the **DNase Inactivation Reagent** from the -20C freezer and allow it to thaw at room temperature during this time
        i. Vortex the **DNase Inactivation Reagent** vigorously to completely resuspend the slurry
21) Add 2µL **DNase Inactivation Reagent** (may be challenging to pipet) and vortex briefly
22) Allow inactivation to occur for 2 minutes at room temperature
23) Centrifuge the reaction for 1.5 minutes at maximum speed to pellet the **DNase Inactivation Reagent**
24) Transfer the RNA (supernatant) to a fresh RNase-free tube
25) Store RNA at -80C or immediately use

RNA ISOLATION USING TRI REAGENT

Max Salick, 2/20/2014
Rev-1:

Reagents

Tri Reagent (i.e. TriZol)
RNase-free ethanol
RNAse-free water
Chloroform (RNAse-free)
Isopropyl alcohol (RNAse-free)
Trypsin / Accutase
FBS-containing medium
Centrifuge capable of reaching 12,000g
Thermocycler
Vortexer

Procedure

1) Make sure thermocycler has available slot
2) Get ice bucket
3) Aspirate media thoroughly, but do no wash
4) Add TRI reagent directly to cells (1mL per 10cm^2 surface area)
5) Pipet the cells up and down several times and transfer to microtube until thoroughly homogenized
6) Centrifuge samples at 12,000 x g for 10 minutes at 4C
7) Transfer cleared supernatant to a new tube (discard the fatty layer above supernatant if present)
8) Supernatant contains RNA; ECM, polysaccharides, and high-MW DNA are in the pellet
9) Incubate homogenized samples for 5 minutes at room temperature
10) In PCR hood, add 200(100)µL chloroform per 1(1/2)mL Tri Reagent
11) Shake samples 15 seconds until chloroform reacts (should look like Pepto-Bismol)
12) Allow samples to sit at room temperature for 2 – 3 minutes
13) Centrifuge at 4°C, 12,000g for 15 minutes
    a. **Make sure that the 12,000g is in the correct units**
14) While centrifuging, label new tubes (same as sample tubes)
15) Remove centrifuge samples and place on ice
16) Tubes should now have a red organic phase containing protein, an interphase containing DNA, and a colorless upper aqueous phase containing RNA
17) Set pipette to 150µL – Pipette aqueous phase from top of spun tubes into the new tubes
18) Add 500(250)µL isopropanol per 1(1/2)mL Tri to aqueous solution
19) Allow samples to stand for 10 minutes at room temperature
20) Centrifuge at 12,000g for 10 minutes at 4°C
21) While centrifuging, prepare 75% ethanol solution by adding RNAse-free ethanol to RNAse-free water
22) Place samples on ice
23) Dump supernatant of each microtube into 50mL tube and place in tray. RNA should be a tiny gel-like pellet on the side and bottom of the tube.
24) Add 1mL(500µL) of 75% ethanol per 1mL(500µL) of TRI
25) Vortex tray full of samples briefly
26) Centrifuge at 7,500g for 5 minutes at 4°C
27) Dump supernatant, allow to air dry for 5-10 minutes (don't let it dry completely, however)
28) Resuspend each RNA pellet in 50µL of RNAse-free H_2O by pipetting several times, and transfer to 0.2mL RNAse-free tube for thermocycling
29) Place in thermocycler at (60C) for 10 minutes
30) Continue treating or freeze at -80C in labeled bag

BIOMATERIALS TESTING (CYTOTOXICITY)

Max Salick, 12/10/2012
Rev 1:

This protocol describes the various steps involved in testing a biomaterial for cytotoxicity using 3T3 cells. Amounts and procedures may vary depending on reagents used, and biomaterials may widely vary with respect to cell attachment.

Seeding

1) Place biomaterials in smallest culture well that fits them. If sample floats, use a washer to weigh down the sample, but make sure that enough sample is exposed to the media so that cells may attach to it
2) Sterilize by whatever means is possible for the material being analyzed. Many materials react to certain sterilization methods in negative ways.
3) Once samples are sterilized as much as possible (the media will contain antibiotics), begin the cell-seeding process
4) Versene treat the cells for 5 minutes at room temperature
5) Aspirate versene and use 3T3 media to wash off the cells and transfer to a conical tube
6) Count number of cells in the tube while spinning it down
7) Aspirate and re-suspend the cells in 3T3 media to the designated concentration
8) Seed directly onto the material, and add enough 3T3 media to ensure that the materials are fully coated

NOTE: The number of cells seeded is highly dependent on sample geometry and material. Generally, for most 3-dimensional foam samples, I use 125,000 cells/cm^2, and for flat 2-dimensional membranes, I use 1,250 cells/cm^2. The area mentioned is dependent on the plate used:
(6-well = 962 sq mm 12-well = 401 sq mm 24-well = 200 sq mm)

After seeding, feed the cells every other day with 3T3 media, ensuring that the samples remain fully submerged

Live/Dead Imaging

This protocol utilizes the EthD-1 / Calcein-AM Live/Dead Mammalian Cell Assessment Kit, available from Life Technologies. Keep vials of this stain frozen at -20°C, and avoid contact with the vials' contents.

1) Wash x2 with PBS, and use these washes to gauge the amount of liquid needed to fully coat the samples. This amount can be used to determine the amount of live/dead stain needed.
2) Prepare the stain based on the following ratios (prepare more or less based on number of samples)
3) 2mL PBS
4) 4uL EthD-1 (red)
5) 1uL Calcein-AM (clear)
6) Apply the stain for 45 minutes at room temperature
7) Transfer the cells to a new plate, if possible
8) Wash gently with PBS
9) Add PBS to keep hydrated
10) Image immediately

MTS Assay

The MTS assay used in this protocol is CellTiter 96 Aqueous One Solution Cell Proliferation Assay from Promega. After thaw, an aliquot can be kept in the 4C fridge for up to 6 weeks.

1) Mix MTS solution. For one well of a **6-well plate**, this amounts to (704uL total) :
2) 587uL media
3) 117uL CellTiter solution
4) For one well of a **12-well plate**, this amounts to (300uL total) :
5) 250uL media
6) 50uL CellTiter solution
7) For one well of a **24-well plate**, this amounts to (150uL total) :
8) 125uL media
9) 25uL CellTiter solution
10) Include extra solution for a **control** (400uL media + 80uL MTS), and pipet 100uL into each of four wells of the microplate. Place the microplate in the incubator with the rest of the samples to ensure that the control experiences similar conditions, but without the cells.
11) Incubate for 1-4 hours, depending on cell type and assay concentration. This should be consistent with the controls established
12) Pipet 100uL of colored media into a 96-well clear microplate, and pipet 100uL of control into a neighboring well.
13) Replace media from tested well with normal media at normal volume
14) Measure the absorbance at 450nm (peak is at 490nm, but the closest filter on our equipment is 450nm)
15) Plates can be re-used, but it is not advisable to use the same well more than once

CALCIUM TRANSIENT STAIN

Max Salick, 12/10/2012
Rev 1:

This protocol describes how to conduct a calcium transient stain utilizing Rhod-2 (Life Technologies). This stain shows the amount of calcium ions present in the cytoplasm. This is particularly effective in observing the transients of neurons and cardiomyocytes. Assessing transient intensity during contraction may be one method of determining the development of the sarcoplasmic reticulum and the maturation of the cardiomyocytes being tested. This test is ***non-destructive*** *and quite easy to conduct.*

Procedure

1) Mix one 50ug aliquot of the Rhod-2 stain with 44.5uL DMSO. This will produce a 100X stain solution.
    a. NOTE: Dissolved aliquot will last one week at 4°C
2) Add 100X stain solution to RPMI/B27, producing enough volume to thoroughly coat all cells being assessed
3) Incubate for 15 minutes
4) Wash cells twice with PBS
5) Feed cells with normal amount of RPMI/B27
6) Incubate for 30 minutes
7) Observe cell contractions using Texas Red filter. A framerate of at least 10 frames per second is required for proper transient analysis.
    a. It is recommended to view contracting cell calcium transients on a heated stage.

PDMS PREPARATION

Max Salick

Notes

PDMS disks have been used to provide a mold for cell-embedded gels during their polymerization. PDMS is also useful as a general soft material for preparation of bioreactors and other bioassay devices. PDMS is used because it is reasonably biologically inert and does not release many toxic residues into its surroundings. Such toxins could have harmful effects on the chemically-sensitive cells. Typically, petri dish-shaped disks are formed, and the required mold shapes are then carved out of these solid PDMS molds.

For this procedure, 30g of polymer base are used. This is enough to create a 3mm-thick disk the size of a petri dish. Scale amounts accordingly for thicker or thinner disks.

Reagents

30g	SYLGARD 184 Silicone Elastomer Base (Dow Corning)
3g	SYLGARD 184 Silicone Elastomer Curing Agent (Dow Corning)

Equipment

Scale (0.1g resolution)

Plastic cups

Tongue depresser

Vacuum

Hot plate (up to 80C)

Glass petri dish

Microscope slide

Transparency sheet

Glass cutter

Procedure

1) Mix base and curing reagent
2) Place plastic cup on scale and tare
3) Add 30g of silicone elastomer base to cup
4) Add 3g of silicone elastomer curing agent to cup
5) Mix thoroughly using tongue depresser (about 2 minutes)
6) Use vacuum to remove bubbles from polymer solution and prepare mold
7) Once thoroughly mixed, place cup into vacuum and run vacuum for approx. 45 minutes

OPTIONAL: Remove the cup every ten minutes and hit the cup sharply to help break up bubbles. If this is done, you only need to vacuum for about 30 minutes.

8) While vacuum is running, break microscope slide using glass cutter. Use these pieces as spacers to place in the petri dish to set the resulting thickness of the PDMS disk. Microscope slides are ~1mm thick.
9) Also while vacuuming, cut circles out of the transparency sheets approximately the same size as the petri dish. Place these sheets on both top and bottom of the petri dish before pouring the PDMS.

Polymerization procedure

10) Once vacuuming is finished, pour the PDMS mixture into the prepared petri dish mold.
11) Place the mold onto a hot plate and heat at 80C for 4 hours.
12) Once the heating is finished, the solution should be thoroughly polymerized. Carefully remove the transparency sheets and PDMS disk from the petri dish without breaking the glass.
13) The PDMS is completed, but may now be extracted to remove excess residues from the disk. If left in the mold, these residues have the potential to harm particularly sensitive cells.

PLASMA TREATMENT OF SURFACES

Max Salick, 2/7/2013
Rev 1:

This procedure describes how to use the Ashton Lab's plasma treater to improve the binding potential of a surface. Plasma treatment will help to increase protein adsorption, and is thus useful for many cell biology applications.

Procedure

1) Start with valve facing to the right
2) Place sample into chamber
3) Turn off the yellow valve in the chemical hood next to the plasma treater
4) Turn on the vacuum and allow to run for 5 minutes
5) Flip RF to high; you should see a purple glow
6) Gently turn the vent nozzle until a pink haze can be seen around the sample
    a. Do not turn the nozzle too far, however, or the plasma will be lost. If this happens, simply re-close the valve and slowly open it again
    b. This often takes several tries. Once a maximum 'glow' has been achieved, allow it to treat the sample for ~5 minutes
7) Once finished, tighten the vent
8) Turn large, long valve back to 'right' position
9) Switch RF level and RF power off
10) Switch off vacuum
11) Return the yellow valve in the hood to its original position
12) Slowly bleed the vent to equalize pressure. Opening this quickly will create a rush of air that will blow the sample around

MICROCONTACT PRINTING SAMPLE PREPARATION

Max Salick, 9/19/2013

This procedure describes how to prepare micropatterned slides for controlling the geometry of cell adhesion. This is started 2 days before the cells are seeded onto the slides.

Procedure

Day 1: PEG Reaction

1) Score gold-coated slides based on the stamp size
    a. For the standard small rectangular slides (that fit 12-well plates), cut 1.2cm x 2cm rectangles out of the slides. 3 'chunks' can be made from each slide, and each 'chunk' can hold 2 stamps. Thus, each slide can accommodate 6 samples.
    a. Use a kimwipe to hold the slide in place, while scoring with the bump part of the glass scoring tool. Do not use the wheel portion.
    b. Snap carefully by hand

2) Store rest of slides in cover slip holder, parafilmed. Place holder in a dessicator, pull vacuum, and make sure slides are protected from light.

3) Get the initiator and PEG solution from the -20C Ashton freezer (door, top shelf)
    a. PEG is a green solution in a larger schlenk flask
    b. Initiator is in a foil-covered, parafilmed jar
    c. PEG needs to be at room temperature for its reaction; set in in the “chemistry set” hood for now

4) In chemical hood, rinse off slides with 100% ethanol (using squirt bottle), draining into a waste beaker
5) Dry off with nitrogen tube
6) Repeat 4 and 5 individually for each slide, placing clean slides face-up in petri dish
7) Do same ethanol / nitrogen rinsing step with PDMS stamps
    a. NOTE: If there are smudges or unclean portions of slides or stamps, add a toluene rinse before the ethanol rinse step to help dissolve off the unwanted residues

8) Conduct Initiator stamp step on each slide…
    a. Re-rinse slide with ethanol and nitrogen
    b. Using p10 pipette, apply 5uL (10uL for large stamp) of initiator to stamp
    c. Smear the initiator evenly onto the stamp using the side of the pipette tip
    d. Dry off the initiator solution on the stamp using nitrogen
    e. Set stamp gently onto the slide, without applying pressure (this would cause smearing of the pattern)
    f. Use the blunt end of a tweezers to press down gently on the stamp to make sure it makes full contact over the entire surface of the stamp
    g. After 10 seconds of contact, remove stamp
    h. Rinse stamp with ethanol and nitrogen and repeat this process until all 'chunks' or slides have been stamped with patterns
9) Replace the air in the Initiator jar with nitrogen, close jar, and parafilm to seal
10) Get 3x schlenk flasks for the reaction (this is for 6 'chunks'. 2 'chunks' fit in each schlenk flask)
11) Rinse the flasks with ethanol
12) Cover ends with clumped kimwipes, and place nitrogen tube inside of schlenk flasks. Increase nitrogen flow to blow out the ethanol and dry out the flasks rapidly
13) Place slides (or chunks) back-to-back gently in the neck of the schlenk flask, so that the patterned surface is facing outward
14) Slowly push slides down the flask so that they are still back-to-back at the bottom of the flask
15) Transfer flasks with samples to the chemistry set hood
16) Seal each flask with a rubber stopper and improve seal using zip-ties
17) Turn on vacuum and use vacuum tube (not syringe) to pull air out of flasks
    a. Turn on vacuum
    b. Flasks are open
    c. Place vacuum tube onto schlenk flask port
    d. Once pulled, close port and remove tube
18) Keep PEG sealed at all times
19) Insert slow nitrogen syringe into PEG to maintain pressure but preventing inflow of lab air
20) Use long syringe to draw up ~7mL of PEG solution
21) Add PEG solution to each schlenk flask individually, so that all slides are covered in PEG solution
22) Use sodium L-ascorbate to initialize reaction
    a. Get sodium L-ascorbate, located in white dry container in Ashton lab dry chemicals (glass) cabinet
    b. Weigh out ~100-150mg
    c. Dissolve in 1.5mL DI H_2O (some located in chemistry set hood)
    d. Vortex for ~10 seconds or until dissolved
    e. Use syringe to add 500uL of Na L-ascorbate to each flask, initializing PEG reaction
23) Prop up flasks in chemistry set hood, inserting a slow nitrogen syringe into each flask and a 'vent' syringe tip into each flask

24) Leave flasks overnight for 16 hours to allow reaction to occur
25) Place PEG solution and Initiator back in -20C freezer
26) Clean off stamps with SDS overnight
    a. Place stamps in large (~1L) beaker with stirbar
    b. Pour some SDS (enough to coat) onto stamps inside of beaker
    c. Add ~200mL MilliQ H2O to beaker
    d. Stir overnight to clean stamps

Day 2: Washing

27) Move treated schlenk flasks to the far hood (without the chemistry set)
28) Cut zip ties and remove rubber stoppers
29) Pour out treatment solution (PEG with sodium L-ascorbate) into waste beaker
30) Rinse by spraying ethanol into flask and swirling to clean out, then dump ethanol into waste beaker (be careful not to dump the slides into the waste beaker)
31) Dump out the slides onto a petri dish or kimwipe and set schlenk flask aside
32) Carefully split apart the back-to-back slides and rinse each individually with ethanol and nitrogen
    a. If there is a smudge spot, use acetone for additional washing, followed by an extra ethanol wash
33) Repeat steps 29 – 32 for all flasks and slides
34) Place slides face-up in petri dish
35) If slides contain more than one pattern per slide, use glass cutter to carefully score and snap into individual patterns
36) Return slides face-up in petri dish, and pour 100% ethanol on them, making sure they are all fully coated
37) Parafilm and tin-foil the petri dish to protect from light
38) Place dish on oscillator for 2 hours for final wash
39) Put petri dish in dessicator until it is time to coat ECM; the slides can be kept in the dessicator for several days if necessary

Day 2 or later: ECM Coating

40) If further sterilization is desired, do one more ethanol wash and allow them to air dry for several minutes
41) Conduct 3X PBS washes of the slides
42) Place slides in the proper 6- 12- or 24-well plate
    a. If desired, place additional ECM coating in the plate before adding the slides in order to adhere the slides more rigidly onto the plate. This is particularly necessary for live cell imaging, timelapse imaging, or brightfield stitches
43) Add ECM and allow it to coat overnight
    a. For cardiomyocytes, the following mixture is known to work:
        i. 12 mL DMEM
        ii. 1 vial matrigel (1mg matrigel)
        iii. 144uL fibronectin
        iv. Take the above reagents, mix cold in the DMEM, and add 1mL to each 12-well containing micropatterned slides
44) Seed cells the following day

COLLAGEN GEL PRODUCTION

Max Salick, 4/24/2012
Rev 1: MS 6/12/2012 – Added table for faster calculations of reagents
Rev 2:

This procedure describes the polymerization of collagen gels for cell culture use. Collagen self polymerizes when neutralized and at raised temperatures. Collagen is kept in an acidic solution at 4C for storage until it is used. While still in its monomeric form, the collagen solution is quite viscous and difficult to pipette. Keep the HEPES solution and collagen solutions on ice throughout the procedure, and mix them and distribute them quickly into their molds.

There is some variability between lots in collagen solutions. The Keely lab does vigorous QC when preparing to purchase another lot, so coordinating with them will help to ensure that a good bottle is purchased.

Reagents

- PBS
- HEPES Buffer Solution (1M) (Invitrogen, 15630-080)
- Collagen Solution (BD Biosciences, Cat# 35424)

Procedure

Prepare HEPES 100mM solution in advance, and keep a large bottle of it next to collagen in a 4C fridge. To prepare HEPES 100mM solution, add 4mL HEPES 1M solution to 36mL PBS.

1) Place HEPES and collagen solution on ice
2) Calculate the amount of collagen, HEPES, cell solution, and media will be mixed to create desired gel.
    a. Collagen is based on desired concentration. Typical amounts range from 1mg/mL (very soft) to 4mg/mL (stiffer). This can be set to match physiologically relevant values.
    b. The volume of HEPES (2X, 100mM) added should be the same as the amount of collagen added.
    c. Calculate the number of cells to add based on the concentration of cells in available cell solution. Typically seeding density is around 100,000 cells per mL.
    d. Add media to reach the desired gel volume.
3) Add cell solution, media, and HEPES solution together in a small tube
4) Quickly add the collagen solution, and place the tube on ice while pipetting the final solution several (~20) times to make a good, homogenous mixture
5) Quickly transfer mixed solution to mold or well
6) All solution to cure at room temperature to 10 minutes
7) <u>Gently</u> transfer mold/plate to incubator and allow 60 minutes of polymerization at 37C

The following table gives volumes of reagents needed to produce 1mL of collagen scaffold, given an initial collagen concentration of 9.49g/mL:

Concentration	**1 mg/mL**	**2 mg/mL**	**3 mg/mL**
Collagen Sol'n	0.105 mL	0.211 mL	0.316 mL
HEPES Buffer	0.105 mL	0.211 mL	0.316 mL
Cell Sol'n	X	X	X
Media	0.79 – X	0.578 – X	0.368 – X

FIBRIN PREPARATION PROTOCOL

Derived from:
Ye KY, Sullivan KE, Black LD (2011). Encapsulation of cardiomyocytes in a fibrin hydrogel for cardiac tissue engineering. *J. Vis. Exp.* **55**, 3251.

Preparation of fibrinogen / thrombin stock solutions ***(done well in advance)***

Fibrinogen Stock Solution:

1) Prepare a 33 mg/mL stock solution of fibrinogen in 20 mM HEPES buffer in 0.9% saline by slowly mixing fibrinogen into the HEPES buffered saline over several hours at 37°C.
2) Allow the solution to settle overnight at 2-8°C.
3) Warm the solution to 37°C
4) Sterile filter the solution through a series of consecutive filters: 40 µm cell strainers, 0.45 µm bottle top filters with glass pre-filters, and 0.2 µm bottle top filters with glass pre-filters.
5) Aliquot the solution into 1 mL and 3 mL aliquots and stored at -20°C.

Thrombin Stock Solution:

1) Prepare a 25 U/mL stock solution of thrombin by adding 500 U of thrombin to 18 mL of 0.9% saline and 2 mL of sterile deionized water
2) Sterile filter through a 0.2 µm filter
3) Aliquot into 500 µl and 250 µl aliquots and freeze at -80°C.

Casting fibrin gels with encapsulated cells

1) To make 1 mL of fibrin gel (3.3 mg/mL final fibrinogen concentration, 25 U/mL final thrombin concentration), create F solution in a conical tube by adding 112 µl of the fibrinogen stock to 558 µl of 20 mM HEPES Buffer in 0.9% saline solution.
2) In a separate conical tube, create a T solution by adding 17 µl of the thrombin stock, and 1.3 µl of 2 N Ca++ (calcium chloride) solution to 135 µl of DMEM. See Table 1.
3) In a third conical tube, prepare a cell solution by spinning down the cells and resuspending the cells in a volume so that the concentration of cell is 29.4 million cells/mL or 6 times the concentration of the desired final concentration of cells in the construct
4) When you are ready to cast the fibrin gel construct, prep a 1 mL syringe with a 18G 1 ½ inch long needle. Have a 21G 1 inch needle ready as well.
5) The fibrin solution is created at a 4:1:1 ratio of F solution: T solution: cell solution. To make one mL of gel, add 667 µL of F solution into a clean 50 mL centrifuge tube, followed by 167 µL of cell solution, and lastly add 167 µl of T solution. Pipette to mix solution together being careful not to introduce bubbles. Once solutions are mixed, the reaction has started and the injection of the constructs should be done immediately.
6) Take the previously prepared syringe with the 18G needle and draw up fibrin solution. Take care not to invert the syringe to prevent bubbles from getting into the needle. Replace 18G needle with a 21G needle. Tap syringe gently to force out air bubbles.

HYALURONIC ACID METHACRYLATE PREPARATION

Max Salick, 10/12/2011
Rev 1: 10/27/2011 MS, Added missing “overnight at 4C” step, fixed minor typos
Rev 2: 11/16/2011 MS, Changed overnight to 24 hours, added NaOH addition suggestions
Rev 3: 11/17/2011 MS, Fixed NaOH addition suggestions

Reagents

- Hyaluronic acid sodium salt from streptomyces equi (Sigma, 53747-1G)
- Methacrylic Anhydride (Sigma)
- 5N NaOH (Sigma, 656046-6x1L)
- 95% EtOH
- Dialysis Supplies (~10,000kDa)

2 Procedure

Day 1: Methacrylation

1) Weigh out [**x = _______**] grams of HA (initial amount corresponds to amount of final product)
2) Dissolve in [**x * 100 = ________**] mL of DI H2O to form a 1% (w/v) solution
3) Heat to 60C with stirring in fume hood until dissolved
4) Once dissolved, solution should be very viscous. Allow to cool to room temperature before continuing
5) While still in fume hood, place solution on ice, and add 10-fold molar excess of methacrylic anhydride DROPWISE to HA solution. This corresponds to **[3.96 * x = ________]** mL of MA solution.
6) Maintain pH at 8-9 in fume hood. Do this by frequently adding 5N NaOH over several hours. Exercise caution while working with 5N NaOH. *Note: This part can be challenging, as it takes a few minutes for the pH meter to react to the addition of NaOH. Experimental observations suggest the following addition amounts:*
7) If pH < 7, add **[2x = ________]** mL NaOH and wait for ~3 minutes
8) If 7 < pH < 8, add **[x = _________]** mL NaOH and wait for ~3 minutes
9) If 8 < pH < 8.25, add **[x/2 = _________]** mL NaOH and watch meter closely. NaOH may need to be added within 30 seconds or so.
10) If 8.25 < pH < 9, watch closely and add amount in (c) when pH hits 8.25
11) If 9 < pH, wait for several minutes for pH to drop to 8.25
12) Allow to react at 4C for 24 hours with stirring

Day 2: Precipitation and Dialysis

1) Chill 95% EtOH on ice
2) Precipitate methacrylated HA into chilled 95% EtOH. 10-fold volume ratio of EtOH:HA should be used. This should correspond to **[1040 x x = ________]** mL of 95% EtOH.
3) Pour out the supernatant. Resulting precipitate should be white and gooey.
4) Dissolve remaining precipitate in **[x * 15 = _________]** mL of DI H2O.
5) Pour solution into 10,000 MWCO dialysis tubing and dialyze for 2 days. Change DI H2O four times at even periods throughout this process.

Day 4: Lyopholization

1) Pour dialyzed solution into 50mL conical tubes and freeze in -80C freezer.
2) Lyophilize for 1 week

POLYMERIZATION OF POLYACRYLAMIDE GELS

Max Salick

Notes

Polymerization of polyacrylamide gels occurs when the monomers (acrylamide and bis-acrylamide) contact initiators (TEMED and aluminum persulfate). Oxygen and temperature have a large impact on how well the gels polymerize. The main focus during this procedure is to reduce the amount of oxygen in the solution, as well as the amount of oxygen in contact with the gel during polymerization. Additionally, the gel solution and the mold in which it polymerizes should be as close as possible to 25°C. This is the ideal temperature at which polymerization occurs.

Avoid shaking the solutions or creating bubbles, as this introduces unwanted oxygen into the solution
Before polymerization, make sure both the solution and *all* components of the mold are at ~25°C.
The initiators must be freshly mixed with DI H_2O. Do not use an initiator solution that is more than one or two hours old. The following procedure saves the mixing of the initiators until the latest possible time, to ensure maximum reactivity.

Reagents

5mL	DI H_2O
1.5mL	Stock polyacrylamide solution
25uL	TEMED
25mg	Ammonium Persulfate
~3mL	50 mM HEPES solution

Equipment

Glass vial with plastic seal and soft rubber stopper
Vacuum with needle
2 mini-centrifuge tubes (~2-3 mL)
Scale (accurate up to 1 mg)
Weighing boats or paper
1000uL, 500uL, 475uL, 25uL, 15uL Micropipettes
Hot bath
Gel mold
Petri Dish
Pipette, with 5mL tip
60-100um Glass Beads

Procedure

1) Get all reagents and equipment to desired temperature
2) Set hot bath to 27°C
3) Micropipette 1.5mL of stock acrylamide solution into glass vial, sealing vial with plastic stopper
4) Place glass vial, as well as all gel mold components into plastic bag
5) Place plastic bag into hot bath, and start timer (15 minutes)
6) Prepare for polymerization
7) Place needle at end of vacuum
8) Prepare scale with tared weighing boat
9) Add 500uL DI H_2O to mini-centrifuge tube and label “AP” (ammonium persulfate)
10) Add 475uL DI H_2O to other mini-centrifuge tube and label “T” (TEMED)
11) Retrieve ammonium persulfate (AP) and TEMED containers from storage. Place AP next to scale, and TEMED next to micropipettes

Degassing (if components have been heated to 25-27°. This usually takes about 15 minutes in the hot bath)

12) Remove plastic bag from hot bath and empty its contents
13) Replace plastic stopper with soft rubber stopper on glass vial
14) Turn on vacuum and puncture soft rubber stopper with needle. This begins the degassing process, removing oxygen from the stock solution. Start timer (5 minutes)

Prepare initiators (during degassing process)

15) Weigh 25mg AP and add to mini-centrifuge tube labeled “AP”
16) Mix AP solution gently until fully dissolved
17) Micropipette 25uL TEMED into mini-centrifuge tube labeled “T”
18) Mix TEMED solution gently
19) Place beads in empty mold (for mechanical testing samples). Use enough to have about 6 or 7 beads evenly distributed in the neck region of the mold.

Polymerize (after 5 minutes of degassing)

20) With vacuum still running, remove needle from glass vial
21) Turn off vacuum
22) Remove rubber stopper from glass vial
23) Quickly micropipette 15uL AP solution into glass vial
24) Quickly micropipette 15uL TEMED solution into glass vial
25) Gently stir solution
26) Pipette final solution into desired mold
27) Allow gel to polymerize for 90-120 minutes

Store gels

28) Remove gels from mold and place in petri dish
29) Coat gels with HEPES solution, and store
30) Aspirate and reapply HEPES solution every ~12 hours for 48 hours
31) Finalize gels with cell coating, as shown in PA Gel Finalization Procedure

PRODUCTION OF POLYACRYLAMIDE STOCK SOLUTION

Max Salick and Laurie Hazeltine

Notes

The two monomers required to produce polyacrylamide gel are *acrylamide* and *bis*. Stock solutions of these reagents can be made and stored at 4°C for a time period along the order of months. The stiffness of the gel is determined by the concentration of the bis monomer in the stock solution. For this reason, stocks of varying amounts of bis are created.

Acrylamide is very hazardous, and may cause cancer and heritable genetic damage. Take extreme caution when dealing with this chemical in its powdered form.
Bis is a light, fibrous solid which may be difficult to measure due to its low required molarity in the solutions.
The final solution must be wrapped in tinfoil to prevent contact with light.

Reagents

55 mL	DI H_2O	
5.5 g	Acrylamide, electrophoresis grade 99+%	*ACROS organics*
70 mg	Bis-Acrylamide, electrophoresis grade (N,N' Methylene bisacrylamide)	*Fisher BioReagents*

Equipment

5 Centrifuge Tubes (~15mL), wrapped in tinfoil and labeled
>70mL Flask
Fume hood (with scale, accurate up to 0.1 g)
Scale (accurate up to 1 mg)
Weighing boats or paper
Stirring Rod
Pipette, with 10mL tip and 25mL tip

Procedure

1) Dilute acrylamide to 10%, and distribute to individual centrifuge tubes
2) Using 25mL pipette, add 55mL DI H_2O to flask
3) Weigh 5.5g acrylamide and mix thoroughly into flask
4) Using 10mL pipette, aliquot 10mL of solution from flask into each centrifuge tube

5) Add varying concentrations of bis-acrylamide to respective tubes
6) Weigh specific amounts of bis-acrylamide using precise scale and add to respective tubes

Concentrations (by weight) range from 0.03% to 0.3%. Higher concentration of bis results in a stiffer hydrogel. Commonly used concentrations are shown below:

Gel #	Bis-acrylamide Concentration	Bis-acrylamide Added
1	0.03%	3mg
2	0.06%	6mg
3	0.1%	10mg
4	0.2%	20mg
5	0.3%	30mg

PEG PRODUCTION

Max Salick (assistance by lab of Kristyn Masters), 11/1/2010

Notes

The following procedure allows one to produce biologically inert poly(ethylene glycol) diacrylate, capable of encapsulating living cells. The procedure has been modified to produce very high-quality PEG, but this also requires that the procedure take a period of ~2 weeks.

Equipment

Day 1
Fume hood
Furnace
Scale
Hot plate w/ mount
Pipette (1000μL)
Stir rod
Rubber stopper
Vacuum
Argon tank
Syringe needles
Syringe (5mL)
Ice
500mL round flask
>50mL graduated cylinder

Day 2
1L Erlenmeyer flask
1L beaker
Ceramic funnel
Filter paper (110mm diam)

Day 6
Hot plate
4L pyrex beaker
Dialysis clamps
Dialysis membrane
Dialysis floats

Day 9
Freezer
Lyophilizer
500mL beaker
50mL conical tubes
Rubber bands
Kimwipes

Reagents

PEG (Sigma-Aldrich, 202444-500g)
Located: On shelves in Masters lab

Acryloyl chloride, 97% (Aldrich, A24109-100g)
Located: 4°C fridge
MW: 90.51
Density: 1.119 g/mL

Triethylamine (TEA) (Aldrich, 471283-100g)
Located: Bases drawer in chemistry room
FW: 101.19
Density: 0.726

Dichloromethane reagent ACS 99.5% (Acros 40692-0040)

Ethyl ether anhydrous (E138-4)
Non-recycled

DI H_2O

Procedure

Day 1: PEG Mixing and Preparation

1) Remove acryloyl chlorine [left fridge, middle shelf] and allow to warm to room temperature in fume hood for 2 hours
2) Prepare 500mL round flask, graduated cylinder (for solvent), and oval stir bar
3) Clean flask, cylinder, and stir bar with soap and water, followed by acetone
4) Dry flask, cylinder, and stir bar in furnace at 100°C for 30 minutes
5) Calculate moles of PEG [main lab, room temp shelf] needed

$$x = amount\ of\ PEG\ to\ produce\ (g) = \underline{\qquad\qquad}$$

$$MW = molecular\ weight\ of\ PEG\ (Da) = \underline{\qquad\qquad}$$

$$Moles\ PEG = \frac{x}{MW} = \underline{\qquad\qquad}$$

6) Calculate amount of acryloyl chloride needed

$$Acryloyl\ chloride\ vol\ (moles) = \frac{x}{MW} * 4 = \underline{\qquad\qquad\qquad}$$

$$Acryloyl\ chloride\ vol\ (mL) = \frac{x}{MW} * 323.5 + 1 = \underline{\qquad\qquad\qquad}$$

7) Calculate amount of triethylamine (TEA) ['BASES' drawer in chem. room] needed

$$TEA\ (moles) = \frac{x}{MW} * 2 = \_\_\_\_\_\_\_\_\_\_$$

$$TEA\ (mL) = \frac{x}{MW} * 278.8 = \_\_\_\_\_\_\_\_\_\_$$

8) Calculate amount of dichloromethane (solvent) [‘FLAMMABLE’ drawer in chem. room] needed

$$Dichloromethane\ (mL) = 3 * x = \_\_\_\_\_\_\_\_\_\_$$

9) Measure dichloromethane with graduated cylinder and pour into round flask
10) Weigh out *x* grams of PEG and add to round flask
11) Pipette TEA into round flask
12) Suspend flask over hot plate and add oval stir rod
13) Place rubber stopper on flask
14) Pull vacuum for 6 minutes

Add argon

15) Place needle at end of argon tube and puncture stopper
    a. **Place extra needle through stopper to act as vent**
16) Turn on argon to fill for 3 minutes
17) Remove argon needles and use a 5mL syringe to add acryloyl chloride dropwise to solution
18) Turn on stir rod at middle setting
19) Puncture stopper with syringe and add 1 drop per 10 seconds
20) Pull vacuum for 6 minutes

Add argon

21) Place needle at end of argon tube and puncture stopper
    a. **Place extra needle through stopper to act as vent**
22) Turn on argon to fill for 3 minutes
23) Place on ice for 2 days
24) Replace ice at 2 hours
25) Replace ice at 6 hours
26) Replace ice following morning
27) Replace ice after 12 hours
28) Replace ice following morning
29) Begin day 2 procedure ~48 hours after initial application of ice

Day 3: Ether rinsing

30) Refrigerate ether at 4°C for 2 hours
31) Prepare large (1 L) beaker, large (1 L) Erlenmeyer flask, and large ceramic funnel [chem. room sink]
32) Clean flask, beaker, and funnel with soap and water, followed by acetone
33) Dry flask, beaker, and funnel in furnace at 100°C for 30 minutes
34) Flask and top portion of funnel should be dry before continuing
35) Place large ceramic filter on flask and place 110mm diameter filter paper in filter
36) Pour (non-recycled) ether into large beaker
37) Wet filter paper with ether
38) Rinse PEG through filter paper with ether

39) Pour 1/3 of ether into round flask
40) Dump round flask through filter
41) Pour 1/3 of ether into round flask
42) Dump round flask through filter
43) Pour remaining ether directly onto filter to wash PEG
44) Take filtered PEG on filter paper and dump into empty ether beaker
45) Wrap ether beaker in foil and punch holes through top
46) Allow to sit in fume hood for 4 days
47) Pour filtered ether into yellow carboy in chemical room

Day 7: Dialysis

48) Clean 4000mL pyrex cylinder, smaller (~400mL) beaker, and plastic funnel
49) Clean cylinder, beaker, and funnel with soap and water, followed by acetone
50) Dry cylinder, beaker, and funnel in furnace at 100°C for 30 minutes
51) Get clamps and floats
52) Dilute PEG in 20*x mL of DI H_2O
53) Get dialysis tubing from box on second shelf in left fridge
54) Fill large pyrex cylinder with DI H_2O

Fill membranes with PEG solution

55) Measure out and cut 25cm of membrane
56) Fold end of membrane twice and clamp
57) Wrap end of tube around funnel and pour PEG solution inside
58) Make sure to leave ~4cm empty region in top of tube to allow space for expansion
59) Fold top end of membrane twice and clamp
60) Place float over top end and submerge in large cylinder

Repeat until all PEG is used

61) Wrap large cylinder in foil
62) Place on hot plate and stir at medium setting (3)

Replace DI H_2O over period of 3 days

63) Replace at 2 hours
64) Replace at 6 hours
65) Replace at 24 hours
66) Replace at 48 hours

Day 10: Lyophilization

67) Clean 500mL beaker
68) Clean beaker with soap and water, followed by acetone
69) Dry beaker in furnace at 100°C for 30 minutes
70) Dump membrane contents into 500mL beaker
71) Aliquot contents into 50mL conical tubes
72) Place conical tubes into -80°C freezer for 4 hours
73) Remove conical tubes from freezer and get lyophillization tube
74) Remove tops from conical tubes and rubber-band kimwipe over top
75) Place tube tops at bottom of lyophilization tube

76) Place conical tubes in lyophilization tube face-up
77) Attach lyophilization tube to lyophilizer at any free nozzle
78) Turn nozzle to "VAC"
79) Label lyophilization tube with initials and date
80) Observe to make sure vacuum needle goes back to green
81) Lyophilize for 4 days

If there are many vessels on the lyophilizer, lyophilize for 5-6 days to ensure proper vacuum drying.

PRODUCTION OF MECHANICAL TEST SAMPLES VIA UV POLYMERIZATION THROUGH MASK

Max Salick, 6/22/2010

Notes

Creating masks to produce a sample of a desired shape can be less expensive, although more difficult, than producing an entire mold to create that shape. The UV mask should be printed in extremely high resolution, so the shape of the resulting samples is as accurate as possible. The most challenging part of creating these samples is handling the liquid solution of the polymer and keeping in the right place during polymerization.

This procedure is for PEG-DA hydrogels, and it results in the creation of 8 dogbone samples of approximately 2cm in length. The addition of EB20 media is done to correlate to the addition of cell solution during a parallel biological test. Most mechanical tests will not need this. The recipe for the polymer can vary greatly.

Equipment

- 2x Petri Dish
- Polymerization Mask (cut to size of petri dish) (p*rinted by ImageSetter)*
- Clear Transparency (cut to size of petri dish)
- UV Lamp *(UVP Black-Ray UV Bench Lamp 115V ~60Hz)*
- Disposable Plastic Pipette / Water dropper
- 50mL Conical Tube
- 50mL 0.22um Steriflip
- Small Metal Spatula
- 30-50um Diameter Glass Beads

Reagents	***Amount***
Poly(ethylene glycol)-diacrylate (PEG-DA)	1g
Phosphate-Buffered Saline (PBS)	6.053mL + extra for sample storage (~5mL)
EB20 Media	283uL
Irgacure-2959	331uL

Procedure

1) Turn on UV light to get it warmed up. It takes a few minutes for it to reach its normal intensity

Solution Preparation

2) Mix 1g PEG with 6.053mL PBS and 283uL EB20 mediain 50mL conical tube. The PBS and EB20 may be mixed and aliquoted ahead of time for multiple sets of samples
3) Vortex to help dissolve PEG into PBS/EB20 solution
4) Leave solution to dissolve while preparing mold

Mold Preparation

5) Take the top side of a petri dish and break off a part of the edge. This allows you to peel the transparency off of the dish easily after polymerization
6) Place four small water drops on the inside of the top part of the petri dish.
7) Place the clear transparency onto the droplets and press it firmly to the dish so it is adhered and flush with the dish
8) Place water drops on the outside of the bottom part of the petri dish

9) Place the mask transparency onto the droplets and press it firmly to the dish so it is adhered and flush with the dish
10) Place the PDMS disk onto the top portion of the dish directly onto the PDMS. Press down on the disk so that it creates a seal with the transparency

Further Solution Preparation

11) Once the PEG has dissolved and the solution is clear once again, sterilize it using the steriflip (this is done to match the parallel biological sample procedure)
12) Add 331uL non-sterile I-2959 to the solution and vortex slightly. Take care not to create bubbles. If bubbles are formed, pipette them out
13) Pour the solution into the PDMS mold so it remains in the reservoir
14) Sprinkle glass beads onto the solution as it sits in the mold. Try to spread them evenly, but do not use too many
15) Place the bottom petri dish side with the mask attached to it directly onto the other side of the mold. Make sure the two sides make a seal and the gel solution is trapped between the two transparencies and the PDMS disk

Polymerization

16) Place mold under UV lamp and expose for 3 minutes
17) After 3 minutes, flip the mold upside-down and expose for another 3 minutes
18) Once finished, remove the mold from the UV lamp and turn off the lamp

Sample Removal and Storage

19) First separate the transparencies from the petri dishes by gently wedging the metal spatula between them
20) Carefully peel the transparencies from the samples and place the samples in the extra petri dish
21) Pour PBS into this dish to hydrate the gels
22) Wash off the mask and clear transparency

MECHANICAL TESTING OF HYDROGELS

Max Salick, 2/22/2009

Notes

The soft, viscoelastic properties of hydrogels make them much more difficult to handle during mechanical testing than solid samples. The procedure is a basic tensile test, however it has been modified significantly to account for the environment that the gels experience during cell culture. Optical methods are used to measure strain, while load data is acquired through the MicroInstron. Stress is calculated by direct optical measurement of cross-sectional slices after the test is finished.

Difficulties in this procedure arise due to the soft nature of hydrogels. It is critical that the samples are held as vertical as possible to ensure that applied stress is axial. During sample preparation, glass beads must be embedded into the sample. These beads must be small enough to not impact the macroscopic mechanical properties of the sample. It is also important that the samples contain enough glass beads to provide sufficient strain data. Having too many beads in the neck region of the sample can make it difficult to discern between them, and not having enough beads can prevent the tester from having enough data for the sample. Other difficulties may arise in the gripping of the samples. So far, no sample has been successfully tested to fracture. Currently, a rough, abrasive surface is used to grip the samples. This is sufficient to test the linear region of the gel up to approximately 60% strain. Gripping the gels too hard can easily damage the sample. The gels also have a tendency to slide out of the grips if they are tightened too much.

Equipment

- MicroInstron 5548 Test Stand
- Environmental Chamber
- Cycling Water Heater (PolyScience Digital Temperature Controller)
- Fiber optic lamp (Fiber-Lite 3100)
- Calipers
- Tin Foil
- Flat Tweezers
- Camera (QImaging Micropublisher 5.0 RTV)

Software

Merlin v4.42
QCapture Pro v5.1.1.14

Procedure

General Preparation – Done once before all testing

1) Fill environmental chamber with DI water and set water bath to 38°C. It will take at least 30 minutes for the water in the chamber to reach the desired temperature (37°C).
2) Initialize Merlin and QCapture Pro
3) Prepare Merlin software
    a. Open “Max” method and ensure that .raw data will be saved
    b. Load “HYDROBON” test, which is a simple 1 mm/min tensile extension
4) Prepare QCapture Pro Software
    a. Click “Digital/Video Capture”
    b. Set exposure time (recommended: 1.0 sec), gain (recommended: 2.3), workspace field, preview workspace field, and adjust camera focus
    c. Under “Acquire” tab, enable “Multiple Image Capture” and set the capture interval to “minimal”

Test – Repeat for each sample (Only if environmental chamber has reached ~37°C)

5) Remove sample from hydrated dish
6) Measure thickness, width, and length of neck region with calipers while still hydrated
7) Place tinfoil “catcher” under grips to prevent sample from falling into environmental chamber
8) Loosen top and bottom grips so and raise test stand so that the sample can easily slide into place
9) Using flat tweezers, *gently* grip sample and tighten softly into top grip
10) Lower test stand and softly tighten bottom of sample into lower grip
11) Adjust sample and grips to ensure axial deformation
12) Remove tinfoil catcher
13) Raise environmental chamber and check that sample is still aligned as vertically as possible in test stand
14) Prepare Merlin for test:
    a. Input sample name
    b. Input dimensions of sample that were previously acquired with calipers
    c. Zero load and displacement
15) Prepare QCapture Pro for test:
    a. Set image folder and name
    b. Set first image number as “1”
    c. Adjust camera position, focus, and gain, as well as fiber optic light, so that beads shine brightly and clearly in the workspace
    d. IMPORTANT – Make sure that the preview and acquiring workspaces both include the neck region of the sample
16) Run test, recording times of image capture
17) After test is completed (when sample reaches fracture or slipping occurs), lower environmental chamber
18) Carefully remove sample and place in petri dish
19) Raise environmental chamber
20) Lower MicroInstron back to 0.0mm displacement
21) Zero load and displacement
22) In Merlin, add “buoy” to end of previous sample’s name
23) Run same test as before, but without the sample. This provides buoyancy data which can be later removed from the test data so that loading from the water is not included in the final results
24) As this test is running, place used sample in labeled, hydrated vial, and prepare next sample

25) Repeat steps 5-24 until all samples are tested
26) After all samples are tested, lower environmental chamber, and turn off temperature controller and fiber optic lamp

APPENDIX B: QRT RT-PCR TAQMAN PRIMERS

All primers were purchased from Life Technologies.

Gene	Encoded Protein	TaqMan Gene Expression Assay ID	Size (bp)
GAPDH	Glyceraldehyde 3-phosphate dehydrogenase	Hs02758991_g1	93
ATP2A2	sarco/endoplasmic reticulum Ca2+-ATPase	Hs00544877_m1	123
MYH6	Alpha myosin heavy chain	Hs01101425_m1	67
MYH7	Beta myosin heavy chain	Hs01110632_m1	73
TNNT2	Cardiac troponin T	Hs00943911_m1	152
ACTA2	Alpha smooth muscle actin	Hs00426835_g1	105

APPENDIX C: FLOW CYTOMETRY RESULTS

The following pages show the flow cytometry analysis conducted to quantify the level of purification achieved by Zeocin treatments. Zeocin was applied over 4 days to a differentiated population of cardiomyocytes derived from the cTnT-GFP promoter line.

Plotting all points against FITC fluorescence provides a bimodal curve, and detecting the percentage of positive cells along this curve gives a rough estimate of cTnT+ cells (shown in plots as CM ALL). However, cardiomyocytes are difficult to singularize due to the strong cell-cell attachments that they develop. Thus, a second round of analysis was conducted to select for single cells only (P1). Finding the percentage of cells within this group that was FITC+ (CM Valid) was deemed a more accurate estimate of cardiomyocyte population during purification.

Day 8 (0 days of purification)

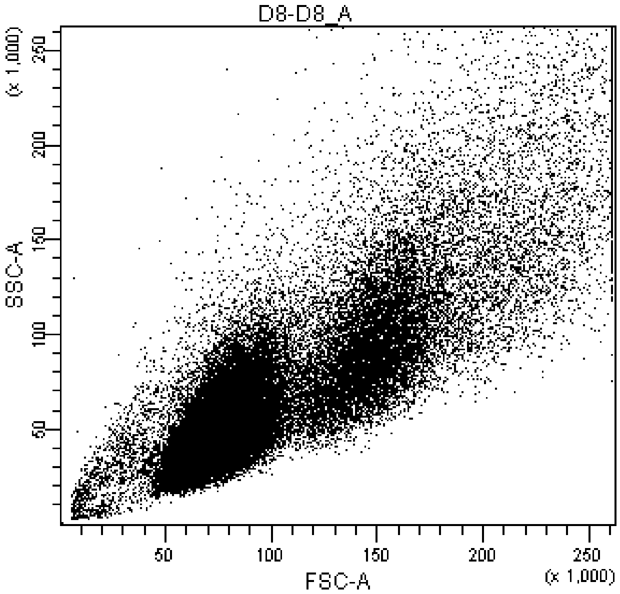

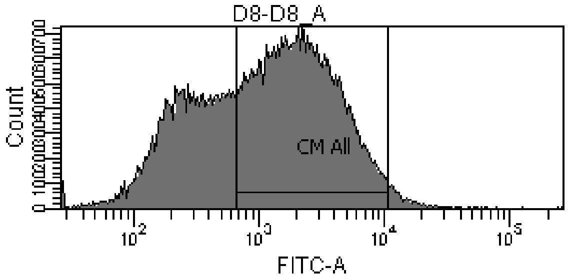

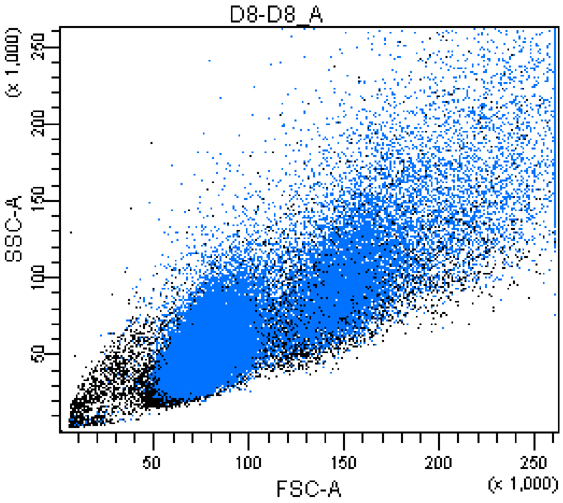

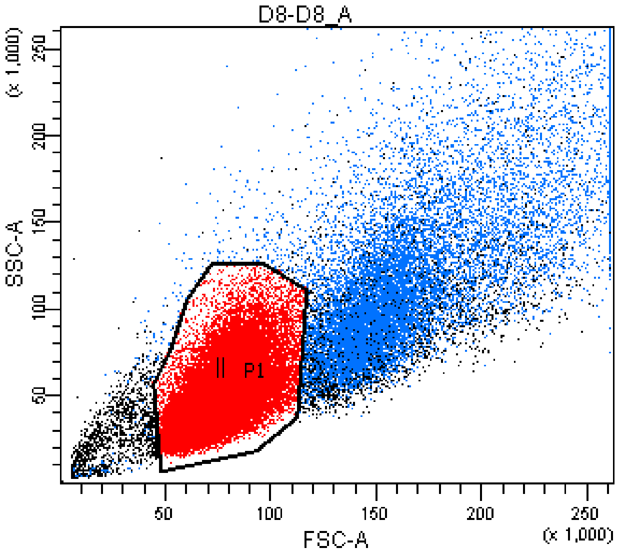

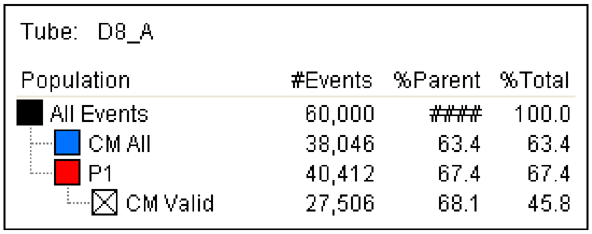
Tube: D8_A

Population	#Events	%Parent	%Total
■ All Events	60,000	####	100.0
🟦 CM All	38,046	63.4	63.4
🟥 P1	40,412	67.4	67.4
☒ CM Valid	27,506	68.1	45.8

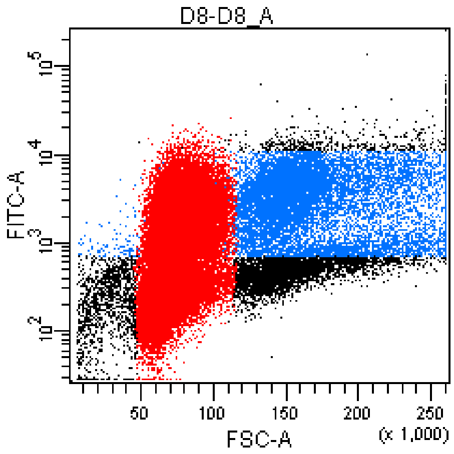

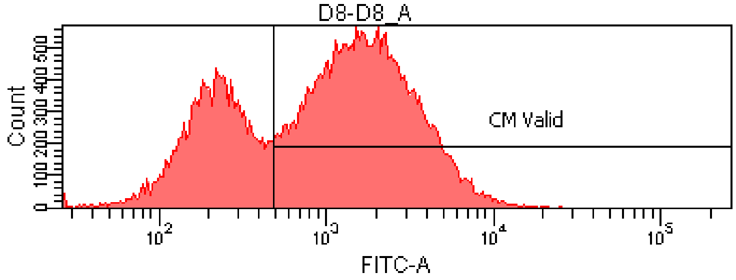

Day 9 (1 day of purification)

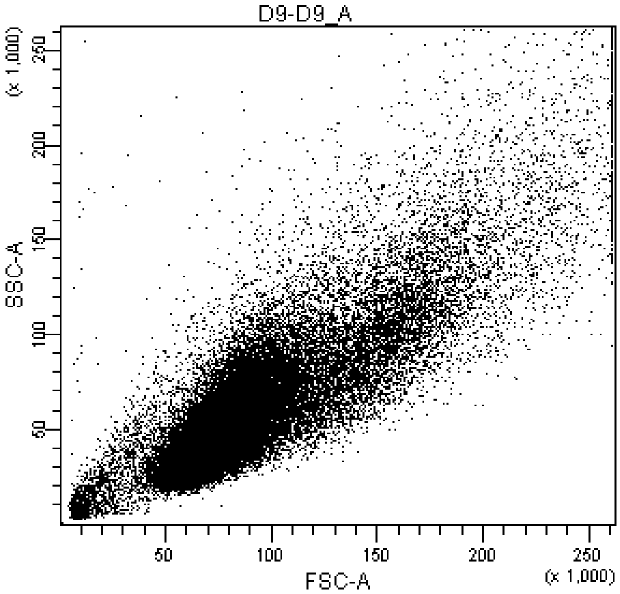

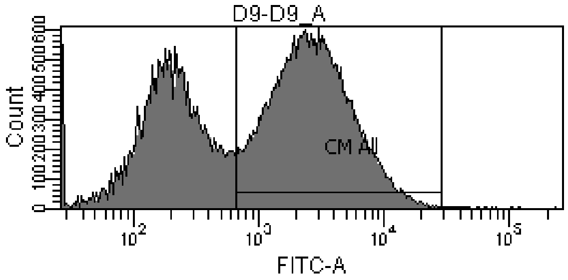

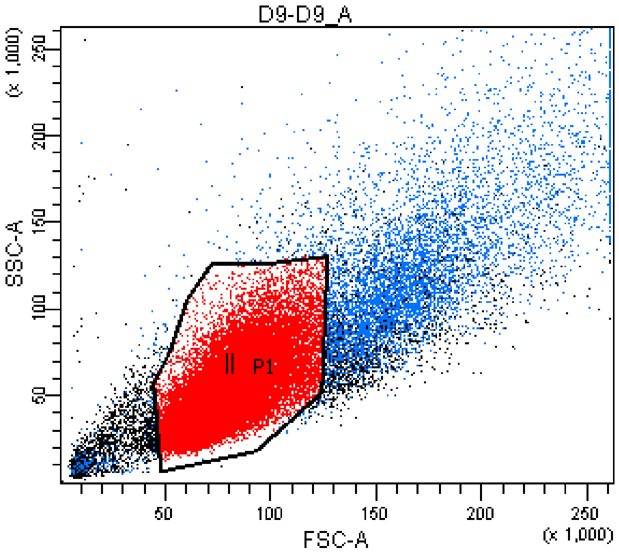

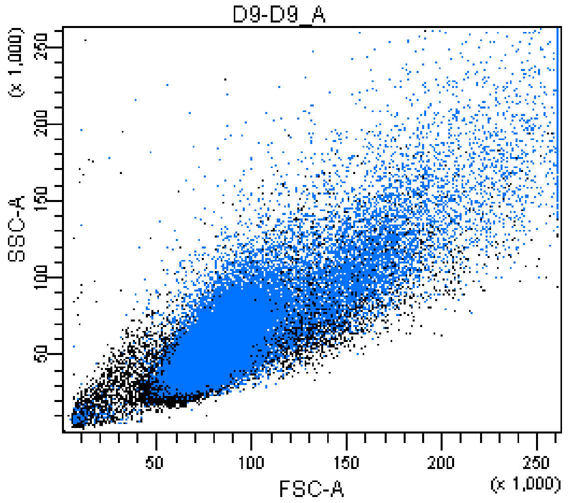

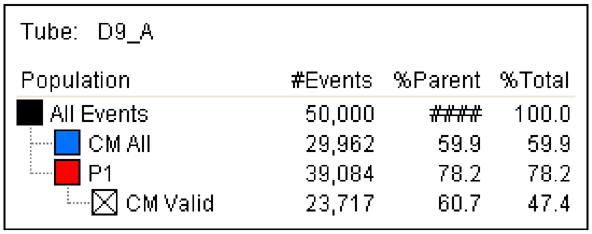

Tube: D9_A

Population	#Events	%Parent	%Total
■ All Events	50,000	####	100.0
🟦 CM All	29,962	59.9	59.9
🟥 P1	39,084	78.2	78.2
☒ CM Valid	23,717	60.7	47.4

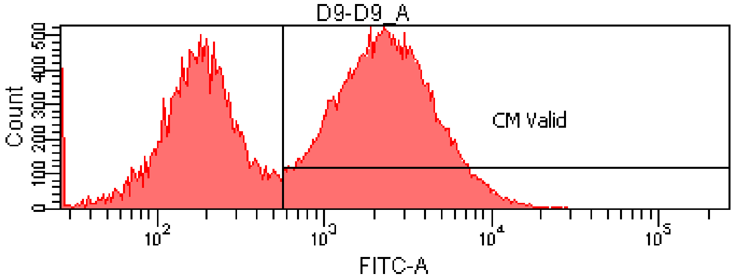

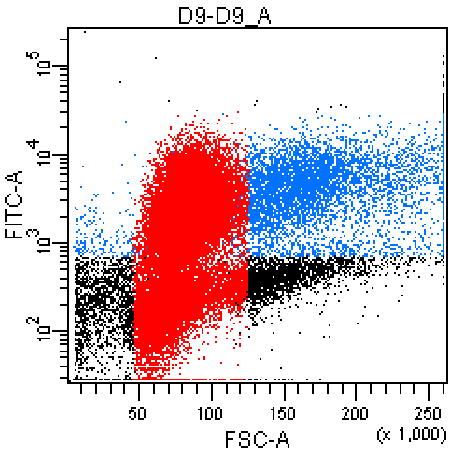

Day 10 (2 days of purification)

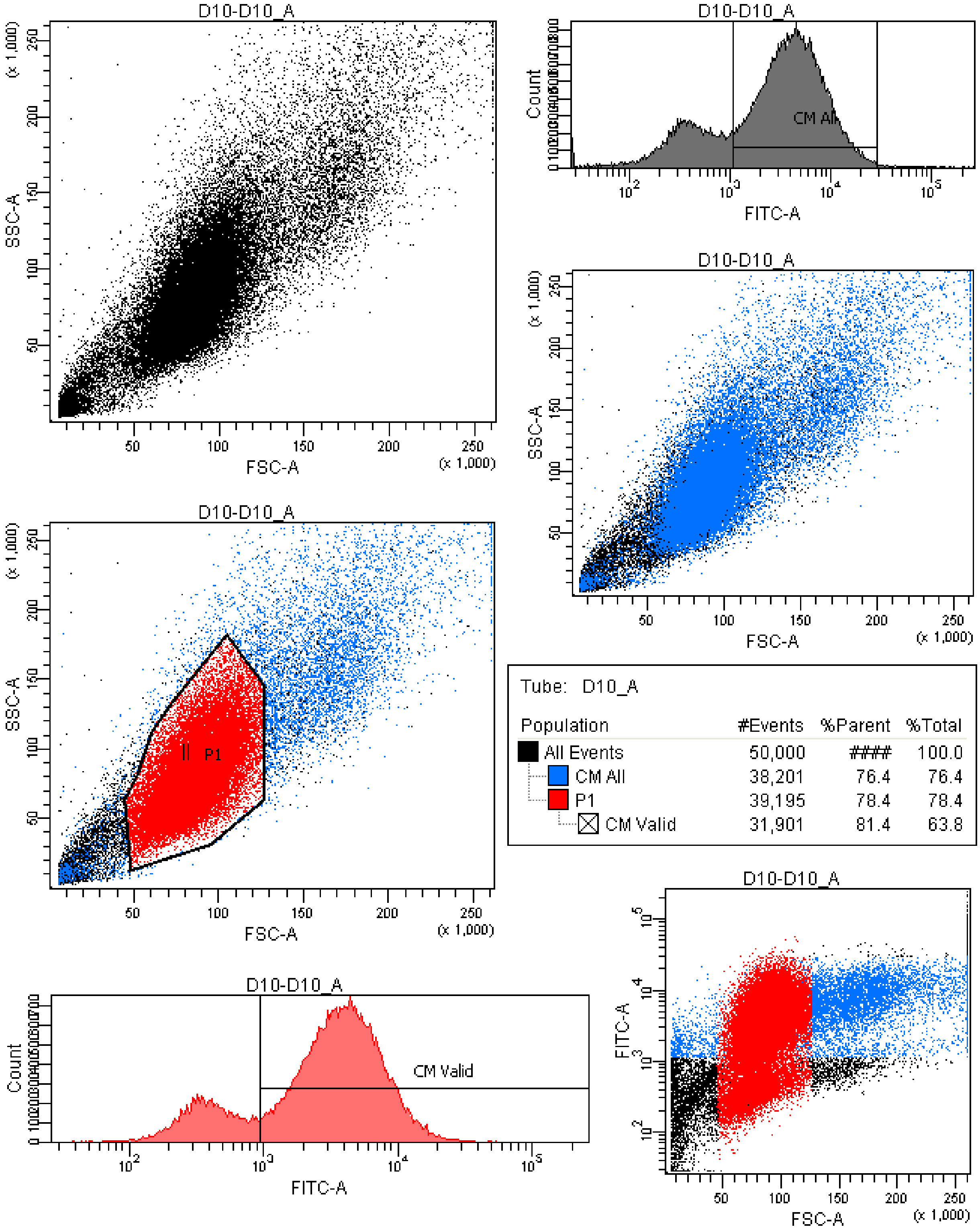

Tube: D10_A

Population	#Events	%Parent	%Total
■ All Events	50,000	####	100.0
🟦 CM All	38,201	76.4	76.4
🟥 P1	39,195	78.4	78.4
☒ CM Valid	31,901	81.4	63.8

Day 11 (day 3 of purification)

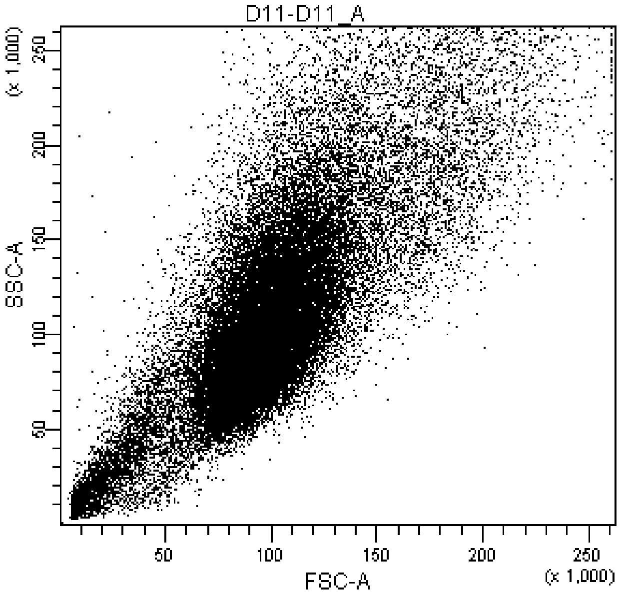

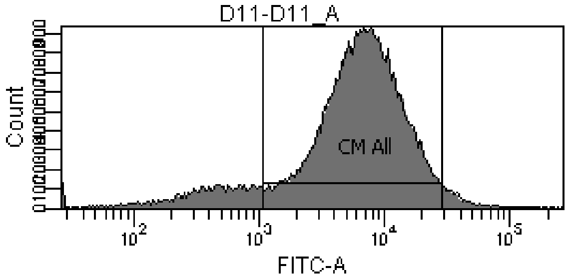

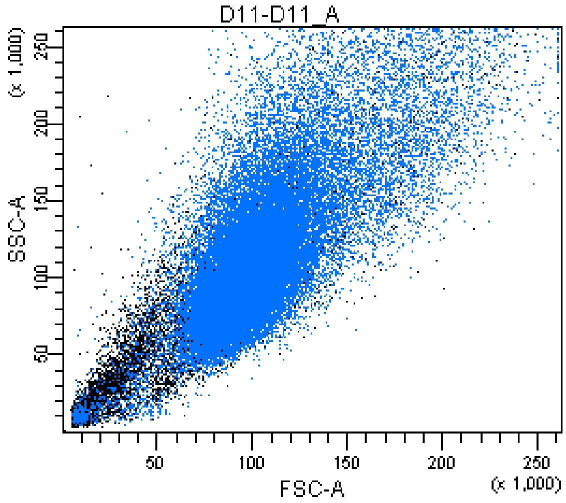

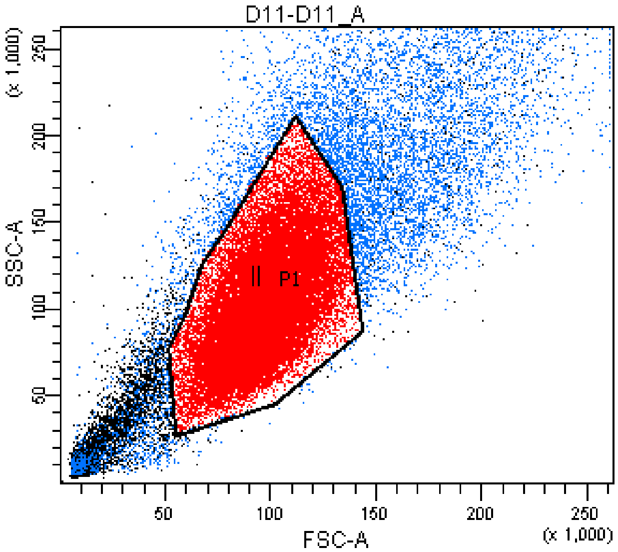

Tube: D11_A

Population	#Events	%Parent	%Total
■ All Events	50,000	####	100.0
🟦 CM All	43,073	86.1	86.1
🟥 P1	35,872	71.7	71.7
☒ CM Valid	33,981	94.7	68.0

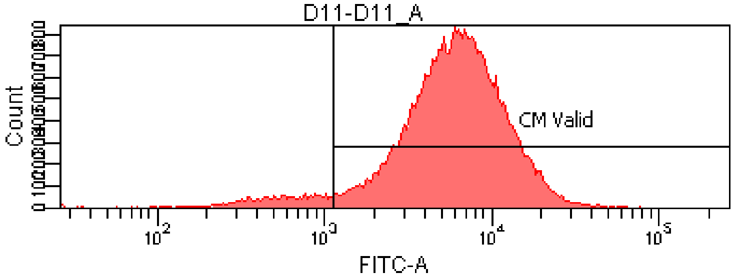

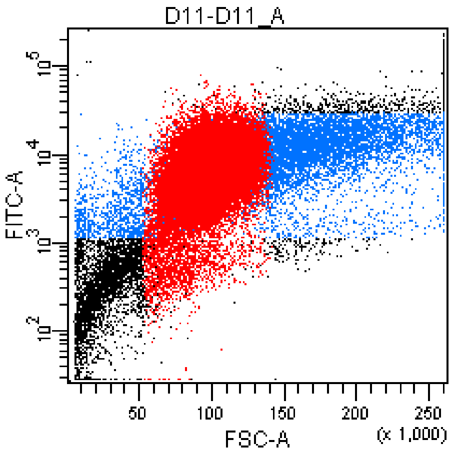

Day 12 (day 4 of purification)

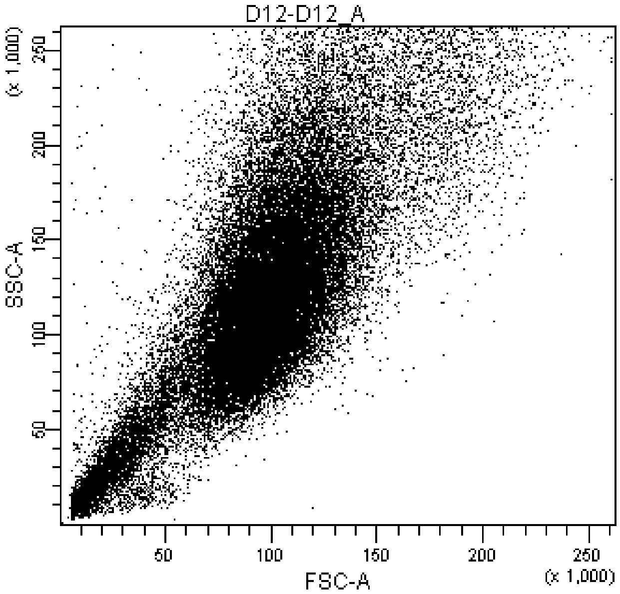

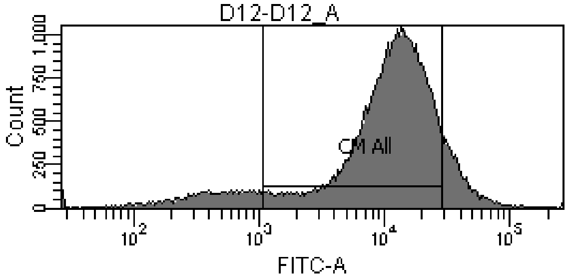

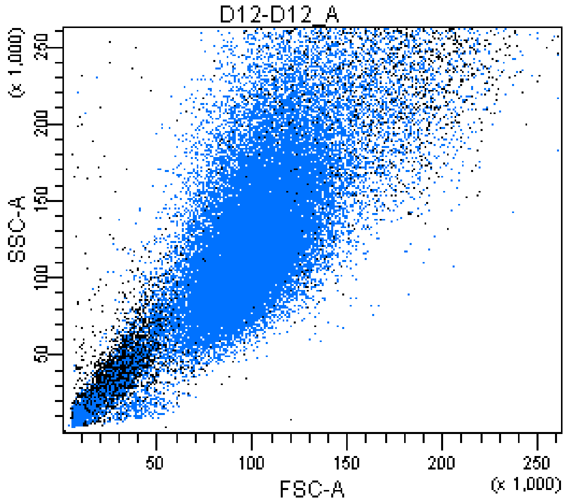

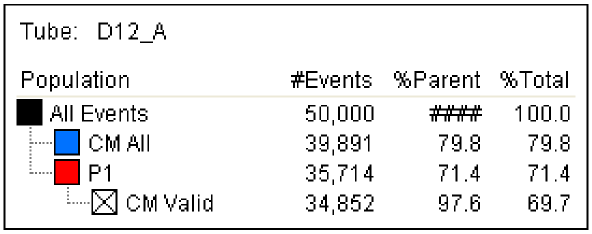

Tube: D12_A

Population	#Events	%Parent	%Total
⬛ All Events	50,000	####	100.0
🟦 CM All	39,891	79.8	79.8
🟥 P1	35,714	71.4	71.4
☒ CM Valid	34,852	97.6	69.7

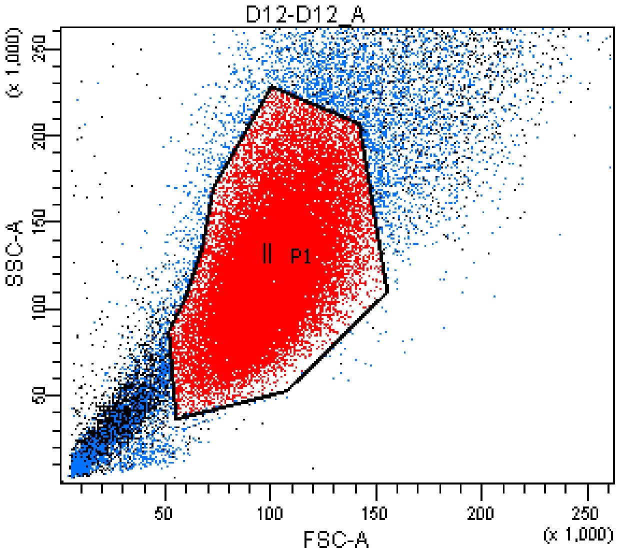

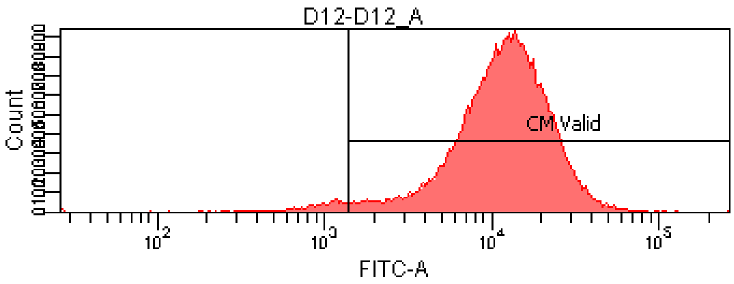

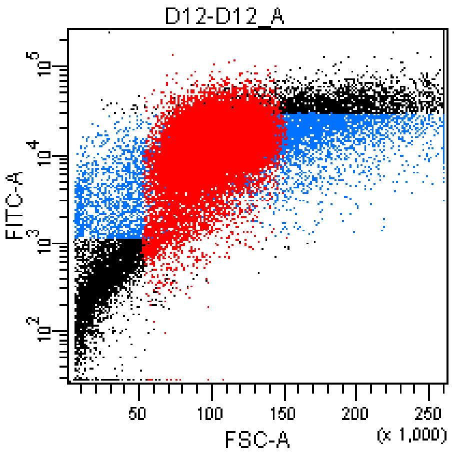

APPENDIX D: MULTI-PARTICLE TRACKING STRAIN ANALYSIS

CODE STRUCTURE

NOTE: Some components of this software utilize the IDL particle tracking package developed by John C. Cocker [1999]. These include the bpass.m, cntfd.m, pkfnd.m, and track.m files, all of which are called on by the main multiparticle_tracker.m file. Due to space considerations, these files are not included in this document. The most updated version is freely available at the following address:

http://physics.georgetown.edu/matlab/code.html

Cocker, JC (1999). Track.m, "Code Repository," physics.georgetown.edu/matlab/code.html. Accessed August 2, 2014.

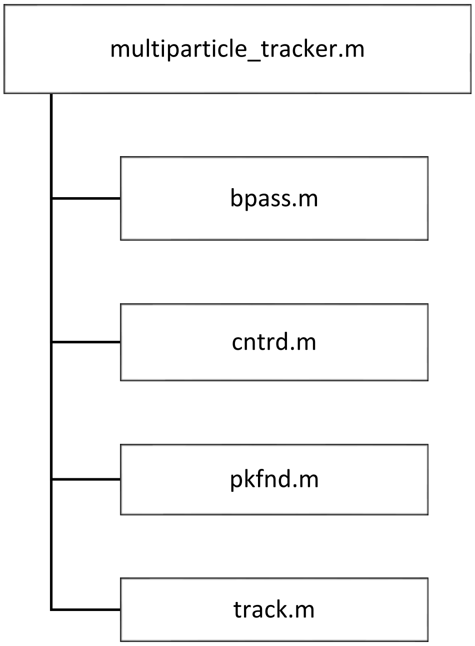

MULTIPARTICLE_TRACKER.M

```
% % Particle Finder
% Max Salick
% 8-5-2011

clc
close all
clear all

format short

% % % % DEFAULT VALUES:
% images=0;
% mindistance=100;
% minxdistance=130;
% poissondatapoints = 30;
% minframechain=2;
% % poissonframes=2;
% combinatorics=13;
%
% param.mem=1;
% param.dim=2;
% param.good=0;
% param.quiet=1;

images=0;

mindistance=16;
minxdistance=130;
poissondatapoints = 30;
minframechain=2;
combinatorics=20;

param.mem=2;
param.dim=2;
param.good=0;
param.quiet=1;

%% Locate Files

disp(['Locate images'])

imagefile = {1 2 3 4 5 6 7 8 9 10 11 12 13 14 15 16 17 18 19 20 21 22 23 24 25 26 27 28 29 30 31
32 33 34 35 36 37 38 39 40 41 42 43 44 45 46 47 48 49 50 51 52 53 54 55 56 57 58 59 60 61 62 63
64 65 66 67 68 69 70 71 72 73 74 75 76 77 78 79 80 81 82 83 84 85 86 87 88 89 90 91 92 93 94 95
96 97 98 99 100 101 102 103 104 105 106 107 108 109 110 111 112 113 114 115 116 117 118 119 120
121 122 123 124 125 126 127 128 129 130 131 132 133 134 135 136 137 138 139 140 141 142 143 144
145 146 147 148 149 150 151 152 153 154 155 156 157 158 159 160 161 162 163 164 165 166 167 168
169 170  171 172 173 174 175 176 177 178 179 180 181 182 183 184 185 186 187 188 189 190 191 192
193 194 195 196 197 198 199 200};

[FileName,PathName] = uigetfile('*.tif','Select the particle-tracking results','C:\Users\Max
Salick\Documents\Work\Lab Data\Mechanical - PA Gel Test','Multiselect','on');

tiffiles=iscell(FileName);

imagenumber = max(size(FileName));

%% Detect if selected stack or multiple images
if tiffiles==1
        disp('Multiple images selected');
    tifstack=0;

else
    disp('TIFF stack selected');
```

```
    tifstack=1;
end

%% If stack, split

    if tifstack==1
    info = imfinfo([PathName FileName]);

    imagenumber = numel(info);

end

%% Run Analysis on Each Image
res = get(0,'ScreenSize');
horres = res(3);
vertres=res(4);

set(0,'defaultTextColor',[.2 .2 .2])

    h= figure('Pointer','crosshair','Position',[6 38 horres/5 vertres-60],'Name','Image
Analysis','MenuBar','none' ...
        ) ;

%     Form image coordinate arrays for particles for individual images

for imagecount = 1:imagenumber
    if tifstack==1
        a = (imread([PathName FileName], imagecount));

    else
    a = double(imread([PathName FileName{imagecount}]));

    end

    if max(size(size(a)))==3
        a=(a(:,:,1)./3+a(:,:,2)./3+a(:,:,3)./3).*1.5-20;
    end

    subplot(3,1,1);
    colormap('gray'), imagesc(a)

    subplot(3,1,2);

    b = bpass(a,1,8);
    colormap('gray'), image(b)
    pk = pkfnd(b,max(max(b))*.4,11);

    cnt = cntrd(b,pk,15);
    subplot(3,1,3)

    siz=size(a);
    scatter(pk(:,1),siz(1)-pk(:,2),1)
    xlim([0, siz(2)])
    ylim([0, siz(1)])

    pause(.000001);
    disp(['Analyzing figure ' num2str(imagecount) ' of ' num2str(imagenumber)])
    cnt(:,2)=siz(1)-cnt(:,2);
    timecolumn = ones(max(size(cnt)),1).*imagecount;
    coords{imagecount}=[cnt(:,1:2) timecolumn];
end

% Stack together image coordinate arrays

trackinput = coords{1};
for n=2:imagenumber
    trackinput = [trackinput;coords{n}];
end

%% Tracking Code
% trackinput contains [x y t] for each particle, sorted by frame
```

```
trackinput(:,1) = trackinput(:,1).*10;

result = track(trackinput, combinatorics,param);

matbuilttable=zeros(max(size(result)),4);
matbuilttable(:,2) = result(:,4);
matbuilttable(:,3)=result(:,3);
matbuilttable(:,4)=result(:,2);
matbuilttable(:,5)=result(:,1)./10;

%% Importing Data

disp('Importing particle-tracking data to table...')

tableimport = matbuilttable;
strains = [1 0 ; 1 0 ];
xstrain = [1 0 ; 1 0];
totalframes = max(tableimport(:,3))+1;
totalparticles = max(tableimport(:,2));
emptyrowrecorder=0;

builttable = zeros(totalframes,totalparticles);
xbuilttable = zeros(totalframes,totalparticles);

disp('Compiling built table...')

for n=1:max(size(tableimport))
    builttable(tableimport(n,3),tableimport(n,2))=tableimport(n,4);
    xbuilttable(tableimport(n,3),tableimport(n,2))=tableimport(n,5);
end
oldbuilttable=builttable;
%% Particle Direction Filter
[builttabley builttablex] = size(builttable);
deletedcolumns=0;
horiz=builttablex;
vert=2;
for horiz = builttablex:-1:1
    removecolumn=0;
    for vert=2:builttabley
        if builttable(vert,horiz)>builttable(vert-1,horiz) && builttable(vert-1,horiz) ~= 0
            removecolumn=1;
        end
    end
    if removecolumn==1;
        builttable(:,horiz)=[];
        xbuilttable(:,horiz)=[];
       deletedcolumns=deletedcolumns+1;
    end
    image(builttable)
end

totalparticles = totalparticles - deletedcolumns;

%% Remove small particle chains
disp('Removing small particle chains...')
for part=totalparticles:-1:1
    if nnz(builttable(:,part))<minframechain
        builttable(:,part)=[];
        xbuilttable(:,part)=[];
    end
end

[totalframes totalparticles] = size(builttable);
h2 = figure('position',[14+horres/5 38 horres/5
vertres/3],'Pointer','crosshair','MenuBar','none');
colormap('gray')
image(builttable);
n=1;

%% Frame-by-frame strain analysis
```

```
disp('Determining frame-by-frame strain data...')
for currentframe = 0:1:(totalframes-2)
    currentframe;

%     Per Frame

strainlist=zeros(1,1);

displacementinterval = zeros(2,2);
relevantparticletracker = 1;

for particle=1:1:totalparticles
    if builttable(currentframe+1,particle)>0 && builttable(currentframe+2,particle)>0
  displacementinterval(1,relevantparticletracker)=builttable(currentframe+1,particle);
  displacementinterval(2,relevantparticletracker)=builttable(currentframe+2,particle);
  relevantparticletracker=relevantparticletracker+1;
    end
end

relevantparticles=relevantparticletracker-1;

recordedstraintracker=1;

for baseparticle=1:relevantparticles-1

    for checkparticle=baseparticle+1:relevantparticles

        distance1=(displacementinterval(1,checkparticle)-displacementinterval(1,baseparticle));

        if distance1>mindistance
            distance2=(displacementinterval(2,checkparticle)-
displacementinterval(2,baseparticle));
            strainlist(1,recordedstraintracker)=(distance2-distance1)/distance1;
            strainlist(2,recordedstraintracker)=distance1;
            strainlist(3,recordedstraintracker)=distance2;

            recordedstraintracker=recordedstraintracker+1;

        end
    end
end

recordedstrains=recordedstraintracker-1;
if strainlist==0
    sums= [0 0];
else
sums=sum(strainlist,2);
end

basesum=sums(2);
means=mean(strainlist,2);
averagestrain=means(1);
stdev=std(strainlist(1,:));

weightedstrainsum=0;
for n=1:recordedstrains
    weightedstrainsum=weightedstrainsum+strainlist(1,n)*strainlist(2,n);
end

averagestrain=averagestrain+1;
weightedstrain=weightedstrainsum/basesum+1;

strains(1,currentframe+2)=averagestrain*(strains(1,currentframe+1));
strains(2,currentframe+2)=weightedstrain*(strains(2,currentframe+1));
stdevs(1,currentframe+2)=stdev;

end

strains=strains-ones(size(strains));
```

```
stdevhigh=stdevs+strains(1,:);
stdevlow=strains(1,:)-stdevs;

%% Plotting

scrsz = get(0,'ScreenSize');

h=figure;

set(h,'Position',[2*horres/5+22 38 scrsz(3)/4 scrsz(4)/3],'MenuBar','none')
disp('Strain component has run successfully!')
disp('-----------------------------')
disp(['Total frames: ' num2str(totalframes) '       Total particles: ' num2str(totalparticles)])
disp(['Minimum initial distance for particle tracking: ' num2str(mindistance) ' pixels'])
disp('---------------------------------------------------------------')
disp(' ')
AverageStrains=strains(1,:)';
area(stdevhigh,'FaceColor',[1 1 .5])
hold on
area(stdevlow,'FaceColor',[1 1 1])
plot(strains')
xlabel('Frame')
ylabel('Strain')
hold off

xlswrite([PathName 'straincalcs_v2.xls'], strains'+1, 'Strains', 'A1');

%% Import Stress Data

disp ('Please select load data...')
[LoadFileName,LoadPathName] = uigetfile('*.raw','Select load .raw file',PathName);

LoadImport = dlmread ([LoadPathName LoadFileName],',',41,0);

fid = fopen([LoadPathName LoadFileName]);
LoadScan = textscan(fid,'%s %s %s %s %s %s %s %s %s %s %s %s %s %s %s %s %s %s %s %s %s %s %s %s
%s %s %s','delimiter',',');

TestName = LoadScan{2}{3};
TestDate = LoadScan{2}{7};
LoadUnit = LoadScan{3}{41};

if max(size(LoadUnit))==8
    loadunit = 'N';
else
    loadunit = 'kgf';
end

disp (['Units are in ' loadunit]);

TestTime = max(LoadImport(:,1));

disp ('Please select buoyancy data...')
[BuoyFileName,BuoyPathName] = uigetfile('*.raw','Select buoyancy .raw file',LoadPathName);

BuoyImport = dlmread ([BuoyPathName BuoyFileName],',',41,0);

disp ('Combining load and buoyancy data...')

widthload = min(size(LoadImport));
widthbuoy = min(size(BuoyImport));
sizeload = max(size(LoadImport));
sizebuoy = max(size(BuoyImport));

combined = zeros(max([sizeload sizebuoy]),1);
load=LoadImport(:,3);
buoy=BuoyImport(:,3);
combined(1:sizeload)=load;
combined(1:sizebuoy)=combined(1:sizebuoy)-buoy;

if max(size(buoy))>max(size(load))
```

```
    timer=BuoyImport(:,1);
else
    timer=LoadImport(:,1);
end

h3 = figure('Position',[horres/5+15 62+vertres/3 horres/2.3 vertres/1.8],'MenuBar','none');
plot(LoadImport(:,1),load,BuoyImport(:,1),buoy,timer,combined);
legend('Load','Buoyancy','Combined')
xlabel('Time (sec)')
ylabel(LoadUnit)

%% Slipping Dialog

button = questdlg('If there is clearly slipping in the load data, the user may choose to only
include data up to the point of slipping.  Is there slipping in this data?','Slip?');

isyes = strncmp(button,'Yes',3);

if isyes ==1
    msgbox('Please select the location on the graph before the sample began to slip','Select Slip
Point')

    [slippointx,slippointy] = ginput(1);
    [min_differenceslip, indexslip] = min(abs(combined(:,1) - slippointy));
    sliptimepercent = (indexslip / max(size(combined)));

    lastimage = floor(sliptimepercent * imagenumber);
    truepercent = lastimage/imagenumber;
    combinedsize = max(size(combined));

    combined = combined(1:floor(truepercent*combinedsize));
    timer = timer(1:floor(truepercent*combinedsize));
    imagenumber = lastimage;
    AverageStrains = AverageStrains(1:lastimage);

h3 = figure('Position',[horres/5+15 62+vertres/3 horres/2.3 vertres/1.8],'MenuBar','none');
plot(timer,combined);
legend('Combined')
xlabel('Time (sec)')
ylabel(LoadUnit)

end

disp('Please input sample cross-section...')

prompt = {'Enter cross-section area (mm^2):'};
dlg_title = 'Cross-section Input';
num_lines = 1;
def = {'20','hsv'};
xsection = inputdlg(prompt,dlg_title,num_lines,def);
xsection = str2num(xsection{1});

xsection=xsection * 10^-6;

if loadunit == 'N'
    combinedstress = combined./xsection;
    loadstress = load./xsection;
    buoystress= buoy./xsection;
end

if loadunit == 'kgf'
    combinedstress = combined./xsection;
    combinedstress = combinedstress / 9.81;
    loadstress = load./xsection;
    loadstress = loadstress / 9.81;
    buoystress= buoy./xsection;
    buoystress = buoystress / 9.81;
end

disp('Linking strain to respective stress data points...')
```

```
ImageInterval = max(timer(:,1)) / (imagenumber-1);

StressStrain = zeros(imagenumber,2);

for strainmix = 1:imagenumber
    time = (strainmix-1)*ImageInterval;
    [min_difference, array_position] = min(abs(timer - time));

    StressStrain(strainmix,2)=combinedstress(array_position);
    StressStrain(strainmix,1)=AverageStrains(strainmix);
end

zeropoint = StressStrain(1,2);
StressStrain(:,2) = StressStrain(:,2)-zeropoint

h4 = figure('Position',[horres/5+15 62+vertres/3 horres/2.3
vertres/1.8],'MenuBar','none','Pointer','crosshair');
plot(StressStrain(:,1),StressStrain(:,2))

title('Stress vs. Strain')
xlabel('Strain (%)')
ylabel('Stress (Pa)')

disp ('Forming linear regression...')
disp('Please select lower bound and upper bound for linear regression...')

[selectedx,selectedy] = ginput(2);

reglowstrain = min(selectedx);
reghighstrain = max(selectedx);

[min_difference, lowindex] = min(abs(StressStrain(:,1) - reglowstrain));
[min_difference, highindex] = min(abs(StressStrain(:,1) - reghighstrain));
indexnumber = highindex-lowindex+1;
str = StressStrain(:,1);
sts = StressStrain(:,2);
X = str(lowindex:highindex);
p = polyfit(X,sts(lowindex:highindex),1);

fitline = [str(lowindex) p(2)+str(lowindex)*p(1); str(highindex) p(2)+str(highindex)*p(1)];

hold on
plot(fitline(:,1),fitline(:,2),'color','red');
disp(' ')
disp(' ')
disp('Analysis complete')
disp('-----------------')
clc

disp('Mechanical Testing Results Report')
disp('---------------------------------')
disp(['Test Name: ' LoadFileName])
disp(['Youngs Modulus: ' num2str(p(1)/1000) ' kPa'])
disp(' ')
disp(' ')
disp('Test Information:')
disp(['Buoyancy File: ' BuoyFileName])
disp(['Cross-Section Area: ' num2str(xsection*1000000) ' mm^2'])
disp(['Number of Strain Images: ' num2str(imagenumber)])
disp(['Number of tracked particles: ' num2str(totalparticles)])
disp(['Linear Fit Strain Range: ' num2str(str(lowindex)) ' to ' num2str(str(highindex))])
disp(' ')
disp(' ')
disp('Analysis Parameters:')
disp(['Minimum Y Distance Between Particles: ' num2str(mindistance)])
disp(['Minimum Consecutive Frames for Single Particle: ' num2str(minframechain)])
disp(['Tracking Combinatorics Variable: ' num2str(combinatorics)])
disp(['Tracking.mem Parameter: ' num2str(param.mem)])
disp(['Tracking.dim Parameter: ' num2str(param.dim)])
disp(['Tracking.good Parameter: ' num2str(param.good)])
disp(['Tracking.quiet Parameter: ' num2str(param.quiet)])
```

```
%% Report
hold off

content= sprintf(['Mechanical Testing Results Report\n---------------------------------\nTest
Name: ' LoadFileName ...
    '\nTest Date: ' TestDate '\nYoungs Modulus: ' num2str(p(1)/1000) ' kPa' ...
'\n\nTest Information:\nBuoyancy File: ' BuoyFileName ...
'\nCross-Section Area: ' num2str(xsection*1000000) ' mm^2\nNumber of Strain Images: '
num2str(imagenumber) ...
'\nNumber of tracked particles: ' num2str(totalparticles) ...
'\nLinear Fit Strain Range: ' num2str(str(lowindex)) ' to ' num2str(str(highindex)) ...
'\n\nAnalysis Parameters:' ...
'\nMinimum Y Distance Between Particles: ' num2str(mindistance) ...
'\nMinimum Consecutive Frames for Single Particle: ' num2str(minframechain) ...
'\nTracking Combinatorics Variable: ' num2str(combinatorics) ...
'\nTracking.mem Parameter: ' num2str(param.mem) ...
'\nTracking.dim Parameter: ' num2str(param.dim) ...
'\nTracking.good Parameter: ' num2str(param.good)]);

reportimage = figure('Position',[10 42 horres/1.6 vertres-110],'Pointer','crosshair');
subplot(2,2,[1]);
reporttext = annotation('textbox',[0.05 0.05 .4 .4])
set(reporttext,'String',content,'Fontsize',7)

plot(StressStrain(:,1),StressStrain(:,2))
title('Stress vs. Strain')
xlabel('Strain (%)')
ylabel('Stress (Pa)')
hold on
plot(fitline(:,1),fitline(:,2),'color','red');

hold off

subplot(2,2,2);
colormap('gray'), imagesc(a)

subplot(2,2,4);
hold on
area(stdevhigh,'FaceColor',[1 1 .5])
hold on
area(stdevlow,'FaceColor',[1 1 1])
plot(strains')
xlabel('Frame')
ylabel('Strain')
```

APPENDIX E: CALCIUM TRANSIENT AUTO ANALYSIS

NOTE: This code is designed to accept inputs in the format of excel workbooks. Data is arranged in columns, such that the first column contains the ROI name, the second column contains the times of each image, and intensity data is given as individual columns starting at F (columns C, D, and E are spacers). Each row is a timestep, and the first row is not used in analysis.

CALCIUM_TRANSIENT_ANALYZER.M

```
% Calcium Transient Analyzer
% Max Salick, 11-5-2012

% This program takes transient intensity data taken from ND elements and
% converts it into normalized transient curves.

clear all
clc
close all

%% Retrieve Data

[excelname,excelpath] = uigetfile('*.xlsx','Select the M-file','Z:\msalick\Current
Experiments');

filepath = [excelpath excelname];
[ndatarough, headertext] = xlsread(filepath, 'Data (ROIs)');
matrixsize = size(ndatarough);
numberofplots = matrixsize(2)-4;
ndatarough(:,1) = ndatarough(:,1) - ndatarough(1,1);
times = ndatarough(:,1);
numtimes = max(size(times));
ndatarough = ndatarough(:,5:matrixsize(2));
plotnames = headertext(1,(7:matrixsize(2)+1))';

plot(times,ndatarough);

%% Spline Smoothing

for k=1:numberofplots
    xx=0:1:round(max(times));
    yy= spline(times,ndatarough(:,k),xx);
    ndata(:,k)=yy;
end

for k=2:numberofplots
    ndata(:,k) = ndata(:,k) - ndata(:,1);
```

```
end

ndata(:,1)=[];

figure
plot(xx,ndata)

%% Normalize

for k=1:numberofplots-1
    ndata(:,k)=ndata(:,k)-min(ndata(:,k));
    ndata(:,k)=ndata(:,k) / max(ndata(:,k));
end

%% Plot Analysis

numtimes=max(size(xx));
for k=1:numberofplots-1
    curve = ndata(:,k);
    [maxv,maxI] = max(curve);
    for kk=1:numtimes-1
        delcurve(kk)=(curve(kk+1)-curve(kk));
    end

      founduptake=0;
    for kk=maxI-100:-1:1
        if  founduptake==0
        if delcurve(kk)<.001  & delcurve(kk-1)<.001  & delcurve(kk-2)<.001 &
curve(kk)<0.4
            startCAuptakeI(k) = kk+1;
            founduptake=1;
        end
        end



    end

    maxCAI(k)=maxI;

    eightypI(k) = maxCAI(k) + dsearchn(curve(maxCAI(k):max(size(curve))),0.8);
    twentypI(k) = maxCAI(k) + dsearchn(curve(maxCAI(k):max(size(curve))),0.2);

    if delcurve(eightypI(k)-2)>0
        eightypI(k) = maxCAI(k) + dsearchn(curve(maxCAI(k):eightypI(k)-10),0.8);
    end

    if delcurve(twentypI(k)-2)>0
            twentypI(k) = maxCAI(k) + dsearchn(curve(maxCAI(k):twentypI(k)-10),0.2);
    end

    CAlosscurve = curve(eightypI(k):twentypI(k));
    CAlosstime = xx(eightypI(k):twentypI(k));


    p = polyfit(CAlosstime'./1000,log(CAlosscurve),1);
    halflife(k) = -.69315 / p(1);
```

```
end

%% Print Results

sheets = round((numberofplots-1)/12+.49999);
scrsz = get(0,'ScreenSize');

for sheetcount=1:sheets

    figure('Position',[10 60 scrsz(3)-20 scrsz(4)-160])

    for k=1:12
   if (sheetcount-1)*12+k<numberofplots
      currentplot=(sheetcount-1)*12+k;
    subplot(4,3,k)
    curve=ndata(:,currentplot);
    plot(xx,ndata(:,currentplot),'Color',[0 0 0])
     line([xx(startCAuptakeI(currentplot)) xx(startCAuptakeI(currentplot))],[0
1]','LineStyle','--','Color',[.6 .6 .6])
     line([xx(maxCAI(currentplot)) xx(maxCAI(currentplot))],[0.7 1]','LineStyle','-
','Color',[1 0 0])
    hold on

plot(xx(eightypI(currentplot):twentypI(currentplot)),curve((eightypI(currentplot):twen
typI(currentplot))),'Color',[1 0 0],'LineWidth',2);
    halflabelxy = [xx(round((eightypI(currentplot)+twentypI(currentplot))/2))
curve(round((eightypI(currentplot)+twentypI(currentplot))/2))];
    halflabel = ['T_1_/_2 = ' num2str(halflife(currentplot))];
    text(halflabelxy(1),halflabelxy(2)+0.1,halflabel,'FontSize',7);

    uptaketime(currentplot) = (xx(maxCAI(currentplot)) -
xx(startCAuptakeI(currentplot)))/1000;
    uptakelabel = ['T_u_p_t_a_k_e = ' num2str(uptaketime(currentplot))];
    text(halflabelxy(1),halflabelxy(2)+0.3,uptakelabel,'FontSize',7);

    hold off
     set(gca,'FontSize',5)
    title(plotnames((sheetcount-1)*12+k),'FontSize',9)
    axis tight
    xlabel('Time(ms)','FontSize',7)
   end
    end
end

dataarray.plotnames = plotnames;
dataarray.uptaketime = uptaketime';
dataarray.halflife = halflife';
save output.mat dataarray
```

APPENDIX F: MICROPATTERNING ROBOT PATTERN ALIGNMENT PROGRAM

CODE STRUCTURE

NOTE: This program utilizes the Horn's quaternion method for absolute orientation, which has been adapted into Matlab format by Matt Jacobson of Xoran Technologies, Inc, and has been made available in the Mathworks File Exchange. It also uses a small piece of code titled num2clip.m, written by Grigor Browning. This program efficiently places values into the clipboard, which is done at the end to allow the user to rapidly work through multiple datasets.

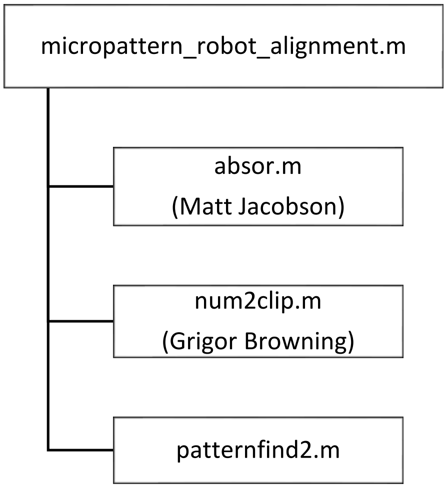

The utilization of absor.m requires the following liability statement to be made for any software that utilizes this software:

Copyright (c) 2009, Matt Jacobson, Xoran Technologies, Inc.
http://www.xorantech.com
All rights reserved.

Redistribution and use in source and binary forms, with or without modification, are permitted provided that the following conditions are met:

- Redistributions of source code must retain the above copyright notice, this list of conditions and the following disclaimer.
- Redistributions in binary form must reproduce the above copyright notice, this list of conditions and the following disclaimer in the documentation and/or other materials provided with the distribution

THIS SOFTWARE IS PROVIDED BY THE COPYRIGHT HOLDERS AND CONTRIBUTORS "AS IS" AND ANY EXPRESS OR IMPLIED WARRANTIES, INCLUDING, BUT NOT LIMITED TO, THE IMPLIED WARRANTIES OF MERCHANTABILITY AND FITNESS FOR A PARTICULAR PURPOSE ARE DISCLAIMED. IN NO EVENT SHALL THE COPYRIGHT OWNER OR CONTRIBUTORS BE LIABLE FOR ANY DIRECT, INDIRECT, INCIDENTAL, SPECIAL, EXEMPLARY, OR CONSEQUENTIAL DAMAGES (INCLUDING, BUT NOT LIMITED TO, PROCUREMENT OF SUBSTITUTE GOODS OR SERVICES; LOSS OF USE, DATA, OR PROFITS; OR BUSINESS INTERRUPTION) HOWEVER CAUSED AND ON ANY THEORY OF LIABILITY, WHETHER IN CONTRACT, STRICT LIABILITY, OR TORT (INCLUDING NEGLIGENCE OR OTHERWISE) ARISING IN ANY WAY OUT OF THE USE OF THIS SOFTWARE, EVEN IF ADVISED OF THE POSSIBILITY OF SUCH DAMAGE.

Jacobson, M (2009). absor.m, http://www.mathworks.com/matlabcentral/fileexchange/26186-absolute-orientation-horn-s-method/content/oldstuff/absorientParams2D.m. Accessed August 2, 2014.

Browning, G (2005). num2clip.m, http://www.mathworks.com/matlabcentral/fileexchange/8472-num2clip--copy-numerical-arrays-to-clipboard. Accessed August 2, 2014.

MICROPATTERN_ROBOT_ALIGNMENT.M

```
% Ashton Lab Robot Alignment Tool
% Max Salick, 6-11-2013

% This code determines the alignment of various shapes imprinted by the
% Ashton Lab micropatterning robot based on fluorescent images.  The images
% are taken after multiple stamps of various imprinted shapes are applied
% to the sample.

% Version 3 Notes:
% This version adds the capability to analyze multiple images.  This allows
% the code to analyze images taken using various channels (FITC, DAPI, etc)
% on the same micropatterned sample.

close all
clear all
clc
global popnames
global popims
global roimarked
global imagedataorig

%% Set Parameters

% Nearest Neighbor Threshold:  This is the maximum distance that two
% members may be to still be considered 'overlapping' (in pixels).  By default, this
% number will be 50.
nnthresh = 50;

disp(['Nearest neighbor threshold: ' num2str(nnthresh) ]);

%% Prompt User to Locate Images

imagenumbertotal = input('Please input the number of images to analyze: ');
PathNamea = ' ';
for k = 1:imagenumbertotal
    [FileNamea,PathNamea] = uigetfile('*.tif','Select an Image Containing
Micropatterns',PathNamea,'Multiselect','off');
    FileName{k} = FileNamea;
    PathName{k} = PathNamea;
end

res = get(0,'ScreenSize');
horres = res(3);
vertres=res(4);

disp(['Number of image files selected: ' num2str(imagenumbertotal)]);

global totalpops
global numpopsvec
numpopsvec = 0;
totalpops = 0;
for imagecount = 1:imagenumbertotal
    if imagenumbertotal>1
    imagedata = imread([PathName{imagecount} FileName{imagecount}]);
    else
        imagedata = imread([PathName{imagecount} FileName{imagecount}]);
    end
```

```
    imagedata = imagedata(:,:,1);
    imsize = size(imagedata);
    imagesc(imagedata)
numpopsvec(imagecount) = input(['Please indicate the number of populations that are
present in this image: ']);
totalpops = totalpops + numpopsvec(imagecount);
end

close

imagecount=1;
if imagenumbertotal>1
    imagedata = imread([PathName{imagecount} FileName{imagecount}]);
    else
        imagedata = imread([PathName{imagecount} FileName{imagecount}]);
end
for k=1:totalpops
    popnamesall{k} = ['Population ' num2str(k)];
    popimsall{k} = logical(0.*imagedata(:,:,1));
end

for imagecount = 1:imagenumbertotal
disp('----------------------------------------')
disp(['Beginning analysis of image ' num2str(imagecount) ' of '
num2str(imagenumbertotal)])
%% Get Image Data Ready, and Normalize

    if imagenumbertotal>1
    imagedata = imread([PathName{imagecount} FileName{imagecount}]);
    else
        imagedata = imread([PathName{imagecount} FileName{imagecount}]);
    end
    imagedata = imagedata(:,:,1);
    imsize = size(imagedata);

numpops = numpopsvec(imagecount);

imagemax = double(max(max(imagedata)));
imagecorrect= double(255/imagemax);
imagedata=imagedata*imagecorrect;
imagedataorig = imagedata;
imagedatamod = imagedata;
rois = zeros(size(imagedata));

%% Set Scale
if imagecount==1

sprintf(['Ashton Lab Robot Alignment Tool, Max Salick 6-11-2013', ...
    '\n-----------------------------', ...
    '\n\nScale must be set...', ...
    '\n      1 - Use scalebar in image to calibrate', ...
    '\n      2 - Direct input of pixel/um ratio', ...
    '\n      3 - Set no scale (arbitrary scale will be set)'])

scalemode = input('Select Option: ');
if scalemode ==1
         colormap('gray')
    imagesc(imagedataorig);
    colormap('gray')
        [scalepointx,scalepointy] = ginput(2);
```

```
        close all
        scaleinput = input('Input the known distance between points: ');
        pixeldist = ((scalepointx(1)-scalepointx(2))^2+(scalepointy(1)-
scalepointy(2))^2)^.5;
        umperpix = scaleinput/pixeldist;
        disp(['Selected scale is ' num2str(umperpix) ' microns per pixel'])
elseif scalemode==2
    umperpix = input('Input known microns-per-pixel: ');
elseif scalemode==3
    sprintf('Setting arbitrary calibration of 1 micron per pixel')
    umperpix = 1;
else
    sprintf('Whoops?');
    stop
end

end

%% ROI Selections

disp(' ')
disp('................')
disp(' ')
disp('Each shape type will be defined as a population.')
disp(' ')

roimarked = zeros(size(imagedataorig));

popnames = popnamesall(sum(numpopsvec(1:imagecount))-
numpopsvec(imagecount)+1:sum(numpopsvec(1:imagecount)));
popims = popimsall(sum(numpopsvec(1:imagecount))-
numpopsvec(imagecount)+1:sum(numpopsvec(1:imagecount)));

disp('Starting pattern selection interface...')

[varargout] = patternfind2(imagedataorig,popnames,popims)

uiwait(patternfind2)

for unloadfromgui = 1:numpopsvec(imagecount)
    popimsall{sum(numpopsvec(1:imagecount))-numpopsvec(imagecount)+unloadfromgui} =
...
        popims{unloadfromgui};
    roimarkedall{sum(numpopsvec(1:imagecount))-numpopsvec(imagecount)+unloadfromgui} =
roimarked;

end

end

%% Prompt User for Predicted Population Offset
disp(' ');
disp('Population selection completed!');
disp(' ');
disp('--------------------------------------------------------')
disp('Starting coordinate detection and matching module...')
disp(' ')
```

```
disp('Please input the designed offset for each population in comparison to Population
1.');

for k=2:totalpops

    offsetx{k} = input(['Population ' num2str(k) ' X offset (um): ']);

    offsetx{k} = offsetx{k}/umperpix;

    offsety{k} = input(['Population ' num2str(k) ' Y offset (um): ']);

    offsety{k} = offsety{k}/umperpix;
end

offsetx{1} = 0;
offsety{1} = 0;

disp(' ');
disp('Patterns selected and defined; determining coordinates and performing nearest-
neighbor computations...')

figure
hold on

%% Convert ROI Data to Population Coordinates

for k = 1:totalpops
  disp(['Finding centroid coordinates of population ' num2str(k) '...'])



    currentrois = popimsall{k}.*roimarkedall{k};
    roiprops = regionprops(currentrois);
    regprops = regionprops(currentrois);

    arealist = [regprops.Area];
    idx = find(arealist > 1);
    posareas = arealist(idx);

    centlist = [regprops.Centroid];
    xlocs = centlist(2.*idx-1);
    ylocs = centlist(2.*idx);

    coords = [xlocs' ylocs'];
    coords(:,2) = imsize(1) - coords(:,2);
    coordsave{k} = coords;

    scatter(coordsave{k}(:,1),coordsave{k}(:,2));
    pause(.000001);

   coordsave{k} = [coords(:,1)-offsetx{k} coords(:,2)-offsety{k}];

   saveareas{k} = posareas;

end

%% Run Nearest-Neighbor Analysis to Produce Valid Coordinate Arrays
```

```
title('All-Population Scatterplot')

hold off
clear coordvalid
clear allmins
clear dists
clear xmiss
clear ymiss
clear xmissave
clear ymissave
for k=2:totalpops
    countup = 1;

    for vi = 1:max(size(coordsave{k}))

        dists {k}(vi,:)= ((coordsave{k}(vi,1)-coordsave{1}(:,1)).^2 +
(coordsave{k}(vi,2)-coordsave{1}(:,2)).^2).^.5;

        [mindist,bestpop1] = min(dists{k}(vi,:));

        if mindist <= nnthresh

            xmiss{k}(vi) = coordsave{k}(vi,1)-coordsave{1}(bestpop1,1);
            ymiss{k}(vi) = coordsave{k}(vi,2)-coordsave{1}(bestpop1,2);

            coordvalid{k}(countup,1) = coordsave{k}(vi,1);
            coordvalid{k}(countup,2) = coordsave{k}(vi,2);
            coordvalid{k}(countup,3) = coordsave{1}(bestpop1,1);
            coordvalid{k}(countup,4) = coordsave{1}(bestpop1,2);
            countup = countup+1;

        end

        allmins{k}(vi) = mindist;

    end
end
%% Find Hatchmark Center via GUI
disp('Producing scatterplot of detected points...')
disp(' ')
disp('>>>Press any key to continue<<<')
pause

pause(1)

disp(' ')
disp('Population coordinates determined.')
disp('Now the global center must be determined to indicate axis of rotation.');

disp(' ')
disp('Zoom is currently enabled.  Please locate the hatchmarks and set the')
disp('zoom so that all hatchmarks are clearly framed withing the figure.')
disp(' ')
disp('When finished, press >ENTER< to begin point selection.')
disp(' ')

imagesc(imagedataorig);
```

```
colormap(gray)
zoom on; % use mouse button to zoom in or out
% Press Enter to get out of the zoom mode.

% CurrentCharacter contains the most recent key which was pressed after opening
% the figure, wait for the most recent key to become the return/enter key
waitfor(gcf,'CurrentCharacter',13)

zoom reset
zoom off
disp('Please select the hatchmarks visible on the sample to determine this center.');
disp(' ')
disp('Select the hatchmarks in the FOLLOWING ORDER:')
disp(' ')
disp(' 1-----2');
disp(' |     |');
disp(' |     |');
disp(' |     |');
disp(' 3-----4');
disp(' ')
[hatch_x, hatch_y] = ginput(4);

globalcent_x = mean(hatch_x);
globalcent_y = mean(hatch_y);



for k = 2:totalpops

% Centering around global center....
ncoordvalid{k}(:,1) = coordvalid{k}(:,1) - globalcent_x;
ncoordvalid{k}(:,3) = coordvalid{k}(:,3) - globalcent_x;
ncoordvalid{k}(:,2) = coordvalid{k}(:,2) - globalcent_y;
ncoordvalid{k}(:,4) = coordvalid{k}(:,4) - globalcent_y;



% Use Horn's quaternion-based method to find optimal transposition matrix
[regParams,Bfit,ErrorStats]= ...
    absor([ncoordvalid{k}(:,1) ncoordvalid{k}(:,2)]', ...
    [ncoordvalid{k}(:,3) ncoordvalid{k}(:,4)]');

transposeinfo{k} = regParams;
absolve_xoff{k} = regParams.t(1)*-umperpix;
absolve_yoff{k} = regParams.t(2)*-umperpix;
absolve_rot{k} = 360-regParams.theta;

fixedcoords{k} = (transposeinfo{k}.M*[ncoordvalid{k}(:,1) ncoordvalid{k}(:,2) ...
    ones(1,max(size(ncoordvalid{k}(:,1))))']')';

fixedcoords{k} = fixedcoords{k}(:,1:2);

origerror{k}= mean(abs(ncoordvalid{k}(:,4) - ncoordvalid{k}(:,2))+ ...
    (abs(ncoordvalid{k}(:,3) - ncoordvalid{k}(:,1))));
newerror(k) =  mean(abs(ncoordvalid{k}(:,4) - fixedcoords{k}(:,2))+ ...
    (abs(ncoordvalid{k}(:,3) - fixedcoords{k}(:,1))));

end

disp(' ')
```

```
disp(' ')
disp(FileName)
disp('----------------------------------------')
disp('Suggested Corrections to Match Populations:')
pastevector = [];
 for k=2:totalpops
     transangle{k} = transposeinfo{k}.theta;
     if transangle{k} > 180
         transangle{k} = transangle{k} - 360;
     end
     pastevector = cat(2,pastevector,[-transposeinfo{k}.t(1)*umperpix  ...
         -transposeinfo{k}.t(2)*umperpix  ...
         transangle{k}]);

     disp(['Population ' num2str(k) ' should be rotated ' ...
         num2str(transangle{k}) ' degrees ( positive=CCW )']);
     disp(['Population ' num2str(k) ' should be translated ' ...
         num2str(-transposeinfo{k}.t(1)*umperpix) ' um in the +X direction']);
     disp(['Population ' num2str(k) ' should be translated ' ...
         num2str(-transposeinfo{k}.t(2)*umperpix) ' um in the +Y direction']);
 disp(' ')
 end

 disp(' ')
 disp('Data has been added to clipboard using the following format:')
 disp('          |            |            |            |           |            |
')
 disp('POP 1: X  |  POP 1: Y  |  POP 1: U  |  POP 2: X  |  POP2: Y  |  POP2:  U  |
POP 3: X ...')
 disp('          |            |            |            |           |            |
')

 num2clip(pastevector);
```

PATTERNFIND2.M

```
function varargout = patternfind2(varargin)

% Begin initialization code - DO NOT EDIT
gui_Singleton = 1;
gui_State = struct('gui_Name',       mfilename, ...
                   'gui_Singleton',  gui_Singleton, ...
                   'gui_OpeningFcn', @patternfind2_OpeningFcn, ...
                   'gui_OutputFcn',  @patternfind2_OutputFcn, ...
                   'gui_LayoutFcn',  [] , ...
                   'gui_Callback',   []);
if nargin && ischar(varargin{1})
    gui_State.gui_Callback = str2func(varargin{1});
end

if nargout
    [varargout{1:nargout}] = gui_mainfcn(gui_State, varargin{:});
else
    gui_mainfcn(gui_State, varargin{:});
end
% End initialization code

% --- Executes just before patternfind2 is made visible.
function patternfind2_OpeningFcn(hObject, eventdata, handles, varargin)
% This function has no output args, see OutputFcn.
% hObject    handle to figure
% eventdata  reserved - to be defined in a future version of MATLAB
% handles    structure with handles and user data (see GUIDATA)
% varargin   command line arguments to patternfind2 (see VARARGIN)

global popnames;
global population_totalnum;
global popims
global imagedataorig
popnames;
population_totalnum;
handles.popnames = popnames;
handles.population_totalnum = population_totalnum;

imagesc(imagedataorig)
set(handles.patternindicate,'String',handles.popnames)

% Choose default command line output for patternfind2
handles.output = hObject;

% Update handles structure
guidata(hObject, handles);

% --- Outputs from this function are returned to the command line.
function varargout = patternfind2_OutputFcn(hObject, eventdata, handles)
% varargout  cell array for returning output args (see VARARGOUT);
% hObject    handle to figure
% eventdata  reserved - to be defined in a future version of MATLAB
% handles    structure with handles and user data (see GUIDATA)

% Get default command line output from handles structure
varargout{1} = handles.output;
```

```
% --- Executes on selection change in patternindicate.
function patternindicate_Callback(hObject, eventdata, handles)
global popims

val = get(hObject,'Value');
handles.pop_currentpop = val;

handles.pop_currentname = handles.popnames{val};
handles.pop_currentname;

imagesc(handles.roimarked-
handles.roimarked.*popims{handles.pop_currentpop}+max(max(handles.roimarked)).*popims{
handles.pop_currentpop})

disp(['Popup menu altered. ' handles.pop_currentname ' selected.'])

handles.output = hObject;
guidata(hObject,handles)

% --- Executes during object creation, after setting all properties.
function patternindicate_CreateFcn(hObject, eventdata, handles)

if ispc && isequal(get(hObject,'BackgroundColor'),
get(0,'defaultUicontrolBackgroundColor'))
    set(hObject,'BackgroundColor','white');
end

% --- Executes on button press in but_finished.
function but_finished_Callback(hObject, eventdata, handles)
global popims
global roimarked
roimarked = handles.roimarked;

varagout.popims = popims;
varargout.roimarked = roimarked;

close(handles.patternfinder)

handles.output = hObject;

% --- Executes on button press in but_selectingtool.
function but_selectingtool_Callback(hObject, eventdata, handles)
global popims
disp('Please select population members to ADD or REMOVE...')

if handles.mode == 1
    handles.pop_currentpop;
    [roix, roiy] = ginput(1);
    roix = floor(roix);
    roiy = floor(roiy);
    handles.selectedroi = handles.roimarked(roiy,roix);
    handles.selectedroi;
    indexroi = handles.roimarked == handles.selectedroi;
    if popims{handles.pop_currentpop}(roiy,roix) ==0 && handles.selectedroi ~= 0

    popims{handles.pop_currentpop} = popims{handles.pop_currentpop} + indexroi;
```

```
    end

    imagesc(handles.roimarked-
handles.roimarked.*popims{handles.pop_currentpop}+max(max(handles.roimarked)).*popims{
handles.pop_currentpop});

elseif handles.mode == 0
    [roix, roiy] = ginput(1);
    roix = floor(roix);
    roiy = floor(roiy);
    handles.selectedroi = handles.roimarked(roiy,roix);
    handles.selectedroi;
    indexroi = handles.roimarked == handles.selectedroi;
    if popims{handles.pop_currentpop}(roiy,roix) ==1
            popims{handles.pop_currentpop} = popims{handles.pop_currentpop} -indexroi;
    end

    imagesc(handles.roimarked-
handles.roimarked.*popims{handles.pop_currentpop}+max(max(handles.roimarked)).*popims{
handles.pop_currentpop});

end

handles.output = hObject;
guidata(hObject,handles)

% --- Executes on button press in radbut_addmode.
function radbut_addmode_Callback(hObject, eventdata, handles)

handles.mode = 1;
disp('Mode switched to ADD population members.')

handles.output = hObject;
guidata(hObject,handles)

% --- Executes on button press in radbut_removemode.
function radbut_removemode_Callback(hObject, eventdata, handles)

handles.mode = 0;
disp('Mode switched to REMOVE population members.')

handles.output = hObject;
guidata(hObject,handles)

% --- Executes on slider movement.
function slid_binaryslider_Callback(hObject, eventdata, handles)
global imagedataorig
handles.binaryval = get(hObject,'Value');
sliderval = handles.binaryval;

handles.roibin = roicolor(imagedataorig,floor(255*sliderval),255);
imagesc(handles.roibin)

handles.output = hObject;
guidata(hObject,handles)

% --- Executes during object creation, after setting all properties.
function slid_binaryslider_CreateFcn(hObject, eventdata, handles)
```

```
if isequal(get(hObject,'BackgroundColor'), get(0,'defaultUicontrolBackgroundColor'))
    set(hObject,'BackgroundColor',[.9 .9 .9]);
end



% --- Executes on button press in but_lockbinary.
function but_lockbinary_Callback(hObject, eventdata, handles)
handles.roimarked = bwlabel(handles.roibin);
imagesc(handles.roimarked);
disp('Image binarized.  You may begin selecting population members.')
handles.mode = 1;

handles.output = hObject;
guidata(hObject,handles)

% --- Executes on button press in but_clearpop.
function but_clearpop_Callback(hObject, eventdata, handles)
global imagedataorig
global popims
popims{handles.pop_currentpop} = zeros(size(imagedataorig));
imagesc(handles.roimarked-
handles.roimarked.*popims{handles.pop_currentpop}+max(max(handles.roimarked)).*popims{
handles.pop_currentpop});

disp([ handles.pop_currentname ' cleared!'])

handles.output = hObject;
guidata(hObject,handles)

% --- Executes on button press in but_autodetect.
function but_autodetect_Callback(hObject, eventdata, handles)
global popims
global selectedrois
global allareas
global findgoodrois

disp('Autodetect selected...')
selectedrois = popims{handles.pop_currentpop}.*handles.roimarked;
selroi_area = regionprops(selectedrois,'Area');
selroi_extent = regionprops(selectedrois,'Extent');
selroi_filledarea = regionprops(selectedrois,'FilledArea');

    arealist = [selroi_area.Area];
    extentlist = [selroi_extent.Extent];
    filledarealist = [selroi_filledarea.FilledArea];
    idx = find(arealist > 1);
    selroi_posarea = arealist(idx);
    selroi_extent = extentlist(idx);
    selroi_filledarea = filledarealist(idx);

minarea = mean(selroi_posarea) * 0.9;
maxarea = mean(selroi_posarea) * 1.1;
minextent = mean(selroi_extent) * 0.9;
maxextent = mean(selroi_extent) * 1.1;
minfilled = mean(selroi_filledarea) * 0.9;
maxfilled = mean(selroi_filledarea) * 1.1;

disp('Used currently selected ROIs to determine ROI property thresholds...')
```

```
% Compare all ROIs to gathered values

allareas = regionprops(handles.roimarked,'Area');
allextent = regionprops(handles.roimarked,'Extent');
allfilled = regionprops(handles.roimarked,'FilledArea');

allarealist = [allareas.Area];
idx1 = find(allarealist > minarea);
idx2 = find(allarealist < maxarea);
allextentlist = [allextent.Extent];
idx3 = find(allextentlist > minextent);
idx4 = find(allextentlist < maxextent);
allfilledlist = [allfilled.FilledArea];
idx5 = find(allfilledlist > minfilled);
idx6 = find(allfilledlist < maxfilled);

goodrois =
intersect(intersect(intersect(intersect(intersect(idx1,idx2),idx3),idx4),idx5),idx6);

disp([num2str(max(size(goodrois))) ' members detected that are similar to the selected
members.']);
disp(['Adding autodetected members to overall population '
num2str(handles.pop_currentpop)]);

findgoodrois = ismember(handles.roimarked,goodrois);
popims{handles.pop_currentpop} = findgoodrois;

imagesc(handles.roimarked-
handles.roimarked.*popims{handles.pop_currentpop}+max(max(handles.roimarked)).*popims{
handles.pop_currentpop});

handles.output = hObject;
guidata(hObject,handles)
```

APPENDIX G: SCANNING GRADIENT FOURIER TRANSFORM MATLAB CODE

CODE STRUCTURE

Note: This code utilizes ‘subaxis.m,’ written by Aslak Grinsted [2001], which provides a useful format for subplotting figures with more control than the default Matlab functions. This software has been provided freely via the Matlab File Exchange. The main code, sft_main_v12.m conducts analysis described in Chapter 7. A supplemental program, sft_checker.m allows users to conduct target analysis of small regions within an image. It calls the sft_scan_echo.m function, which produces displays of the Fourier transforms and intensity plots that are particularly useful for understanding the algorithms, and for debugging purposes.

Three additional m-files are produced by the code during processing. These are batchparams.m, currentjob.m, and currentpath.m. These files save the status of long batch-processed jobs, allowing a user to continue where the left off for large sample sets.

Grinsted, A (2001). subaxis.m, http://www.mathworks.com/matlabcentral/fileexchange/authors/131455. Accessed August 2, 2014.

Main SGFT Code:

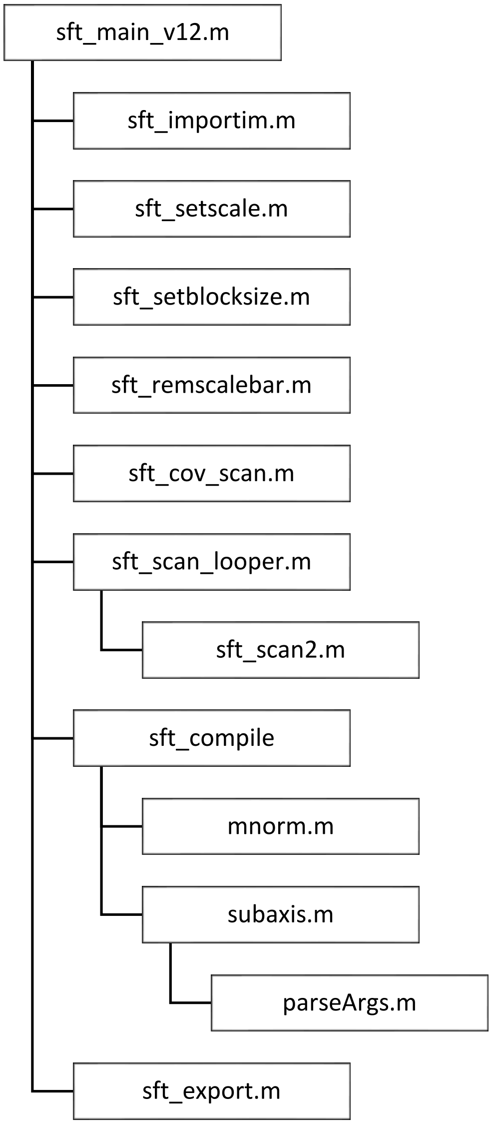

Targeted analysis / debugging tool:

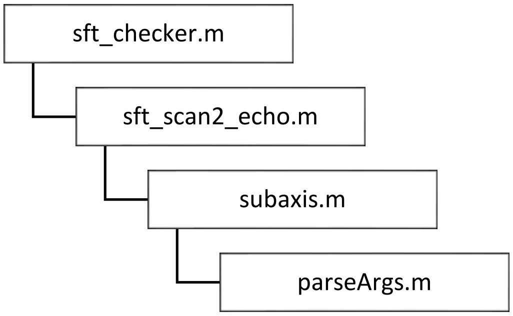

SFT_MAIN_V12.M

```
% Scanning Fourier Transform
% Max Salick, 7-7-2014

% This code combines gradient analysis (for direction determination) with
% one-directional Fourier transforms (for pattern detection) to
% quantitatively assess regions of repeating patterns within heterogeneous
% 2-D image sets. This code has been designed for determination of
% sarcomere organization within cardiomyocyte cultures, but may be utilized
% for a variety of applications within and outside of the field of biology.

% Feel free to use this software freely, as long as proper credit is given
% to the original author.

%% STARTUP
% Fresh start
clc
close all
clear all

% Set initial values
data = [];

% Acquire resolution data for current monitor
res = get(0,'ScreenSize');
horres = res(3);
vertres = res(4);

% Identify software
disp('Sarcomere Analysis, Max R. Salick 7-7-2014')
disp('This software is free to use and edit by third parties, as long as')
disp('acknowledgement is given to the original author.')
disp('------------------------------')

disp(' ')
disp('Is this a [RERUN]? (copy all parameters saved from previous run)')
rerun = input('>> [YES = 1], [NO = 0] :');

if rerun == 0

disp(' ')
disp('Is this being run on a [SINGLE IMAGE] or a [BATCH OF IMAGES]?');

batchmode = input('>> [SINGLE = 0], [BATCH = 1] : ');

else
    batchmode = 0;
end

switch batchmode
%% SINGLE START
  case 0
      if rerun == 0
    disp('SINGLE IMAGE mode selected.')
    disp(' ')
    disp('>> Please locate image.  Image must be in TIF format.')
```

```
    [FileName,PathName] = uigetfile('*.tif','Multiselect','off','Locate Image');

    disp('Image located.')
    disp(' ')
    disp('Please provide estimate of [PATTERN SIZE] (distance in um between
neighboring stripes).');
    disp('This helps to optimize the scanning window size, improving signal-to-
noise.');
    patestimate = input('>> PATTERN SIZE (default value = 2) : ');
    disp(' ')
    disp('Please provide a [SCANNING RESOLUTION].');
    disp('This is the distance between pixels of neighboring scans.');
    disp('Smaller values provide higher-resolution results, at the cost of computation
time.');
    scanjump = input('>> SCANNING RESOLUTION (default value = 16) : ');
      else
        load rerunparams
      end

% Import and normalize image data

[imagedata, imagesize, imhor, imvert] = sft_importim(PathName, FileName);



%% Set Scale

if rerun == 0
umperpix = sft_setscale(imagedata,vertres,imhor,imvert)

%% Set Blocksize

blocksize = sft_setblocksize(patestimate,umperpix)



%% Remove Scalebar

imagedataorig = sft_remscalebar(imagedata,imhor,imvert,vertres);

end

%% Save rerun parameters
save('rerunparams','scanjump','patestimate','blocksize','FileName','PathName','imageda
taorig','umperpix');

disp(' ');
disp('------------------------------------');
disp('PARAMETERS SET!  BEGINNING ANALYSIS.')
disp('------------------------------------');
disp(['File Name: ' FileName]);
disp(['Path Name: ' PathName]);
disp(['um Per Pixel: ' num2str(umperpix)]);
disp(['Pattern Width Estimate: ' num2str(patestimate)]);
disp(['Scanjump: ' num2str(scanjump)]);
disp(['Blocksize: ' num2str(blocksize)]);
disp('------------------------------------');
disp(' ');

close all
```

```
%% Local Contrast Filtering and Normalizing

im = sft_imfilter(imagedataorig,blocksize);

%% COVERAGE loop

[m_full_cov,im_noedge] = sft_cov_scan(im,scanjump,blocksize);
im = im_noedge;

imagesc(im)

%% GRADIENT + FFT Loop

[imagesize, m_full_str, m_full_dir, m_full_sl, quiver] = ...
    sft_scan_looper(imvert, imhor, m_full_cov, im, blocksize, scanjump, umperpix);

%% Reporting and Data Summarization



[data, m_im, m_orig, m_cov, m_sl, m_dir, m_quiver, m_str,fillbins] = ...
    sft_compile(m_full_cov, imagesize, blocksize, m_full_sl, m_full_dir, ...
    m_full_str, quiver, im, imagedataorig, scanjump, umperpix);



%% Save Data

sft_export(PathName, FileName, m_str, m_cov, fillbins, umperpix, ...
    blocksize, scanjump, timer, data)



    disp('---------------------------------------------');
    disp(['Analysis completed for ' FileName '!']);
    disp('---------------------------------------------');

%% ------------------------------------------------------
%% BATCH MODE
%% ------------------------------------------------------
%% Load Batch File Names
    case 1
     disp('BATCH mode selected.')
     disp(' ')

     disp('Please select from the following options:')
     disp('NOTE: Images must be in same folder, and must have same parameters)')
     disp(' ')
     disp('1 - Continue currently loaded batch from last uncompleted image')
if exist('currentjob.m')
     disp('    (currently loaded batch detected)');
else
     disp('    (currently loaded batch not detected. This option is not recommended)')
end
     disp(' ')
     disp('2 - Start new batch by selecting images manually')

     disp(' ')
     disp('3 - Load in batch info from text file containing image names')
```

```
     disp(' ')
     batchtype = input('>> [CONTINUE = 1], [NEW = 2], [NEW FROM TXT = 3] : ');
     disp(' ')
     switch batchtype
         case 1

          if exist('currentjob.m')
    batch = importdata('currentjob.m');
    PathName = importdata('currentpath.m');
    disp('Reading existing job status information...')
    [batch.importfilenames' batch.importfilestatus'];
    totalimagestorun = length(batch.importfilenames);
          else
             disp('No existing job status information.  Starting new job batch.')
             batchtype=2;
             disp(' ')
             disp('Please locate images.  Image must be in TIF format.')
             disp('Images must all be in the same folder.')

          [FileName,PathName] = uigetfile('*.tif','Multiselect','on','Locate Image');
          totalimagestorun = length(FileName);
          batch.importfilenames = FileName;
          for ind1 = 1:totalimagestorun
           batch.importfilestatus{ind1} = 0;
          end

          save('currentjob.m','batch');
          save('currentpath.m','PathName');
          [batch.importfilenames' batch.importfilestatus'];

          end

          case 2
          disp('Please locate images.  Image must be in TIF format.')
          disp('Images must all be in the same folder.')

          [FileName,PathName] = uigetfile('*.tif','Multiselect','on','Locate Image');
          totalimagestorun = length(FileName);
          batch.importfilenames = FileName;
          for ind1 = 1:totalimagestorun
           batch.importfilestatus{ind1} = 0;
          end

          save('currentjob.m','batch');
          save('currentpath.m','PathName');
          [batch.importfilenames' batch.importfilestatus'];

         case 3

        disp('Please select the job file (text file containing file names of
images).')
        disp('The job file should be in the same directory as the images.')
        disp('The images should be listed with extensions, and should be ENTER-
delimited.')
        [jobfilename,PathName] = uigetfile('*.txt','Multiselect','off','Locate
Image');

        fid = fopen([PathName jobfilename],'r');
        batch.importfilenamesa = textscan(fid,'%s');
        batch.importfilenames = batch.importfilenamesa{1};
```

```
        totalimagestorun = length(batch.importfilenames);
          for ind1 = 1:totalimagestorun
           batch.importfilestatus{ind1} = 0;
          end

          save('currentjob.m','batch');
          save('currentpath.m','PathName');
          [batch.importfilenames' batch.importfilestatus'];
     end

    save('currentjob.m','batch');
    save('currentpath.m','PathName');

    disp(' ')
    disp('Current job status (0=PENDING 1=COMPLETE 2=ERROR):')
    disp(' ')
    [batch.importfilenames' batch.importfilestatus']

%% Set Batch Parameters

    if batchtype == 1
        batchparams = importdata('batchparams.m');
        umperpix = batchparams.umperpix;
        scanjump = batchparams.scanjump;
        blocksize = batchparams.blocksize;
        patestimate = batchparams.patestimate;

    else
        disp(' ')
        disp('Batch parameters must be set.')
        disp('Once set, these parameters will be applied to ALL images in the batch.')
        disp(' ')

        disp(' ')
    disp('Please provide estimate of [PATTERN SIZE] (distance in um between 
neighboring stripes).');
    disp('This helps to optimize the scanning window size, improving signal-to-
noise.');
    patestimate = input('>> PATTERN SIZE (default value = 2) : ');
    disp(' ')
    disp('Please provide a [SCANNING RESOLUTION].');
    disp('This is the distance between pixels of neighboring scans.');
    disp('Smaller values provide higher-resolution results, at the cost of computation 
time.');
    scanjump = input('>> SCANNING RESOLUTION (default value = 16) : ');

    FileName = [batch.importfilenames{1}];

    [imagedata, imagesize, imhor, imvert] = sft_importim(PathName, FileName);

% Set Scale

umperpix = sft_setscale(imagedata,vertres,imhor,imvert)

% Set Blocksize

blocksize = sft_setblocksize(patestimate,umperpix)
```

```
% Save rerun parameters

    end

save('batchparams.m','scanjump','patestimate','blocksize','umperpix');

disp(' ');
disp('------------------------------------');
disp('PARAMETERS SET!  BEGINNING ANALYSIS.')
disp('------------------------------------');
disp(['Path Name: ' PathName]);
disp(['um Per Pixel: ' num2str(umperpix)]);
disp(['Pattern Width Estimate: ' num2str(patestimate)]);
disp(['Scanjump: ' num2str(scanjump)]);
disp(['Blocksize: ' num2str(blocksize)]);
disp('------------------------------------');
disp(' ');

totalimagestorun = length(batch.importfilenames);

while 1==1

for ind1 = 1:totalimagestorun+1
    checkjobstatus = batch.importfilestatus{ind1};
    if checkjobstatus == 0
        currentjob = ind1;
        FileName = [batch.importfilenames{currentjob}];
        break
    end

end

disp(' ')
disp('--------------------------------------------------')
disp(['Next file selected: ' FileName])
disp(['This is file ' num2str(currentjob) ' / ' num2str(totalimagestorun)]);
disp(datestr(now))
disp('--------------------------------------------------')
disp(' ')

try

close all

[imagedata, imagesize, imhor, imvert] = sft_importim(PathName, FileName);
imagedataorig = imagedata;

% Local Contrast Filtering and Normalizing
im = sft_imfilter(imagedataorig,blocksize);

% COVERAGE loop
[m_full_cov,im_noedge] = sft_cov_scan(im,scanjump,blocksize);
im = im_noedge;

imagesc(im)
colormap(gray)
% GRADIENT + FFT Loop
```

```
[imagesize, m_full_str, m_full_dir, m_full_sl, quiver] = ...
    sft_scan_looper(imvert, imhor, m_full_cov, im, blocksize, scanjump, umperpix);

% Reporting and Data Summarization
[data, m_im, m_orig, m_cov, m_sl, m_dir, m_quiver, m_str,fillbins] = ...
    sft_compile(m_full_cov, imagesize, blocksize, m_full_sl, m_full_dir, ...
    m_full_str, quiver, im, imagedataorig, scanjump, umperpix);

% Save Data
sft_export(PathName, FileName, m_str, m_cov, fillbins, umperpix, ...
    blocksize, scanjump, timer, data)



    disp('---------------------------------------------');
    disp(['Analysis completed for ' FileName '!']);
    batch.importfilestatus{currentjob} = 1;
    disp('---------------------------------------------');
    save('currentjob.m','batch')

catch
    disp(['WARNING: ERROR HAS OCCURED FOR SAMPLE ' FileName]);
    batch.importfilestatus{currentjob} = 2;
     save('currentjob.m','batch')

end

end

end
```

SFT_IMPORTIM.M

```
function [imagedata, imagesize, imhor, imvert] = ...
   sft_importim(PathName, FileName)
% Imports image and its parameters, given a path and file name.

    imagedata = imread([PathName FileName]);
    imagedata = imagedata(:,:,1);
    if mean(mean(imagedata))<127
        imagedata = 255-imagedata;
    end
imagemax = max(max(imagedata));
imagecorrect= 255./imagemax;
imagedata = imagedata.*imagecorrect;
imagesize = size(imagedata);
imhor = imagesize(2);
imvert = imagesize(1);


end
```

SFT_SETSCALE.M

```
function umperpix = sft_setscale(imagedata,vertres,imhor,imvert)

% Provides user with many options of determining scale of the image.

  umperpix=1;
 disp('Scale must be set...')
 disp('      1 - Use scalebar in image to calibrate')
 disp('      2 - Direct input of pixel/um ratio')
 disp('      3 - Set no scale (FOR TROUBLESHOOTING PURPOSES ONLY!)')
 disp('      4 - Use last-used pixel/um ratio')

scalemode = input('Select Option: ');
if scalemode ==1
    disp(' ')
    disp('Please select scalebar.  First, click directly on the scalebar.')
    disp('The image will then zoom in onto the location that was selected.')
    disp('Once this is done, select both ends of the scalebar to calibrate.')
    disp(' ')
    disp('PRESS ANY KEY TO BEGIN')
    pause



    figure('position',[50,50,floor((vertres-100)*imhor/imvert),vertres-100])
         colormap('gray')
    imagesc(imagedata);

        [scalepointlocx,scalepointlocy] = ginput(1);
        scalepointlocx = max(scalepointlocx,76);
        scalepointlocy = max(scalepointlocy,76);

        scalepointlocx = min(scalepointlocx,imhor-76);
        scalepointlocy = min(scalepointlocy,imvert-76);

        scalefocus = imagedata(scalepointlocy-75:1:scalepointlocy+75, ...
               scalepointlocx-75:1:scalepointlocx+75);
           close all
           figure('position',[50,50,vertres-100,vertres-100])
           imagesc(scalefocus);

        disp('Please select either end of scalebar, being as precise as possible.');
        [scalepointx,scalepointy] = ginput(2);
        close all
        scaleinput = input('Input the known distance between points: ');
        pixeldist = ((scalepointx(1)-scalepointx(2))^2+(scalepointy(1)-
scalepointy(2))^2)^.5;
        umperpix = scaleinput/pixeldist;
        disp(['Selected scale is ' num2str(umperpix) ' microns per pixel'])
            save('umperpix','umperpix')
elseif scalemode==2
    umperpix = input('Input known microns-per-pixel: ');
    save('umperpix','umperpix')
elseif scalemode==3
    sprintf('Setting arbitrary calibration of 1 micron per pixel')
    umperpix = 1;
elseif scalemode==4
    load umperpix
    disp(['Selected scale is ' num2str(umperpix) ' microns per pixel'])
```

```
else
    sprintf('Whoops! Unknown input detected!');
    stop
end
     colormap('gray')
end
```

SFT_SETBLOCKSIZE.M

```
function blocksize = sft_setblocksize(patestimate,umperpix)

% Sets blocksize to include ~8 patterns.  This was found to be an optimal
% number of patterns within each scan to give an adequate, but localized,
% representation of patterning in the region.

disp(' ')
disp('Setting blocksize to include ~8 pattern widths within each frame')

blocksize = 2*(floor((patestimate*8/umperpix)/2));

% Make blocksize non-prime.
while isprime(blocksize)==1
    blocksize=blocksize+1;
end
disp(['Setting BLOCKSIZE = ' num2str(blocksize)]);

end
```

SFT_REMSCALEBAR.M

```
function imagedataorig = sft_remscalebar(imagedata,imhor,imvert,vertres)

% Manually remove scalebar from image.  The targetted region will be
% blurred to prevent it from being analyzed and giving false results.  Also
% can be used on debris in the image that is not representative.

    disp(' ');
disp('Scalebar must now be removed to keep detection software from falsely including
it in the data');
disp('Please outline the scalebar, then right click and select "FILL AREA" ');
    disp(' ')
    disp('PRESS ANY KEY TO BEGIN')
    pause
figure('position',[50,50,floor((vertres-100)*imhor/imvert),vertres-100]);
    colormap('gray')
    imagesc(imagedata);
```

```
    title('Select scalebar/debris. Right click and select "fill area" when finished.')

    imagedataorig=roifill;

end
```

SFT_COV_SCAN.M

```
function [m_full_cov,im_noedge] = sft_cov_scan(im,scanjump,blocksize)

% This function scans the image and determines regions that have enough
% positive signal to be included in the analysis.

% The output, m_full_cov, is an array with 1s indicating regions with
% adequate signal, and 0s indicating regions that will be skipped to reduce
% computation time of Fourier analysis.

disp('Beginning preliminary COVERAGE scan loop...')
disp(' ')

disp('First scan loop will determine regions that contain cells.')
disp('Edges of positive regions will be reduced (within 0.75 blocksizes).')
disp('This reduces the false positives that result from edge effects during')
disp('Fast Fourier Transform image analysis.')

filterbox = floor(blocksize/10);

imagesize = size(im);
meanintense = mean(mean(im));
m_full_cov = zeros(imagesize);
for xloc = ceil(blocksize/2)+1:scanjump:imagesize(2)-(ceil(blocksize/2)+1)
    for yloc = ceil(blocksize/2)+1:scanjump:imagesize(1)-(ceil(blocksize/2)+1)
        section = im(yloc-blocksize/2:yloc+blocksize/2-1,xloc-
blocksize/2:xloc+blocksize/2-1);
        if mean(mean(section))>(meanintense)/2  % This skips blank areas
            m_full_cov(yloc-scanjump/2:yloc+scanjump/2,xloc-
scanjump/2:xloc+scanjump/2)=1;
        end
    end
end

disp(' ')
disp('Positive regions of image detected.')
disp('Removing edges of image...')

D = bwdist(1-m_full_cov);
D(D>blocksize*.75) = blocksize*.75;
D = (D/(blocksize*.75));
% D2 = imfilter(D,fspecial('disk',4*filterbox),'same');

im_noedge = double(im).*D;
```

```
disp(' ')
disp('First scan loop (COVERAGE) completed!')

end
```

SFT_SCAN_LOOPER.M

```
function [imagesize, m_full_str, m_full_dir, m_full_sl, quiver] = ...
    sft_scan_looper(imvert, imhor, m_full_cov, im,  ...
                    blocksize, scanjump, umperpix)

%   This file coordinates "sft_scan.m", giving the scan locations and
%   spacings, and constructing output arrays based on the sft_scan values.

%  Scans through the entire image to detect patterning.  First conducts
%  gradient analysis to determine directionality of the image.  Next, 1-D
%  Fourier transforms are taken in the determined directions, and peak
%  detection of averaged Fourier transforms is conducted to assess the
%  amount of organization at the scanned areas.  Spacing between patterns
%  is determined spatially using intensity profiles across the image in the
%  known direction of patterning.

disp('Beginning second scan loop.  This will utilize gradient methods')
disp('to determine the orientation of patterns within the image, and')
disp('will then apply 1D Fourier transforms in this direction to determine')
disp('pattern strength.')
disp(' ')

disp('Initializing main FFT scan loop...')
disp(' ')

fftw('planner','exhaustive')

[GX,GY] = gradient(im);
orientim = atan2(-GY,GX);

imagesize = [imvert imhor];
m_full_str = zeros(imagesize);
m_full_dir = zeros(imagesize);
m_full_sl = zeros(imagesize);
quiver = zeros(imagesize);
totaltoscan = sum(sum(m_full_cov));

tic
scanned=0;

mstart = zeros(scanjump);
mstart(floor(scanjump)/2,1:end)=1;

for xloc = ceil(blocksize/2)+1:scanjump:imagesize(2)-(ceil(blocksize/2)+1)
```

```
    timer = toc;
    timeremain = timer*totaltoscan/scanned - timer;
    minremain = floor(timeremain/60);
    secremain = floor(timeremain - 60*minremain);
    disp([num2str(ceil(100*scanned/totaltoscan)) '% complete. ' ...
        num2str(minremain) ':' num2str(secremain) ' remaining.'])

    for yloc = ceil(blocksize/2)+1:scanjump:imagesize(1)-(ceil(blocksize/2)+1)

       if m_full_cov(yloc, xloc) == 1
         scanned = scanned+scanjump^2;
         section = im(yloc-blocksize/2:yloc+blocksize/2-1,xloc-
blocksize/2:xloc+blocksize/2-1);
         orientsection = orientim(yloc-blocksize/2:yloc+blocksize/2-1,xloc-
blocksize/2:xloc+blocksize/2-1);
         section = section-min(min(section)).*255/max(max(1+section-
min(min(section))));

 [fourstrengthval,sarclength,meandirect] =
sft_scan2(section,orientsection,blocksize,umperpix);



m_full_str(yloc-scanjump/2:yloc+scanjump/2,xloc-
scanjump/2:xloc+scanjump/2)=fourstrengthval;
m_full_dir(yloc-scanjump/2:yloc+scanjump/2,xloc-
scanjump/2:xloc+scanjump/2)=meandirect;
m_full_sl(yloc-scanjump/2:yloc+scanjump/2,xloc-scanjump/2:xloc+scanjump/2)=sarclength;

m = imrotate(mstart,double(meandirect*180/pi),'bilinear','crop');
quiver(yloc-scanjump/2:-1+yloc+scanjump/2,xloc-scanjump/2:-1+xloc+scanjump/2)=m;

        end
    end

end

disp(' ')
disp('Analysis complete!')

end
```

SFT_SCAN2.M

```
function [fourstrengthval,sarclength,meandirect] =
sft_scan_echo(section,orientsection,blocksize,umperpix)

%  Scans through the entire image to detect patterning.  First conducts
%  gradient analysis to determine directionality of the image.  Next, 1-D
%  Fourier transforms are taken in the determined directions, and peak
%  detection of averaged Fourier transforms is conducted to assess the
%  amount of organization at the scanned areas.  Spacing between patterns
```

```
%  is determined spatially using intensity profiles across the image in the
%  known direction of patterning.




        [M, N] = size(section);
        w1 = cos(linspace(-pi/2, pi/2, M));
        w2 = cos(linspace(-pi/2, pi/2, N));
        w = w1' * w2;



orientangles = orientsection(orientsection~=0);
orientangles(3.1415 < orientangles) = [];
orientangles(-3.1415 > orientangles) = [];
orientangles(1.56 < orientangles & orientangles <1.58) = [];
orientangles(-1.56 > orientangles & orientangles > -1.58) = [];

C = sum(cos(orientangles.*2)); % Center of mass X (circular form)
S = sum(sin(orientangles.*2));

meandirect = 0;
if C>0
meandirect = (atan(S/C))/2;
else
    meandirect = (atan(S/C)+pi)/2;
end

if meandirect<0
    meandirect = meandirect+pi;
end

if isnan(meandirect)==1
    meandirect=0;
end



npixels = floor(blocksize/1.1);
clear fourlina
fourlina = {zeros(1,npixels) zeros(1,npixels) zeros(1,npixels) zeros(1,npixels)
zeros(1,npixels)};
warning('off','signal:findpeaks:noPeaks');
k=0;
fourlinsum = 0;
for Doff=-8:1:8
    k=k+1;
    xi = [blocksize/2-blocksize*cos(meandirect)/2.2-Doff*sin(meandirect); ...
          blocksize/2+blocksize*cos(meandirect)/2.2-Doff*sin(meandirect)];
    yi = [blocksize/2+blocksize*sin(meandirect)/2.2-Doff*cos(meandirect); ...
          blocksize/2-blocksize*sin(meandirect)/2.2-Doff*cos(meandirect)];



       fourlina{k} = improfile(section,double(xi),double(yi),npixels);
       FOUR{k} = abs(fft(fourlina{k}));

       fourlinsum = fourlinsum+FOUR{k};

end
```

```
linesmade = k;

fourlin_ave = smooth(fourlinsum ./ linesmade);

fourlin_ave = fourlin_ave(1:ceil(0.5*npixels));
for k=length(fourlin_ave):-1:1
    fourlin_ave(k) = fourlin_ave(k)-min(fourlin_ave(1:k));
end

[pks,locs] = findpeaks(fourlin_ave,'sortstr','descend');

    if isempty(pks) == 0

        Fdomain = locs(1);

        fourstrengthval = pks(1);

    else
        fourstrengthval = 0;



    end

str_four = fourstrengthval;



%% 1D Profile Strength/Spacing Determination - Spacial Domain Analysis

combodists = [];
for k=1:3
    fourlina{k} = smooth(fourlina{k});

    linemean = mean(fourlina{k});
    linezeros = fourlina{k} - linemean;
cross = find(diff(sign(linezeros)));

cross_l = linezeros(cross);
cross_r = linezeros(cross+1);

cross_spats = cross + cross_l./(cross_l-cross_r);

if length(cross_spats)>2
cross_dists = umperpix.*[diff(cross_spats(1:2:end)); diff(cross_spats(2:2:end))];
combodists = [combodists(:) ; cross_dists];

end
end

if length(combodists)>1
sl_spatial = mean(combodists);
else
    sl_spatial = 0;
end
```

```
fourstrengthval = str_four;
sarclength = sl_spatial;

end
```

SFT_COMPILE.M

```
function [data, m_im, m_orig, m_cov, m_sl, m_dir, m_quiver, m_str, fillbins] = ...
    sft_compile(m_full_cov, imagesize, blocksize, m_full_sl, m_full_dir, ...
    m_full_str, quiver, im, imagedataorig, scanjump, umperpix)

% Takes output matrices and compiles them into data arrays.  Produces
% figures to report the resutls.

disp(' ')
disp('Producing report of results...')

m_cov = m_full_cov(ceil(blocksize/2):imagesize(1)-1-
ceil(blocksize/2),ceil(blocksize/2):imagesize(2)-1-ceil(blocksize/2));
ind = find(m_cov);
nonind = find(1-m_cov);

m_sl = m_full_sl(ceil(blocksize/2):imagesize(1)-1-
ceil(blocksize/2),ceil(blocksize/2):imagesize(2)-1-ceil(blocksize/2));
m_dir  = m_full_dir(ceil(blocksize/2):imagesize(1)-1-
ceil(blocksize/2),ceil(blocksize/2):imagesize(2)-1-ceil(blocksize/2));
m_quiver = quiver(ceil(blocksize/2):imagesize(1)-1-
ceil(blocksize/2),ceil(blocksize/2):imagesize(2)-1-ceil(blocksize/2));
m_str = (m_full_str(ceil(blocksize/2):imagesize(1)-1-
ceil(blocksize/2),ceil(blocksize/2):imagesize(2)-1-ceil(blocksize/2)).^1);
loweststrength = min(m_str(ind));
m_str = m_str + loweststrength.*(1-m_cov);

m_im = (im(ceil(blocksize/2):imagesize(1)-1-
ceil(blocksize/2),ceil(blocksize/2):imagesize(2)-1-ceil(blocksize/2)));
m_orig = (255-imagedataorig(ceil(blocksize/2):imagesize(1)-1-
ceil(blocksize/2),ceil(blocksize/2):imagesize(2)-1-ceil(blocksize/2)));


figure
subaxis(16,4,1,1,1,12,'spacing',.025,'holdaxis',1,'margin',.01)
colormap('gray')
image(m_orig/4)
title('Original Image')
axis image
axis off

subaxis(16,4,2,1,1,12)
image(m_im/2)
axis image
axis off
title('Filtered Image (Local Contrast)')

subaxis(16,4,4,1,1,12)
```

```
image(62.*(m_str-min(min(m_str)))/(max(max(m_str))-min(min(m_str))))
title('Sarcomere Regions')
axis image
axis off

subaxis(16,4,3,1,1,12)
image((cat(3,min(255,double(m_im)+floor(255.*m_quiver)),m_im,m_im))./255);
title('Sarcomere Direction Quiver Plot')
axis image
axis off

m_dist = umperpix.*(bwdist(1-m_cov));

m_sp_dist = m_dist(1:scanjump:end,1:scanjump:end);
m_sp_str = m_str(1:scanjump:end,1:scanjump:end);
m_sp_dir = m_dir(1:scanjump:end,1:scanjump:end);
m_sp_sl = m_sl(1:scanjump:end,1:scanjump:end);
m_sp_cov = m_cov(1:scanjump:end,1:scanjump:end);
[coveredY,coveredX] = size(m_sp_dist);
[Ymesh,Xmesh] = meshgrid(1:coveredY,1:coveredX);
Ymesh = Ymesh';
Ymesh = coveredY-Ymesh;
Xmesh = Xmesh';



lanewidth = (umperpix.*scanjump) .* max(max((m_sp_cov.*Xmesh)') -
min((m_sp_cov.*Xmesh)'));

data = [Xmesh(m_sp_cov>0.5) ...  % 1
                Ymesh(m_sp_cov>0.5)...  % 2
                m_sp_dist(m_sp_cov>0.5) ...  % 3
                m_sp_str(m_sp_cov>0.5) ...  %4
                m_sp_dir(m_sp_cov>0.5) ... %5
                m_sp_sl(m_sp_cov>0.5) ...  %6
                m_sp_cov(m_sp_cov>0.5) .* lanewidth];  %7



%% Alignment Distribution
subaxis(16,4,1,13,1,3)
rose([data(:,5)+pi; data(:,5)],1800)
title('Rose Plot of Alignments (unweighted)')

[n,bins] = histc(data(:,5).*180./pi,[0:1:180]);

fillbins = zeros(size(n));
subaxis(16,4,2,13,3,3)
for k =1:max(size(data))
    fillbins(bins(k)) = fillbins(bins(k)) + (data(k,4));
end
fillbins(end)=[];
plot((smooth(fillbins)))
axis([0 180 0 1.1*max(fillbins)])

title('Weighted Histogram of Alignments')

figure
image(cat(3,255.*mnorm((double(m_im)-
double(m_im).*mnorm(m_str))),uint8(255.*mnorm(double(m_im))),255.*mnorm(double(m_im).*
mnorm(m_str))));
```

```
disp(' ')
disp('Data compiled and reported in "data" array.')

end
```

MNORM.M

```
function B = mnorm(A)

B = (A-min(min(A)))./(max(max(A))-min(min(A)));
end
```

SFT_EXPORT.M

```
function sft_export(PathName, FileName, m_str, m_cov, fillbins, umperpix, ...
    blocksize, scanjump, timer, data)

% Exports data arrays into .m files that contain X, Y, distance from edge,
% pattern strength, patern direction, and pattern spacing.  Also exports
% the data into an Excel workbook.

disp(['Exporting data to ' PathName FileName '.m'])
disp(['Exporting data to ' PathName FileName ' Excel Workbook'])

percsarc = (nnz(m_str>5)) / (nnz(m_cov)) * 100;

savefile = [PathName 'output_' FileName '.m'];
params.umperpix=umperpix;
params.blocksize=blocksize;
params.scanjump=scanjump;
params.timer=timer;

save(savefile, 'data','params')

dataexport = {'x', 'y', 'edgedist(um)', 'strength', 'direction',...
    'sarclength', 'lanewidth'};
dataexport2 = [data(:,1) data(:,2) data(:,3) ...
    data(:,4) data(:,5) data(:,6) data(:,7)];

paramexport = {'path', 'file', 'umperpix', 'blocksize', 'scanjump', 'time'; ...
    PathName FileName params.umperpix params.blocksize params.scanjump ...
    params.timer};
sumexport = {'% Area Containing Sarcomeres(>5)' percsarc; ...
    'Average Sarcomere Strength' mean(mean(m_str)); ...
```

```
    '% Weighted Alignment Within 20 Degrees'
100*sum(fillbins(70:110))/sum(fillbins);...
'% Weighted Alignment Within 15 Degrees' 100*sum(fillbins(75:105))/sum(fillbins);...
'% Weighted Alignment Within 10 Degrees' 100*sum(fillbins(80:100))/sum(fillbins); ...
'Average Sarcomere Length' mean(data(:,6)) ;
'Sarcomere Length Std. Dev.' std(data(:,6))};

disp(' ');
disp(['Average Sarcomere Strength: ' num2str(mean(mean(m_str))) ]);
disp(['% Area Containing Sarcomeres(>5): ' num2str(percsarc) '%']);
disp(['% Weighted Alignment Within 20 Degrees: '
num2str(100*sum(fillbins(70:110))/sum(fillbins)) '%']);
disp(['% Weighted Alignment Within 15 Degrees: '
num2str(100*sum(fillbins(75:105))/sum(fillbins)) '%']);
disp(['% Weighted Alignment Within 10 Degrees: '
num2str(100*sum(fillbins(80:100))/sum(fillbins)) '%']);
disp(['Average Sarcomere Length: ' num2str(mean(data(:,6))) ' um' ]);
disp(['Sarcomere Length Std. Dev.: ' num2str(std(data(:,6))) ' um']);

xlswrite([PathName 'output_' FileName '.xls'], paramexport, 'parameters');
xlswrite([PathName 'output_' FileName '.xls'], dataexport2, 'data','A3');
xlswrite([PathName 'output_' FileName '.xls'], dataexport, 'data');
xlswrite([PathName 'output_' FileName '.xls'], sumexport, 'summary');



end
```

SFT_CHECKER.M

```
figure
 imagesc(im);
 axis image;
 colormap(gray);
 [xloc,yloc] = ginput(1);
 xloc = ceil(xloc);
 yloc = ceil(yloc);
section = im(yloc-blocksize/2:yloc+blocksize/2-1,xloc-blocksize/2:xloc+blocksize/2-1);
section = section-min(min(section)).*255/max(max(1+section-min(min(section))));

[GX,GY] = gradient(im);
orientim = atan2(-GY,GX);
orientsection = orientim(yloc-blocksize/2:yloc+blocksize/2-1,xloc-
blocksize/2:xloc+blocksize/2-1);

 [fourstrengthval,sarclength,meandirect] =
sft_scan2_echo(section,orientsection,blocksize,umperpix);

 meandirect
 fourstrengthval
 sarclength
```

SFT_SCAN2_ECHO.M

```
function [fourstrengthval,sarclength,meandirect] =
sft_scan_echo(section,orientsection,blocksize,umperpix)

%  Scans through the entire image to detect patterning.  First conducts
%  gradient analysis to determine directionality of the image.  Next, 1-D
%  Fourier transforms are taken in the determined directions, and peak
%  detection of averaged Fourier transforms is conducted to assess the
%  amount of organization at the scanned areas.  Spacing between patterns
%  is determined spatially using intensity profiles across the image in the
%  known direction of patterning.




        [M, N] = size(section);
        w1 = cos(linspace(-pi/2, pi/2, M));
        w2 = cos(linspace(-pi/2, pi/2, N));
        w = w1' * w2;



orientangles = orientsection(orientsection~=0);
orientangles(3.1415 < orientangles) = [];
orientangles(-3.1415 > orientangles) = [];
orientangles(1.56 < orientangles & orientangles <1.58) = [];
orientangles(-1.56 > orientangles & orientangles > -1.58) = [];

C = sum(cos(orientangles.*2)); % Center of mass X (circular form)
S = sum(sin(orientangles.*2));

subaxis(2,2,1,1);
imagesc(orientsection);
 axis image;
colormap(gray);

meandirect = 0;
if C>0
meandirect = (atan(S/C))/2;
else
    meandirect = (atan(S/C)+pi)/2;
end

if meandirect<0
    meandirect = meandirect+pi;
end

if isnan(meandirect)==1
    meandirect=0;
end
 subaxis(2,2,2,1)
 imagesc((section));
 colormap(gray);
 axis image

npixels = floor(blocksize/1.1);
```

```
clear fourlina
fourlina = {zeros(1,npixels) zeros(1,npixels) zeros(1,npixels) zeros(1,npixels)
zeros(1,npixels)};
warning('off','signal:findpeaks:noPeaks');
k=0;
hold on
fourlinsum = 0;
for Doff=-8:1:8
    k=k+1;
    xi = [blocksize/2-blocksize*cos(meandirect)/2.2-Doff*sin(meandirect); ...
          blocksize/2+blocksize*cos(meandirect)/2.2-Doff*sin(meandirect)];
    yi = [blocksize/2+blocksize*sin(meandirect)/2.2-Doff*cos(meandirect); ...
          blocksize/2-blocksize*sin(meandirect)/2.2-Doff*cos(meandirect)];

       fourlina{k} = improfile(section,double(xi),double(yi),npixels);
       FOUR{k} = abs(fft(fourlina{k}));
line(xi,yi);
       fourlinsum = fourlinsum+FOUR{k};

end

hold off

linesmade = k;

fourlin_ave = smooth(fourlinsum ./ linesmade);

fourlin_ave = fourlin_ave(1:ceil(0.5*npixels));
for k=length(fourlin_ave):-1:1
    fourlin_ave(k) = fourlin_ave(k)-min(fourlin_ave(1:k));
end
 subaxis(2,2,1,2)
 plot(fourlin_ave);
[pks,locs] = findpeaks(fourlin_ave,'sortstr','descend');

    if isempty(pks) == 0

        Fdomain = locs(1);

        fourstrengthval = pks(1);

    else
        fourstrengthval = 0;

    end

str_four = fourstrengthval;

%% 1D Profile Strength/Spacing Determination - Spacial Domain Analysis
 subaxis(2,2,2,2)
 plot(fourlin_ave);

combodists = [];
for k=1:3
    fourlina{k} = smooth(fourlina{k});
    plot(abs(fourlina{k}),'b')

    hold on
```

```
    linemean = mean(fourlina{k});
    linezeros = fourlina{k} - linemean;
cross = find(diff(sign(linezeros)));

cross_l = linezeros(cross);
cross_r = linezeros(cross+1);

cross_spats = cross + cross_l./(cross_l-cross_r);

scatter(cross + cross_l./(cross_l-cross_r),
linemean*ones(size(cross)),'r','linewidth',3);

if length(cross_spats)>2
cross_dists = umperpix.*[diff(cross_spats(1:2:end)); diff(cross_spats(2:2:end))];
combodists = [combodists(:) ; cross_dists];

end
end

if length(combodists)>1
sl_spatial = mean(combodists);
else
    sl_spatial = 0;
end

fourstrengthval = str_four;
sarclength = sl_spatial;

end
```